การสังเคราะห์อนุภาคระดับนาโนเมตรของแบเรียมเซอร์โคเนียมไททาเนตด้วยกระบวนการโซโนเคมี

SONOCHEMICAL SYNTHESIS OF BARIUM ZIRCONIUM TITANATE NANOPARTICLES

ศุภมาส วิรุญจิตร
SUPAMAS WIRUNCHIT

วิทยานิพนธ์นี้เป็นส่วนหนึ่งของการศึกษาตามหลักสูตรปริญญาปรัชญาดุษฎีบัณฑิต
สาขาวิชานาโนวิทยาและนาโนเทคโนโลยี
วิทยาลัยนาโนเทคโนโลยีพระจอมเกล้าลาดกระบัง
สถาบันเทคโนโลยีพระจอมเกล้าเจ้าคุณทหารลาดกระบัง
พ.ศ. 2558
KMITL-2015-NT-D-001-005

SONOCHEMICAL SYNTHESIS OF BARIUM ZIRCONIUM TITANATE NANOPARTICLES

SUPAMAS WIRUNCHIT

A THESIS SUBMITTED IN PARTIAL FULFILLMENT
OF THE REQUIREMENT FOR THE DEGREE OF
DOCTOR OF PHILOSOPHY IN NANOSCIENCE AND NANOTECHNOLOGY
COLLEGE OF NANOTECHNOLOGY
KING MONGKUT'S INSTITUTE OF TECHNOLOGY LADKRABANG
2015

KMITL-2015-NT-D-001-005

วิทยาลัยนาโนเทคโนโลยีพระจอมเกล้าลาดกระบัง
สถาบันเทคโนโลยีพระจอมเกล้าเจ้าคุณทหารลาดกระบัง
ใบรับรองวิทยานิพนธ์

ัวข้อวิทยานิพนธ์	การสังเคราะห์อนุภาคระดับนาโนเมตรของแบเรียมเซอร์โคเนียมไททาเนตด้วยกระบวนการโซโนเคมี
hesis Title	Sonochemical Synthesis of Barium Zirconium Titanate Nanoparticles
ักศึกษา	นางสาวศุภมาส วิรุญจิตร
หัสประจำตัว	53670103
ริญญา	ปรัชญาดุษฎีบัณฑิต
าขาวิชา	นาโนวิทยาและนาโนเทคโนโลยี
าจารย์ที่ปรึกษาวิทยานิพนธ์	ผศ.ดร.นราธิป วิทยากร
าจารย์ที่ปรึกษาวิทยานิพนธ์ร่วม	-
มายเลขวิทยานิพนธ์	KMITL-2015-NT-D-001-005

คณะกรรมการสอบวิทยานิพนธ์		ลายมือชื่อ
ร.สิรพัฒน์	ประโทนเทพ	
ศ.ดร.นราธิป	วิทยากร	
ศ.ดร.วิษณุ	เพชรภา	
ศ.ดร.วรรณวิลัย	วิทยากร	
ศ.ดร.ธีระชัย	บงการณ์	

น / เดือน/ ปี ที่สอบ วันศุกร์ที่ 26 มิถุนายน พ.ศ. 2558 เวลา 13.30 น. เป็นต้นไป
ถานที่สอบ ณ อาคารวิจัยนาโนเทคโนโลยีสิรินธร ชั้น 1 ห้องประชุมนาโน

วิทยาลัยนาโนเทคโนโลยีพระจอมเกล้าลาดกระบังรับรองแล้ว

(ผู้ช่วยศาสตราจารย์ ดร.อนุชิต จารุวนาวัฒน์)
คณบดี

วันที่ 6 **เดือน** สิงหาคม **พ.ศ.2558**

หัวข้อวิทยานิพนธ์	การสังเคราะห์อนุภาคระดับนาโนเมตรของแบเรียมเซอร์โคเนียมไททาเนตด้วยกระบวนการโซโนเคมี
นักศึกษา	นางสาว ศุภมาส วิรุญจิตร
รหัสประจำตัว	53670103
ปริญญา	ปรัชญาดุษฎีบัณฑิต
สาขาวิชา	นาโนวิทยาและนาโนเทคโนโลยี
พ.ศ.	2558
อาจารย์ที่ปรึกษาวิทยานิพนธ์	ผศ. ดร. นราธิป วิทยากร

บทคัดย่อ

งานวิจัยนี้ศึกษาการสังเคราะห์ผงผลึกในระบบแบเรียมไททาเนต-แบเรียมเซอร์โคเนต ($BaTiO_3$-$BaZrO_3$) ด้วยวิธีโซโนเคมี (Sonochemical method) โดยใช้แบเรียมคลอไรด์ไดไฮเดรต ($BaCl_2 \cdot 2H_2O$) ไทเทเนียมเตตระคลอไรด์ ($TiCl_4$) และเซอร์โคเนียมออกซิคลอไรด์ออกตะไฮเดรต ($ZrOCl_2.8H_2O$) เป็นสารตั้งต้น โดยทำการศึกษาอิทธิพลของความเข้มข้นของสารตั้งต้น บรรยากาศที่ใช้ในการสังเคราะห์ เวลาที่ใช้ในการเกิดปฏิกิริยา ความเข้มข้นของเซอร์โคเนียมไอออน (Zr^{4+}) และความเข้มข้นของโซเดียมไฮดรอกไซด์ (NaOH) ซึ่งเป็นสารช่วยตกตะกอน (Precipitant) ที่มีผลต่อผงผลึกในระบบแบเรียมไททาเนต-แบเรียมเซอร์โคเนต จากนั้นจะทำการวิเคราะห์ผงผลึกแบเรียมไททาเนตที่ได้โดยจะทำการตรวจสอบโครงสร้างผลึกด้วยเทคนิคการเลี้ยวเบนของรังสีเอกซ์ (XRD) ตรวจสอบเอกลักษณ์ด้วยเทคนิคฟูเรียร์ทรานสฟอร์มอินฟราเรดสเปกโทรสโกปี (FT-IR) และเทคนิครามานสเปกโทรสโกปี ตรวจสอบลักษณะสัณฐานวิทยาและขนาดของอนุภาคด้วยกล้องจุลทรรศน์อิเล็กตรอนแบบส่องกราด (SEM) ซึ่งในงานวิจัยนี้ได้ประสบความสำเร็จในการสังเคราะห์ผงผลึกในระบบแบเรียมไททาเนต-แบเรียมเซอร์โคเนต ด้วยวิธีการโซโนเคมีภายใต้สภาวะความเป็นเบสที่สูง ซึ่งจากผลที่ได้จากเทคนิค XRD พบว่าผงผลึกที่ได้มีความบริสุทธิ์สูงและมีเฟสที่สอดคล้องกับสารมาตรฐานในระบบแบเรียมไททาเนต-แบเรียมเซอร์โคเนต ซึ่งมีโครงสร้างเป็นแบบคิวบิก (Cubic structure) ต่อมาทำการวิเคราะห์ด้วยเทคนิค FT-IR และ Raman จะพบการสั่นแบบยืดหดของพันธะ Ti-O และ Zr-O เกิดขึ้นภายในโครงสร้างเพอรอฟสไกต์ของสารในระบบแบเรียมไททาเนต-แบเรียมเซอร์โคเนต โดยอนุภาคของสารในระบบแบเรียมไททาเนต-แบเรียมเซอร์โคเนตที่เตรียมได้จะมีลักษณะเป็นทรงกลมและมีการกระจายตัวที่แคบโดยจะมีขนาดของอนุภาคเฉลี่ยประมาณ 123 ± 23 นาโนเมตร ที่ระบุด้วยเทคนิค SEM

คำสำคัญ: **แบเรียมไททาเนต ($BaTiO_3$) แบเรียมเซอร์โคเนต ($BaZrO_3$) แบเรียมเซอร์โคเนียมไททาเนต ($BaZr_xTi_{1-x}O_3$) วิธีโซโนเคมี (Sonochemical method)**

Thesis Title	Sonochemical synthesis of barium zirconium titanate nanoparticles
Student	Miss Supamas Wirunchit
Student ID	53670103
Degree	Doctor of Philosophy
Program	Nanoscience and Nanotechnology
Year	2015
Thesis Advisor	Asst. Prof. Dr. Naratip Vittayakorn

ABSTRACT

In this research, nanoparticles of barium titanate – barium zirconate system ($BaTiO_3$-$BaZrO_3$) were synthesized via sonochemical method using barium chloride dihydrate ($BaCl_2{\cdot}2H_2O$) as the barium source titanium tetrachloride ($TiCl_4$) as the titanium source and zirconium oxychloride octahydrate ($ZrOCl_2{\cdot}8H_2O$). The effects of precursor concentrations, synthesis atmosphere, sonication time, Zr^{4+} concentration and the concentration of sodium hydroxide (NaOH) on the precipitation of barium titanate – barium zirconate system ($BaTiO_3$-$BaZrO_3$) powders were investigated. The as-synthesized barium titanate – barium zirconate system ($BaTiO_3$-$BaZrO_3$) powders were characterized by X-ray diffraction technique (XRD), Fourier transform infrared spectroscopy (FT-IR) and Raman spectroscopy. The powder morphology was determined by scanning electron microscopy (SEM). The spherical nanoparticles of barium titanate – barium zirconate system ($BaTiO_3$-$BaZrO_3$) were prepared successfully by the sonochemical method in a strong alkaline environment. The XRD patterns show that the main diffraction peaks correspond to cubic $BaTiO_3$, $BaZr_{0.25}Ti_{0.75}O_3$, and $BaZrO_3$ particles. The FT-IR and Raman spectra indicat the presence of the bonding vibration of Ti-O and Zr-O stretching within the $BaTiO_3$, $BaZr_xTi_{1-x}O_3$, and $BaZrO_3$ structure. The $BaTiO_3$-$BaZrO_3$ system particles from the sonochemical synthesis show a monosized, spherical shape and a narrow size distribution. The average diameter of the sonochemically synthesized particles is 123 ± 23 nm, as identified by SEM.

Keywords: Barium titanate ($BaTiO_3$), Barium Zirconate ($BaZrO_3$), Barium zirconium titanate ($BaZr_xTi_{1-x}O_3$), Sonochemical method, Nanosphericalparticles

ACKNOWLEDGMENTS

This thesis was accomplished in the Electroceramic Research Laboratory, College of Nanotechnology, King Mongkut's Institute of Technology Ladkrabang, Bangkok, Thailand.

I wish to acknowledge many people who have helped and assisted me, and shared my problems or just listened during the preparation of this thesis. First of all, I would like to thank, with deep appreciation, Assistant Professor Dr. Naratip Vittayakorn for his unending patience and invaluable suggestions, recommendations, inspirations and supports throughout my educational life, since being an undergraduate student.

I would also like to thank Assistant Professor Dr. Banjong Boonchom and Mr. Anucha Ruangphanit for their kind advice, help and valuable information.

I would like to express my gratitude to Associate Professor Dr. Wisanu Pecharapa, Assistant Professor Dr. Wanwilai Vittayakorn, Assistant Professor Dr. Teerachai Bongkarn and Dr. Sirapat pratontep, for their helpful advice, useful comments and suggestions and devotion of their time to serve as members of the Examining Committee.

I am indebted to the many people who influenced, helped and had fun in working with me when preparing this thesis, and those that are too numerous to mention. My profound thanks are conveyed to members of the Electroceramic Research Laboratory who gave me so much assistance.

Special thanks go to Buddhism & Tradition club KMITL and my Nano-family, Mr. Pathompong legsompud, Mr. Kraisak Watthanarangsart, Mr. Wiriya Samransom, Mr. Sarunyu Saksakulkrai, Miss Teantong Chonsut, Miss Benjaporn Saetang, Miss Thanyarat Suhadcho, Miss Napassorn Jensupakarn, Mr. Paopoom keidkong, Mr. Supphawat Settapong and Mr. Kopchai Unkeaw, who relaxed, helped, cheered and encouraged me. Their advice and experience influenced and drove me to this point.

I wish to acknowledge the Royal Golden Jubilee (RGJ) Ph.D. Program for all its financial support.

Finally, I wish to dedicate this thesis to my parents, Mr. Wanchai Wirunchit and Mrs. Jumnien Wirunchit, for their support, understanding and patience.

SUPAMAS WIRUNCHIT

TABLE OF CONTENTS

LIST OF TABLES

LIST OF FIGURES

Figure Page

Figure Page

CHAPTER 1

INTRODUCTION

1.1 Overview

Many researchers have focused recently on the lead-free ceramic materials and their applications in various electronic devices because of environmental and human health issues [1-4]. Barium titanate ($BaTiO_3$) was the first of lead-free piezoelectric ceramic material to be studied widely since its discovery in the 1940s [5]. It is well known that the improved performance of the material in electroceramics can be done by doped of a compound which is an effective way, especially substitution of Ti^{4+} with Zr^{4+} in $BaTiO_3$, which has received much attention because of their electrical properties and tunable structure to specific applications. The formation of the solid solution $Ba(Zr_xTi_{1-x})O_3$ with partial substitution of Ti^{4+} (ionic radius 0.745 nm) by Zr^{4+} (ionic radius 0.86 nm) resulted in an increase in the lattice parameter and changes that occur with crystalline, the dielectric properties and phase transition temperatures compared with pure $BaTiO_3$ [6]. Previous research have been studied the submicron-sized of $Ba(Zr_xTi_{1-x})O_3$ powders have suggested that $Ba(Zr_xTi_{1-x})O_3$ is still tetragonal at Zr substitutions up to 0.2 mol%, then changes to pseudo-monoclinic in the range between 0.2 to 0.6 mol% before changing to a rhombohedral at Zr content as 20 mol%. The $Ba(Zr_xTi_{1-x})O_3$ is a cubic at room temperature when increase Zr content more than 20 mol% [7]. The phase transition of pure BT from tetragonal to cubic (nornal ferroelectric to paraelectric) at 130 °C. There are also behavioral changes such as phase transition temperature from 130 to 110 °C at the composition 10 mol% of Zr, $Ba(Zr_xTi_{1-x})O_3$ ceramics. In addition, the $Ba(Zr_xTi_{1-x})O_3$ ceramics exhibit Tc shifts to higher temperature with increase in frequency at around 30 mol% of Zr substitutions, which is typical diffuse paraelectric to ferroelectric phase transition behavior [8]. The Zr-rich compositions (at above 30 mol%) exhibit like relaxor ferroelectric behavior, showing a diffuse phase transitions and dielectric dispersion [9]. Since these phase boundary compositions and phase transition temperatures will hinge on the size of crystalline primary particles, it is expected that nanopowders might behave differently [10]. While the particle size is reduced, this may influence in the size of domains around tens of nanometers. The particles tend to be stable, presumably due to the high surface energy, because the crystal structure nearest a high symmetry (cubic). This observation was reported perovskite structured such$BaTiO_3$, $PbTiO_3$, and $Pb(Zr_{0.52}Ti_{0.48})O_3$; (PZT) have in a range of critical particle size different [11]. Moreover, the critical particle size

is important that this occurs is still unknown, and it seems to vary depending on the route for the synthesis.

The production of high performance ceramic materials with functional devices requires the highest purities, homogeneity powders, well controlled particle morphology and narrow size distribution. Thus, many research groups have focused on the quality of processing for synthesis of $Ba(Zr_xTi_{1-x})O_3$ (BZT) high performance product powders. The conventional solid state method, is a traditional way of preparing $Ba(Zr_xTi_{1-x})O_3$ ceramics, is the reaction between $BaCO_3$, ZrO_3 and TiO_2 at high temperature. The complete phase formation of BZT by This fabrication method is required calcinations at high temperature and repeated cycles of mixing respective oxides. Nevertheless, this fabrication method has several drawbacks such as low purity [16, 17], long processing time [12, 13], frequent need for grinding steps [17], multiple calcinations [14, 15] and submicrometer size crystals [12, 13, 18]. So this method is not suitable for obtaining narrow particle size distribution [12, 14, 18]. In 2005, J. Bera *et al.* [14] have used solid state reaction method for formation the $Ba(Zr_xTi_{1-x})O_3$ solid solution. They reported that formation mechanism of the $Ba(Zr_xTi_{1-x})O_3$ solid solution can be explained by multistep reactions. At a temperature lower than 1,300oC, the raw materials which are $BaTiO_3$ and $BaZrO_3$, did not form $Ba(Zr_xTi_{1-x})O_3$ solid solution directly. In the initial stage, the temperature ranging from 700 to 800 °C displayed the formed separately of the raw materials. Subsequently, a single perovskite phase of $Ba(Zr_xTi_{1-x})O_3$ was form by the diffusion of $BaTiO_3$ into the $BaZrO_3$ at a temperature as high as 1,600 °C. In order to eliminate the defects of conventional solid state reaction method by many new wet-chemical synthesizing methods which have been developed such as sol–gel method [19, 20], aqueous co-precipitation method [21], hydrothermal method [22, 23], combustion method [24] and direct synthesis from solution (DSS) [25], are the most popular methods to do that. However, although these chemical methods are suitable for preparing high quality BZT nanopowders, the synthesis process is complicated and takes a very long time. In addition, the calcinations process is still required to achieve complete phase formation. It is really difficult to get the nanoparticles with uniform size under the calcination process [12, 18]. So the calcination process should be undesirable step during the fabrication process of nanopowder. This research provides an interesting sonochemical method, which is one of the wet chemical processes technique that fulfills the requirements for synthesizing extremely fine particles with spherical morphology and a narrow size distribution [26, 27]. The sonochemical method can be employed to synthesize metallic and organic covers, and especially almost all inorganic nanoparticles, in a short period of time [28-31]. It also can use the acoustic cavitation from an ultrasonic

wave to accelerate or generate the chemical reaction. The creation, growth and collapse of a bubble, which are formed in liquid, are the main event of sonochemistry. At the initial stage, the solute vapor diffuses into the volume of the bubble that leads to bubble growth. Subsequently, the bubble growth until its size reaches maximum value and is collapsed in the last stage. During ultrasonication, the small bubble generated in aqueous solution collapses which caused an extremely high pressure of ~20 MPa, temperature of about 5,000 K and a very high cooling rate of ~ 10^{10} $K.S^{-1}$ in a much localized space. Then, it is expected that all is unique properties of the sonochemically synthesized particles [32-34]. In the previous research such as simple metal oxides [35, 36], core/shell nanocomposites [37, 38], metals [39, 40], carbides [41], nitrides [35], sulfides [35, 42] and precious metals [43, 44] were synthesized successfully by this method. Until now, studies have reported the multicationic oxides based on a perovskite structure (ABO_3) which synthesized by the sonochemical method quite a few, and there is no report to the best of authors' knowledge on the direct sonochemical synthesizing of $(BaZr_xTi_{1-x}O_3)$; x = 0.00 - 0.60 powders.

In this study, a synthesis nanosized complex perovskite $Ba(Zr_xTi_{1-x})O_3$ with x = 0.00 - 0.60 has been conducted using high-intensity ultrasound irradiation by varying the synthesis parameters, including the concentration of precipitating agent, the synthesis atmosphere, the concentration of the starting solution, sonication time, the power of ultrasound irradiation and Zr/Ti molar ratio. In addition, all products were investigated carefully in order to understand their effect on the morphology and the perovskite phase formation of the powders. The procedure of the $Ba(Zr_xTi_{1-x})O_3$ nanopowders formation by sonochemical method also was examined.

1.2 Scope of this work

The aim of this research was to synthesize a complex perovskite $Ba(Zr_xTi_{1-x})O_3$ nanopowders (where x = 0.00, 0.05, 0.20, 0.40 and 0.60) using high-intensity ultrasound irradiation via varying the synthesis parameters, including the synthesis atmosphere, concentration of precipitating agent, concentration of the starting solution, sonication time and Zr/Ti molar ratio. In this process, barium chloride dihydrate ($BaCl_2.2H_2O$), zirconium oxychloride octahydrate ($ZrOCl_2.8H_2O$) and titanium chloride ($TiCl_4$) were employed as the starting material, and sodium hydroxide (NaOH) was used as precipitating agent. The crystallographic information, including phase purity crystal structure, crystallite size and lattice constant of the product powders, were determined using X-ray diffraction technique (XRD). The particle size and

morphological studies were carried out using scanning electron microscope (SEM). Furthermore, the crystal structures and functional groups were confirmed using Raman and Fourier transform-infrared spectroscopy (FT-IR).

1.3 Objectives of this work

This research emphasizes on the synthesis of a nanosize complex perovskite barium zirconium titanate ($Ba(Zr_xTi_{1-x})O_3$) to achive the following purpose:

1.3.1 To synthesize the single phase of a complex perovskite $Ba(Zr_xTi_{1-x})O_3$ nanopowders (where x = 0.00, 0.05, 0.20, 0.40 and 0.60) by the sonochemical process via varying the synthesis parameters, including the synthesis atmosphere, concentration of precipitating agent, concentration of the starting solution, sonication time and Zr/Ti molar ratio.

1.3.2 To determine the optimum conditions for the synthesis of the $Ba(Zr_xTi_{1-x})O_3$ nanopowders by the sonochemical process.

1.3.3 To investigate the influence of the synthesis atmosphere, concentration of precipitating agent, concentration of a starting solution, sonication time, power of ultrasound irradiation and Zr/Ti molar ratio on the perovskite phase formation of the $Ba(Zr_xTi_{1-x})O_3$ nanopowders obtained by the sonochemical process.

1.3.4 To determine the characteristics of a complex ternary metal oxide $Ba(Zr_xTi_{1-x})O_3$ nanopowders obtained by obtained by sonochemical process via varying the synthesis parameters, including the synthesis atmosphere, concentration of precipitating agent, concentration of the starting solution, sonication time and Zr/Ti molar ratio.

CHAPTER 2

LITERATURE REVIEW

2.1 Nanostructured materials

Nanotechnology is a technology related to small structures or small material with generally dimensions ranging from subnanometer to hundreds of nanometers. Generally, material in the micrometer often display physical properties similar to bulk materials. Generally, material in the micrometer often display physical properties similar to bulk materials. The materials at the nanometer scale may have different physical properties distinctive different from those of bulk materials. The materials are available in this range will characteristic or properties feature outstanding due to the change of atoms or molecules to bulk form to come up in this size range. For example, Crystals with dimensions in the nanometer scale have a low melting point, which is different from bulk materials with a melting point of 1,000 ° C. In addition, the lattice constant also reduced due to the surface energy and the number of atoms or ions plays a significant role in the thermal stability. The stability of the crystal structure is generally stable at high temperatures, but for crystal structures with dimensions in the nanometer scale can be stabilized at much lower temperatures. So when the material is reduced in to the nanometer scale ferroelectrics and ferromagnetics may have lost their ferroelectricity and ferromagnetism. Characteristics on dimensions that are small enough in the few of nanometers, the bulk semiconductors become insulators. Similarly, Au nanocrystals to demonstrate the catalyst at low temperatures excellent. The bulk gold did not show any catalytic properties.

Nanostructured materials, are a low dimensional materials composed of building units of nanoscale or submicron size at least in one direction and exhibiting size effects, as a part of nanotechnology. The dimensions of nanostructured materials include zero-dimensional (0D), one-dimensional (1D), two-dimensional (2D) and three-dimensional (3D) nanomaterials. They are the main types of nanostructured materials based on the dimensions [45].

2.1.1 Zero-dimensional nanostructured materials (0D nanostructured materials)

The field of 0D nanostructured materials has been studied and developed continuously significantly from 10 years in the past. There are many physical and chemical methods have been developed for use in the fabrication 0D nanostructured materials that can control the size and shape as well. The 0D nanostructured materials, which was synthesized, have wide variety kinds such as heterogeneous particles arrays, hollow spheres, uniform particles arrays (quantum dots), core–shell quantum dots, onions and nanolenses [46-50]. Figure 2.1 shows the SEM and TEM images of different types of 0D nanostructured materials. Moreover, 0D nanostructured materials, such as quantum dots has been widely studied in single-electron transistors [51], lasers [52], solar cells [52] and light emitting diodes (LEDs) [54] .

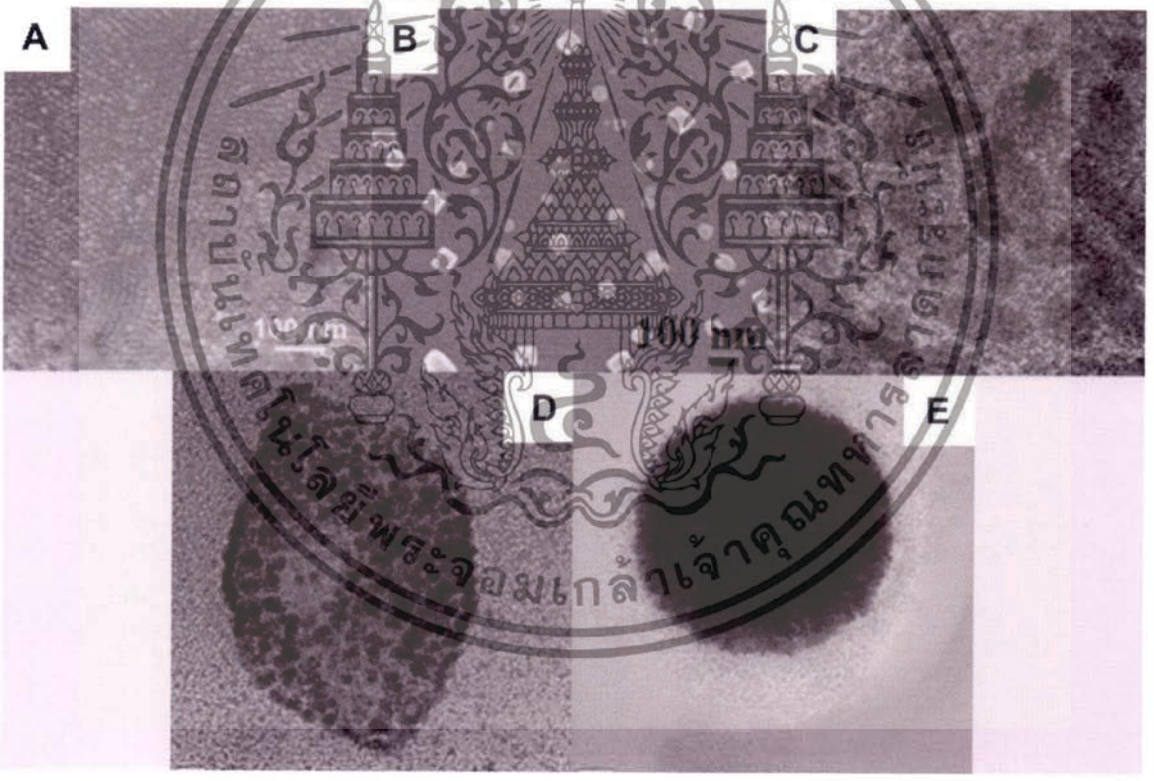

Figure 2.1 The SEM and TEM image of 0D nanostructured materials. (A) Quantum dots, (B) nanoparticles arrays, (C) core–shell nanoparticles, (D) hollow cubes and (E) nanospheres [45].

2.1.2 One-dimensional nanostructured materials (1D nanostructured materials)

1D nanostructured materials has been steadily increasing attention in the past decade due to importance of their properties. And a variety of potential applications of them. It is commonly recognized that the 1D nanostructured materials are ideal systems for exploring many of novel phenomena at the nanoscale and to determine the dependence of functionality properties, size and dimension. In addition, they also play an important role in agencies in electronics manufacturing and interconnects, electrochemical energy and optoelectronic devices with a nanoscale dimensions. The field of 1D nanostructured materials have been the focus of research such as Iijima and co-worker [55] have conducted pioneering research on nanotubes have received significant attention. The 1D nanostructured materials have a profound effect on nanodevices, nanoelectronics and systems, alternative energy resources, nanocomposite materials and national security [56]. In Figure 2.2 shows the 1D nanostructured materials, such as nanorods, nanotubes, nanoribbons, nanowires, hierarchical nanostructures, and nanobelts [57-72].

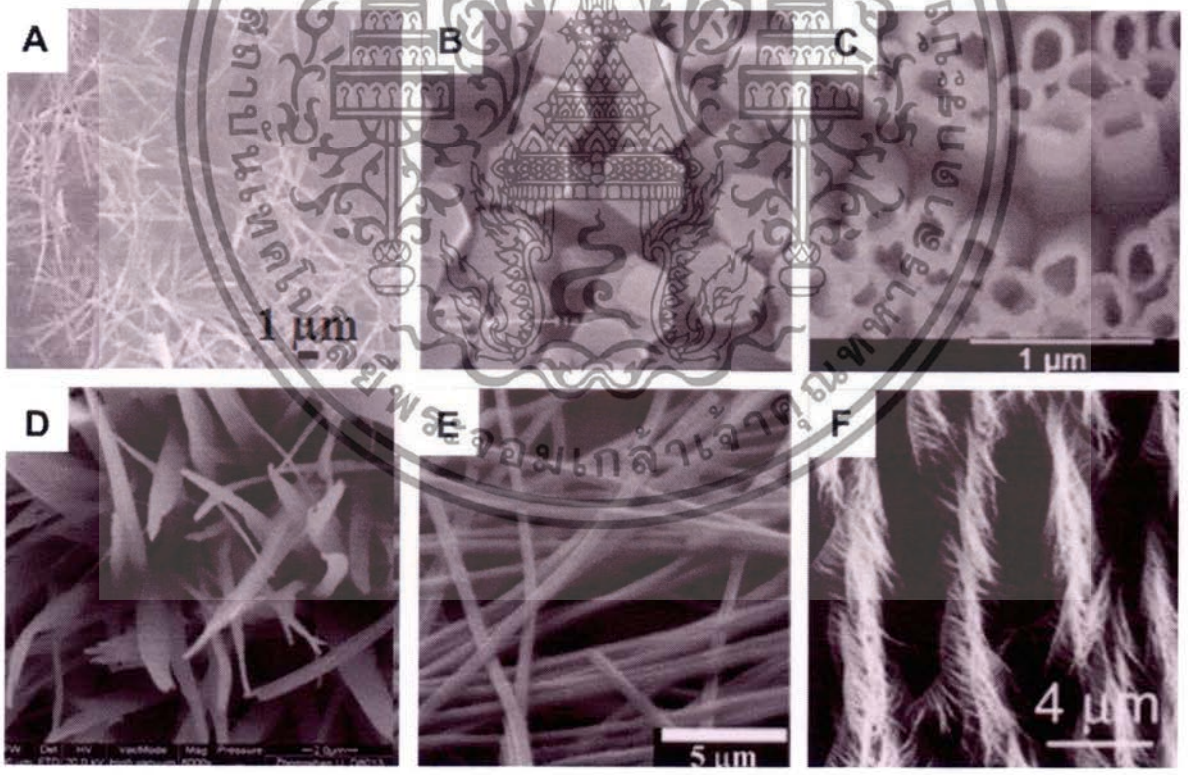

Figure 2.2 The SEM image of 1D nanostructured materials. (A) nanowires, (B) nanorods, (C) nanotubes, (D) nanobelts], (E) nanoribbons, and (F) hierarchical nanostructures [45].

2.1.3 Two-dimensional nanostructured materials (2D nanostructured materials)

In recent years, the synthesis 2D nanostructured materials which have two dimensions outside of the nanometric size range, has become a focus of research. Due to their characteristics of many low dimensional as distinct from the bulk properties. In the last few years, many research have focused much attention and development of 2D nanostructured materials [73-75]. In addition, this 2D nanostructured materials is interesting, especially for monitoring the use and development of new sensors nanoreactors nanocontainers and photocatalysis. And continues to be attractive for a basic understanding of the mechanism of nanostructure growth [76]. In Figure 2.3 shows the 2D nanostructured materials, such as branched structures, junctions (continuous islands), nanodisks, nanowalls, nanoplates, nanosheets and nanoprisms [77-83].

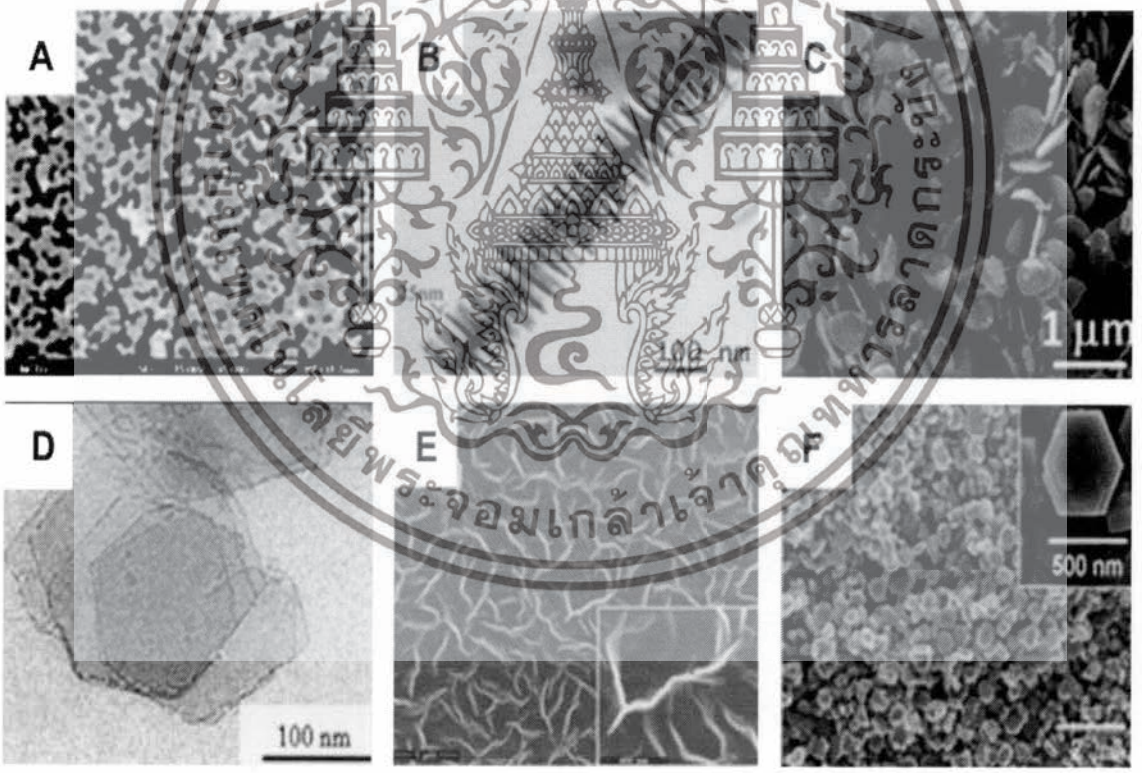

Figure 2.3 The SEM and TEM image of 2D nanostructured materials. (A) Junctions (continuous islands), (B) branched structures, (C) nanoplates, (D) nanosheets, (E) nanowalls and (F) nanodisks [45]

2.1.4 Three-dimensional nanostructured materials (3D nanostructured materials)

In the past 10 years, many 3D nanostructured materials have been synthesized and given attracted considerable from a lot of research interest due to the large specific surface area and other superior properties than their bulk counterparts that arise from quantum size effects [84-98]. It is well known that an important factors in the ultimate performance and applications of nanostructured materials, severe depending on the size, shape, dimensions and morphology, which is indicative of the behaviors of them. Thus, the synthesis 3D nanostructured materials with a controlled structure and morphology have been very much interested. Furthermore, the nanostructures of 3D nanostructured materials are important because of the variety of applications in the areas of catalyst materials, electrode for batteries and magnetic materials [84-98]. Due to their higher surface area and supply enough absorption sites for all relevant molecules in small spaces [99]. As a result, a lot of research has to pay attention to the 3D nanostructured, recently. On the other hand, the material has a porosity in three dimensions could lead to improved transport of molecules [99-101]. In Figure 2.4 shows the typical 3D nanostructured materials, such as nanocoils, nanopillers, nanoflowers, nanocones and nanoballs [102-106].

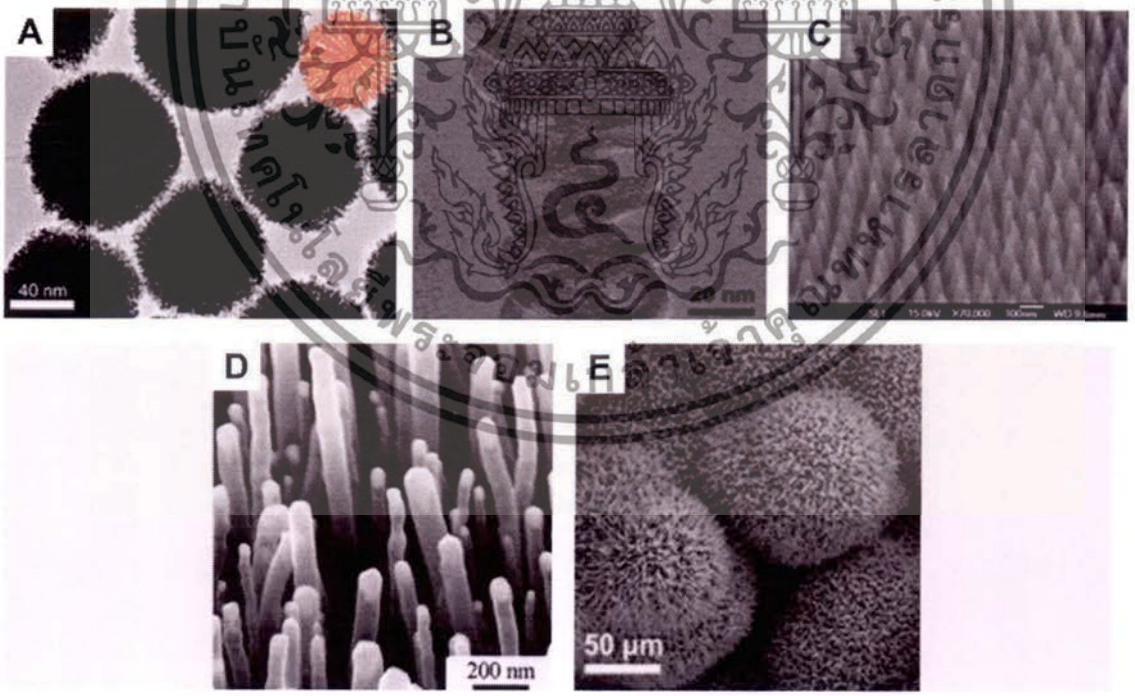

Figure 2.4 The SEM and TEM image of 3D nanostructured materials. (A) nanoballs (dendritic structures), (B) nanocoils, (C) nanocones, (D) nanopillers and (E) nanoflowers [45]

2.2 Grain size effects on ferroelectric ceramics

Since the discovery of the high dielectric constant of ferroelectric barium titanate in the 1940s, ceramic materials based on this compound have been widely utilized in the manufacture of ceramic capacitors and related electro-ceramic applications [5].

The dielectric constant of ceramic BaTiO3 depends strongly on the grain size. Coarse-grained ceramics of pure $BaTiO_3$ (grain size ≈ 20 ~ 50 μm) show K ≈ 1500 ~ 2000 at room temperature (K_{RT}). In the past six decades, several investigators such as H. Kniekamp and W. Heywang [107], G. H. Jonker and W. Noorlander [108], N. C. Sharma and JE. R. McCartney [109] reported that the dielectric constant increases markedly with decreasing grain size, attaining values of 6000 for ceramic bodies with grain sizes of 1 μm or less. In the hot-pressed $BaTiO_3$ with grain size ≈ 1 μm, Brandmayr et. al. [110] reported dielectric constant value (K_{RT}) of ≈ 6000 at room temperature. At even smaller grain size (<1 μm), however, the same authors observed a strong decrease of dielectric constant (K_{RT}). It was concluded that the dielectric constant at room temperature of $BaTiO_3$ ceramics reaches to a maximum value at a grain size of about 1 μm.

G. Arlt et al. [111-112] observed that the width of the 90° domains reveals a dependence on the grain size of $BaTiO_3$ fine-grained ceramics. The observation of domains, the measurements of the dielectric constant and elastic coefficients (Young's modulus), and a theoretical analysis confirm that the equilibrium domain width is dependent on the grain size with a ratio $d_{domain} \sim (\text{grain size})^{1/2}$ as shown in Figure 2.5. They have also repeated that the equilibrium domain width decreases with grain size less than 10 μm and is effectively constant at grain size > 10 μm. Thus, they explained that the high dielectric constant, K_{RT} ≈ 5000 ~ 6000, of fine-grained $BaTiO_3$ is due to the domain size effects. Recently, however, G. Arlt and N. A. Pertsev [114] have reported again that, based on careful theoretical calculations, the high domain density cannot cause the observed large dielectric constant in fine grained (grain size ≈ 1 μm) $BaTiO_3$ ceramics. Instead, they concluded the increase of dielectric constant with decreasing grain size comes mainly from the internal stress. As shown on Figure 2.6,

they believed that with grain sizes smaller than 1 μm, the decreased dielectric constant is due to ferroelectric structure changes.

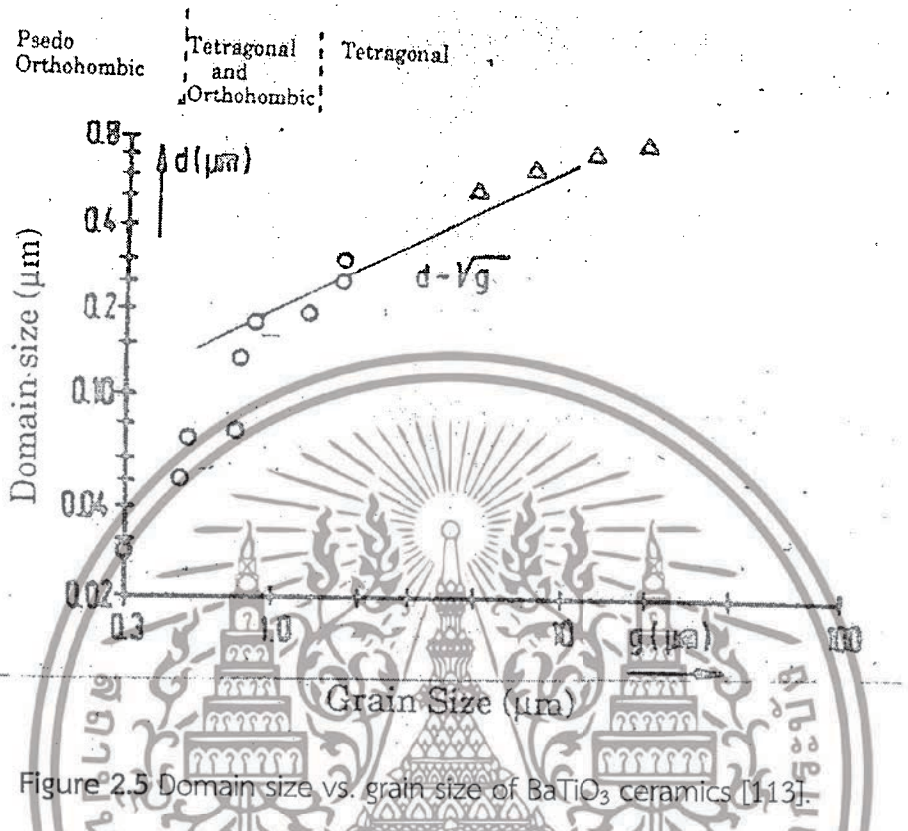

Figure 2.5 Domain size vs. grain size of $BaTiO_3$ ceramics [113].

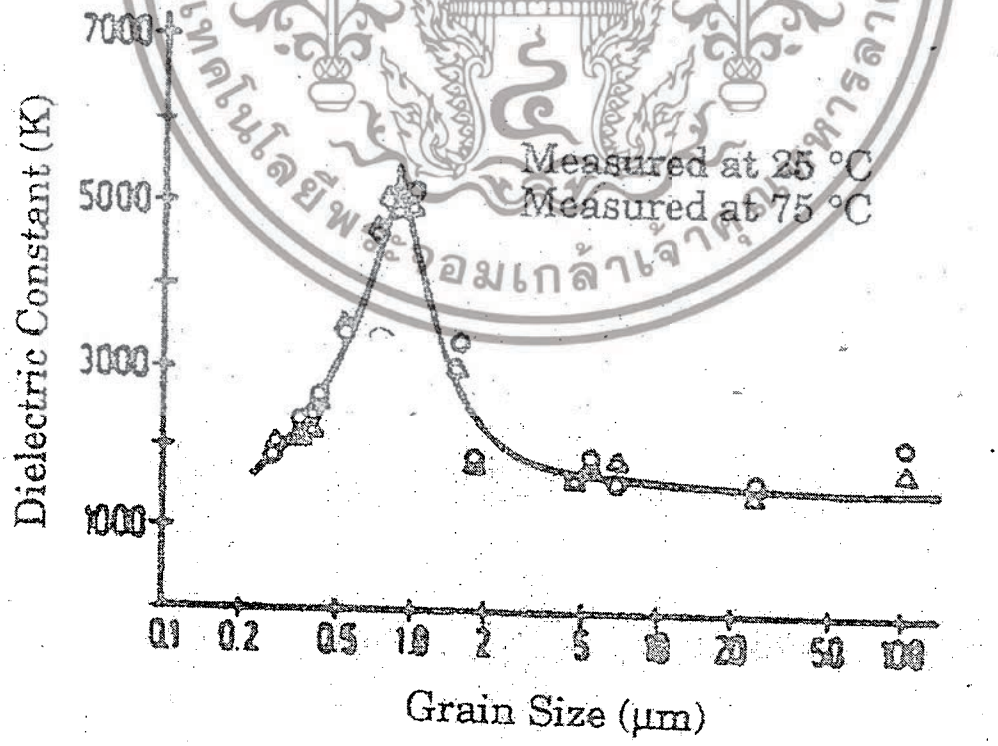

Figure 2.6 Dielectric constant versus grain size of $BaTiO_3$ ceramics [113].

In grain size less than 1 μm, it is believed that there are other important factors to be considered possibly the electric filed energy and the surface energy of the grain can no longer to be neglected, and even the grain is forced by stress to become more cubic structure. The crystallographic structure is modified and the lower is the value of the crystallographic deformation (c2a -1).

The piezoelectric activities have shown an increase with increasing grain size in BaTiO3 ceramics. As shown in Figure 2.7, the longitudinal strain level drops off as grain size decreases from 50 μm to 1 μm [115]. This is believed to be due to the clamping of domain walls by internal stress during the E-filed cycling in fine-grained $BaTiO_3$ ceramics. Furthermore, piezoelectric-activity should disappear when material cubic because the volume of 90° twinned domain decreases with decreasing grain size due to the internal stress effects on fine grain $BaTiO_3$ ceramics.

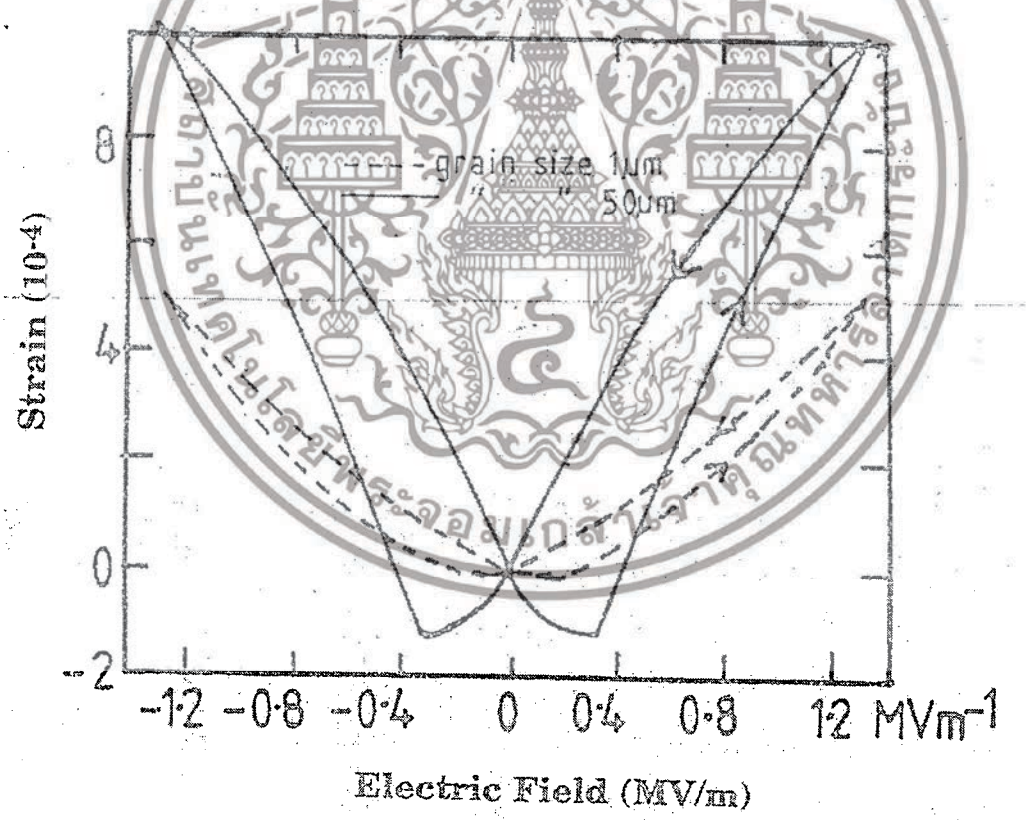

Figure 2.7 Electric field vs. longitudinal strains for coarse and fine grain sizes in $BaTiO_3$ ceramics [115].

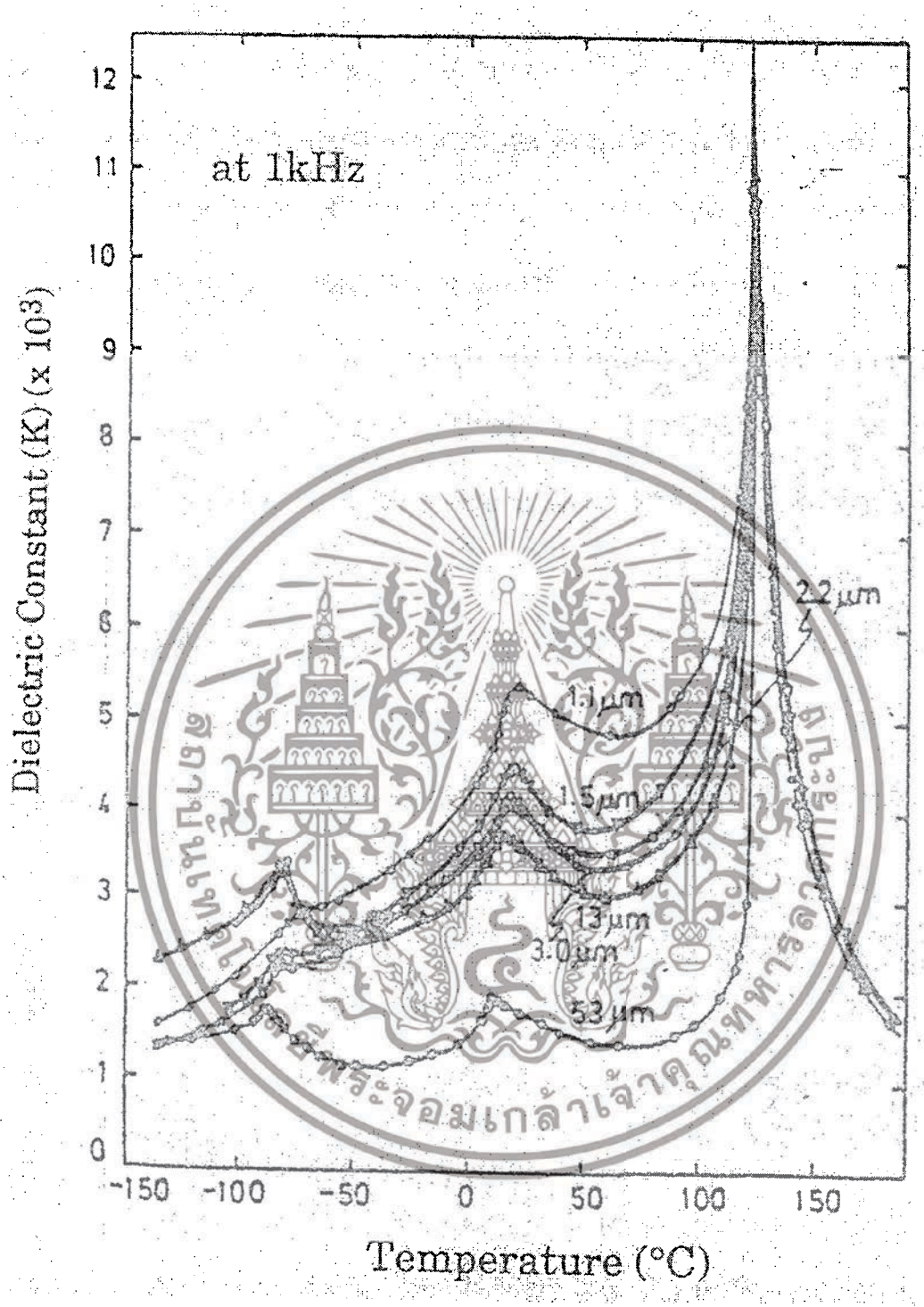

Figure 2.8 Temperature dependence of dielectric constant in various grain sizes high purity $BaTiO_3$ ceramics [116].

In single crystal $BaTiO_3$, the crystal transforms from cubic structure to tetragonal ($T_{c->t}$), orthorhombic ($T_{t->0}$), and rhombohedral ($T_{0->t}$) on cooling at, 130 °C, 0 °C, and -90 °C, respectively. K. Kinoshita and A. Yamaji [116] (Figure 2.8) have shown that above the phase transition temperature (ferroelectric ⟶ paraelectric), T_c grain size has no observable effects on dielectric properties such as dielectric constant K, maximum of dielectric constant (K_{max}), and variation of T_c with a range of 1 μm to 50 μm. In addition, the tetragonal-to-orthorhombic and orthorhombic-to-rhombohedral transition temperatures are raised by about 10 °C with the same range of grain size. W. R. Buessem et al. [117] and A. J. Bel et al. [118] proposed the internal stress model and calculated the modified Devonshire equations in terms of compressive and tensile stress. In addition to the high dielectric constant in fine-grained (grain size ~ 1 μm) ceramics at room temperature, they have shown that the transition ($T_{t->0}$) temperature between tetragonal and orthorhombic structure has increased by 10 °C similar to 1 μm fine-grained materials. Based on the internal stress model, the internal stress develops only below transition temperature (Tc) since it depended on clamping of the ferroelectric tetragonality deformation due to the difficulties in 90° domain formations in fine-grained (grain size ~ 1 μm) ceramics. Thus, this model cannot predict the variation of ferroelectric-paraelectric phase transition ($T_{c->t}$) temperature with varying of grain size.

In summary, the grain size and/or stress dependence of the dielectric constant and transition parameters of $BaTiO_3$ ceramics were reviewed based on theoretical and experimental approaches as listed in Table 2.1. Generally, the dielectric constant, KRT, of this system is made up from the intrinsic dielectric constant resulting from ferroelectric phenomena and is affected by external factors such as electric field and stress, the extrinsic dielectric constant that results from domain wall motion, grain boundary, and defects such as space charges [119].

The observed increase of the tetragonal/orthorhombic transition temperature can be explained with respect to the earlier theories by the existence of internal stress in the grains. In spite of the early results regarding the increase of T_c in the fine-grained ceramic $BaTiO_3$, it is believed that the variation of Curie point (ferroelectric-paraelectric transition temperature,T_c) with grain size is not related with the internal stress, but with grain boundary phases associated with defects (space charges, etc.) [119].

Table 2.1 Grain size effects on barium titanate ($BaTiO_3$) system (decreasing grain size) [119].

Authors	Year	Grain size (μm)	K @ 25 °C	K_{max}	T_c	Model	Comments
Kniepkamp and Heywang	1954	~ 1	3500	-	-	-	
Avan'eva et al.	1960	~ 1	6000	-	-	-	- Chemically pure $BaTiO_3$
Brandmayr	1965	0.4 ~ 3	6000 @ 1 μm	-	-	-	- The K decrese below 1 μm grain size
Buessem et al.	1966	1 ~ 10	6000 @ 1 μm	-	-	Interal Stress Model	- Devonshire theory - Single domain state at 1 μm grain size
Samara	1969 1971	-	-	X-tal ceramics	-	Hydrostatic Pressure effects	- Different behavior between crystal and ceramics
Martirena and Burfoot	1975	-	-	-	-	A Gaussian distribution model	- No agreements with experimental results.
Kinoshita and Yamaji	1976	1.1 ~ 53	5000 @ 1.1 μm		-	Internal stress model	- No observation of the variation of T_c
Arlt et al.	1980 1985	0.7 ~ 50	5500 @ 0.7 μm			Domain density model	- Domain size decreases with decreasing grain size. Ratio $d \sim (\text{grain size})^{1/2}$
Dudkevih	1981	-	-	-	-	Soft mode model	- Not applicable for the grain size (> 1μm)
Bell et al.	1985	-	6000 @ 1 μm			Internal stress model	- Devonshire theory - A large change of T_c is not seen in experimental
Shaikh et al.	1989	0.3 ~ 10	~ 4000 @ 0.4 μm			Grain boundary model	- Only for grain sizes (≤0.4 μm)

2.3 Fabrication of the barium zirconate titanate powders

The Barium zirconate titanate ($Ba(Zr_xTi_{1-x})O_3$; BZT) is a complex perovskite which has Zr^{4+} and Ti^{4+} occupy in B-site. The BZT, which has tunable structural and electrical properties of specific applications, has received much attention. Characteristics of the ferroelectric phase transition of $Ba(Zr_xTi_{1-x})O_3$ ceramics depend strongly on Zr content from normal ferroelectric to relaxor ferroelectric behavior [14]. The Zr^{4+} is an effective substituent in $Ba(Zr_xTi_{1-x})O_3$, which decreases and shifts the Curie temperature to below room temperature [121]. Furthermore, the Zr^{4+} ion (0.86Å) has a larger ionic size than Ti^{4+} (0.745Å) that expands the lattice and is more stable chemically. Therefore, the substitution of Ti with Zr would depress the conduction by electron hopping between Ti^{4+} and Ti^{3+} [122-124].

The conventional solid state method is a traditional way of preparing $Ba(Zr_xTi_{1-x})O_3$ ceramics. In 2005, J. Bera *et al.* [14] have used solid state reaction method for formation the $Ba(Zr_xTi_{1-x})O_3$ solid solution from $BaCO_3$, ZrO_2 and TiO_2. They reported that formation mechanism of the $Ba(Zr_xTi_{1-x})O_3$ solid solution can be explained by multistep reactions. At a temperature lower than 1,300°C, the raw materials which are $BaCO_3$, ZrO_2 and TiO_2, did not form $Ba(Zr_xTi_{1-x})O_3$ solid solution directly. Because the formation of Ba(ZrxTi1-x)O3 require energy (133 kcal/mol) higher than BaTiO3 (34.3 kcal/mol) and BaZrO3 (48.4 kcal/mol). In the initial stage, the temperature ranging from 700 to 800 °C displayed the formed separately of the raw materials. Subsequently, a single perovskite phase of $Ba(Zr_xTi_{1-x})O_3$ was form by the diffusion of $BaTiO_3$ into the $BaZrO_3$ at a temperature as high as 1,600 °C. (as shown in Figure 2.9).

In order to obtain perovskite $Ba(Zr_xTi_{1-x})O_3$ nanoparticles with high quality. Many new wet-chemical synthesizing methods which have been developed, such as sol–gel method [19, 20], aqueous co-precipitation method [21], hydrothermal method [22, 23], combustion method [24] and direct synthesis from solution (DSS) [25], to replace conventional solid state reaction method. The synthesis of the nanosized of $Ba(Zr_xTi_{1-x})O_3$ particles via the wet-chemical methods make the developing new electronic nanodevices from $Ba(Zr_xTi_{1-x})O_3$ system very attractive [24, 125].

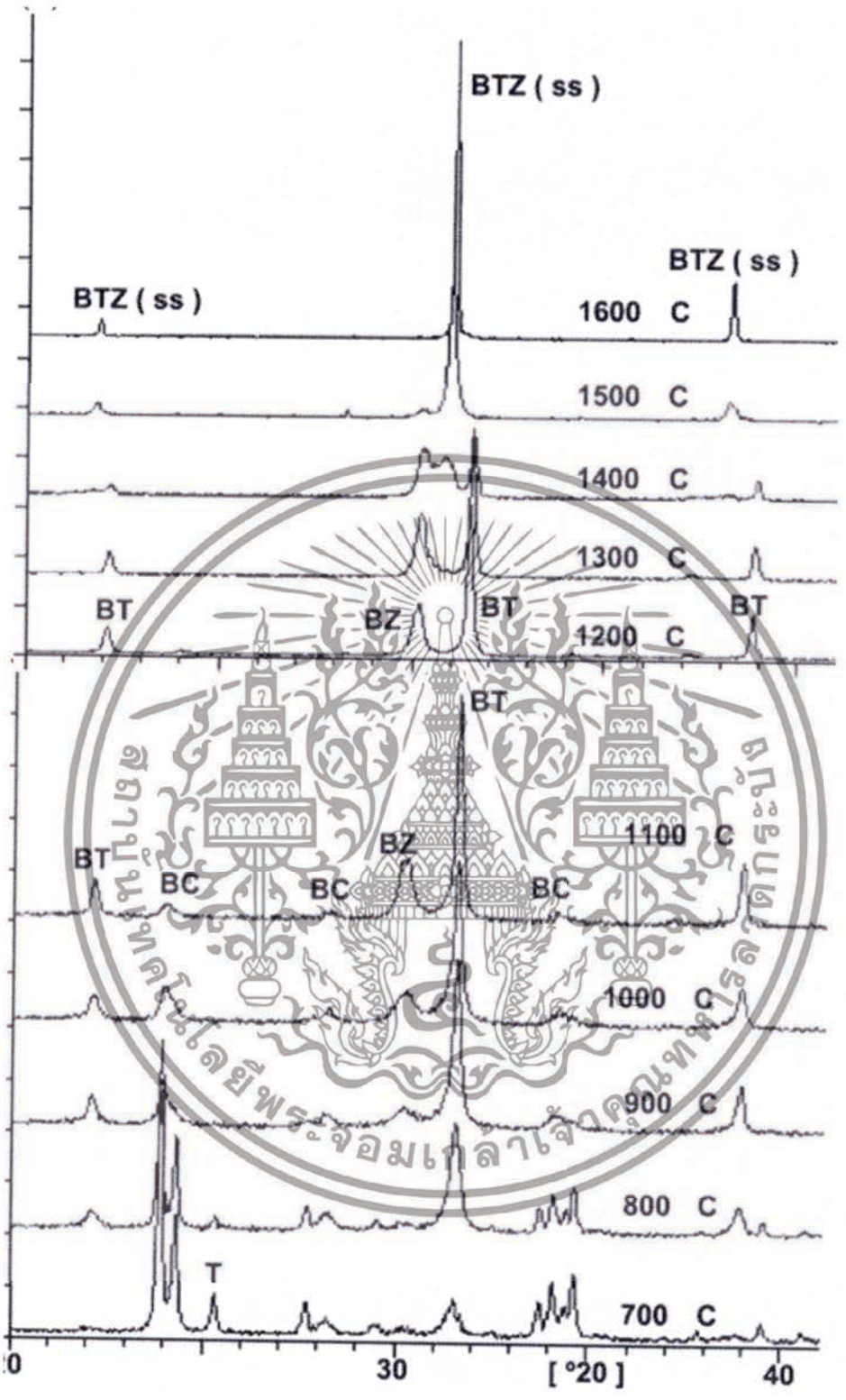

Figure 2.9 XRD pattern of the $BaTiO_3$- $BaZrO_3$ powders [14].

In 2011, P. Julphunthong *et al.* [24] have used the combustion technique by usage urea $(NH_2)_2CO$ as a fuel to reduce the reaction temperature for synthesis barium zirconate titanate ($Ba(Zr_xTi_{1-x})O_3$) powder. Unfortunately, after the combustion process needed to be calcined the powder at 1,000°C for 5 h in order to obtain a pure perovskite structure (as shown in Figure 2.10 and 2.11). Generally, after the calcination process always observed submicron sizes with irregular morphology of the powder [18, 120]. It is really difficult to get the nanoparticles with uniform size under the calcination process [18, 120]. So the calcination process should be undesirable step during the fabrication process of nanopowder.

Figure 2.10 XRD pattern of the $Ba(Zr_xTi_{1-x})O_3$ powders calcined at various temperatures for 2 h: (ω) $BaCaO_3$; (ρ) ZrO_2; (β) Ba_2TiO_4 [24].

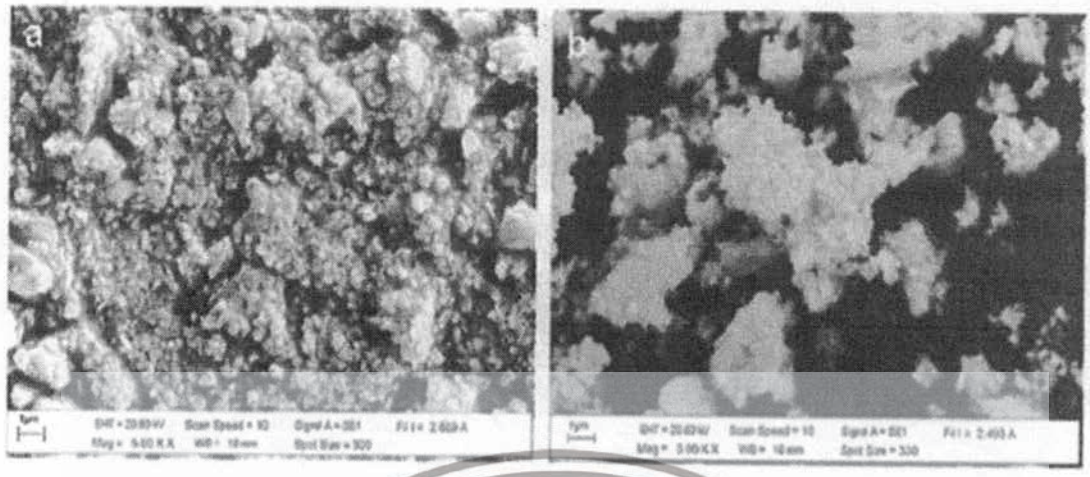

Figure 2.11 SEM image of the $Ba(Zr_xTi_{1-x})O_3$ powders (a) calcined at 700°C for 2 h (b) calcined at 1000°C for 2 h [24].

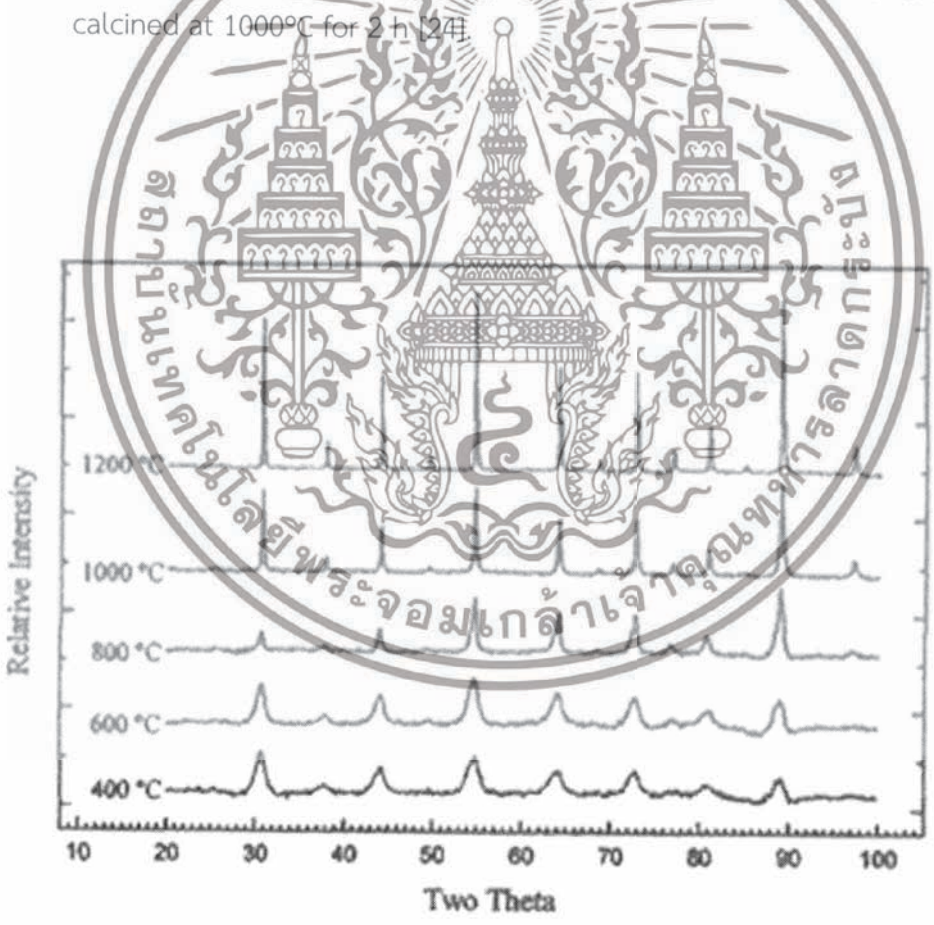

Figure 2.12 XRD pattern of the $BaZr_{0.5}Ti_{0.5}O_3$ powders calcined at various temperatures [19].

M. Veitu et al. [19] has proposed an alkoxide sol–gel synthesis method for synthesis the homogeneous $BaZr_{0.5}Ti_{0.5}O_3$ nanopowders. By using [Ba(O Pr^i_2)] and $[TiZr(OPr^i)_8.Pr^iOH]_2$ as a precursor synthesized the hetero-trimetallic Ba-Ti-Zr framework under CO_2-free argon (Ar) or nitrogen atmosphere. The most advantageous characteristics of this method are the outstanding control of the composition of resulting powders and high purity. However, in order to obtain the crystallize $Ba(Zr_xTi_{1-x})O_3$ needs to be calcined the hydrolyzed dried gel at temperatures above 400°C (Figure 2.12). In addition, morphology of the BZT system revealed well defined crystallites in the range between 10-20 nm as shown in Figure 2.13.

Figure 2.13 TEM image of the $BaZr_{0.5}Ti_{0.5}O_3$ powders calcined at 800°C [19].

J. Q. Qi *et al.* [126] developed a new method, to prepare $Ba(Zr_xTi_{1-x})O_3$ nanoscaled powders near room temperature under ambient pressure, which is called direct synthesis from solution (DSS). The powders of $Ba(Zr_xTi_{1-x})O_3$ nanocrystalline can be obtained by mixing between a base solution of barium hydroxide which dissolving into warm water, with hot base solution of tetrabutyltitanate and isopropanal solution of zirconium isopropoxide–isopropanol. The particle size of the $Ba(Zr_xTi_{1-x})O_3$ nanoparticles fell within the range of 25 to 120 nm from this synthesis method. (as shown in Figure 2.14)

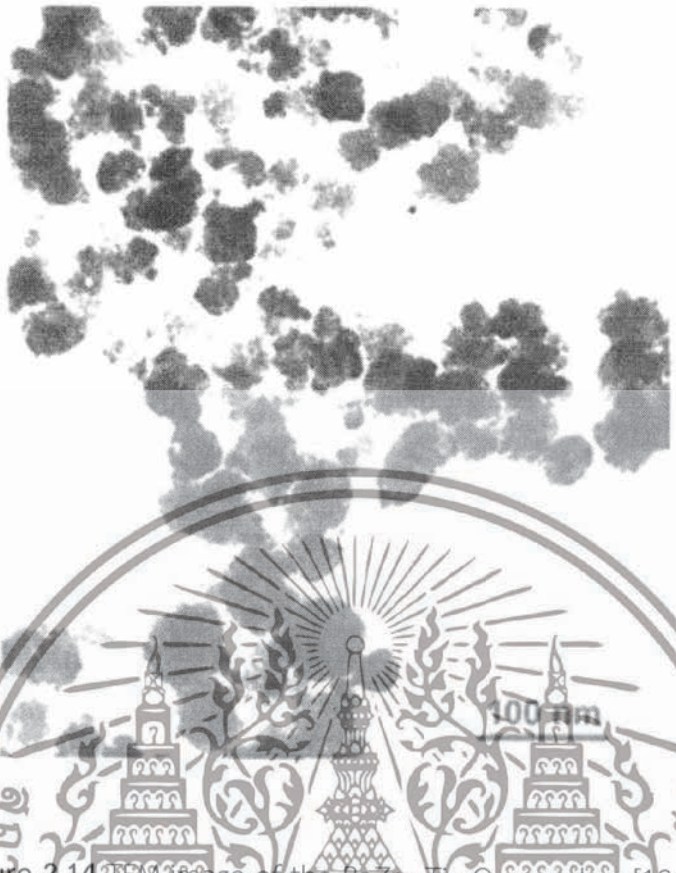

Figure 2.14 TEM image of the $BaZr_{0.5}Ti_{0.5}O_3$ powders [126].

Recently, S. B. Reddy et al. [21] have used the aqueous co-precipitation method for synthesis the single phase nanocrystalline powder of $Ba(Zr_xTi_{1-x})O_3$ successfully at a temperature < 100°C. At initial stage, the chloride solution of Ba, Ti and Zr ions were mixed together. Then, dripped slowly the mixture into a heated strong base solution with pH>12.0 (as shown in Figure 2.15 and 2.16). The nanocrystalline $Ba(Zr_xTi_{1-x})O_3$ was obtained successfully with a strongly based concentration at a temperature of about 80°C. The product powders displayed an average particle size of 30 nm. The synthesis temperature and precipitant concentration as a parameter play an important role for increasing product purity [21]. Nevertheless, the particles obtained by this method have a mixture of shapes such as cubes, elliptical, acicular and spherical with truncated edges [21]. The shape and particle size are not being control. The widerange particle size distribution and difference shape morphology have been the important problem to create the abnormal grain growth in the sintering process [18].

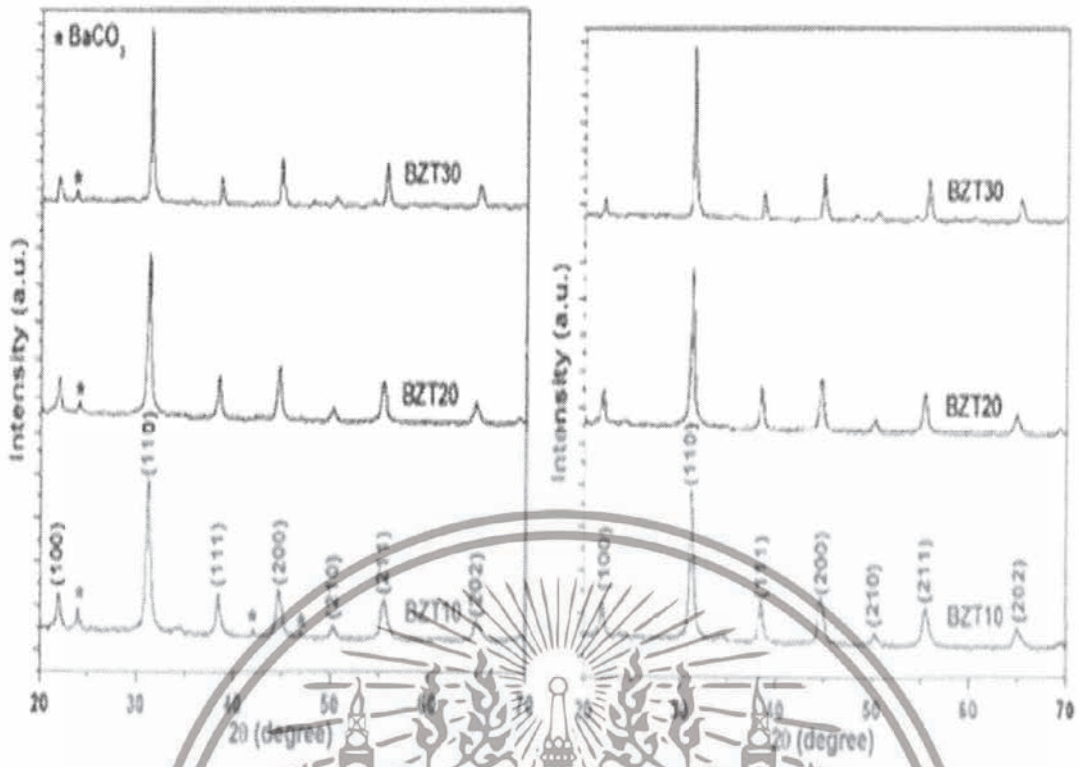

Figure 2.15 XRD pattern of the $Ba(Zr_xTi_{1-x})O_3$ powders (a) 10 M NaOH, (b) 15 M NaOH [21].

Figure 2.16 TEM image of the $Ba(Zr_xTi_{1-x})O_3$ powders prepared using 15 M NaOH [21].

2.4 Sonochemical method

In order to obtain the spherical morphology with a narrow particle size distribution of $Ba(Zr_xTi_{1-x})O_3$ nanoparticles, the wet-chemical methods were developed so far for eliminate abnormal grain growth during the sintering process [18, 19, 21, 126-128]. A new technique that fulfills the requirements for synthesizing extremely fine particles with a narrow size distribution and spherical morphology seems to be the sonochemical synthesis at ambient temperature [26, 27]. The sonochemical method uses ultrasonic irradiation to accelerate or generate the chemical reaction for create an acoustic cavitation phenomenon. Acoustic cavitation phenomenon, is created from the ultrasonic irradiation in a liquid, is the formation, growth, and implosive collapse of bubbles. In this phenomenon generates a localized hot spot with an extremely high pressure of ~20 MPa, a temperature of approximately 5,000 K and a very high heating-cooling rate of ~ 10^{10} $K.s^{-1}$ [26, 32], as shown in Figure 2.17 and 2.18. These ephemeral, localized hot spots can drive many chemical reactions, such as decomposition, dissolution, oxidation, reduction, and promotion of polymerization [26, 32].

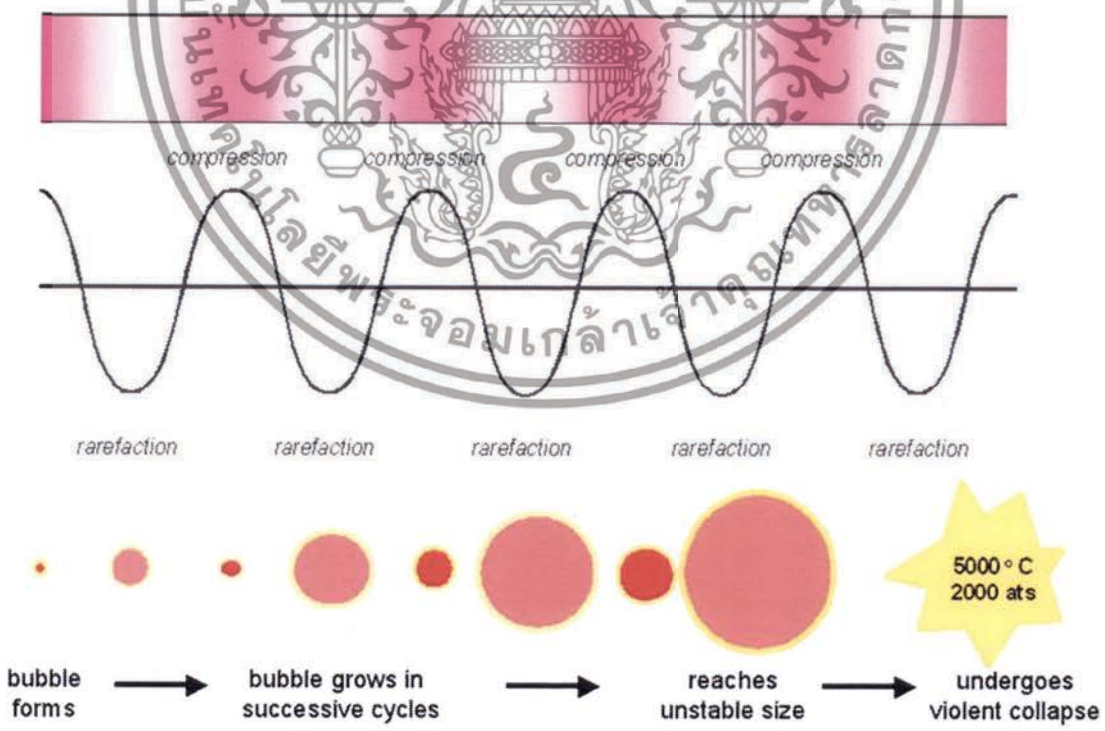

Figure 2.17 Acoustic cavitation phenomenon from ultrasonic irradiation [129].

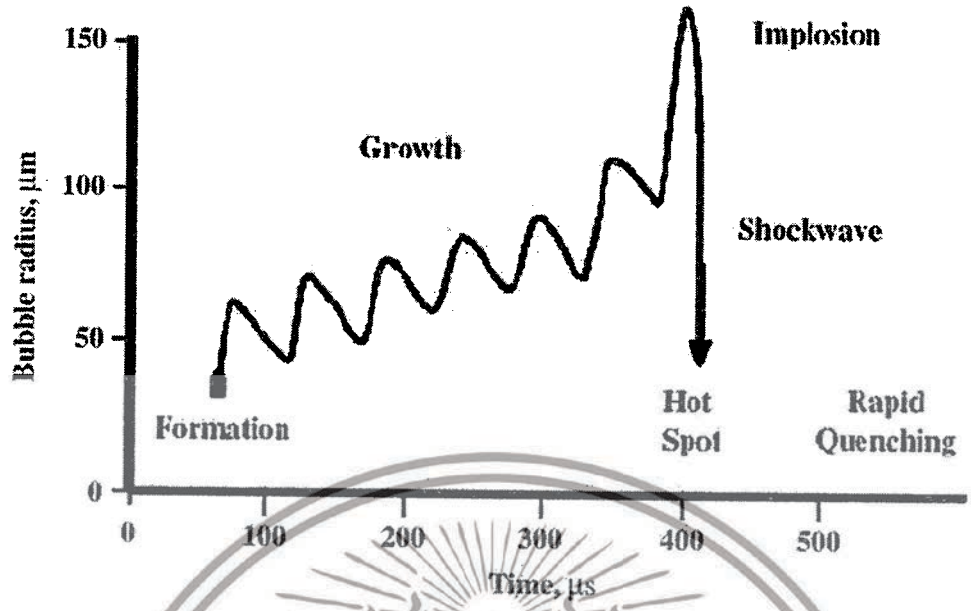

Figure 2.18 To generate a localized hot spot which is formation, growth, and implosive collapse of bubbles in a liquid [129].

By using these transient extreme conditions, various kinds of novel materials, organic, inorganic and with unusual properties such as simple metal oxides [35, 36], core/shell nanocomposites [37, 38], metals [39, 40], carbides [41], nitrides [35], sulfides [35, 42] and precious metals [43, 44] were synthesized successfully. Until now, studies have reported the multicationic oxides based on a perovskite structure (ABO_3) which synthesized by the sonochemical method quite a few, and there is no report to the best of authors' knowledge on the direct sonochemical synthesizing of ($BaZr_xTi_{1-x}O_3$) powders.

Many researchers pay attention to sonochemical method and have to take this method to the synthesis nanoparticles. T. Akita et al [131] have succeeded in preparing the gold - Palladium (Au-Pd) nanoparticles by the sonochemical method at 20 minutes of the reaction time. The TEM images (as shown in Figure 2.19) showed that the particles have a spherical in shape with a narrow size distribution. The average particle size is approximately 13 ± 3.2 nm.

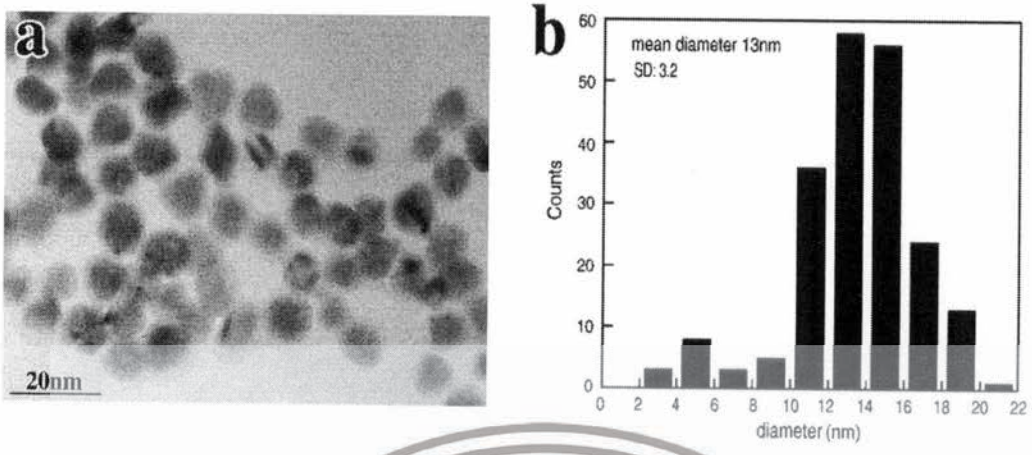

Figure 2.19 (a) SEM images and (b) Size distribution pattern of Au-Pd nanoparticles [131].

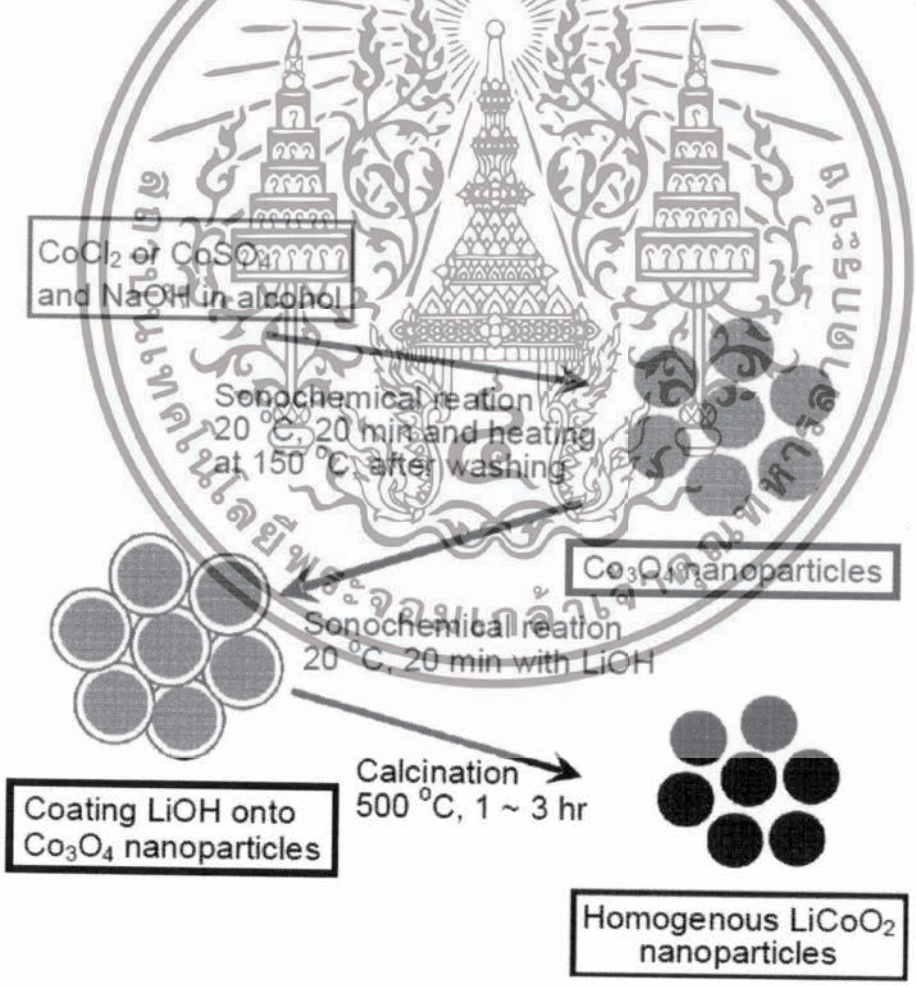

Figure 2.20 The steps in the synthesis of lithium cobalt dioxide ($LiCoO_2$) nanoparticles [132].

J.P. Park et al [132] synthesized lithium cobalt dioxide ($LiCoO_2$) nanoparticles, which is commonly used as cathod material in a rechargeable lithium batteries, successfully by the sonochemical method. The steps in the synthesis, as shown in Figure 2.20, the first step will be preparation of cobalt oxide (Co_3O_4) particles in the nanometer scale, as shown in Figure 2.21 (b). The substrate is prepared from sodium hydroxide (NaOH) and cobalt chloride ($CoCl_2$) or cobalt sulfate ($CoSO_4$) by the sonochemical process at 20 kHz 220W for 20 minutes. The second stage will take the lithium hydroxide (LiOH) coated onto cobalt oxide nanoparticles (Co_3O_4) by the same method above. The XRD results showed phase of lithium hydroxide (LiOH), which is a precursor to remain, as shown in Figure 2.21 (a). Then, the product powders was Calcined at 500°C for 1-3 hours. The XRD results showed that the phase purity of the lithium cobalt dioxide ($LiCoO_2$) occurs at 500 °C for 3 hours (as shown in Figure 2.22 (a)) and a particle size of 10-30 nm in diameter, as shown in Figure 2.22 (b).

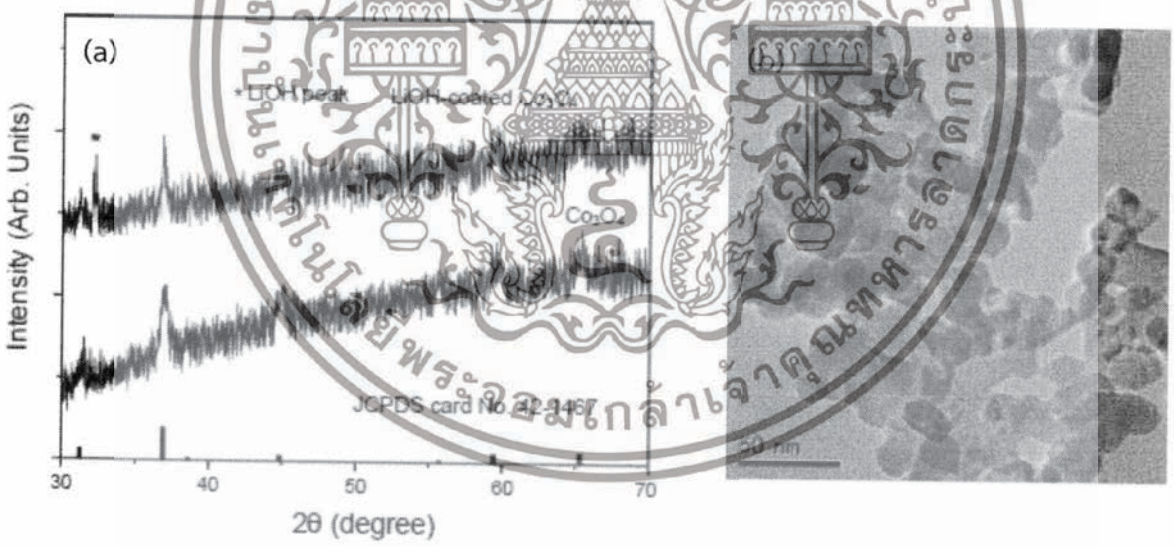

Figure 2.21 (a) XRD results and (b) TEM images of lithium cobalt dioxide ($LiCoO_2$) nanoparticles [132].

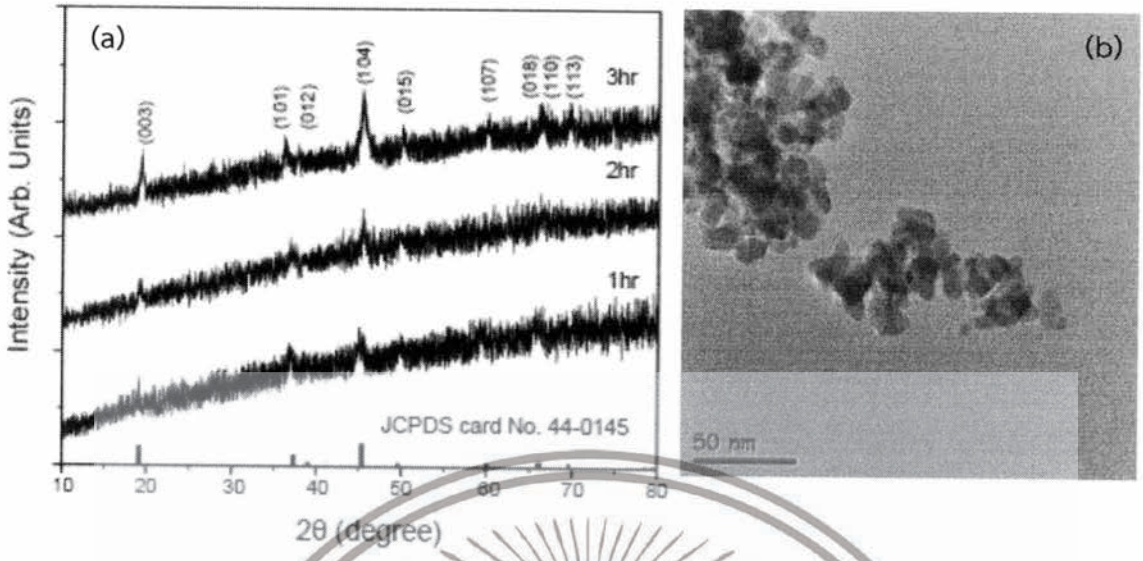

Figure 2.22 (a) XRD results and (b) TEM images of lithium cobalt dioxide ($LiCoO_2$) nanoparticles with calcined at 500 °C for 3 hours [132].

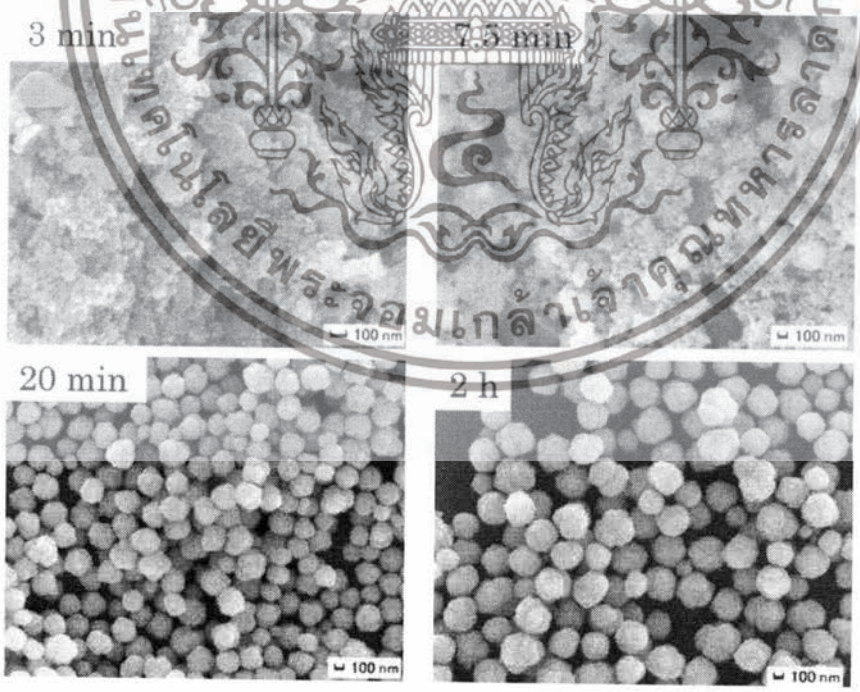

Figure 2.23 SEM images of $BaTiO_3$ nanoparticles at the difference reaction time [133].

In 2010, F. Dang et al [133] were synthesized barium titanate ($BaTiO_3$) successfully by sonochemical method. Using barium chloride ($BaCl_2$) and titanium tetrachloride chloride ($TiCl_4$) as a substrate. The results of the study in the reaction time with 3, 7.5, 20 and 120 minutes as shown in Figure 2.23. At 3 minutes, the barium titanate particles begin integration of small spherical particles occurs. After that increase the reaction time to two hours, the particles are spherical shape with an average particle size of approximately 200 nm and has a narrow size distribution, as shown in Figure 2.24.

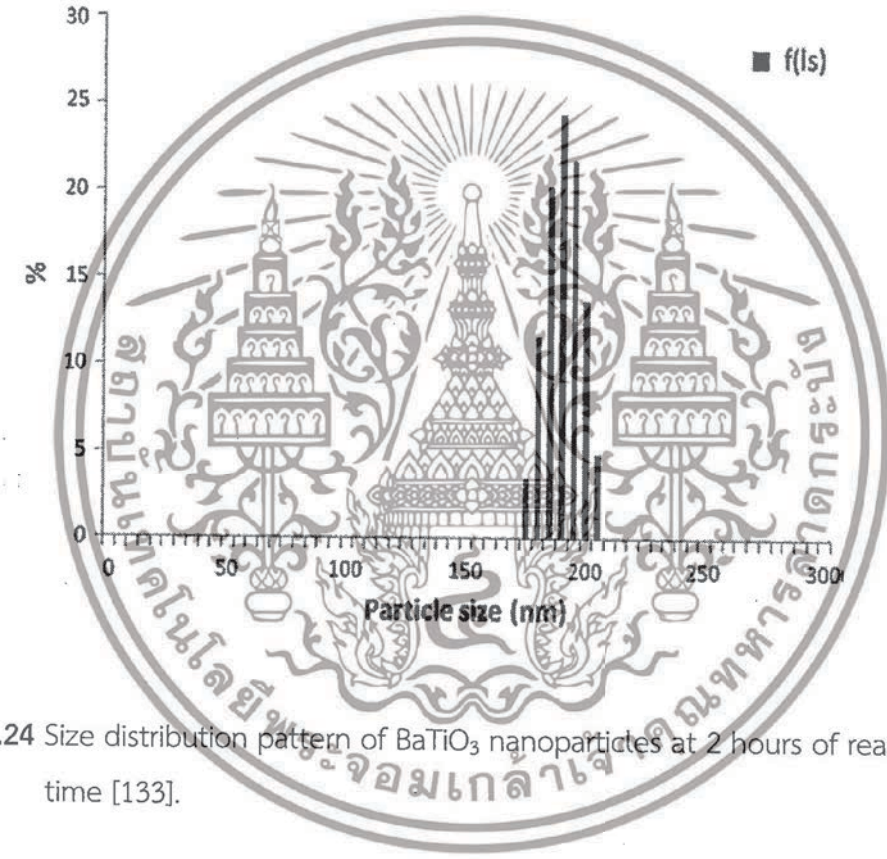

Figure 2.24 Size distribution pattern of $BaTiO_3$ nanoparticles at 2 hours of reaction time [133].

CHAPTER 3

EXPERIMENTAL PROCEDURES

In this chapter presents the details of the experimental procedures adopted for the synthesis and characterization of the complex perovskite barium zirconium titanate ($Ba(Zr_xTi_{1-x})O_3$; BZT) nanopowders. Firstly, the complex perovskite barium zirconium titanate nanopowders were synthesized by the sonochemical method via varying the synthesis parameters, including the concentration of precipitating agent, synthesis atmosphere, concentration of the starting solution, sonication time, Zr/Ti molar ratio and the power of ultrasound irradiation. Then, the process to investigate crystal structure, morphology, particle size and phase formation of barium zirconium titanate nanopowders are described.

3.1 The chemical materials

The chemical purity and supplier of starting materials are listed in Table 3.1.

Table 3.1 Specifications of the starting material powders used in this study.

Materials	Chemical formula	Purity (%)	Manufacturer
Barium chloride dihydrate	$BaCl_2.2H2O$	≥99.80	Sigma-Aldrich Company Inc., USA
Titanium chloride	TiCl4	≥99.90	Wako Pure Chemical Industries, Ltd., Japan
Zirconium oxychloride octahydrate	$ZrOCl_2.8H2O$	≥99.50	Inframat Advanced Materials, USA
Sodium hydroxide	NaOH	97.70	Carlo Erba Reagenti SpA Company, France
Formic Acid	HCOOH	85.00	Carlo Erba Reagenti SpA Company, France
Argon gas	Ar	>99.998	Praxair Company, Ltd., Thailand

3.2 Laboratory equipment and instruments

3.2.1 Beaker (50, 100, 250, 500 and 1000 ml)
3.2.2 Pipette (1, 2, 5 and 10 ml)
3.2.3 Cylinder (25, 50 and 100 ml)
3.2.3 Volumetric Flask (100, 250, 500 and 1000 ml)
3.2.4 Sonication Vessel 250 ml
3.2.5 Weighing Papers
3.2.6 Watch Glass
3.2.7 Dropper Tube
3.2.8 Stirring Rod
3.2.9 Centrifuge Tube
3.2.10 Pestle and Mortar
3.2.11 Wash Bottle
3.2.12 Magnetic Bar
3.2.13 Stainless Spatula
3.2.14 Spoon
3.2.15 Forceps
3.2.16 Aluminium Foil
3.2.17 pH Indicator Paper
3.2.18 Copper Conductive Tapes
3.2.19 Laboratory Balance (Sartorius Model BSA series, USA)
3.2.20 Sonometer (Sonics Model VCX-750, USA)
3.2.21 Magnetic stirring hotplate (Heidolph Model MR Hei-Standard, Germany)
3.2.22 Thermal Oven (Memmert Model Schutzart IP 20, Germany)
3.2.23 Centrifuge (Labnet Model Spectrafuge 6C, USA)
3.2.24 Ultrasonic Cleaner with Heat (ST144H 3/4 Gal, USA)
3.2.25 X-ray diffractometer (Panalytical Model X'Part^3, The Netherlands)
3.2.26 Field emission scanning electron microscope (JEOL Model JSM-6335F, Japan)
3.2.27 Fourier transform infrared spectrometer (Perkin Elmer Model Spectrum GX, USA)
3.2.28 Raman spectrometer (Thermo scientific Model DXR Raman Microscope, USA)

3.3 Solution preparation

Figure 3.1 Schematic flow chart of Ti^{4+} solution preparation.

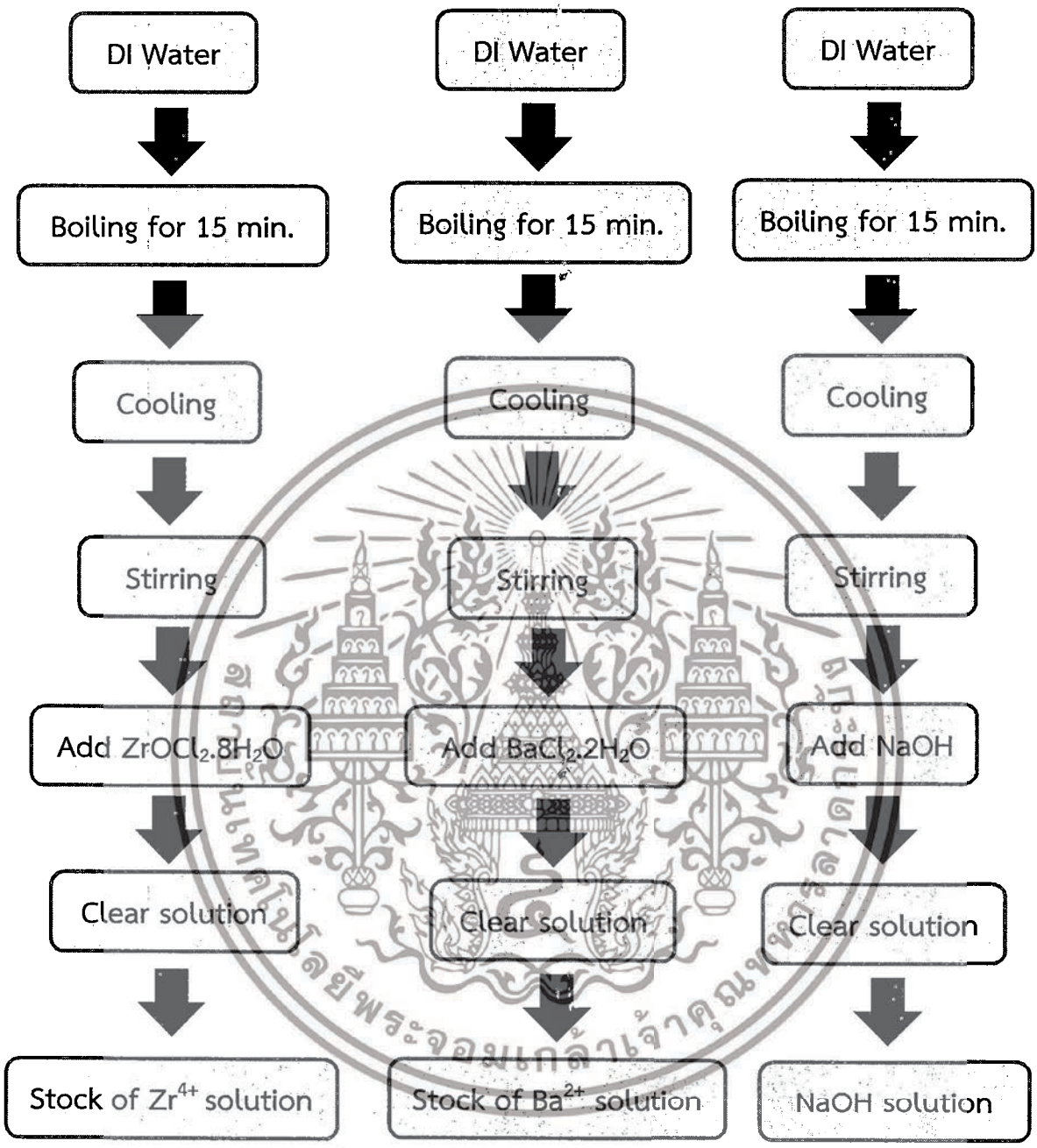

Figure 3.2 Schematic flow chart of solution preparation.

In this research, all the reagents used in experiments are analytical reagent grade (AR grade) and high purity. The barium chloride dihydrate ($BaCl_2 \cdot 2H2O$, ≥99.8% Sigma-Aldrich), zirconium oxychloride octahydrate ($ZrOCl_2 \cdot 8H2O$, ≥99.5% Inframat Advance material) and titanium tetrachloride ($TiCl_4$, ≥99.9% Wako) were used as the

rawmaterials. Sodium hydroxide (Carlo Erba 97.7%) was used as the precipitating agent. The deionized water used in this experiment should be boiled previously at 100°C for 15 minutes to remove the CO_2 dissolved in it. In order to obtain the stock of Ti^{4+} solution, $TiCl_4$ was dripped very slowly into deionized water at a temperature below than 5°C and stirred vigorously until the solution was clear. Then, the separate stoichiometric amounts of $BaCl_2 \cdot 2H2O$ and $ZrOCl_2 \cdot 8H2O$ were dissolved typically in deionized water in order to obtain the barium (Ba^{2+}) and zirconium (Zr^{4+}) solution, respectively. These stocks of precursor solution were prepared freshly for each part of experiments. In order to acquire the precipitating agent of sodium hydroxide (NaOH) solution, NaOH was dissolved into deionized water. The solution preparation procedures of all solution in this experiment show in Figure 3.1 and Figure 3.2.

3.4 Synthesis of a complex perovskite barium zirconium titanate ($Ba(Zr_xTi_{1-x})O_3$; BZT) nanopowders.

The complex perovskite barium zirconatetitanate ($Ba(Zr_xTi_{1-x})O_3$; BZT) powder products, with the composition (x) = 0.00, 0.05, 0.20, 0.04 and 0.60, were synthesized by the sonochemical method without the calcination process, which was in accordance with the reaction (3.1):

$$BaCl_2 \cdot 2H_2O_{(aq)} + (1-x)TiCl_{4(aq)} + xZrOCl_2 \cdot 8H_2O_{(aq)} + (6-2x)NaOH_{(aq)} \longrightarrow$$
$$Ba(Zr_xTi_{1-x})O_{3(s)} + (6-2x)NaCl_{(aq)} + (13-x)H_2O_{(aq)} \qquad (3.1)$$

In this study, the synthesis process used was divided into five sections according to the synthesis parameters that include the concentration of precipitating agent, synthesis atmosphere, concentration of the starting solution, sonication time, Zr/Ti molar ratio and the power of ultrasound irradiation.

3.4.1 The concentration of precipitating agent

This section study the effect of the concentration of precipitating agent on the $Ba(Zr_xTi_{1-x})O_3$ (x = 0.0) phase formation. The 1 mol.L^{-1} of barium and titanium solution were used as the stock of precursor solution in this section. The mixture targeted the ratio of Ti and Ba ion in the solution constantly at 1:1. Firstly, the appropriate proportions of titanium and barium solution was pipetted from the stock solution, in order to obtain a homogeneous mixed solution by mixing the stock solution together with continuous stirring. Subsequently, setting up the sonication equipment for the sonochemical process. The sodium hydroxide (NaOH) solution, use as the precipitating agent, was loaded into a sonication vessel after setting up the equipment. In order to study the effect of the concentration of NaOH solution by using the concentration varied from 5 to 20 mol.L^{-1}. After that, the sonication vessel which contained the NaOH solution, was added the mixed precursor solution with drop by drop at a rate of about 25 ml.min^{-1}. Then, ultrasonic irradiation for 30 minutes by pulse ultrasonication (Sonics VCX-750, 20 kHz, 750 W) in the 2 s mode; and a pause in 1 s mode was performed in this experiment. In order to obtain better quality of nanoparticles. Using the pulse ultrasonic mode for synthesis the powder gives a narrower particle size distribution than synthesized powder in continuous ultrasonic mode, has been reported [44]. This could be a scene from an uneven distribution of ultrasonic energy in the ultrasonic vessel [44]. The white precipitation was formed instantaneously during the process of adding mixed solution. The precipitate, which contained in the sonication vessel when the irradiation time was over, was cooled to room temperature by immersing in tap water. Then, the centrifugal filtration used to filter out the recovered precipitate, and washed with 0.1 mol.L^{-1} formic acid (HCOOH) to remove any possible carbonate contamination (CO_3^{2-}) and deionized water until the pH value reduced to 7. The 0.1 mol.L^{-1} of $AgNO_3$ solution was used to check the remained chloride ion by the supernatant with no white sediment remained, which confirmed that the chloride ion was not retained. Eventually in order to obtain the powder products, the washed precipitates were dried in an oven overnight with the temperature about 80°C. The process of the synthesis in this section was shown in Figure 3.3

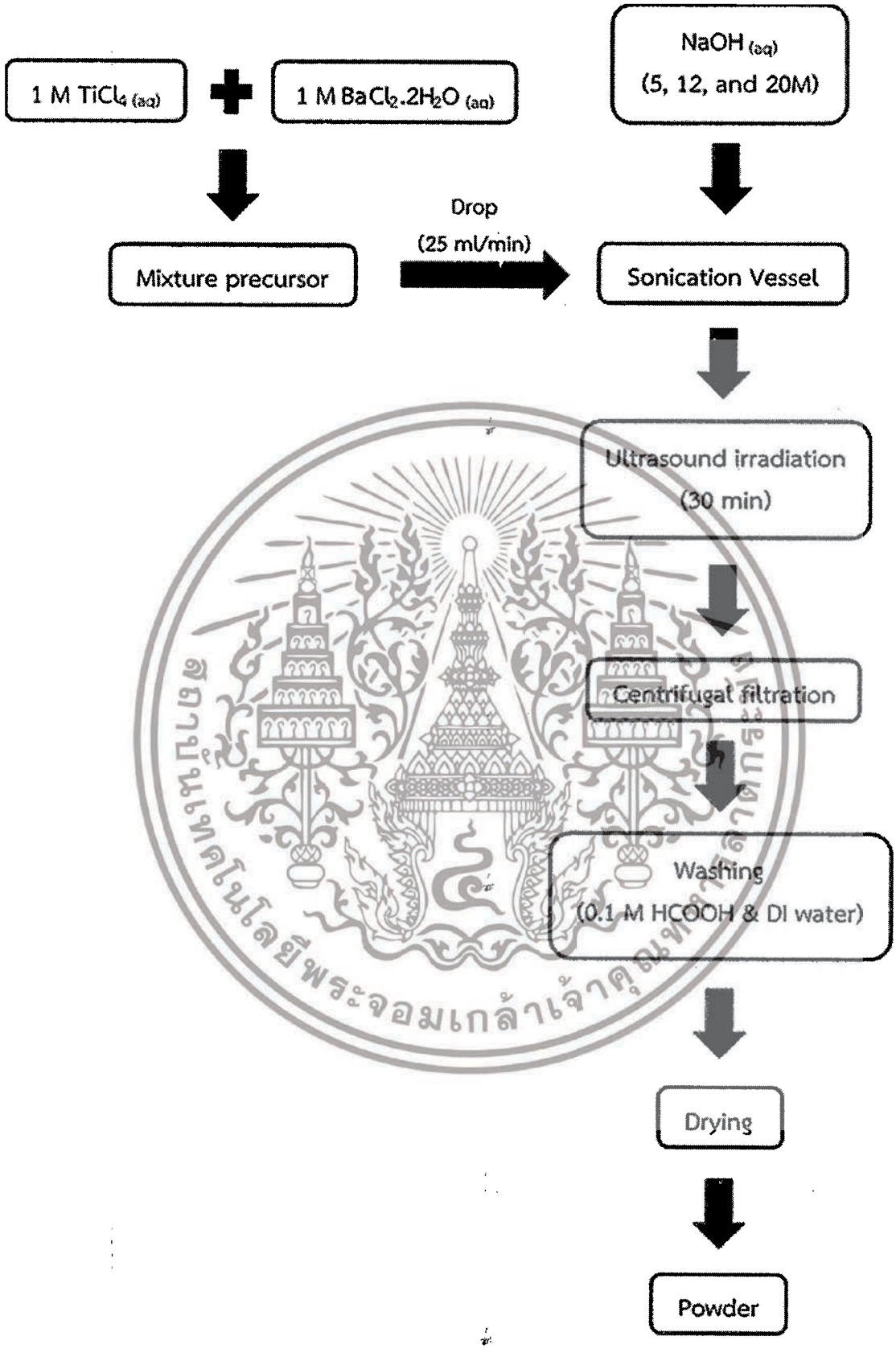

Figure 3.3 Schematic flow chart of BZT powder synthesis with varies concentration of $NaOH_{(aq)}$.

3.4.2 The synthesis atmosphere

This section study the effect of the synthesis atmosphere on the $Ba(Zr_xTi_{1-x})O_3$ (x = 0.0) phase formation. The 1 mol.L^{-1} of barium and titanium solution were used as the stock of precursor solution in this section. The mixture targeted the ratio of Ti and Ba ion in the solution constantly at 1:1. Firstly, the appropriate proportions of titanium and barium solution was pipetted from the stock solution, in order to obtain a homogeneous mixed solution by mixing the stock solution together with continuous stirring. Subsequently, setting up the sonication equipment for the sonochemical process. Regarding the synthesis system, the effect of synthesis atmosphere on the phase formation was studied. The powder synthesized in a closed system with Ar gas was compared with that in open air. The 20 mol.L^{-1} of sodium hydroxide (NaOH) solution, use as the precipitating agent, was loaded into a sonication vessel after setting up the equipment. And then, the sonication vessel which contained the NaOH solution, was added the mixed precursor solution with drop by drop at a rate of about 25 ml.min^{-1}. Therefore, a high pH value reached 14 during the process. Then, ultrasonic irradiation for 30 minutes by pulse ultrasonication (Sonics VCX-750, 20 kHz, 750 W) in the 2 s mode; and a pause in 1 s mode was performed in this experiment, In order to obtain better quality of nanoparticles. Using the pulse ultrasonic mode for synthesis the powder gives a narrower particle size distribution than synthesized powder in continuous ultrasonic mode, has been reported [44]. This could be a scene from an uneven distribution of ultrasonic energy in the ultrasonic vessel [44]. The white precipitation was formed instantaneously during the process of adding mixed solution. The precipitate, which contained in the sonication vessel when the irradiation time was over, was cooled to room temperature by immersing in tap water. Then, the centrifugal filtration used to filter out the recovered precipitate, and washed with 0.1 mol.L^{-1} formic acid (HCOOH) to remove any possible carbonate contamination (CO_3^{2-}) and deionized water until the pH value reduced to 7. The 0.1 mol.L^{-1} of $AgNO_3$ solution was used to check the remained chloride ion by the supernatant with no white sediment remained, which confirmed that the chloride ion was not retained. Eventually in order to obtain the powder products, the washed precipitates were dried in an oven overnight with the temperature about 80°C. The process of the synthesis in this section was shown in Figure 3.4

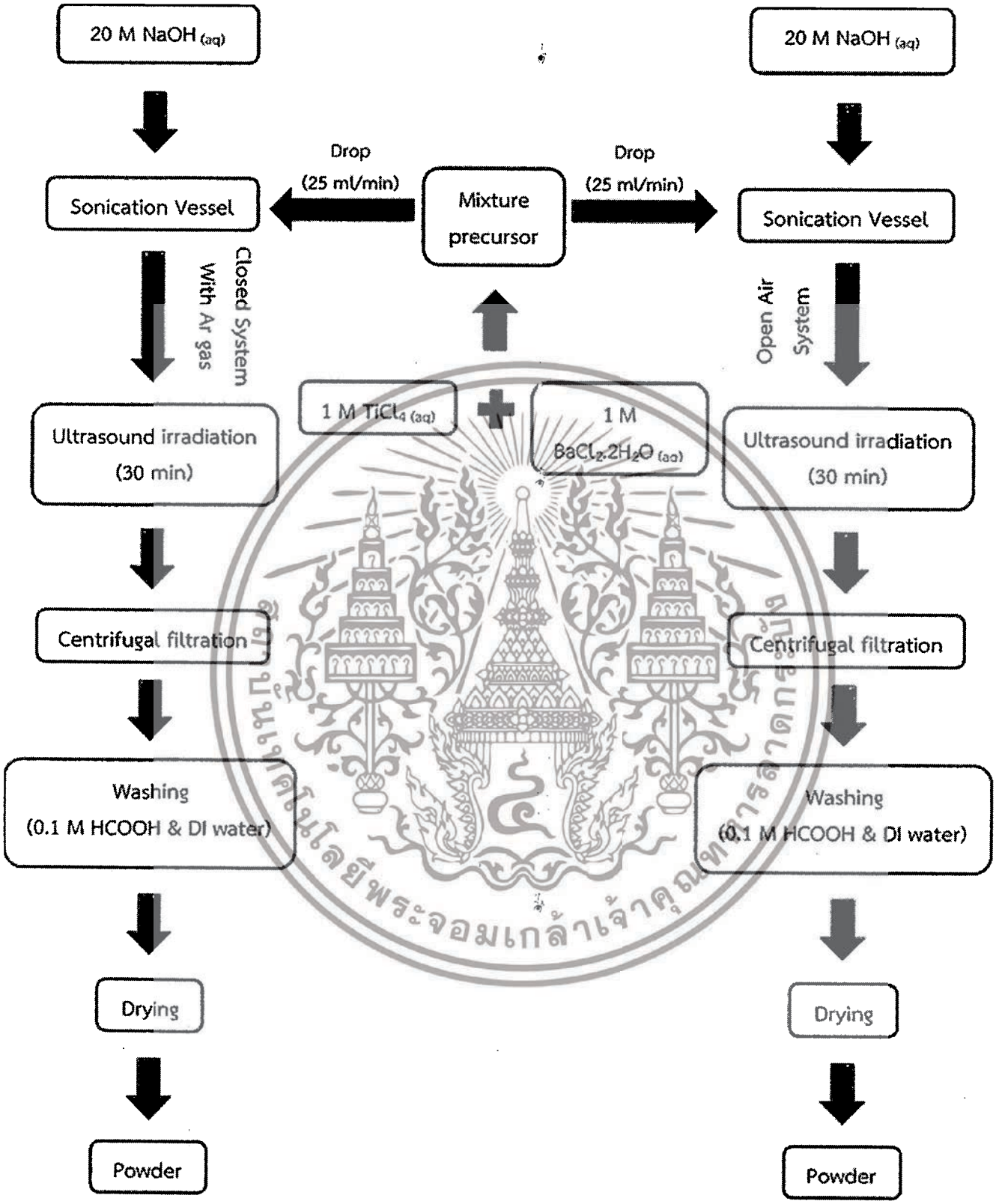

Figure 3.4 Schematic flow chart of BZT powder synthesis with study the effect of synthesis atmosphere.

3.4.3 The concentration of the starting solution

This section study the effect of the concentration of the starting solution on the $Ba(Zr_xTi_{1-x})O_3$ (x = 0.0) phase formation. Firstly, the appropriate proportions of titanium and barium solution was pipetted from the stock solution, in order to obtain a homogeneous mixed solution by mixing the stock solution together with continuous stirring. In order to study the effect of Ti and Ba ion concentration on the perovskite phase formation, The concentrations of titanium and barium solution were varied from 0.01 $mol{\cdot}L^{-1}$ to 1.5 $mol{\cdot}L^{-1}$. The mixture targeted the ratio of Ti and Ba ion in the solution constantly at 1:1. Subsequently, setting up the sonication equipment for the sonochemical process in the close system with Ar gas. The 20 $mol.L^{-1}$ of sodium hydroxide (NaOH) solution, use as the precipitating agent, was loaded into a sonication vessel after setting up the equipment. And then, the sonication vessel which contained the NaOH solution, was added the mixed precursor solution with drop by drop at a rate of about 25 $ml.min^{-1}$. Therefore, a high pH value reached 14 during the process. Then, ultrasonic irradiation for 30 minutes by pulse ultrasonication (Sonics VCX-750, 20 kHz, 750 W) in the 2 s mode; and a pause in 1 s mode was performed in this experiment, in order to obtain better quality of nanoparticles. Using the pulse ultrasonic mode for synthesis the powder gives a narrower particle size distribution than synthesized powder in continuous ultrasonic mode, has been reported [44]. This could be a scene from an uneven distribution of ultrasonic energy in the ultrasonic vessel [44]. The white precipitation was formed instantaneously during the process of adding mixed solution. The precipitate, which contained in the sonication vessel when the irradiation time was over, was cooled to room temperature by immersing in tap water. Then, the centrifugal filtration used to filter out the recovered precipitate, and washed with 0.1 $mol.L^{-1}$ formic acid ($HCOOH$) to remove any possible carbonate contamination (CO_3^{2-}) and deionized water until the pH value reduced to 7. The 0.1 $mol.L^{-1}$ of $AgNO_3$ solution was used to check the remained chloride ion by the supernatant with no white sediment remained, which confirmed that the chloride ion was not retained. Eventually in order to obtain the powder products, the washed precipitates were dried in an oven overnight with the temperature about 80°C. The process of the synthesis in this section was shown in Figure 3.5

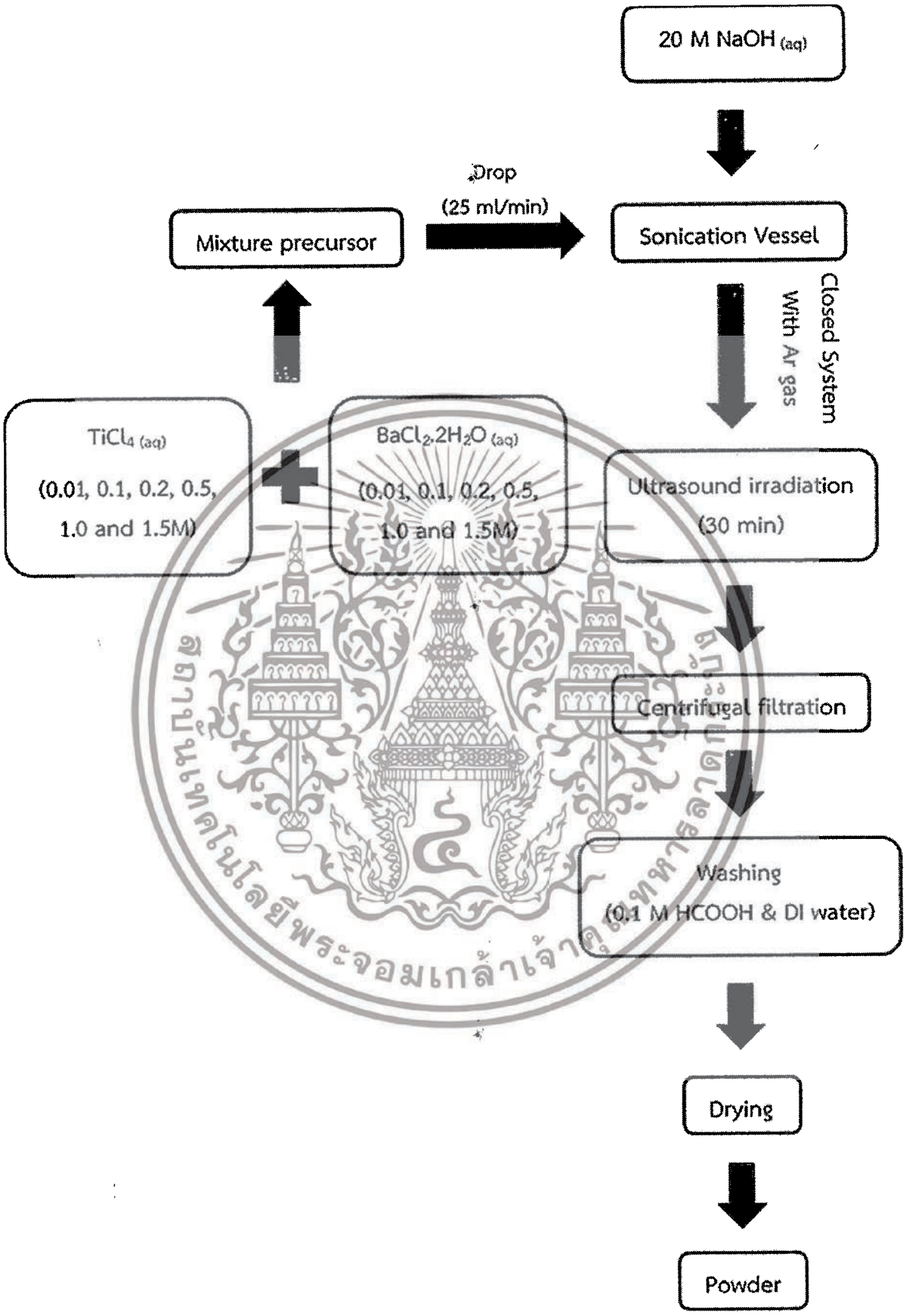

Figure 3.5 Schematic flow chart of BZT powder synthesis with varies concentration of starting solution.

3.4.4 The sonication time

This section study the effect of the synthesis atmosphere on the $Ba(Zr_xTi_{1-x})O_3$ (x = 0.0) phase formation. The 1 $mol.L^{-1}$ of barium and titanium solution were used as the stock of precursor solution in this section. The mixture targeted the ratio of Ti and Ba ion in the solution constantly at 1:1. Firstly, the appropriate proportions of titanium and barium solution was pipetted from the stock solution, in order to obtain a homogeneous mixed solution by mixing the stock solution together with continuous stirring. Subsequently, setting up the sonication equipment for the sonochemical process in the close system with Ar gas. The 20 $mol.L^{-1}$ of sodium hydroxide (NaOH) solution, use as the precipitating agent, was loaded into a sonication vessel after setting up the equipment. And then, the sonication vessel which contained the NaOH solution, was added the mixed precursor solution with drop by drop at a rate of about 25 $ml.min^{-1}$. Therefore, a high pH value reached 14 during the process. Then, ultrasonic irradiation under ambient Ar gas for a given time in this section (5, 10, 15, 30 and 60 minutes) by pulse ultrasonication (Sonics VCX-750, 20 KHz, 750 W) in the 2 s mode; and a pause in 1 s mode was performed in this experiment, In order to obtain better quality of nanoparticles. Using the pulse ultrasonic mode for synthesis the powder gives a narrower particle size distribution than synthesized powder in continuous ultrasonic mode, has been reported [44]. This could be a scene from an uneven distribution of ultrasonic energy in the ultrasonic vessel [44]. The white precipitation was formed instantaneously during the process of adding mixed solution. The precipitate, which contained in the sonication vessel when the irradiation time was over, was cooled to room temperature by immersing in tap water. Then, the centrifugal filtration used to filter out the recovered precipitate, and washed with 0.1 $mol.L^{-1}$ formic acid (HCOOH) to remove any possible carbonate contamination (CO_3^{2-}) and deionized water until the pH value reduced to 7. The 0.1 $mol.L^{-1}$ of $AgNO_3$ solution was used to check the remained chloride ion by the supernatant with no white sediment remained, which confirmed that the chloride ion was not retained. Eventually in order to obtain the powder products, the washed precipitates were dried in an oven overnight with the temperature about 80°C. The process of the synthesis in this section was shown in Figure 3.6.

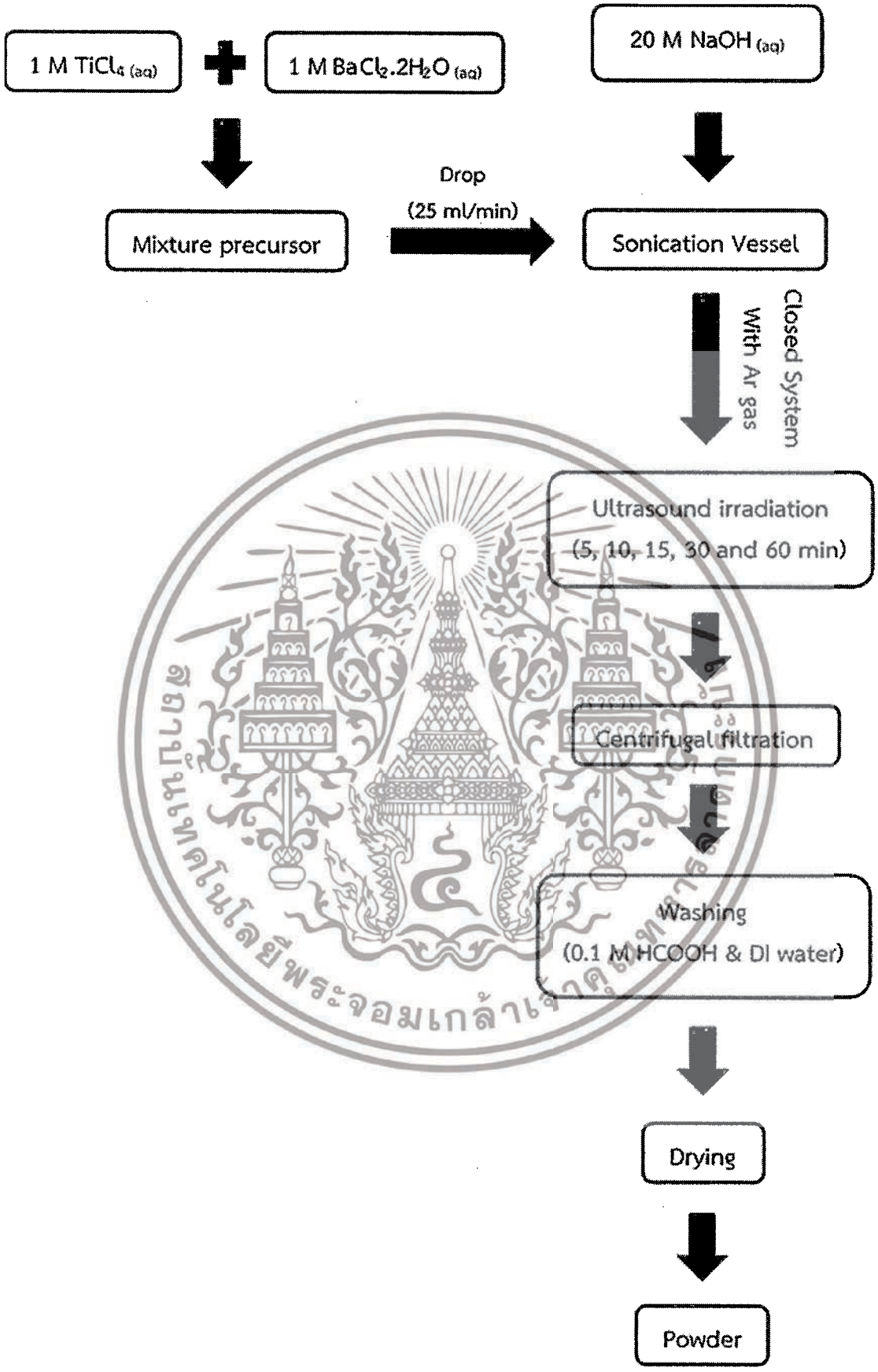

Figure 3.6 Schematic flow chart of BZT powder synthesis with varies sonication time.

3.4.5 The Zr/Ti molar ratio

This section study the effect of the Zr/Ti molar ratio on the $Ba(Zr_xTi_{1-x})O_3$ with the composition (x) = 0.00, 0.05, 0.20, 0.04 and 0.60 phase formation. The 1 $mol.L^{-1}$ of barium zirconium and titanium solution were used as the stock of precursor solution in this section. The appropriate proportions of titanium zirconium and barium solution was pipetted from the stock solution, in order to obtain a homogeneous mixed solution by mixing the stock solution together with continuous stirring. Subsequently, setting up the sonication equipment for the sonochemical process in the close system with Ar gas. The 20 $mol.L^{-1}$ of sodium hydroxide (NaOH) solution, use as the precipitating agent, was loaded into a sonication vessel after setting up the equipment. And then, the sonication vessel which contained the NaOH solution, was added the mixed precursor solution with drop by drop at a rate of about 25 $ml.min^{-1}$. Therefore, a high pH value reached 14 during the process. Then, ultrasonic irradiation under ambient Ar gas for a given time in this section (5, 10, 15, 30 and 60 minutes) by pulse ultrasonication (Sonics VCX-750, 20 kHz, 750 W) in the 2 s mode; and a pause in 1 s mode was performed in this experiment, In order to obtain better quality of nanoparticles. Using the pulse ultrasonic mode for synthesis the powder gives a narrower particle size distribution than synthesized powder in continuous ultrasonic mode, has been reported [44]. This could be a scene from an uneven distribution of ultrasonic energy in the ultrasonic vessel [44]. The white precipitation was formed instantaneously during the process of adding mixed solution. The precipitate, which contained in the sonication vessel when the irradiation time was over, was cooled to room temperature by immersing in tap water. Then, the centrifugal filtration used to filter out the recovered precipitate, and washed with 0.1 $mol.L^{-1}$ formic acid (HCOOH) to remove any possible carbonate contamination (CO_3^{2-}) and deionized water until the pH value reduced to 7. The 0.1 $mol.L^{-1}$ of $AgNO_3$ solution was used to check the remained chloride ion by the supernatant with no white sediment remained, which confirmed that the chloride ion was not retained. Eventually in order to obtain the powder products, the washed precipitates were dried in an oven overnight with the temperature about 80°C. The process of the synthesis in this section was shown in Figure 3.7.

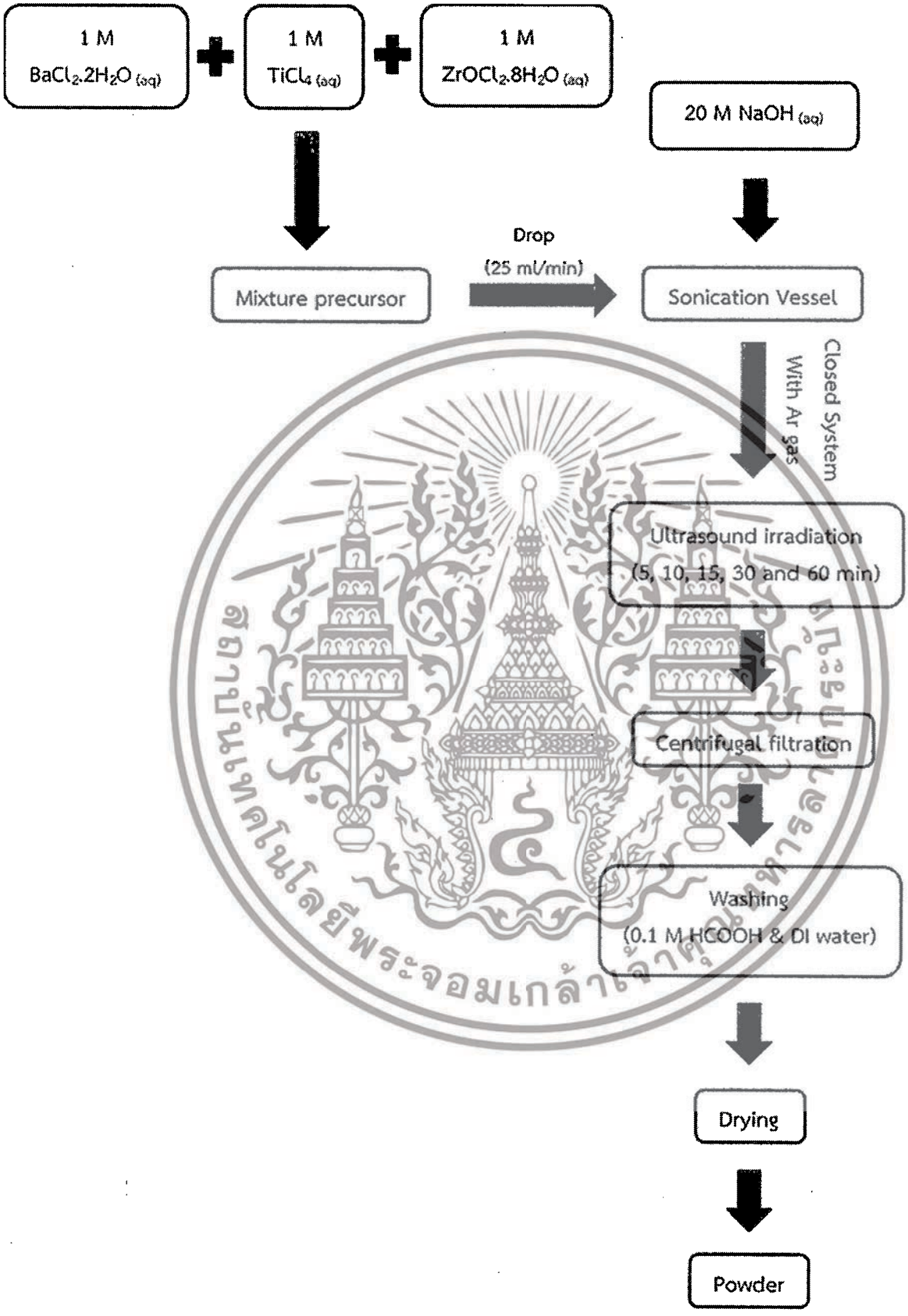

Figure 3.7 Schematic flow chart of BZT powder synthesis with varies Zr/Ti molar ratio.

3.4.6 Power of the ultrasound irradiation

This section study the effect of the Power of the ultrasound irradiation on the $Ba(Zr_xTi_{1-x})O_3$ with the composition (x) = 0.00 and 0.40 phase formation. The 1 $mol.L^{-1}$ of barium, zirconium and titanium solution were used as the stock of precursor solution in this section. The appropriate proportions of titanium zirconium and barium solution was pipetted from the stock solution, in order to obtain a homogeneous mixed solution by mixing the stock solution together with continuous stirring. Subsequently, setting up the sonication equipment for the sonochemical processin the close system with Ar gas. The 20 $mol.L^{-1}$ of sodium hydroxide (NaOH) solution, use as the precipitating agent, was loaded into a sonication vessel after setting up the equipment. And then, the sonication vessel which contained the NaOH solution, was added the mixed precursor solution with drop by drop at a rate of about 25 $ml.min^{-1}$. Therefore, a high pH value reached 14 during the process. Then, ultrasonic irradiation under ambient Ar gas for 30 minutes by pulse ultrasonication (Sonics VCX-750, 20 kHz, 750 W) in the 2 s mode; and a pause in 1 *s* mode was performed in this experiment, In order to obtain better quality of nanoparticles. Using the pulse ultrasonic mode for synthesis the powder gives a narrower particle size distribution than synthesized powder in continuous ultrasonic mode, has been reported [44]. This could be a scene from an uneven distribution of ultrasonic energy in the ultrasonic vessel [44]. The white precipitation was formed instantaneously during the process of adding mixed solution. And then, the power of ultrasound irradiation was set up for study in this effect by varying the amplitude mode with maximum amplitude = 20, 40 and 80%. The precipitate, which contained in the sonication vessel when the irradiation time was over, was cooled to room temperature by immersing in tap water. Then, the centrifugal filtration used to filter out the recovered precipitate, and washed with 0.1 $mol.L^{-1}$ formic acid (HCOOH) to remove any possible carbonate contamination (CO_3^{2-}) and deionized water until the pH value reduced to 7. The 0.1 $mol.L^{-1}$ of $AgNO_3$ solution was used to check the remained chloride ion by the supernatant with no white sediment remained, which confirmed that the chloride ion was not retained. Eventually in order to obtain the powder products, the washed precipitates were dried in an oven overnight with the temperature about 80°C.

3.5 Characterization

The crystal structure, phase nucleation and influence of the fuel-to-oxidizers molar ratio, calcination temperatures and dwell times of calcination to phase formation of as-synthesized and calcined powders, were studied and characterized by the X-ray diffraction technique (XRD), Fourier transform infrared (FTIR) and Raman spectrometer spectroscopy. The particle size and morphology of the powders obtained were investigated through a field emission scanning electron microscope (FE-SEM).

3.5.1 X-ray diffraction technique (XRD)

Figure 3.8 The X-ray diffractometer (Panalytical Model X'Part[3])

The perovskite phase formation, structure and crystallite size of the products were carried out by X-ray powder diffraction using an X-ray diffractometer (Panalytical Model X'Part[3], The Netherlands) (as shown in figure 3.8) with Cu Kα radiation (λ=0.15406 nm). The acceleration voltage was 35 kV with a 150 mA current flux. X-ray diffraction (XRD) was taken of the powders attached to a glass slide, and data were

collected in the 2θ range from 20° to 60°, with a scanning rate of 1°/min and sample interval of 0.02°. Crystallite size and microstrain were calculated by the X-ray line broadening method using Scherrer equation [134]. The Scherrer equation relies on utilizing the following equation:

$$D = K\lambda/\beta\cos\theta, \quad (3.2)$$

where λ is the CuK_α radiation of wavelength (1.5406Å), β is the full width at haft-maximum (FWHM) in radian and θ is the scattering angle. Also, K is the shape factor (a constant equal to 0.94) and *D* is the crystallite size normalized to the reflecting planes.

3.5.2 Raman spectrometer

The Raman spectrometer (as shown in figure 3.9) was used for confirm phase identification of the final powder product, which determines the characteristic vibrations of atoms in molecules and compound. In order to support the crystal structure identification of synthesized powders by the Raman spectra were recorded in the 100—1,000 cm^{-1} wave number ranges with a Thermo Scientific DXR Raman microscope (532-nm excitation of the laser) at room temperature.

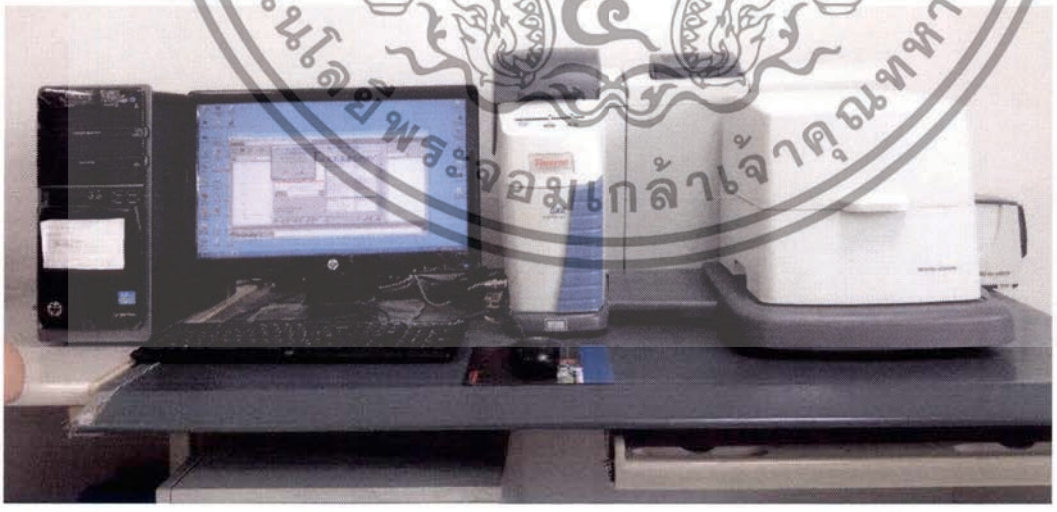

Figure 3.9 The Raman spectrometer (Thermo scientific Model DXR Raman Microscope)

3.5.3 Fourier transform infrared (FTIR) spectroscopy

The Fourier transform infrared spectrometer (FT-IR) (as shown in figure 3.10) was used for characterizing the final powder product and confirm phase identification, which determines the adsorption of infrared radiation, due to characteristic vibrations and rotations of atoms in molecules and compound. The FT-IR spectra were recorded in the range of 4,000–400 cm^{-1}, with 8 scans on a Perkin Elmer, FT-IR SPECTRUM GX and a resolution of 4 cm^{-1} using KBr pellets (KBr, spectroscopy grade, Merck) at room temperature.

Figure 3.10 Fourier transform infrared spectrometer (Perkin Elmer Model Spectrum GX)

3.5.4 Field emission scanning electron microscope (FE-SEM)

The Field emission scanning electron microscope (JEOL Model JSM-6335F) (as shown in figure 3.11) used to characterize initially the particle size and morphology of the resulting as-prepared products, equipped with energy-dispersive X-ray spectroscopy (EDS) capabilities. The powders were dispersed firstly in ethyl alcohol using an ultrasonic bath for 15 min. Then, dispersion was dropped on copper tape and dried. In order to minimize charging effects under FE-SEM imaging conditions, these

samples were coated conductively with gold by sputtering for 15 s. The average particle size of powders obtained was examined using the linear intercept method.

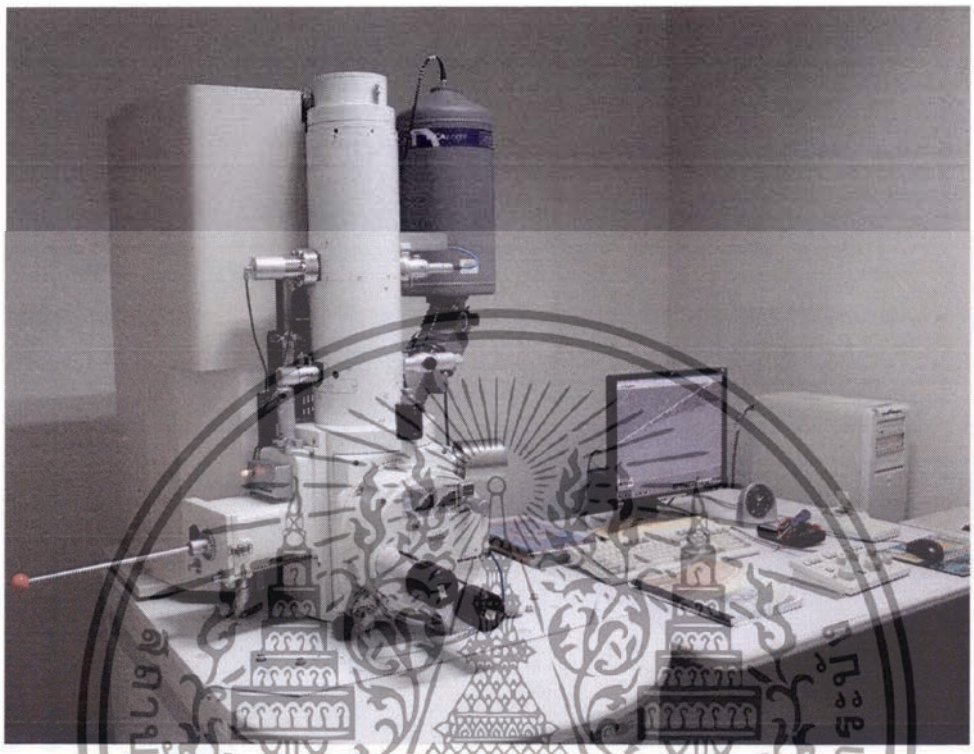

Figure 3.11 Field emission scanning electron microscope (JEOL Model JSM-6335F)

CHAPTER 4

RESULTS AND DISCUSSION

Supamas Wirunchit, Thitirat Charoonsuk[a] and Naratip Vittayakorn[a,b,c]

[a]*Electroceramics Research Laboratory, College of Nanotechnology, King Mongkut's Institute of Technology Ladkrabang, Bangkok 10520, Thailand.*

[b]*Department of Chemistry, Faculty of Science, King Mongkut's Institute of Technology Ladkrabang, Bangkok 10520, Thailand*

[c]*Advanced Materials Research Unit, Faculty of Science, King Mongkut's Institute of Technology Ladkrabang, Bangkok 10520, Thailand*

Published in April 2015

RSC Advances

Vol (5) p. 38061-38074

In this chapter discusses the results of experiments, including characterization and analysis of the complex perovskite barium zirconium titanate ($Ba(Zr_xTi_{1-x})O_3$; BZT) nanopowders were synthesized via sonochemical method. The results of the influence of the synthesis parameters (the concentration of precipitating agent, the synthesis atmosphere, the concentration of the starting solution, sonication time, Zr/Ti molar ratio and the power of the ultrasound irradiation) were presented and discussed. Then, the crystal structure, morphology, particle size and phase formation of barium zirconium titanate nanopowders are described. In order to know the optimum conditions for the synthesis of barium zirconium titanate powder by sonochemical method. The barium zirconium titanate ($Ba(Zr_xTi_{1-x})O_3$; BZT) nanopowders that must be of high purity and small size in the nanometer respectively.

The complex perovskite barium zirconium titanate ($Ba(Zr_xTi_{1-x})O_3$; BZT) powder products, with the composition (x) = 0.00, 0.05, 0.20, 0.04 and 0.60, which was in accordance with the reaction (4.1). They were synthesized by the sonochemical method without the calcination process.

$$BaCl_2{\bullet}2H_2O_{(aq)} + (1-x)TiCl_{4(aq)} + xZrOCl_2{\bullet}8H_2O_{(aq)} + (6-2x)NaOH_{(aq)} \longrightarrow Ba(Zr_xTi_{1-x})O_{3(s)} + (6-2x)NaCl_{(aq)} + (13-x)H_2O_{(aq)} \quad (4.1)$$

4.1 The effect of the precipitating agent concentration on the complex perovskite barium zirconium titanate ($Ba(Zr_xTi_{1-x})O_3$ phase formation.

To change the parameters have a dramatic effect on the perovskite phase formation. In this section study the effect of the concentration of precipitating agent (NaOH) with 5, 12 and 20 $mol.L^{-1}$ on the $Ba(Zr_xTi_{1-x})O_3$ (x = 0.0) phase formation in the open air. The 1 $mol.l^{-1}$ of barium and titanium solution were used as the stock of precursor solution. The Ba, Ti and Zr ion ratio in the mixed solution targeted constantly at 1:1:0. The mixture solution was irradiated with an ultrasonic horn for 30 minutes at 80% of the maximum ultrasound irradiation amplitude. This study exposed the concentration of NaOH with a striking effects on the $Ba(Zr_xTi_{1-x})O_3$ (x = 0.0) phase formation.

Figure 4.1 shows the XRD pattern of $Ba(Zr_xTi_{1-x})O_3$ (x = 0.0) powders that was irradiated with an ultrasonic horn for 30 min in the open air system with a different NaOH concentrations. It can be seen that the powders synthesized with 5 $mol.L^{-1}$ NaOH

illustrate only X-ray peaks of the unwanted phase correspond with the literature [128] that is $BaCO_3$ and $Ba(OH)_2(H_2O)_3$ phase. No perovskite structure characteristic diffraction peaks could be discerned, indicating that no reaction was yet been triggered for synthesis with 5 $mol.L^{-1}$ of NaOH concentration. Moreover, the XRD pattern did not display any explicit of Ti-precursor phase indicated that the Ti-precursor phase in this condition is in the amorphous form [135]. The perovskite phase was developed at a NaOH concentration as high as 12 $mol.L^{-1}$, accompanied by the unwanted phase of $BaCO_3$ (JCPDS file no. 41-0373) and $Ba(OH)_2(H_2O)_3$ (JCPDS file no. 77-2333). In addition, the perovskite phase prominently displayed with increasing NaOH concentration to 20 $mol.L^{-1}$, the $BaCO_3$ and $Ba(OH)_2(H_2O)_3$ phase decreased dramatically. This observation suggests that the unwanted phase of $BaCO_3$ and $Ba(OH)_2(H_2O)_3$ were also decreased with escalating NaOH concentration. Diffraction peaks of the perovskite phase are indexed with the $BaTiO_3$ cubic structure in the *Pm3m* space group from JCPDS card No. 31-0174. Intensity of the perovskite pattern increased significantly with increasing NaOH concentration. The increasing of perovskite phase at high hydroxide concentration might be due to increasing formation of the complex polymeric chain network of bimetallic Ba-Ti hydroxides [136].

Nevertheless, a low intensity peak of $BaCO_3$ was still present in products synthesized with 20 $mol.L^{-1}$ of NaOH concentration in open air system.

The problem of forming $BaCO_3$ at a high NaOH concentration should be attributed to using the open air synthesis system, in which the Ba-hydroxide in the solution can react easily with CO_2 in air or carbonate species in the solution.

The volume fraction of the perovskite phase formation was considered at various NaOH concentration. The amounts of perovskite, $BaCO_3$ and $Ba(OH)_2(H_2O)_3$ phases relate with a volume fraction of the perovskite phase formation which were approximated by calculating the ratio of the main X-ray peak intensities of perovskite $BaTiO_3$, $BaCO_3$, and $Ba(OH)_2(H_2O)_3$ phase using the following equation [137]:

$$\% \text{ perovskite} = \frac{I_{perov}}{I_{perov}+I_{BaCO_3}+I_{Ba(OH)_2(H_2O)_3}} \times 100 \qquad (4.2)$$

where I_{perov}, I_{BaCO_3} and $I_{Ba(OH)_2(H_2O)_3}$ stand for the intensities belonging to the strongest reflection peak of (110) perovskite, ($BaCO_3$, and $Ba(OH)_2(H_2O)_3$, respectively. A volume fraction increase of the perovskite $BaTiO_3$ phase formation, resulting from

the sonochemical process at various the concentration of precipitating agent, is shown in Table 4.1.

Table 4.1 Fraction of perovskite phase formed and lattice parameter (*a*) as a function of the concentration of precipitating agent

NaOH concentration ($mol.L^{-1}$)	Lattice parameter (*a*) (Å)	% perovskite
5	-	0.00
12	4.0328 ± 0.0057	73.14
20	4.0317 ± 0.0039	89.96

Note: The lattice parameter (*a*) of the $BaTiO_3$, which is cubic structure in the *Pm3m* space group from JCPDS card No. 31-0174, is 4.0310 Å.

Figure 4.2 shows the FT-IR spectroscopic studies of the powder products at various NaOH concentrations that was irradiated with an ultrasonic horn for 30 minutes in the open air system. The FT-IR band for the all products were observed at around 3,500 cm^{-1}, due to O–H asymmetric stretching (υ_3) and bending mode (υ_2) of O–H at around 1,600 cm^{-1}, respectively, arising from the water present in the surface of the barium titanante nanoparticle [138]. As shown in Figure 4.2, FT-IR spectrum of the powder synthesized with 5 $mol.L^{-1}$ NaOH indicated peaking of the characteristic band at around 1,450, 1,300, 1,100 and 890 cm^{-1}, which corresponded to the anti-symmetric carbonate group stretching vibration of $BaCO_3$ [139, 140]. And did not appear the Ti-O vibrations band of the perovskite phase same with XRD result. The absorption band at around 600 cm^{-1}, represents the characteristic infrared absorptions of the Ti-O vibrations. The TiO_6 stretching vibration connected to the barium which situated band around 603 cm^{-1} [141-143]. By increasing the NaOH concentration, the absorption bands of about 603 cm^{-1} became increasingly stronger, indicating that the $BaTiO_3$ phase was created initially at about 12 $mol.L^{-1}$ NaOH and the asymmetric stretch vibration of the carbonate groups decreased significantly. In addition, the perovskite phase prominently displayed with increasing NaOH concentration to 20 $mol.L^{-1}$, the $BaCO_3$ phase decreased dramatically. This result indicated that, $BaTiO_3$ crystallites grew increasingly by increasing the NaOH concentration, which was also consistent with the XRD determined previously.

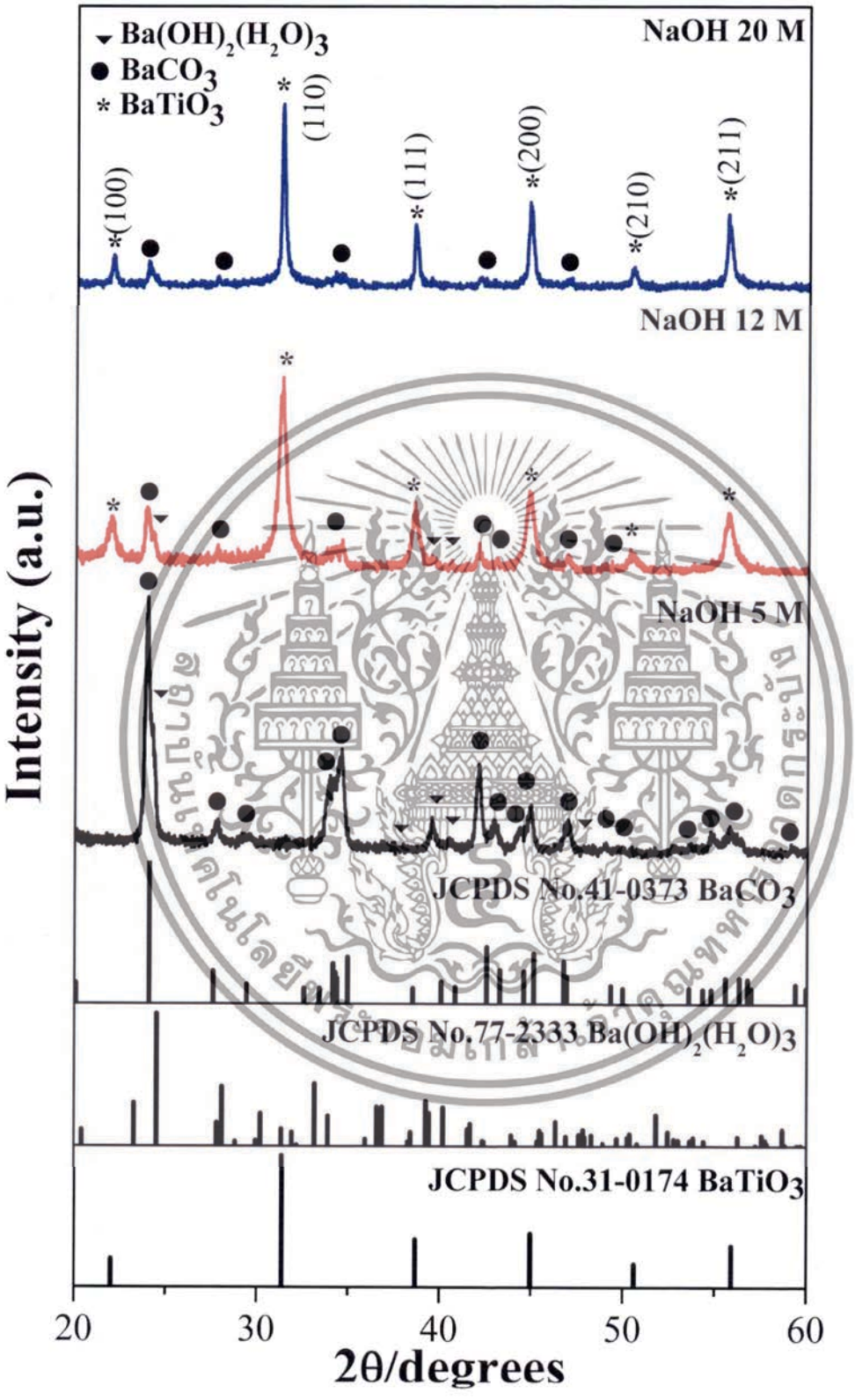

Figure 4.1 The XRD pattern of $Ba(Zr_xTi_{1-x})O_3$ (x = 0.0) powders that sonicated for 30 minutes at various NaOH concentrations in the open air system.

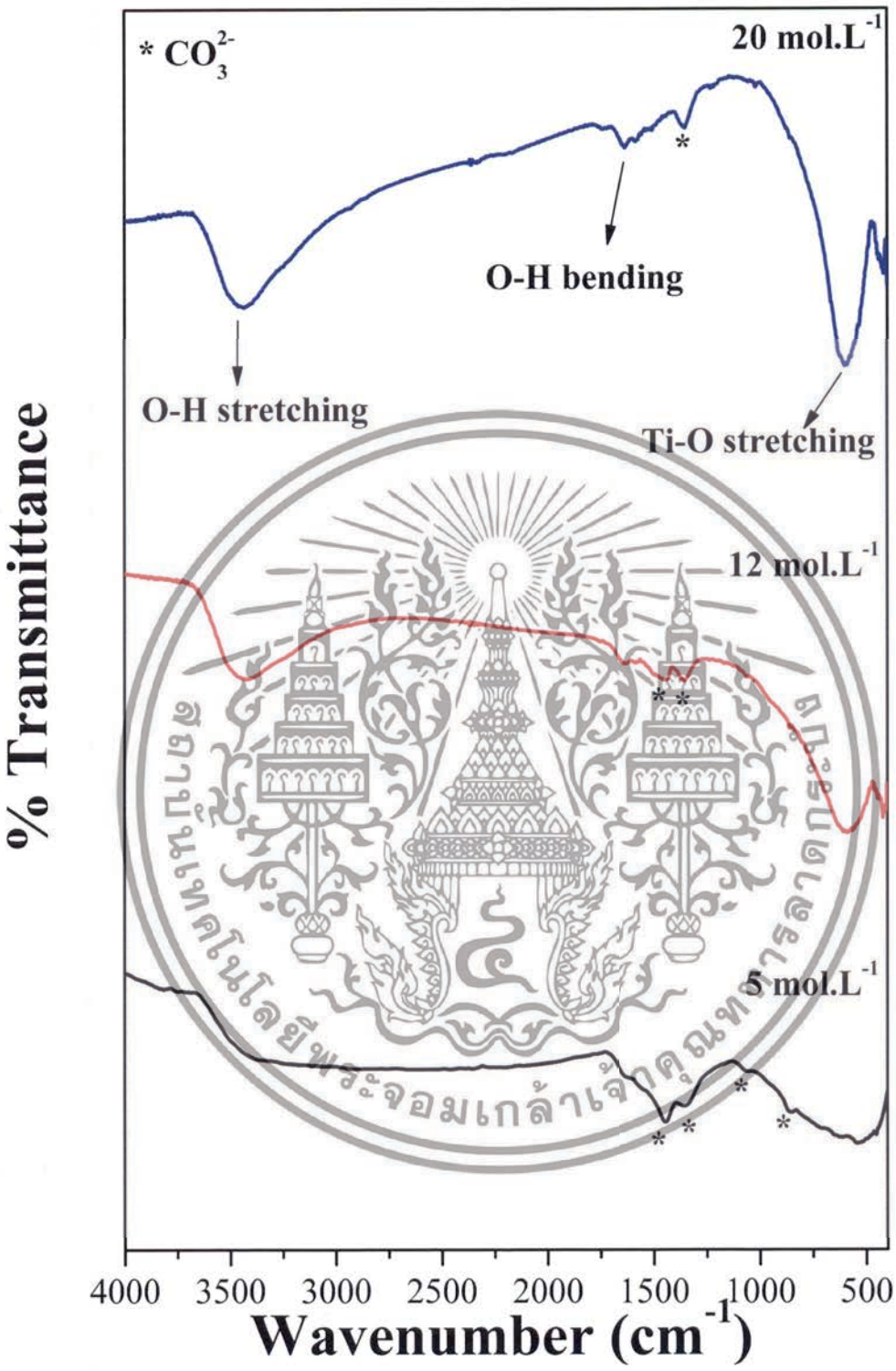

Figure 4.2 The FT-IR spectrum of $Ba(Zr_xTi_{1-x})O_3$ (x = 0.0) powders that sonicated for 30 minutes at various NaOH concentrations in the open air system.

Raman spectroscopy is a highly sensitive spectroscopic technique generally used for probing structure in atomic scale on the basis of vibrational symmetry [144]. Cubic $BaTiO_3$ has no inherent Raman-active modes, which are however, expected for non-centrosymmetric tetragonal structure. Raman spectra of as-synthesized powders, synthesized at different NaOH concentration, are presented in Figure 4.3. It can be seen that the powders synthesized with 5 $mol.L^{-1}$ NaOH display the symmetric stretching mode of C – O bond from minimal $BaCO_3$ traces, which correspond at around 134, 155 and 808 cm^{-1} [145, 146]. The perovskite phase started to form with increasing NaOH concentration, the $BaCO_3$ phase decreased dramatically, which consistent with the XRD (Figure 4.1) and FT-IR (Figure 4.2) results, respectively.

It is well known that $BaTiO_3$ has five atoms, and fifteen degrees of freedom divided into the optical representations, $3F_{1u} + F_{2u}$, while another F_{1u} symmetry mode corresponds to the acoustical branch. The $BaTiO_3$ spectra revealed the presence of a tetragonal structure, mainly characterized by the $A_1(TO_1)$, $A_1(TO_2)$, $E(TO_2)$, $A_1(TO_3)$ and $A_1(LO)$/$E(LO)$ Raman modes, while no Raman-active mode was predicted for the cubic phase (Pm3m) [147]. The Raman shift peak of the powder products (with 12 and 20 $mol.L^{-1}$), is located at around 181, 295, 521 and 707 cm^{-1} and assigned to the transverse optical (TO) modes of A_1 symmetry. The peak at 181 cm^{-1} arises due to interference from harmonic coupling between the three $A_1(TO)$ phonons. The peak at 707 cm^{-1} is related to the highest frequency of the longitudinal optical mode (LO) with A_1 symmetry [147]. Regarding the other compositions, the Raman spectra nearly corresponds to those of $BaTiO_3$ that present a cubic structure, which is in agreement with the XRD result.

Then, the powder products that are to examine the morphology using a field emission scanning microscope (FE-SEM). FE-SEM micrographs of all powder products, sonochemically synthesized for 30 minutes of ultrascnic irradiation at various NaOH concentrations in the open air system, are demonstrated in Figure 4.4. As shown in Figure 4.4, two type of morphological particles were observed at 5 $mol.L^{-1}$ NaOH (Figure 4.4 (a)), a small one with agglomerated form and large particle with irregular morphology. The morphology of the particle changed significantly with increased NaOH concentration to a narrow size distribution, and a more spherical shape was observed clearly. Figure 4.4 (c) shows the histogram of particle size distribution which illustrates a narrow size distribution of the nanoparticles. The average particle size decreased significantly with increasing NaOH concentration, and when measured by FE-SEM was found to be 172 ± 11 nm and 84 ± 16 nm powder synthesized with 12 $mol.L^{-1}$ and 20 $mol.L^{-1}$ of NaOH concentration, respectively.

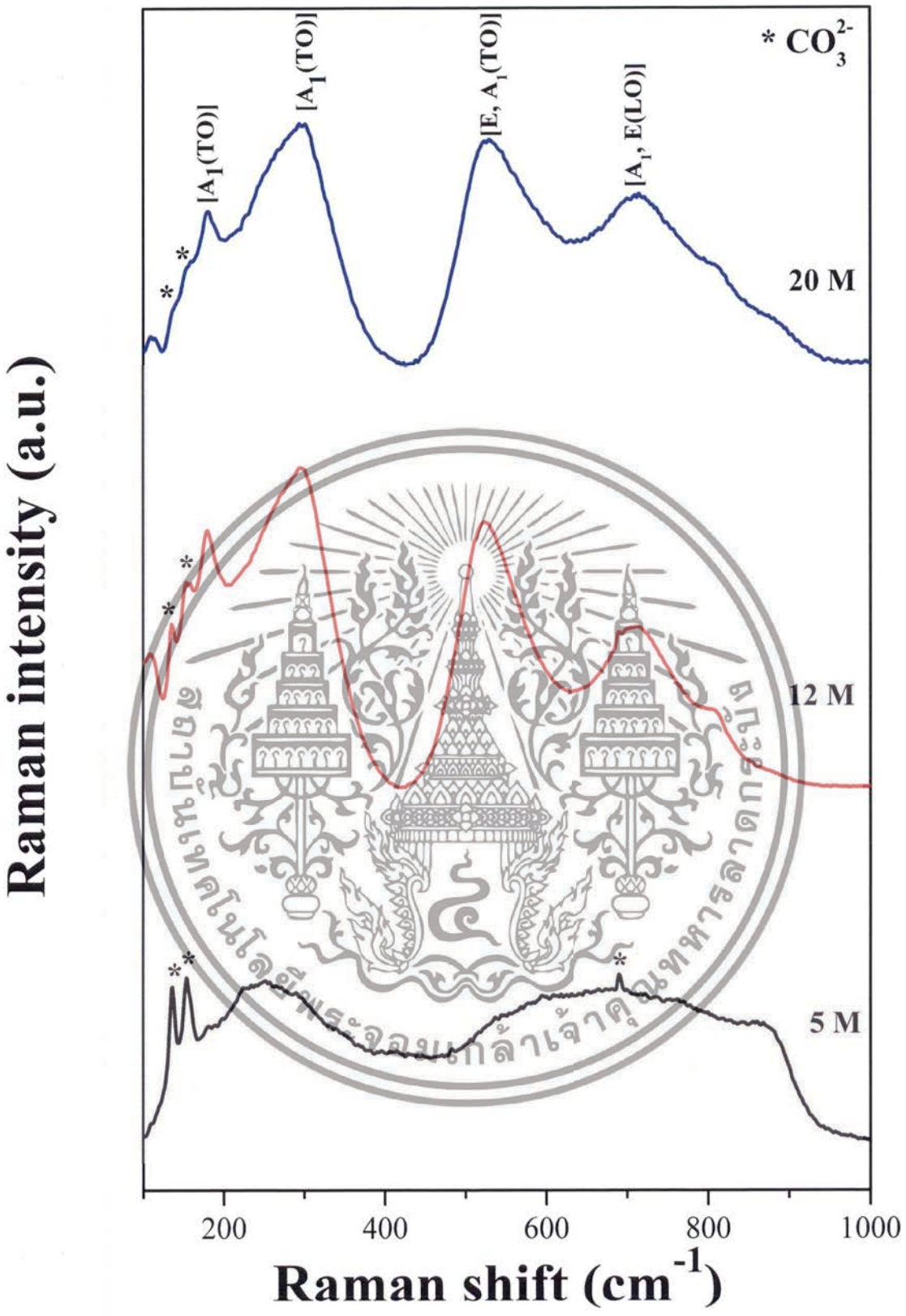

Figure 4.3 Raman spectrum of $Ba(Zr_xTi_{1-x})O_3$ (x = 0.0) powders that sonicated for 30 minutes at various NaOH concentrations in the open air system.

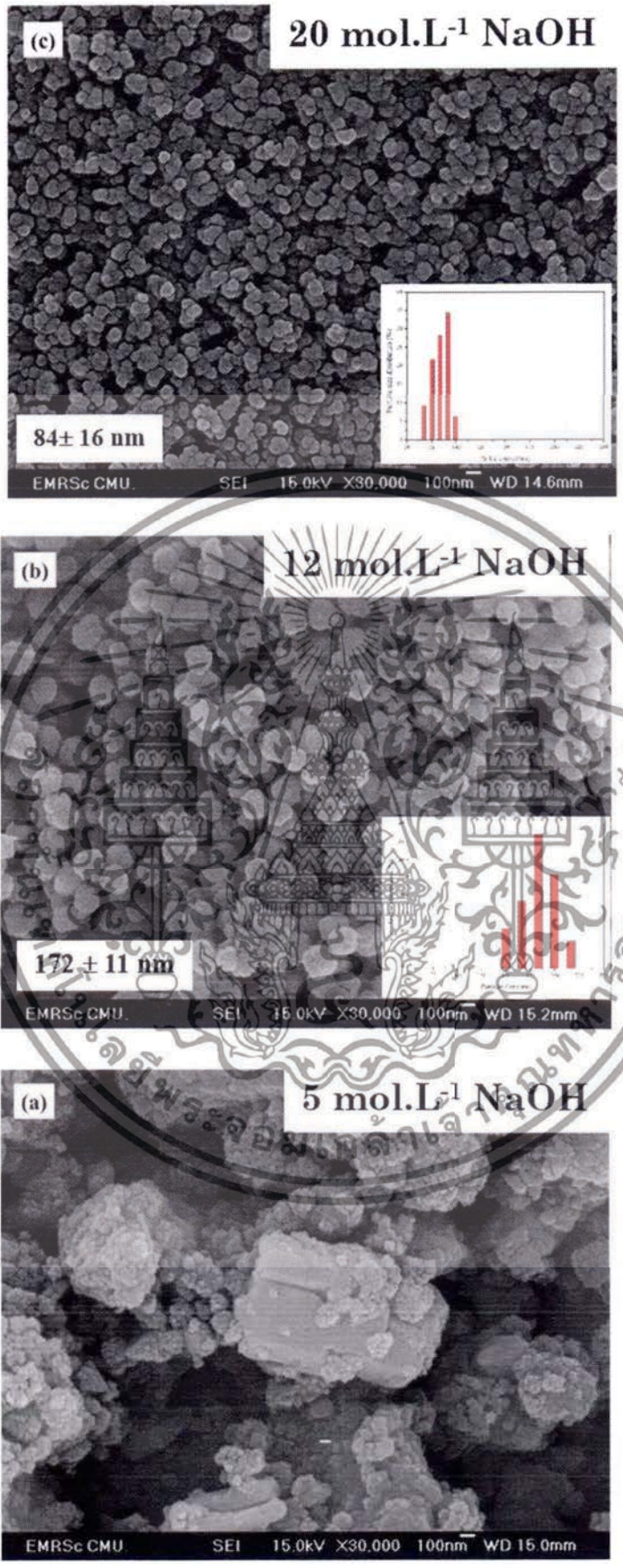

Figure 4.4 FE-SEM images of $Ba(Zr_xTi_{1-x})O_3$ (x = 0.0) powders that sonicated for 30 minutes at various NaOH concentrations in the open air system.

Figure 4.5 shows FE-SEM image and the energy dispersive X-ray (EDX) patterns of $Ba(Zr_xTi_{1-x})O_3$ (x = 0.0) powders that sonicated for 30 minutes in the open air system with 5 mol.L^{-1} NaOH, indicated that the agglomerated cluster was the Ti-amorphous phase, while the large particle was the $BaCO_3$ phase. The results corresponded well with the XRD pattern (Figure 4.1).

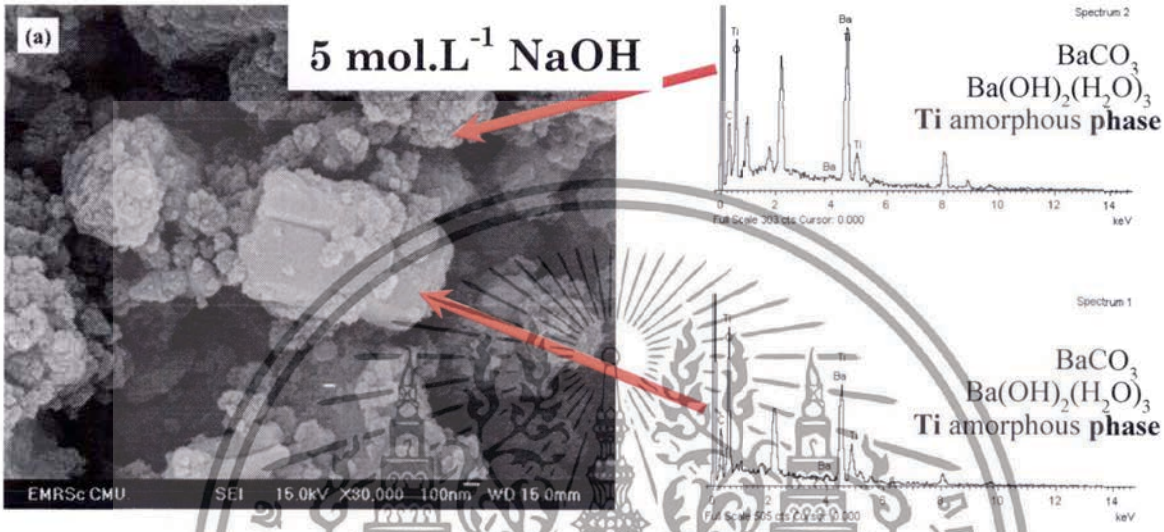

Figure 4.5 FE-SEM image and the energy dispersive X-ray (EDX) patterns of $Ba(Zr_xTi_{1-x})O_3$ (x = 0.0) powders that sonicated for 30 minutes at 5 mol.L^{-1} NaOH in the open air.

From all results (XRD, FT-IR, Rman and FE-SEM results) above, It can be seen that the 20 mol.L^{-1} NaOH is an optimal condition for synthesis the $Ba(Zr_xTi_{1-x})O_3$ powders with the sonochemical method.

This is consistent with the research of R. Vijayalakshmi *et al.* [148] have succeeded in the synthesis of barium titanate ($BaTiO_3$) with hydrothermal method. It uses 240 ° C for 20 hours and then studied the concentration of NaOH was changed to 1%, 2% and 3% respectively. The particles made from synthetic 1% NaOH was found that the particles are spherical and have a relatively uniform distribution. When the concentration was increased to 2% NaOH showed that the particles are spherical, and begin to change into rod structure mixed in the products. However, the 3% NaOH found that the deformation is characterized by small rods. The diameter of 20-30 nm and a length of more than 90 nm. Moreover, it also found that the particles that are larger when the concentration of NaOH increases. The result would be inconsistent

with this research is that when the concentration of sodium hydroxide increases the particles that are smaller and the particles can be characterized sphere, as shown in the Table 4.2. In addition, a study by W. Wang *et al.* [149] have sisthesized the ($BaTiO_3$ by sol-gel - hydrothermal method. As a result of the influence of the concentration of potassium hydroxide (KOH) different at 0.5, 1, 4 and 8 $mol.L^{-1}$, respectively, the concentration of KOH is 0.50 $mol.^{L-1}$, the characteristics of the particles. It will be larger and there does not appear to be homogeneous. The concentration of KOH increased to 1 $mol.L^{-1}$ found that the particles are spherical and have a uniform dispersion of the particles have a size of around 375 nm. When the concentration of KOH increased the size of the particles that are smaller and have a narrow distribution. This results will be consistent with this research, which is the particle size decreased with increasing the NaOH concentration.

Table 4.2 show the results of the $BaTiO_3$ which synthesized by the different method

	Sol-gel-Hydrothemal method	Hydrothemal method	Sonochemical method
Stating materials	$C_{16}H_{36}O_4Ti$ and $Ba(C_2H_3O_2)_2$	$BaCl_2$ and $TiCl_4$	$BaCl_2 \cdot 2H_2O$ and $TiCl_4$
Conditions	120 °C for 12 h. 0.5-8 $mol.L^{-1}$ of KOH	240 ° C for 20 h. 1-3% of NaOH	20 $mol.L^{-1}$ of NaOH, $Ba^{2+}:Ti^{4+}$ = 1:1, reaction time for 30 min
Shape	Sphere	Nanorod	Nanosphere
Particle size	120-375 nm.	The diameter of 20-30 nm and a length of more than 90 nm.	83.85 ± 11.38 nm.
Distribution	narrow distribution	narrow distribution	narrow distribution
Researcher	W. Wang *et al.* [149]	R. Vijayalakshmi *et al.* [148]	This research

4.2 The effect of the synthesis atmosphere on the complex perovskite barium zirconium titanate ($Ba(Zr_xTi_{1-x})O_3$ phase formation.

In this section study the effect of the synthesis atmosphere on the $Ba(Zr_xTi_{1-x})O_3$ (x = 0.0) phase formation in the open air and Ar atmosphere. The 1 $mol.l^{-1}$ of barium and titanium solution were used as the stock of precursor solution, and used 20 $mol.L^{-1}$ NaOH as the precipitating agent. The Ba, Ti and Zr ion ratio in the mixed solution targeted constantly at 1:1:0. The mixture solution was irradiated with an ultrasonic horn for 5, 30 and 60 minutes at 80% of the maximum ultrasound irradiation amplitude. This study exposed the synthesis atmosphere with a striking effects on the $Ba(Zr_xTi_{1-x})O_3$ (x = 0.0) phase formation.

Figure 4.6 shows the evolution of XRD pattern of $Ba(Zr_xTi_{1-x})O_3$ (x = 0.0) powders obtained after sonication for 5, 30 and 60 minutes in 20 $mol.L^{-1}$ NaOH in the open air system (a) and closed system with Ar gas (b). In the open air system, the XRD pattern shows the mixed phase of the perovskite, $BaCO_3$ and $Ba(OH)_2(H_2O)_3$ phase. The unwanted phase of $BaCO_3$ (JCPDS file no. 41-0373) and $Ba(OH)_2(H_2O)_3$ (JCPDS file no. 77-2333) decreased significantly with increasing sonication time. Nevertheless, the $BaCO_3$ remained at 60 minutes sonication time. For the powder synthesized in Ar atmosphere, The $BaCO_3$ phase disappeared after only five minutes sonication time. The relatively small XRD pattern shows good agreement with the perovskite structure. However, the intensity of the perovskite phase is quite low indicating that the product has a low crystallinity. The crystallinity of the product was improved significantly with increasing the sonication time. A sharp XRD pattern was observed clearly at 60 minutes sonication time. The XRD pattern indicates that the synthesized powder shows good agreement with the cubic $BaTiO_3$ structure with *Pm3m* space group (JCPDS file no. 31-0174). Based on XRD results, Rietveld refinement analysis gives a lattice parameters a = 4.0415±0.0004 Å, which was slightly larger than that of the reported value a = 4.031 Å (JCPDS file no. 31-0174). This slight expansion of lattice parameters (a) might be due to the presence of a trace amount of the OH group trapped in the crystal lattice, which can be confirmed by solvothermal treatment with Dimethylformamide (DMF). The intensities and positions of the peaks match very well with those data reported in the literature [25, 126]. No peaks of any other phases are detected, indicating the high purity of the product. The results indicated that the impurity $BaCO_3$ phase can be reduce or eliminate when product was synthesized at high concentration of precipitating agent (20 $mol.L^{-1}$ NaOH) and in the closed system with Ar atmosphere.

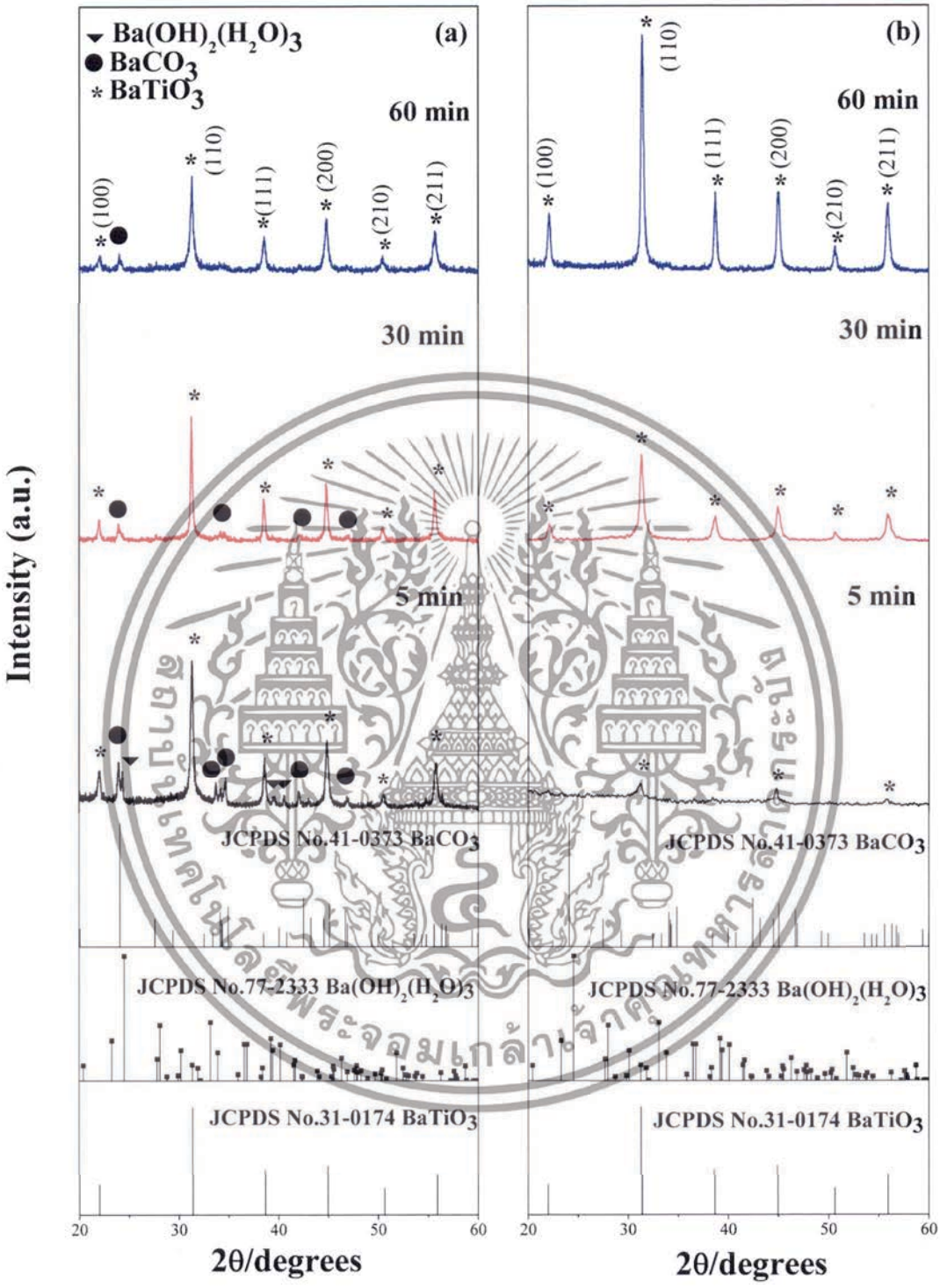

Figure 4.6 The XRD pattern of $Ba(Zr_xTi_{1-x})O_3$ (x = 0.0) powders that sonicated for 5, 30 and 60 minutes with 20 mol.L^{-1} NaOH in the open air (a) and Ar atmosphere (b).

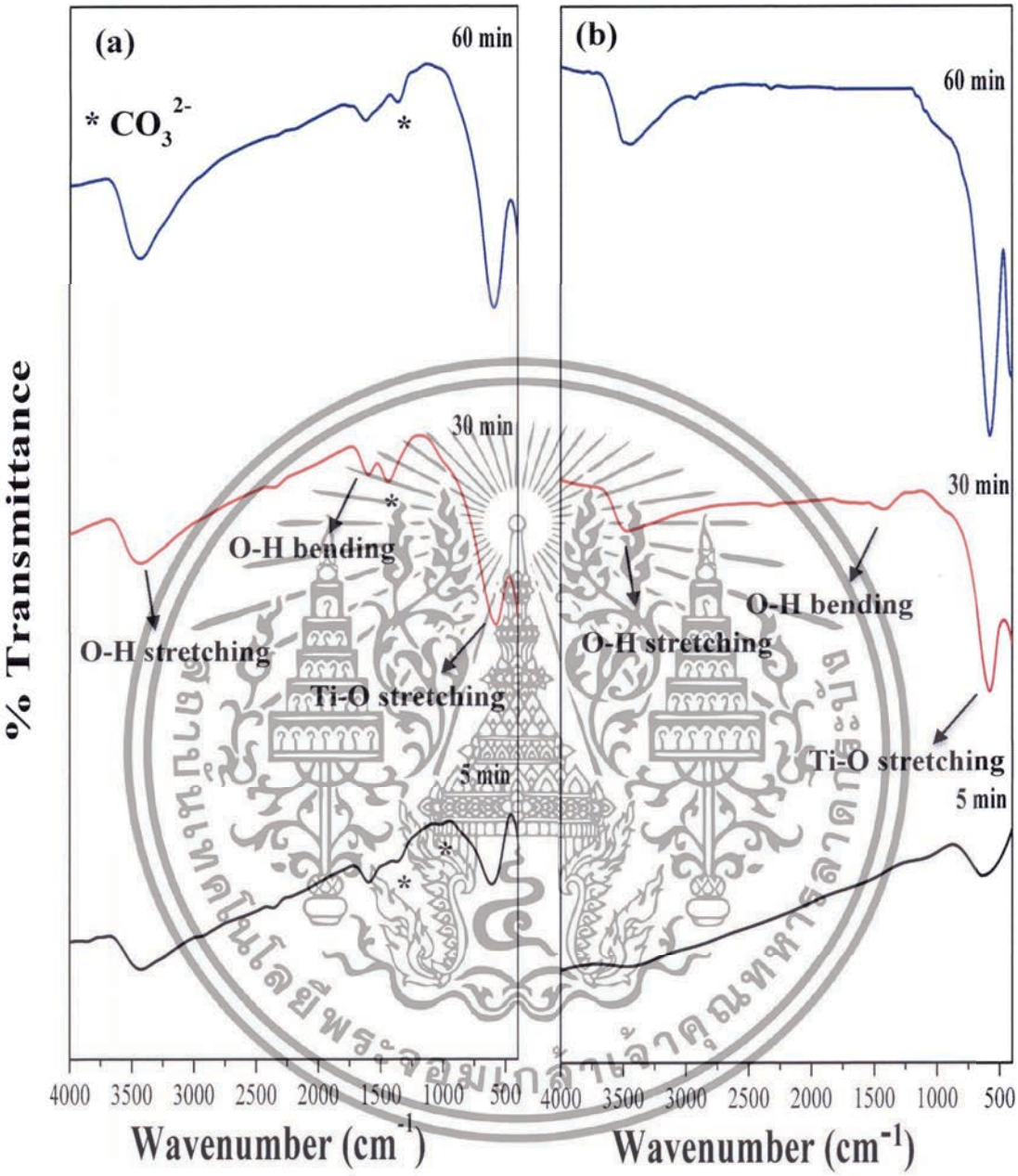

Figure 4.7 The FT-IR spectrum of $Ba(Zr_xTi_{1-x})O_3$ (x = 0.0) powders that sonicated for 5, 30 and 60 minutes with 20 mol.L^{-1} NaOH in the open air (a) and Ar atmosphere (b).

Figure 4.7 shows the evolution of FT-IR spectroscopic of the powder products obtained after sonication for 5, 30 and 60 minutes in 20 mol.L^{-1} NaOH in the open air system (a) and closed system with Ar gas (b). The FT-IR band for the all products were observed at around 3,500 cm^{-1}, due to O–H asymmetric stretching (υ_3) and bending mode (υ_2) of O–H at around 1,600 cm^{-1}, respectively, arising from the water present in the surface of the barium titanante nanoparticle [138], as shown in Figure 4.7 (a) and (b). In the open air system (Figure 4.7 (a)), FT-IR spectrum of the powder products indicated peaking of the characteristic band at around 1,400 and 1,000 cm^{-1}, which corresponded to the anti-symmetric carbonate group stretching vibration of $BaCO_3$ [139, 140]. The absorption band at around 600 cm^{-1}, represents the characteristic infrared absorptions of the Ti-O vibrations, which is due to TiO_6 stretching vibration connected to the barium [141-143]. By increasing the sonication time, the absorption bands of about 600 cm^{-1} became increasingly stronger, and the asymmetric stretch vibration of the carbonate groups decreased significantly. In addition, the perovskite phase prominently displayed with increasing sonication time to 60 minutes, the $BaCO_3$ phase decreased dramatically. This result indicated that, $BaTiO_3$ crystallites grew increasingly by increasing the reaction time. Nevertheless, the $BaCO_3$ remained at 60 minutes sonication time. which was also consistent with the XRD determined previously. For the powder synthesized in Ar atmosphere (Figure 4.7 (b)), the $BaCO_3$ phase disappeared after only five minutes sonication time. The FT-IR spectrum show the absorption band at around 600 cm^{-1}, represents the characteristic infrared absorptions of the Ti-O vibrations, which is due to TiO_6 stretching vibration connected to the barium. Furthermore, the absorption bands of Ti-O stretching vibrations became increasingly stronger with increasing the sonication time. From this results could conclude that the impurity $BaCO_3$ phase can be reduce or eliminate when product was synthesized at high concentration of precipitating agent (20 mol.L^{-1} NaOH) and in the closed system with Ar atmosphere, as the same XRD results.

Raman spectra of powders products, synthesized at different ultrasonic reaction times with 20 mol.L^{-1} NaOH in the open air system and closed system with Ar gas, are presented in Figure 4.8 (a) and (b) respectively. In the open air system (Figure 4.8 (a)), all powder products display the symmetric stretching mode of C – O bond from minimal $BaCO_3$ traces, which correspond at around 134, 155 and 808 cm^{-1}[145, 146]. It is well known that $BaTiO_3$ has five atoms, fifteen degrees of freedom per unit cell, octahedral rotational symmetry in the cubic phase, and fifteen degrees of freedom divided into the optical representations, $3F_{1u} + F_{2u}$, while another F_{1u} symmetry mode corresponds to the acoustical branch. The $BaTiO_3$ spectra revealed the presence of a tetragonal structure, mainly characterized by the $A_1(TO_1)$, $A_1(TO_2)$, $E(TO_2)$, $A_1(TO_3)$ and

A_1(LO)/E(LO) Raman modes, while no Raman-active mode was predicted for the cubic phase (*Pm3m*) [144]. When the reaction time at 5 minutes, the Raman shift peaks located at around 181, 295, 521 and 707 cm^{-1} match well with the typical Raman peaks of $BaTiO_3$ [150]. The bands around 295 and 521 cm^{-1} are assigned to the transverse optical (TO) modes of A_1 symmetry, whereas the peak at 181 cm^{-1} arises due to interference from anharmonic coupling between the three A_1(TO) phonons. The peak at 707 cm^{-1} is related to the highest frequency longitudinal optical mode (LO) with A_1 symmetry [151]. With increasing reaction time, the symmetric C - O stretching vibration becomes weaker. The decreasing of symmetric C - O stretching vibration band in Raman is corresponded well with FT-IR spectrum. For the powder synthesized in Ar atmosphere (Figure 4.8 (b)), the $BaCO_3$ phase disappeared after only five minutes sonication time. When increased the sonication time to 30 minutes, the Raman shift peaks located at around 181, 295, 521 and 707 cm^{-1} was appeared, which match well with the typical Raman peaks of $BaTiO_3$. The bands around 295 and 521 cm^{-1} are assigned to the transverse optical (TO) modes of A_1 symmetry, whereas the peak at 181 cm^{-1} arises due to interference from anharmonic coupling between the three A_1(TO) phonons. The peak at 707 cm^{-1} is related to the highest frequency longitudinal optical mode (LO) with A_1 symmetry.

The morphology and particle size were studied also by a field emission scanning microscope (FE-SEM). FE-SEM micrographs of all powder products, sonochemically synthesized at different ultrasonic reaction times with 20 $mol.L^{-1}$ NaOH in closed system with Ar gas, are demonstrated in Figure 4.9. As shown in Figure 4.9 (a), a large amount of $BaTiO_3$ nanocrystals was created initially from the Ba and Ti-based precursor under ultrasonic irradiation before aggregation of $BaTiO_3$ particles from large particles. Sphere-like particles were obtained after 30 minutes, and the particle size increased slightly after 60 minutes under ultrasonic irradiation. The $BaTiO_3$ particles showed a monosized spherical shape that was different from that in other preparation methods. The products had a spherical or very close to spherical morphology, and the particle size distribution was rather narrow. In addition, the average grain size was increased from 100 ± 11 nm to 123 ± 13 nm in diameter by increasing the reaction times from 30 min to 60 min, respectively, as seen in Figure 4.9 (a-c).

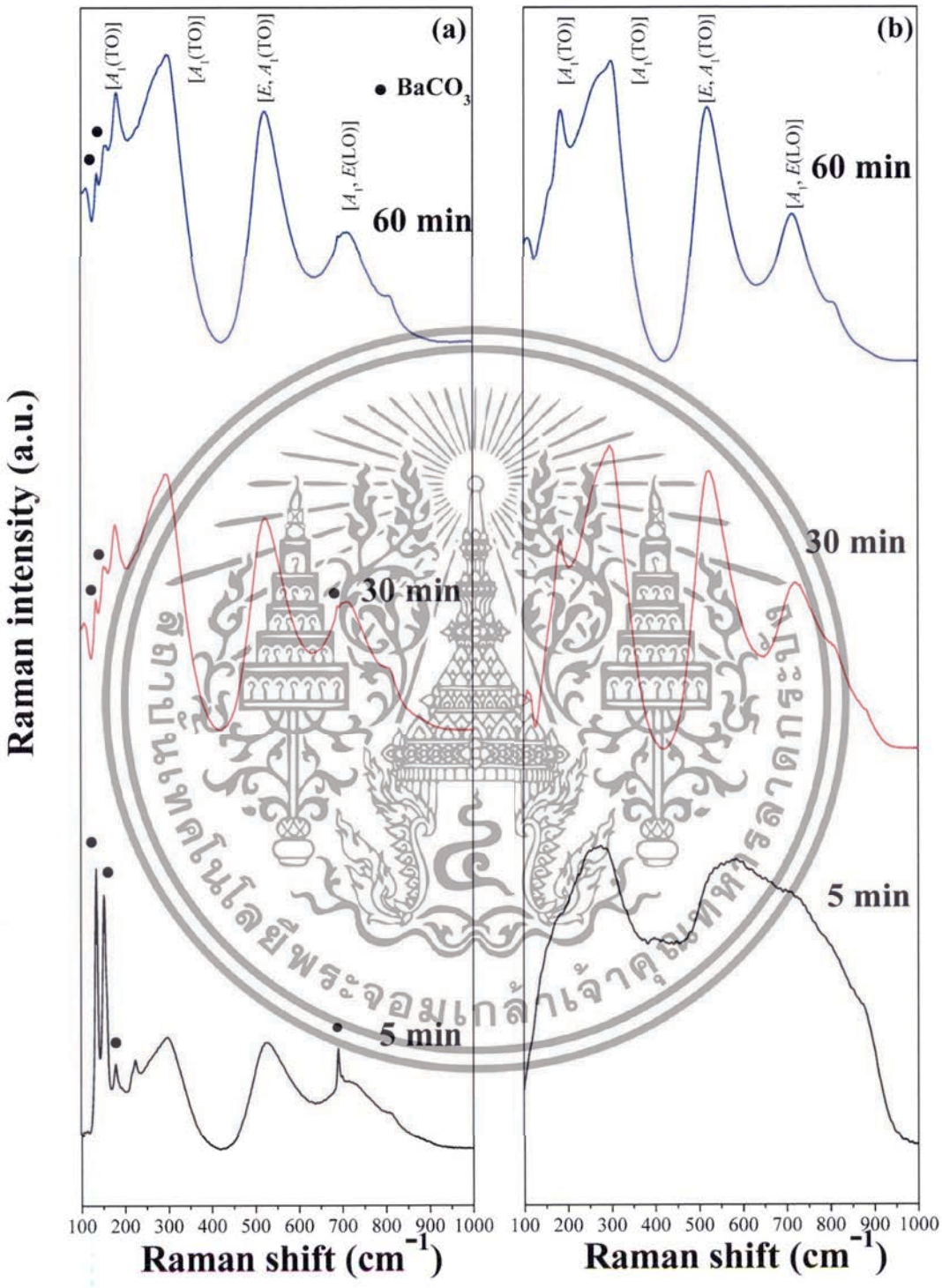

Figure 4.8 Raman spectrum of $Ba(Zr_xTi_{1-x})O_3$ (x = 0.0) powders that sonicated for 5, 30 and 60 minutes with 20 mol.L^{-1} NaOH in the open air (a) and Ar atmosphere (b).

Figure 4.9 FE-SEM images of $Ba(Zr_xTi_{1-x})O_3$ (x = 0.0) powders that sonicated for 5, 30 and 60 minutes with 20 mol.L^{-1} NaOH in Air atmosphere.

4.3 The effect of the starting solution concentration on the complex perovskite barium zirconium titanate ($Ba(Zr_xTi_{1-x})O_3$ phase formation.

To change the parameters have a dramatic effect on the perovskite phase formation. In this section study the effect of the starting solution concentration (Ba^{2+} and Ti^{4+} solution) with 0.01, 0.1, 0.2, 0.5, 1.0 and 1.5 $mol.L^{-1}$ on the $Ba(Zr_xTi_{1-x})O_3$ (x = 0.0) phase formation in the close system with Ar gas. The Ba, Ti and Zr ion ratio in the mixed solution targeted constantly at 1:1:0. The mixture solution was irradiated with an ultrasonic horn for 30 minutes at 80% of the maximum ultrasound irradition amplitude in 20 $mol.L^{-1}$ NaOH. This study exposed the starting solution concentration with a striking effects on the $Ba(Zr_xTi_{1-x})O_3$ (x = 0.0) phase formation.

Figure 4.10 shows the XRD pattern of $Ba(Zr_xTi_{1-x})O_3$ (x = 0.0) powders that was irradiated with an ultrasonic horn for 30 minutes in different precursor solution concentrations with 20 $mol.L^{-1}$ NaOH in the close system with Ar gas. At low precursor concentration ($\leq$ 0.2 mol L^{-1}), the XRD pattern displayed the $BaCO_3$ phase and $Ba(OH)_2(H_2O)_3$ phase; the perovskite phase was not observed at 0.01 $mol.L^{-1}$ precursor concentration. At 0.1 mol L^{-1}, the perovskite phase started to form and the unwanted phase $BaCO_3$ and $Ba(OH)_2(H_2O)_3$ phase decreased. With increased the precursor concentration to 0.5 mol L^{-1}, the $BaCO_3$ peak disappears, and Pure perovskite phase was obtained in this condition. Increasing of precursor concentration to 1.5 mol L^{-1}, the intensity of the XRD pattern decreased while the full width at haft-maximum (FWAH) value was increased, indicating the nanocrystals tend to become smaller. The average crystallite size of the powders obtained can be determined from the XRD pattern according to Scherrer's equation [134]:

$$D = K\lambda/\beta\cos\theta \qquad (4.3)$$

where λ is the CuKα radiation of wavelength (1.5406Å), β is the full width at haft-maximum (FWHM) in radian and θ is the scattering angle. Also, K is the shape factor (a constant equal to 0.94) and D is the crystallite size normalized to the reflecting planes. The crystalline size calculated form Scherrer equation is summarized in Table 4.3 and confirmed this assumption.

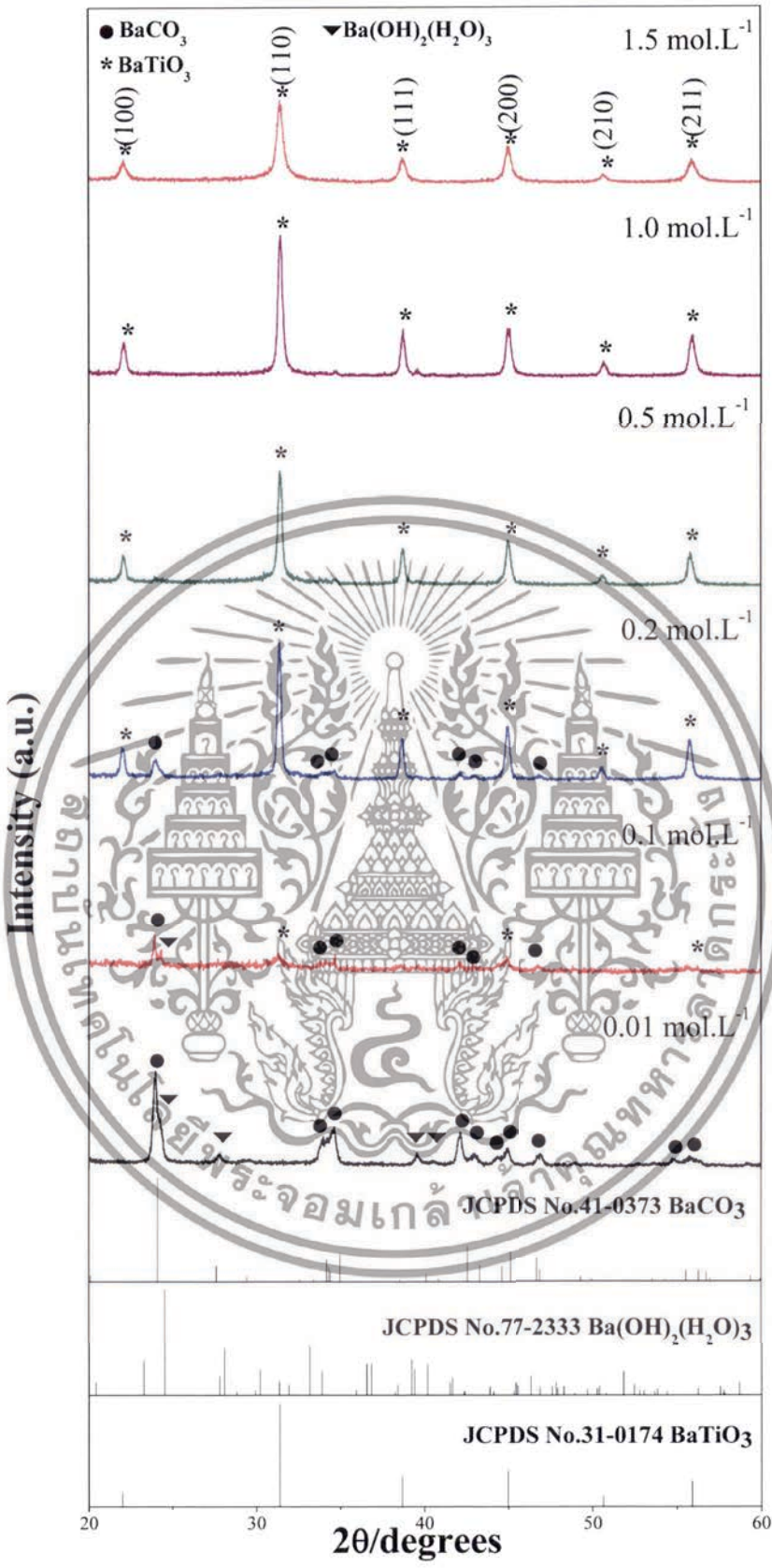

Figure 4.10 The XRD pattern of $Ba(Zr_xTi_{1-x})O_3$ (x = 0.0) powders that sonicated for 30 minutes at various the starting solution concentrations in 20 mol.L^{-1} NaOH in Ar atmosphere.

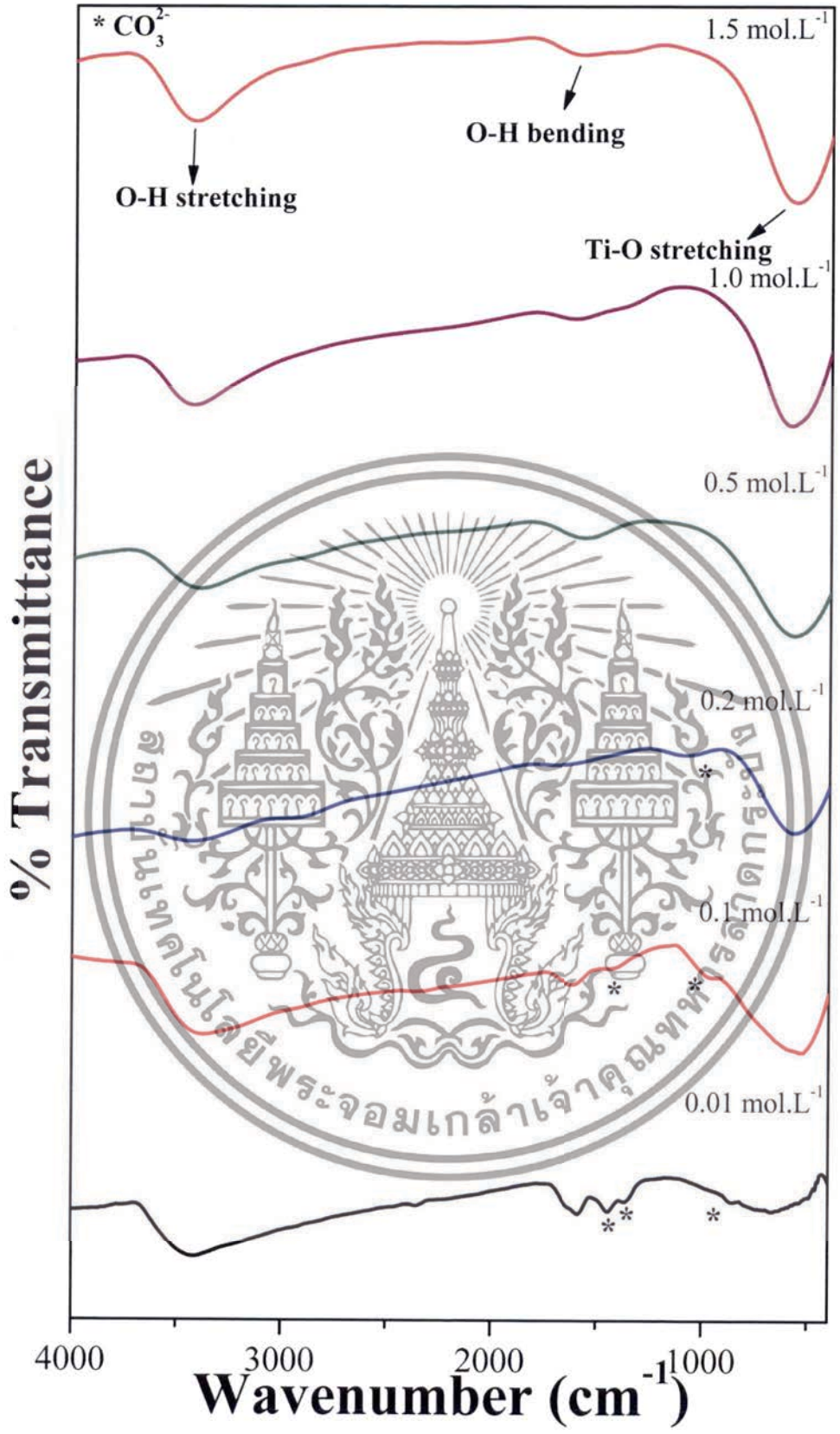

Figure 4.11 The FT-IR spectrum of $Ba(Zr_xTi_{1-x})O_3$ (x = 0.0) powders that sonicated for 30 minutes at various the starting solution concentrations in 20 mol.L^{-1} NaOH in Ar atmosphere.

Figure 4.12 Raman spectrum of $Ba(Zr_xTi_{1-x})O_3$ (x = 0.0) powders that sonicated for 30 minutes at various the starting solution concentrations in 20 mol.L^{-1} NaOH in Ar atmosphere.

Figure 4.11 shows the FT-IR spectroscopic of $Ba(Zr_xTi_{1-x})O_3$ (x = 0.0) powders that was irradiated with an ultrasonic horn for 30 minutes in different precursor solution concentrations with 20 mol.L^{-1} NaOH in the close system with Ar gas. The FT-IR band for the all products were observed at around 3,500 cm^{-1}, due to O–H asymmetric stretching (υ_3) and bending mode (υ_2) of O–H at around 1,600 cm^{-1}, respectively, arising from the water present in the surface of the barium titanante nanoparticle [138]. As shown in Figure 4.11, at low precursor concentration (≤ 0.2 mol L^{-1}), the FT-IR spectrum displayed the anti-symmetric carbonate group stretching vibration of $BaCO_3$ at around 1,450, 1,300 and 850 cm^{-1} [139,7/4]. At 0.1 mol L^{-1}, the perovskite phase started to form and the unwanted $BaCO_3$ phase decreased. The absorption band at around 600 cm^{-1}, represents the characteristic infrared absorptions of the Ti-O vibrations [8/4, 9/4, 10/4]. The band situated around 600 cm^{-1} is due to TiO_6 stretching vibration connected to the barium. By increasing the precursor concentration, the absorption bands of about 600 cm^{-1} became increasingly stronger, indicating that the pure $BaTiO_3$ phase was obtained at about 0.5 mol.L^{-1} of precursor concentration and the asymmetric stretch vibration of the carbonate groups decreased significantly. This result indicated that, $BaTiO_3$ crystallites grew increasingly by increasing the precursor concentration, which was also consistent with the XRD determined previously.

Raman spectroscopy is a highly sensitive spectroscopic technique generally used for probing structure in atomic scale on the basis of vibrational symmetry [11/4]. Cubic $BaTiO_3$ has no inherent Raman-active modes, which are however, expected for non-centrosymmetric tetragonal structure. Raman spectra of as-synthesized powders, synthesized at different NaOH concentration, are presented in Figure 4.12. It can be seen that the powders synthesized with 0.01 mol.L^{-1} of precursor solution display the symmetric stretching mode of C – O bond from minimal $BaCO_3$ traces, which correspond at around 134, 155 and 808 cm^{-1} [12/4, 13/4], and did not appear the Raman peak which a characteristic of the $BaTiO_3$ phase. The perovskite $BaTiO_3$ phase started to form with increasing the precursor solution concentration, the $BaCO_3$ phase decreased dramatically, When the precursor solution concentration increased to 0.5 mol.L^{-1}, the $BaCO_3$ phase disappeared, and the pure perovskite phase was obtained which consistent with the XRD (Figure 4.10) and FT-IR (Figure 4.11) results, respectively.

It is well known that $BaTiO_3$ has five atoms, and fifteen degrees of freedom divided into the optical representations, $3F_{1u} + F_{2u}$, while another F_{1u} symmetry mode corresponds to the acoustical branch. The $BaTiO_3$ spectra revealed the presence of a tetragonal structure, mainly characterized by the $A_1(TO_1)$, $A_1(TO_2)$, $E(TO_2)$, $A_1(TO_3)$ and $A_1(LO)/E(LO)$ Raman modes, while no Raman-active mode was predicted for the cubic phase (*Pm3m*) [14/4]. The Raman shift peak of the powder products (with > 0.1 mol.L^{-1}

^{1} of the precursor solution cincentration), is located at around 181, 295, 521 and 707 cm^{-1} and assigned to the transverse optical (TO) modes of A_1 symmetry. The peak at 181 cm^{-1} arises due to interference from harmonic coupling between the three A_1(TO) phonons. The peak at 707 cm^{-1} is related to the highest frequency of the longitudinal optical mode (LO) with A_1 symmetry [14/4]. Regarding the other compositions, the Raman spectra nearly corresponds to those of $BaTiO_3$ that present a cubic structure, which is in agreement with the XRD result.

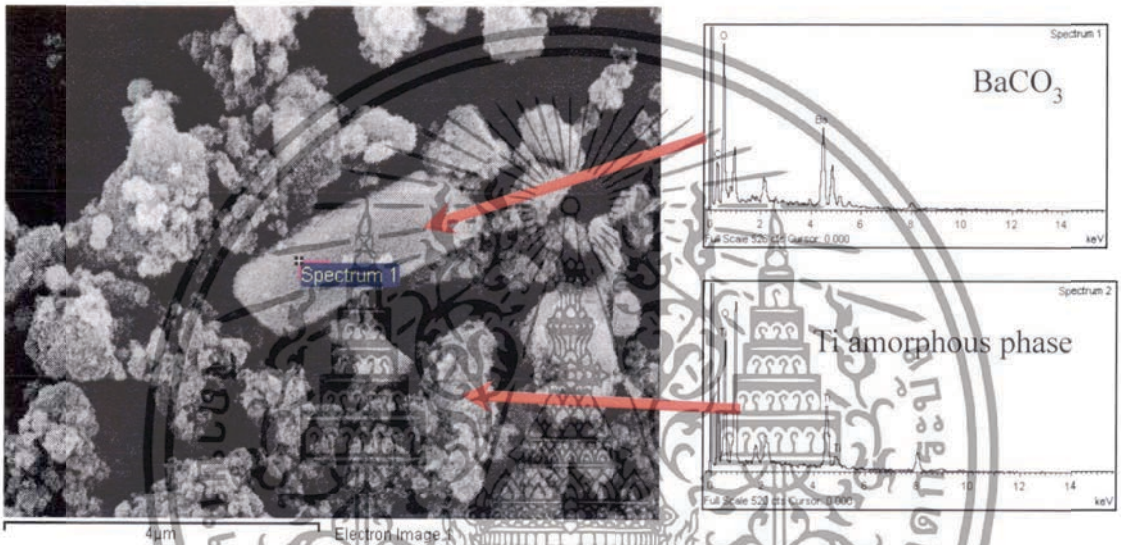

Figure 4.13 FE-SEM image and the energy dispersive X-ray (EDX) patterns of $Ba(Zr_xTi_{1-x})O_3$ (x = 0.0) powders that sonicated for 30 minutes at 0.01 $mol.L^{-1}$ of precursor solution concentration with 20 $mol.L^{-1}$ NaOH in the Ar atmosphere.

Figure 4.13 displayed the morphology of the powder product synthesized with 0.01 $mol.L^{-1}$ of precursor concentration. As shown in Figure 4.13, two types of morphology particles were observed clearly; small particle with agglomerated from and large particle with irregular morphology. The EDX indicated that the agglomerated cluster was Ti-amorphous phase while the large particle was the $BaCO_3$ phase. The results correspond well with the XRD pattern.

With increase the precursor concentration, the morphology of the particle changed significantly, as shown in Figure 4.14. The particles morphology shows more spherical in shape. And narrow size distribution was observed clearly with increasing the precursor concentration. The particle size distribution histrogram in Figure 4.14 (c) illustrations that the nanoparticles have narrow size distribution ranges with the average particle dispersity (D_{SEM99}/D_{SEM50}) of 1.54. Average particle size decreases significantly with increasing the precursor concentration. The average particle sizes measured by FE-SEM were found to be 123±43 nm for powder synthesized in 0.5 mol.L^{-1} of precursor concentration and decreased to 50±11 nm for 1.5 mol.L^{-1} of precursor concentration, respectively. As shown in Table 4.3, The crystallite size of powder was found to be 37±14 nm and 16±01 nm when synthesized in 0.5 mol.L^{-1} and 1.5 mol.L^{-1} of precursor concentration, respectively. It is interesting to note that the particle size becomes close to the crystallite size with increasing the precursor concentration indicating that the particles synthesized at high precursor concentration are composed of fewer crystallites. Generally, the size of the particles that precipitate out of solution be influenced by the relative rates of nuclei formation and crystallite growth. The high nucleation rate condition can produce a large number of small crystallites [120, 22/4]. At higher values of precursor concentration, a larger number of cation ions are diffusing in the solution leading to higher degree of supersaturation of perovskite and higher nucleation rate [18, 39]. As a result, the size of the final particles decreases with increasing precursor concentration while a large number of small crystallites are formed. The structural and morphological characterizations converge in demonstrating that the sonochemical synthesis process leads to the formation of the cubic $BaTiO_3$ phase with 100-nm grade nanopowders and a narrow size distribution.

Table 4.3 Fraction of Crystalline size and Particle size by Scherrer method and SEM, respectively as a function of the Starting solution concentration.

Starting solution concentration (mol.L^{-1})	Scherrer method Crystalline size (nm)	SEM Particle size (nm)
0.5	37 ± 14	123 ± 43
1.0	29 ± 9	94 ± 28
1.5	16 ± 1	50 ± 11

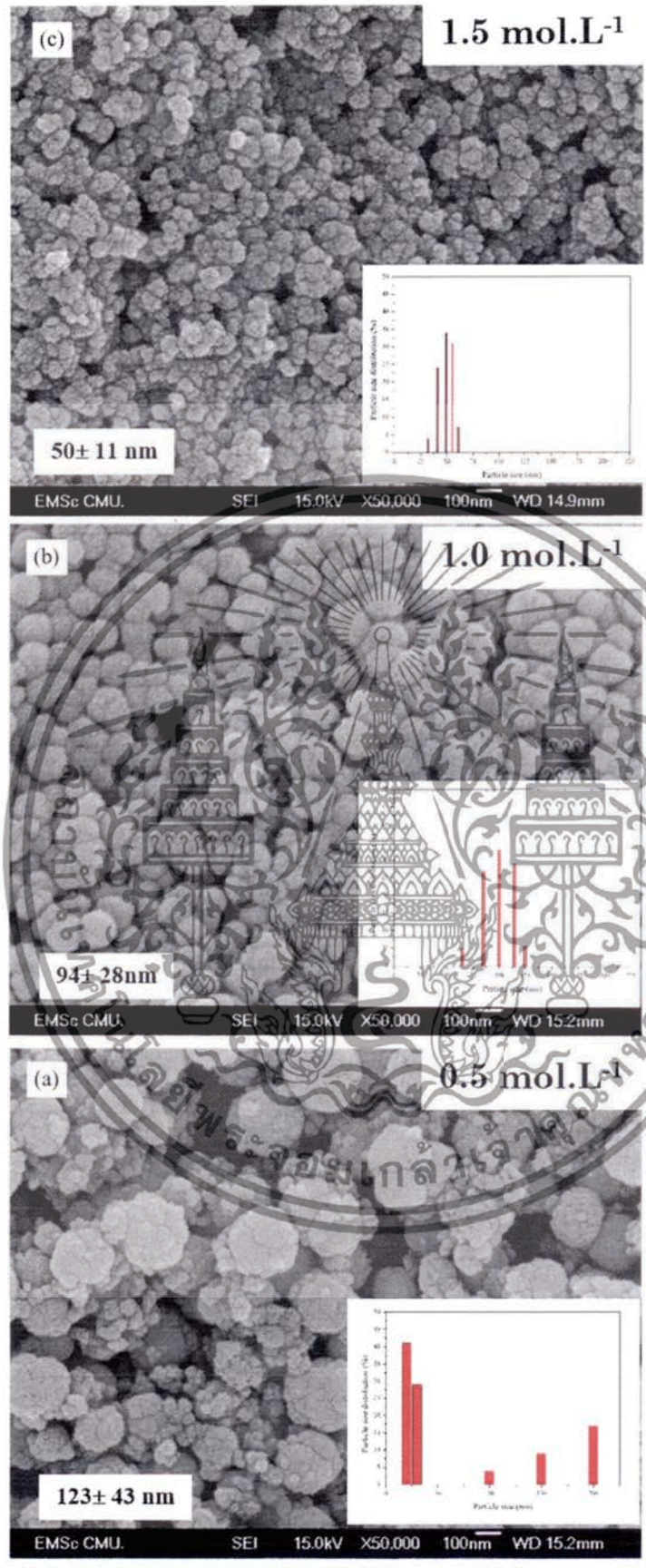

Figure 4.14 FE-SEM images of $Ba(Zr_xTi_{1-x})O_3$ (x = 0.0) powders that sonicated for 30 minutes at various the precursor solution concentrations with 20 $mol.L^{-1}$ NaOH in the Ar atmosphere.

4.4 The effect of the sonication time on the complex perovskite barium zirconium titanate ($Ba(Zr_xTi_{1-x})O_3$ phase formation.

In this section study the effect of the sonication time on the $Ba(Zr_xTi_{1-x})O_3$ (x = 0.0) phase formation in the Ar atmosphere. The 1 $mol.l^{-1}$ of barium and titanium solution were used as the stock of precursor solution, and used 20 $mol.L^{-1}$ NaOH as the precipitating agent. The Ba, Ti and Zr ion ratio in the mixed solution targeted constantly at 1:1:0. The mixture solution was irradiated with an ultrasonic horn for 5, 10, 15, 30 and 60 minutes at 80% of the maximum ultrasound irradiation amplitude. This study exposed the sonication time with a striking effects on the $Ba(Zr_xTi_{1-x})O_3$ (x = 0.0) morphology and size distribution.

Figure 4.15 shows the evolution of XRD pattern of $Ba(Zr_xTi_{1-x})O_3$ (x = 0.0) powders obtained after sonication for 5, 10, 15, 30 and 60 minutes in 20 $mol.L^{-1}$ NaOH in the closed system with Ar gas. The pure perovskite structure was observed clearly at 5 min sonication time by using a strong base solution (20 $mol.L^{-1}$ NaOH) and high precursor concentration (1.0 $mol.L^{-1}$), with the powder synthesized in a closed system with Ar gas. The $BaCO_3$ phase or unwanted phase were not found at all. However, the intensity of the perovskite phase is quite low indicating that the product has a low crystallinity. The crystallinity of the product was improved significantly with increasing time of ultrasonic irradiation. A sharp XRD pattern was observed clearly at 60 minutes sonication time. The XRD pattern indicates that the synthesized powder shows good agreement with the cubic $BaTiO_3$ structure with *Pm3m* space group (JCPDS file no. 31-0174). Increasing of sonication time, the intensity of the XRD pattern increased while the full width at haft-maximum (FWAH) value was decreased, indicating the nanocrystals tend to become larger. The average crystallite size of the powders obtained can be determined from the XRD pattern according to Scherrer's equation (Equation 4.3). The crystalline size calculated form Scherrer equation is summarized in Table 4.4 and confirmed this assumption

Raman spectra of powders products, synthesized at different ultrasonic reaction times with 20 $mol.L^{-1}$ NaOH in the closed system with Ar gas, are presented in Figure 4.16. As shown in Figure 4.16, the $BaCO_3$ phase disappeared after only five minutes sonication time. When increased the sonication time to 10 min, the Raman shift peaks located at around 181, 295, 521 and 707 cm^{-1} was appeared, which match well with the typical Raman peaks of $BaTiO_3$. The bands around 295 and 521 cm^{-1} are assigned to the transverse optical (TO) modes of A_1 symmetry, whereas the peak at 181 cm^{-1} arises due to interference from anharmonic coupling between the three A_1(TO)

phonons. The peak at 707 cm^{-1} is related to the highest frequency longitudinal optical mode (LO) with A_1 symmetry. Raman results are in agreement with the XRD result.

Figure 4.15 The XRD pattern of $Ba(Zr_xTi_{1-x})O_3$ (x = 0.0) powders synthesized at different ultrasonic reaction times with 20 $mol.L^{-1}$ NaOH in the closed system with Ar gas.

Figure 4.16 Raman spectrum of $Ba(Zr_xTi_{1-x})O_3$ (x = 0.0) powders synthesized at different ultrasonic reaction times with 20 mol.L^{-1} NaOH in the closed system with Ar gas.

The morphology and particle size were studied also by a field emission scanning microscope (FE-SEM). FE-SEM micrographs of all powder products, sonochemically synthesized at different ultrasonic reaction times with 20 mol.L^{-1} NaOH in closed system with Ar gas, are demonstrated in Figure 4.17. As shown in Figure 4.17 (a), nanocrystals of $Ba(Zr_xTi_{1-x})O_3$ (x = 0.0) was firstly formed under ultrasonic irradiation, and then nanocrystals readily agglomerated into aggregated particles in a short period of time in order to minimize the high surface energy. The particle size and shape of the cluster are difficult to identify. With increase the sonication time, the spherical in shape and uniform particle are observed clearly (Figure 4.17 (b-e)). Sphere-like particles were achieved evidently after 10 minutes of the sonication time, and the particle size slightly increased after 60 minutes under ultrasonic irradiation. In addition, the average grain size was increased from 68 ± 26 nm to 132 ± 20 nm in diameter by increasing the reaction times from 10 minutes to 60 minutes, respectively, as seen in Figure 4.9 (b-e) and summarized in Table 4.4. Furthermore, the particles showed a monosized spherical shape that was different from that in other wet chemical synthesizing methods [19, 20, 17/4, 25]. The products had a slightly spherical morphology, and the particle size distribution was rather narrow. Moreover, with increasing the sonication time further, the formation of neck between the particles was observed. The formation of neck is coursed by high velocity of interparticle collision generated by ultrasonic irradiation [Fig. 4(d)]. The high velocity of interparticle collision can make surface diffusion, as the melting point started from the surface area of nanoparticles [32]. Surface diffusion is a typical mass transport in the sintering mechanism that produces surface smoothing [39], particle joining [27, 23/4], grain boundary formation [32, 23/4], neck growth [23/4], and pore rounding. However, volume shrinkage and densification was not originate, due to the sonochemical method generated the local thermal energy which difference from thermal energy of the sintering process [26].

Table 4.4 Fraction of Crystalline size and Particle size by Scherrer method and SEM, respectively as a function of the sonication time.

Sonication time (min)	Scherrer method Crystalline size (nm)	SEM Particle size (nm)
10	21 ± 16	68 ± 26
15	26 ± 11	86 ± 24
30	29 ± 9	94 ± 28
60	31 ± 7	132 ± 20

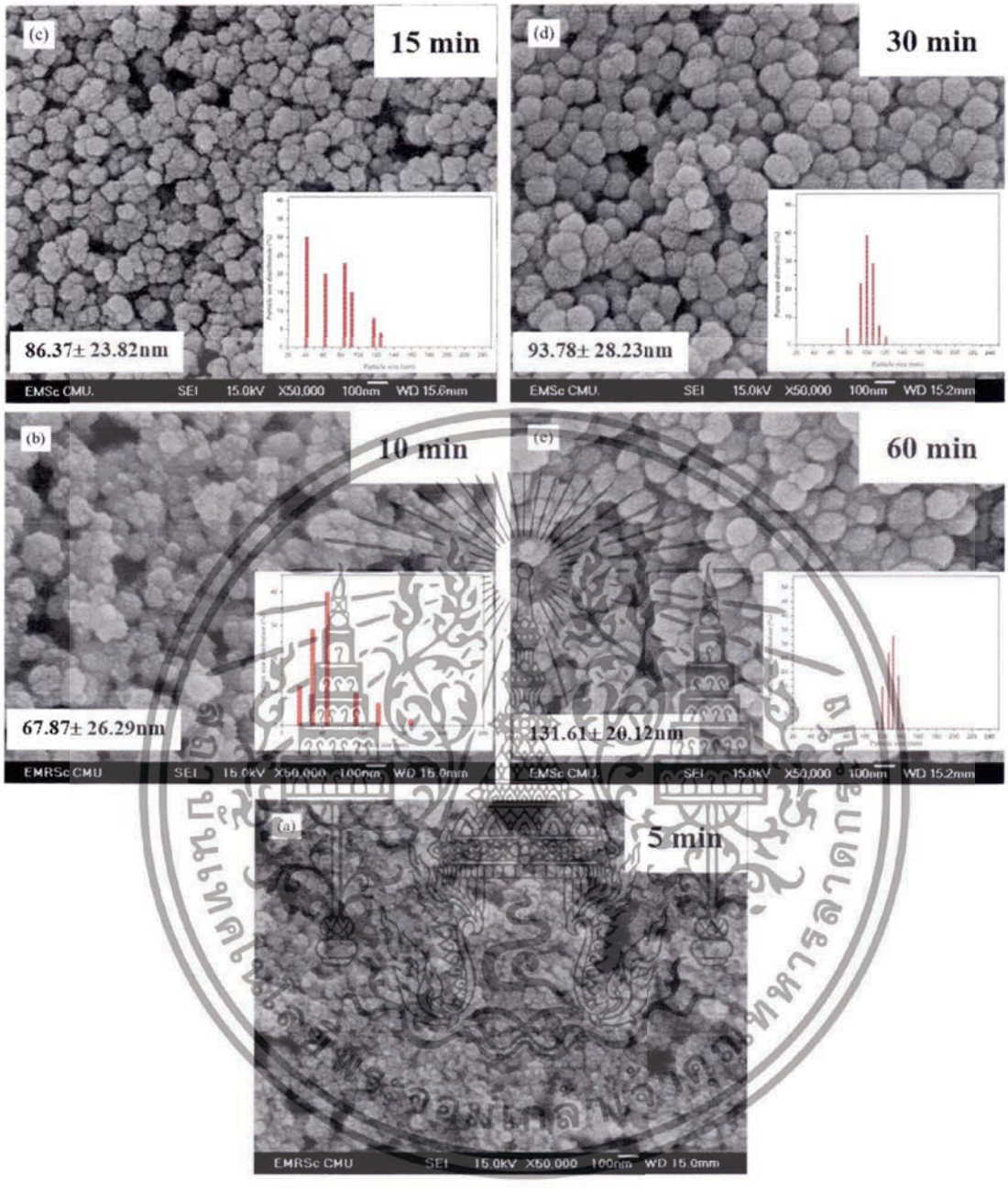

Figure 4.17 FE-SEM images of $Ba(Zr_xTi_{1-x})O_3$ (x = 0.0) powders synthesized at different ultrasonic reaction times with 20 mol.L^{-1} NaOH in the closed system with Ar gas.

4.5 The effect of the Zr/Ti molar ratio on the complex perovskite barium zirconium titanate ($Ba(Zr_xTi_{1-x})O_3$ phase formation.

In this section study the effect of the Zr/Ti molar ratio on the $Ba(Zr_xTi_{1-x})O_3$ (with x = 0.00, 0.05, 0.20, 0.40 and 0.60) phase formation in the close system with Ar gas. The 1 $mol.l^{-1}$ of barium, zirconium and titanium solution were used as the stock of precursor solution. The mixture solution was irradiated with an ultrasonic horn for 5 to 60 minutes at 80% of the maximum ultrasound irradiation amplitude in 20 $mol.L^{-1}$ NaOH.

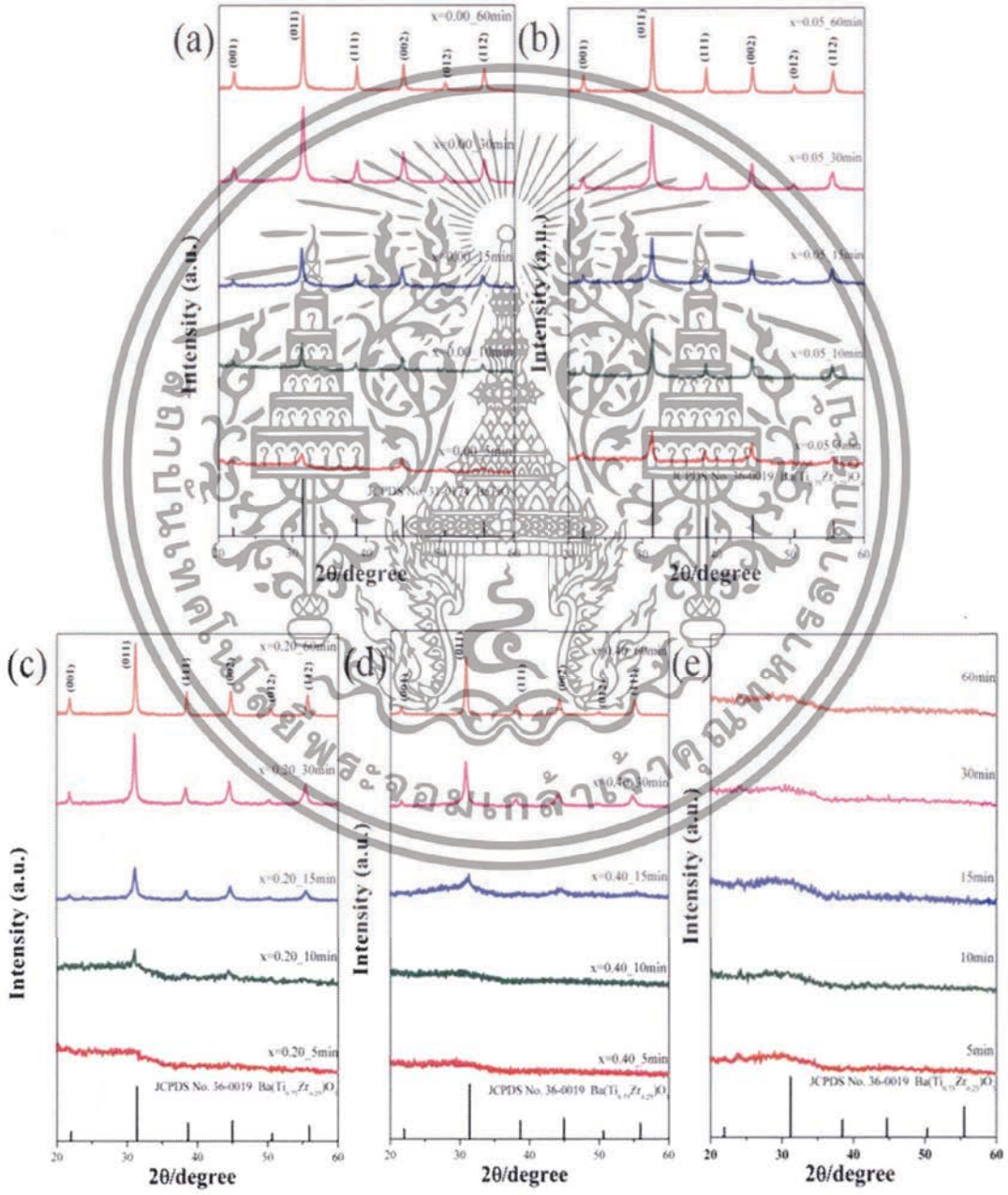

Figure 4.18 The XRD pattern of $Ba(Zr_xTi_{1-x})O_3$, with x = 0.00, 0.05, 0.20, 0.40 and 0.60 nanoparticles at different ultrasonic reaction times; (a) x = 0.00, (b) x = 0.05, (c) x = 0.20, (d) x = 0.40 and (e) x = 0.60.

The evolution of XRD patterns of $Ba(Zr_xTi_{1-x})O_3$; x = 0.00, 0.05, 0.20, 0.40 and 0.60 powders synthesized in different sonication times is shown in Figures 4.18. Figure 4.18 (a) (x = 0.00) shows the XRD pattern of the perovskite phase as observed at 5 minutes sonication time. There was no detection of the $BaCO_3$ phase or unwanted phase, which indicated that powder synthesized in Ar-gas can eliminate formation of the $BaCO_3$ phase. However, intensity of the perovskite phase was quite low, which meant that the powder had low crystallinity. High crystallinity was achieved by increasing sonication time. Sharp peaks of perovskite phase were observed for powder synthesized at 60 minutes sonication time. A similar trend was observed for the composition, x = 0.05 (Figure 4.18 (b)). By increasing the composition, x = 0.20 and 0.40, the XRD pattern of perovskite phase with low intensity started to form at 10 and 15 minutes sonication time, respectively (Figure 4.18 (c) and (d)). Intensity of the perovskite structure increased with increasing sonication time. XRD results indicated that when Zr concentration increases, the sonication time must be increased in order to obtain a pure perovskite phase. Sharp well-defined peaks were evident clearly in all products synthesized at 60 minutes sonication time. When compared to traditional solid state synthesis, the result indicated that the BZT phase was formed completely during the sonochemical synthesis, without further heating or calcination. However, as shown in Figure 4.18 (e), no strong crystal phases can be found from the XRD pattern for the composition x = 0.60, meaning that the samples are composed of an amorphous phase. The formation of amorphous phase might be related to the difference regions of sonochemical activity. It has been known that there are two regions of sonochemical activity, as postulated by Suslick and co-workers [26, 154]. One is the inside of the collapsing bubbles and the other is the interfacial region between the cavitation bubbles and the surrounding solution. The inside of the collapsing bubbles generate extremely high temperature (>5000 K), pressure (>20 MPa) and very high cooling rates (excess of 10^{10} $K.s^{-1}$), where the temperature in the interfacial region is much lower than the interior of the collapsing bubbles, it is still high enough to rupture chemical bonds and induce a variety of reactions [153]. If the reaction takes place inside the collapsing bubbles, the final product obtained is amorphous as a result of the extremely rapid cooling rate (>10^{10} $K.s^{-1}$) which occurs during the collapse. On the other hand, if the reaction occurs within the interfacial region, one would expect to get nanocrystalline products. In the present case, since amorphous powders were obtained at high Zr/Ti ratio, we propose that the formation of $Ba(Zr/Ti)O_3$ at high Zr/Ti ratio probably occurs inside the collapsing bubbles meanwhile the formation of $Ba(Zr/Ti)O_3$ at low Zr/Ti ratio probably occurs at interfacial region of the collapsing bubbles. Similar behavior was observed in stibnite (Sb_2S_3) nanorod that synthesized by sonochemical method [155]. Besides, another factor

might relate to the difference in formation constant of the complex metallic hydroxide network. At high Zr concentration, hetero-trimetallic Ba-Ti-Zr-hydroxide may have difficulty in forming a network [152]. All compositions of powders synthesized at 60 minutes sonication time were selected in order to identify the crystal structure.

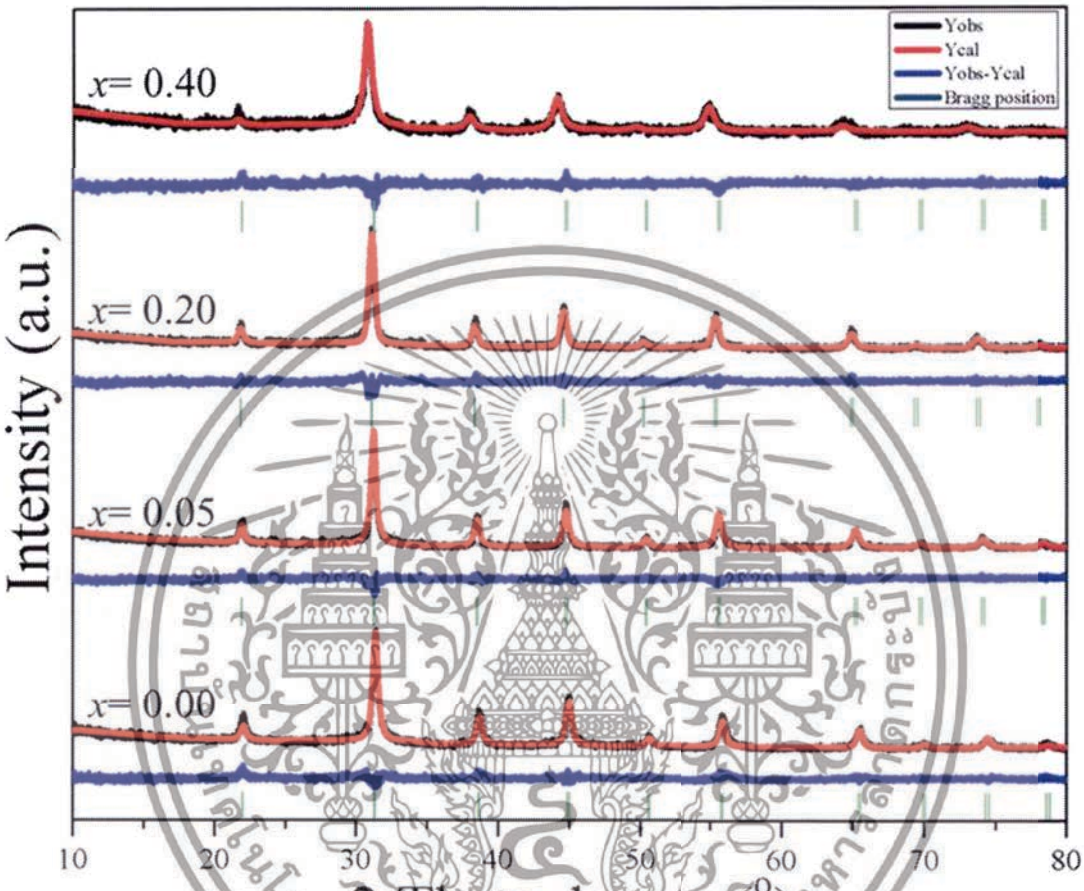

Figure 4.19 Rietveld refinement that fits $Ba(Zr_xTi_{1-x})O_3$, with x = 0.00, 0.05, 0.20 and 0.40 nanoparticles synthesized at 60 minutes ultrasonic irradiation time.

Figure 4.19 displays the XRD pattern of $Ba(Zr_xTi_{1-x})O_3$, with x = 0.00, 0.05, 0.20 and 0.40 nanoparticles, synthesized for 60 minuites sonication time. Characteristics of the tetragonal perovskite structure such as splitting (002) and (200) in a range from 44° to 46° were not observed in all of the samples. One symmetric peak observed at 2θ ~ 44° to 46° in all of the samples confirmed that all compositions had a cubic symmetry. This agreed well with previous reports that used a solid state and co precipitation method [40, 145, 156-157]. Furthermore, the XRD pattern displayed a

progressive peak shift toward the lower diffraction angle with increased Zr^{4+}. This phenomenon can be explained qualitatively with respect to the unit cell volume caused by the substitution of Zr^{4+} at the Ti-site. According to Shannon's effective ionic radii, with a coordination number of 6, the ionic radius of B-site ions (Zr^{4+}) has a radius of 0.86 Å, which is close to the radius of Ti^{4+} (0.745 Å) [157]. Therefore, Zr^{4+} can enter into the six fold coordinated B-site of the perovskite structure to substitute Ti^{4+}, due to radius matching. Rietveld refinement using data from 20° to 60° of the XRD results was conducted to achieve lattice parameters and the calculated unit cell volume (v) of $Ba(Zr_xTi_{1-x})O_3$,; x = 0.00, 0.05, 0.20, and 0.40 powders are also reported in Table 4.5. These values increase with increased Zr^{4+} content by replacing Ti^{4+}-site (0.745 Å) with large Zr^{4+} (0.86Å) ions, respectively. When compared with previous results of BZT powders prepared by a mixed oxide method, as reported by Chen et al. [156], the sonochemical BZT powder transition from tetragonal to cubic phase did not occur, whereas the solid state reaction power phase transition occurred at x = 0.20. The absence of phase transition in BZT powder synthesized by the sonochemical method might be related to some entrapped hydroxyl groups on the crystal surface or in the crystal lattice. It is well known that many wet chemical syntheses generate OH species in the solution during the process, and OH groups are incorporated easily into the perovskite lattice, as defects are shown to be similar to a "loose packed" structure. Ordinarily, hydroxyl (-OH) groups play an important role in the synthesis of perovskite nanopowders via wet-chemical processes, especially in a very high OH^- concentration (pH > 12) [127, 138, 160-163]. The powder products can contain much chemical bonding with the two types of OH- species. Weakly bonded OH- species are adsorbed on particle surfaces, while strongly bonded OH- species are entrapped in the crystal lattice, to form lattice OH- defects [127]. These defects can affect the stability of lattice vibration and decrease tetragonality to form a metastable cubic phase, which leads to the absence of phase transition [127].

According to the literature [158, 159], the quality of data from structural refinement is checked generally by R-values (R_p, R_{exp}, R_{wp}), and the appropriate fit (G), which is defined by $G^2=X^2$. X^2 or "Chi squared", can be determined from the expected and weighted profile of R factors ($X^2 = (R_{wp}/R_{exp})^2$). Additionally, the difference between experimental profiles of XRD patterns and calculated data varies slightly in scale of intensity, as illustrated by the line, $Y_{observed}$-$Y_{calculated}$. Furthermore, the crystalline size of all compositions was calculated using the Scherer equation from the FWHM of the 110 planes in the XRD pattern, which is shown in Table 4.6. The crystalline size decreased with increasing the Zr^{4+} content.

Table 4.5 The lattice parameter, Unite cell volume and X^2 of $Ba(Zr_xTi_{1-x})O_3$, with x = 0.0, 0.05, 0.2 and 0.4 nanoparticles.

Composition	Lattice parameter (a) (Å)	Unite cell volume (v) (Å^3)	X^2
x = 0.00	4.0295 ± 0.0004	65.43	1.1770
x = 0.05	4.0432 ± 0.0003	66.10	1.0293
x = 0.20	4.0641 ± 0.0004	67.12	1.2619
x = 0.40	4.0931 ± 0.0011	68.57	1.3481

The Raman spectra were clearly showed in Figure 4.20. All the Raman peaks of the composition x = 0.00, 0.05, 0.20 and 0.40 were similarly observed. The 4 broadening peaks at around 186, 303, 522 and 715 cm^{-1} are assigned to the [A_1(TO) + E(LO)], [A_1(TO)], [E, A_1(TO)] and [A_1, E(LO)] Raman-active modes of tetragonal (*P4mm*) symmetry [160]. It is noteworthy that despite the XRD data (Figure 4.18) shows the cubic (*Pm3m*) symmetry, whereas the Raman spectra show the tetragonal (*P4mm*) crystal structure. This is because of the hydroxyl defect from high basic environment. The OH^- groups can substitute in sub-lattice to form metastable cubic phase. However, hydroxyl defect existed as the interstitial defects in many unit cells but not all. So, some unit cell can stabilize in tetragonal structure. Nevertheless, the characterization by using XRD gives the results in a static and average symmetry while the result in a dynamic and local symmetry could be characterized by Raman spectroscopy [160]. Therefore, the Raman results were not correlated with the results from XRD data in this situation. In fact, the crystal structure of product powders may exhibit the mixture between tetragonal and cubic crystal structure. However, the hydroxyl defects could be removed by chemical treatment with DMF [127, 163]. From the literature, the OH^- species on particle surfaces could be eliminated by thermal heat treatment above 300°C, and above 1,100°C for eliminating the lattice OH^- species [127, 162-163]. Moreover, this Figure also revealed that all of Raman peaks disappeared when the composition (x) of Zr/Ti ratio was increased to 0.60. The present of very broad hump demonstrated the predominantly amorphous phase character. This result can confirm that the product powder at this condition was stabilized in the amorphous phase.

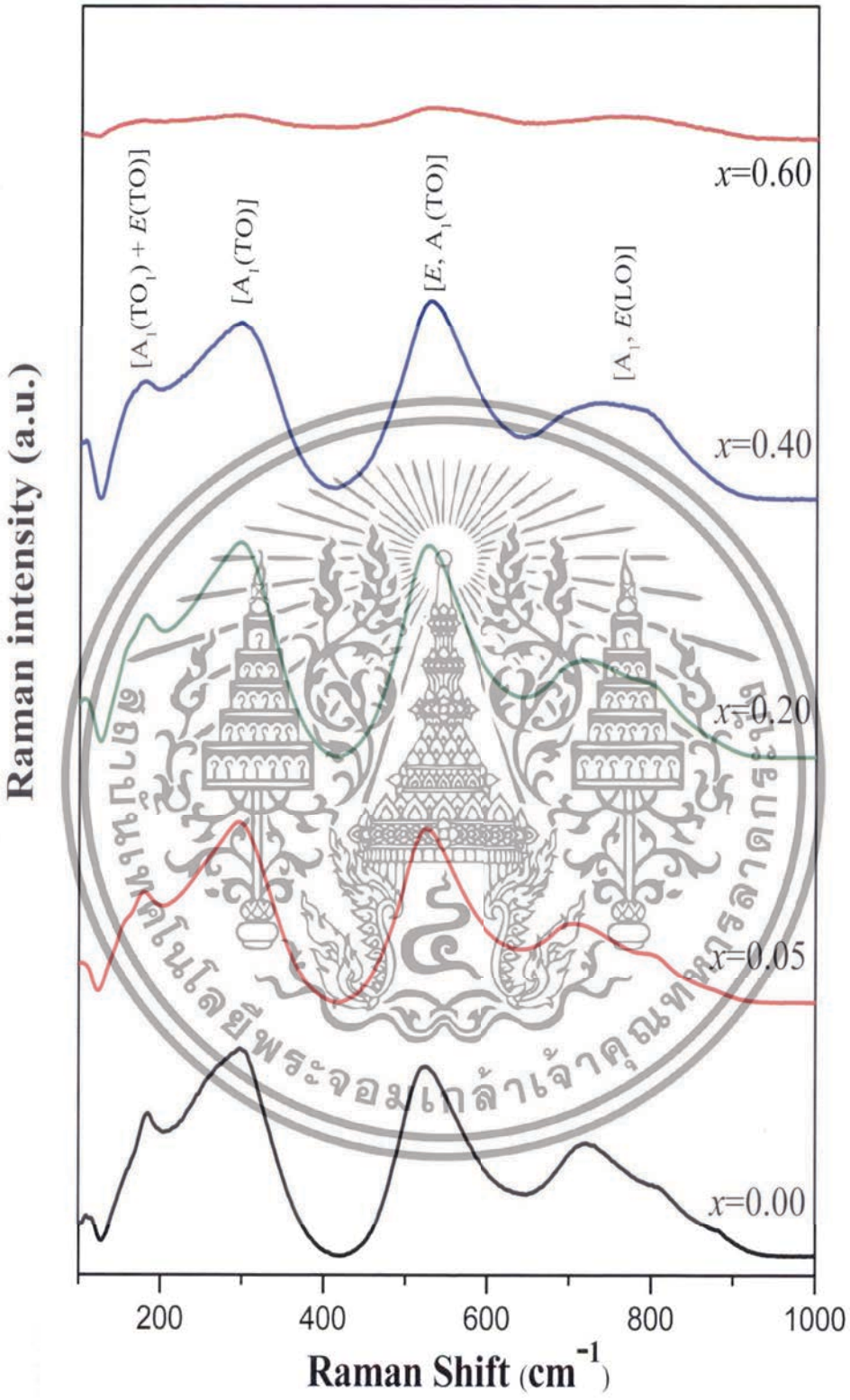

Figure 4.20 Raman spectrum of $Ba(Zr_xTi_{1-x})O_3$, with x = 0.00, 0.05, 0.20, 0.40 and 0.60 powders synthesized at 60 minutes sonication time.

Figure 4.21 FT-IR spectrum of $Ba(Zr_xTi_{1-x})O_3$, with x = 0.00, 0.05, 0.20, 0.40 and 0.60 powders synthesized at 60 minutes sonication time.

Furthermore, the FT-IR spectrum of product powders at various Zr/Ti ratios were studied and reported in Figure 4.21. The appearance of the band at around 3,600 and 1,600 cm^{-1} for all composition are attributed to O-H stretching and O-H bending vibration, respectively. For the corresponding of previously result, it may believe that the O-H vibration bands in composition of 0.00 - 0.40 Zr/Ti ratios come from the OH^- defects, which existed on surface particles and in sub-lattice. On the other hand, the O-H vibration band in 0.60 composition of Zr/Ti ratio may from the mixture between OH^- species defects and -OH groups from amorphous phase. Moreover, the absorption peak at around 520 cm^{-1} was used to indicate the difference of trimetallic Ba-Ti-Zr hydroxides amorphous and crystalline BZT phase. This peak mainly assigned to the characteristic peak of perovskite structure, associating with the absorption vibration of Ti-O and Zr-O asymmetric stretching in BO_6 octahedra [20, 138]. The 0.00-0.40 composition showed the strong of this vibration band, thus confirming that the product powders at these conditions were formed of BZT solid solution without the impurity and/or the other phases. Interestingly, the BO_6 vibration band was disappeared for 0.60 composition of Zr/Ti ratio while the O-H absorption band exhibit large intensity. This suggested that the BZT solid-solution phase was not found at this condition. So, it can confirm that the product powder maystabilized in the form of trimetallic Ba-Ti-Zr hydroxides amorphous phase. The result from FT-IR spectra showed corresponding well with the result form XRD (Figure 4.19) and Raman spectra (Figure 4.20).This observation clearly demonstrates that the multicaticnic perovskite $Ba(Zr_xTi_{1-x})O_3$; x = 0.0 — 0.4 solid solution was formed completely during the sonochemical process itself, without the need of further calcination or a heating process.

The morphology and particle size were studied also by FE-SEM, and FE-SEM micrographs of all aggregated particle products, sonochemically synthesized for 60 minutes of ultrasonic irradiation, are demonstrated in Figures 4.22, with the average particle size shown in Table 4.6. The difference between the XRD crystallite size and SEM particle size is thought to associate with the existence of a hierarchical structure [145]. The SEM particle size may stem from a secondary mesostructure consisting of a primary crystallite size. A large number of BZT nanocrystals were created initially from the Ti- and Zr- based precursor under ultrasound irradiation before aggregating BZT particles from large particles. The BZT particles showed a monosized spherical shape different from that in other preparation methods [8, 156, 164]. The products showed a spherical or almost spherical morphology, and the particle size distribution was rather narrow.

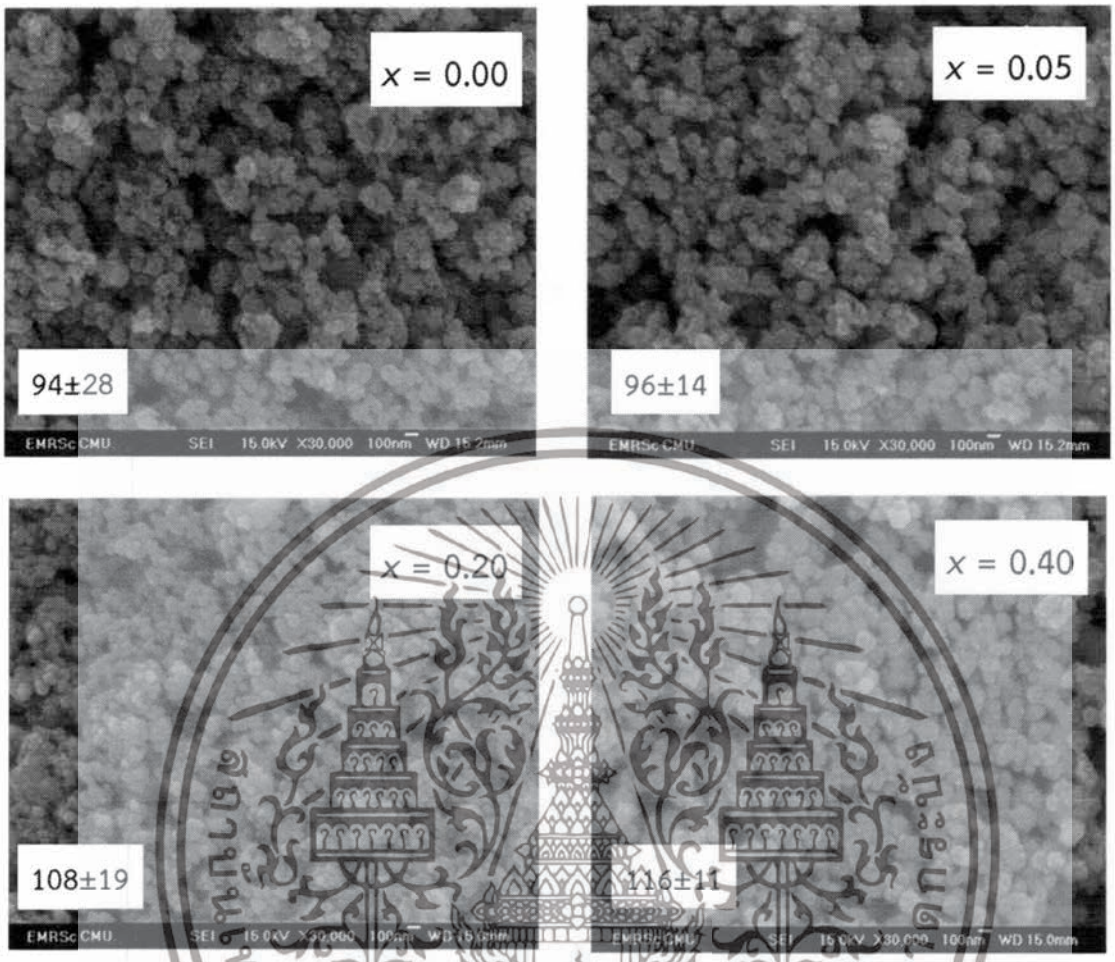

Figure 4.22 FE-SEM images of $Ba(Zr_xTi_{1-x})O_3$, with x = 0.00, 0.05, 0.20, and 0.40 powders synthesized at 60 min sonication times.

Table 4.6 The crystallite size and particles size of $Ba(Zr_xTi_{1-x})O_3$, with x = 0.0, 0.05, 0.2 and 0.4 nanoparticles.

Composition	*Crystallite size (nm)*	*Perticle size (nm)*
x = 0.00	29 ± 9	94 ± 28
x = 0.05	30 ± 7	96 ± 14
x = 0.20	33 ± 13	108 ± 19
x = 0.40	34 ± 12	116 ± 11

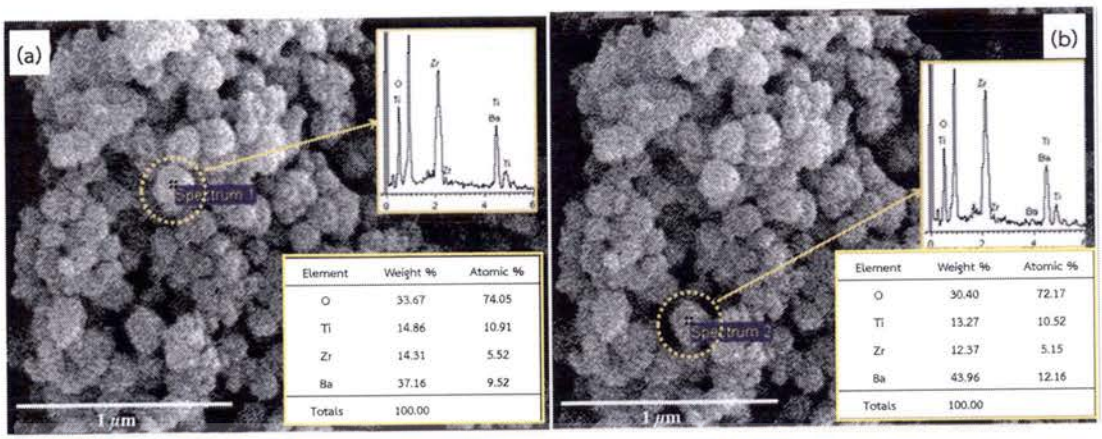

Figure 4.23 FE-SEM image and the energy dispersive X-ray (EDX) patterns of $Ba(Zr_xTi_{1-x})O_3$, with x = 0.40 powders synthesized at 60 min sonication time.

The SEM/EDX analysis at different points on the surface of individual particles was performed in order to confirm the homogeneity of the powder products. Figure 4.23 (a) and (b) display the EDX spectra at different points on the surface of individual particles. It can be seen from these figures that the concentrations of various elements (Ba, Ti, Zr and O) involved in the individual particle are very close to each other indicating to the homogeneity of the powder products. The result from SEM/EDX spectra showed good correspondence with the result from XRD (Figure 2.19). This observation clearly demonstrates that the multicationic perovskite $Ba(Zr_xTi_{1-x})O_3$, with x = 0.0–0.4 solid solution was formed completely during the sonochemical process itself, without the need for further calcination or a heating process.

4.6 The effect of the power of ultrasound irradiation on the complex perovskite barium zirconium titanate ($Ba(Zr_xTi_{1-x})O_3$ phase formation.

In this section study the power of ultrasound irradiation on the $Ba(Zr_xTi_{1-x})O_3$ (with x = 0.00 and 0.40) phase formation in the close system with Ar gas. The 1 $mol.l^{-1}$ of barium, zirconium and titanium solution were used as the stock of precursor solution. The mixture solution was irradiated with an ultrasonic horn for 30 min at 20%, 40% and 80% of the maximum ultrasound irradiation amplitude in 20 $mol.L^{-1}$ NaOH.

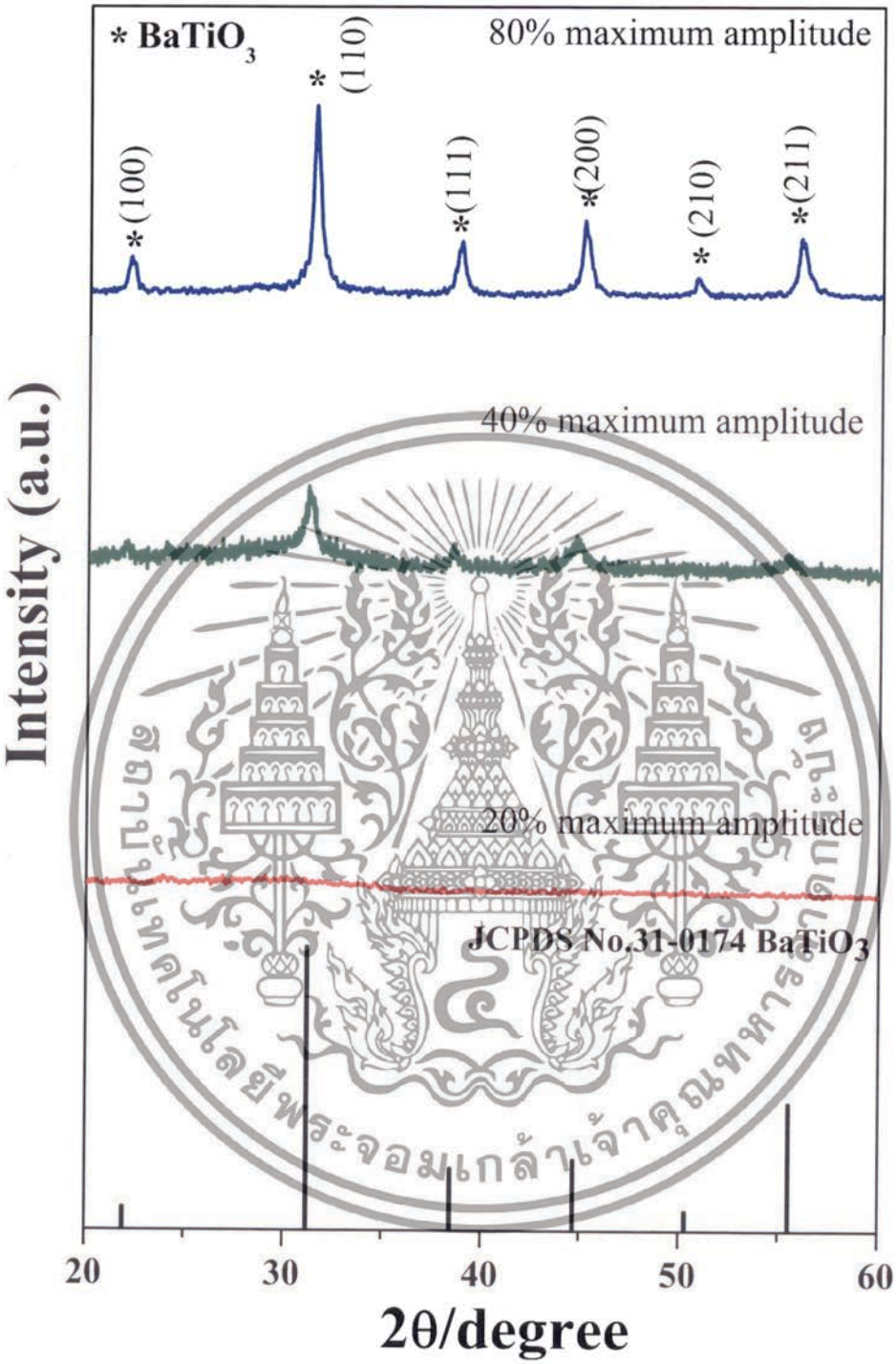

Figure 4.24 The XRD pattern of $Ba(Zr_xTi_{1-x})O_3$, with x = 0.00, nanoparticles at different power of ultrasound irradiation.

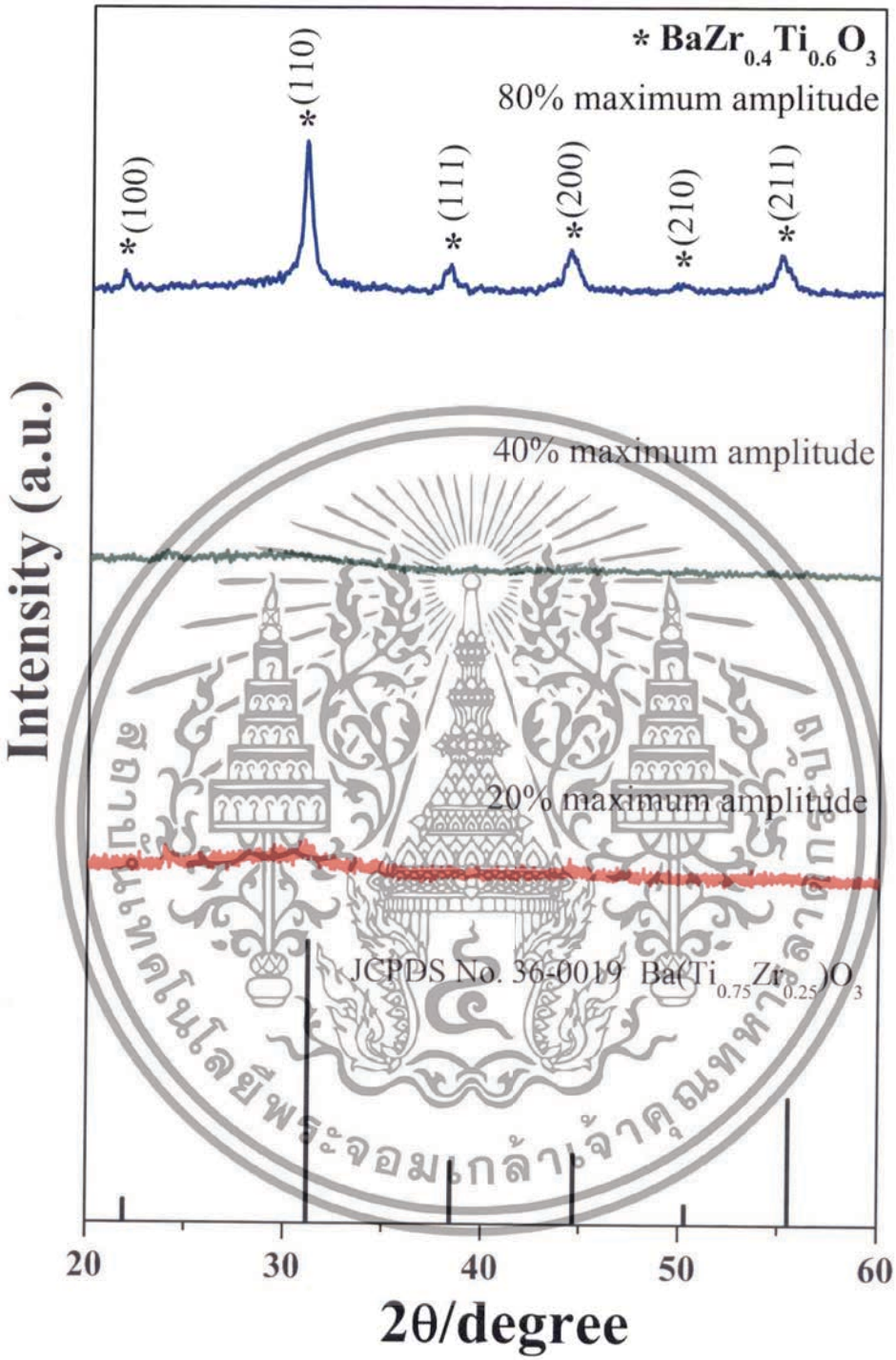

Figure 4.25 The XRD pattern of $Ba(Zr_xTi_{1-x})O_3$, with x = 0.40, nanoparticles at different power of ultrasound irradiation.

The evolution of XRD patterns of $Ba(Zr_xTi_{1-x})O_3$ with x = 0.0 and 0.40 powders, respectively synthesized in different power of ultrasound irradiation is shown in Figures 4.24 and 4.25. Figure 4.24 shows the XRD pattern of the $Ba(Zr_xTi_{1-x})O_3$ with x = 0.00 powders as observed at 40% of the maximum ultrasound irradiation amplitude that the samples are composed of an amorphous phase. One is the inside of the collapsing bubbles and the other is the interfacial region between the cavitation bubbles and the surrounding solution. The inside of the collapsing bubbles generate extremely high temperature, pressure and very high cooling rates, where the temperature in the interfacial region is much lower than the interior of the collapsing bubbles, it is still high enough to rupture chemical bonds and induce a variety of reactions. At 40% of the maximum ultrasound irradiation amplitude. There was no detection of the $BaCO_3$ phase or unwanted phase, which indicated that powder synthesized in Ar-gas can eliminate formation of the $BaCO_3$ phase. However, intensity of the perovskite phase was quite low, which meant that the powder had low crystallinity. High crystallinity was achieved by increasing power of ultrasound irradiation to 80% of the maximum ultrasound irradiation amplitude. For the $Ba(Zr_xTi_{1-x})O_3$ with x = 0.40 powders, as shows in Figure 4.25, the XRD pattern of perovskite phase as observed at 80% of the maximum ultrasound irradiation amplitude. XRD results indicated that when Zr concentration increases, the amplitude of the ultrasound irradiation must be increased in order to obtain a pure perovskite phase. Sharp well-defined peaks were evident clearly in all products synthesized at 80% maximum amplitude of the ultrasound irradiation. As shown in Figure 4.24 and 25, no strong crystal phases can be found from the XRD pattern for the composition x = 0.00 at 20% of the maximum ultrasound irradiation amplitude and at < 40% of the maximum ultrasound irradiation amplitude of the composition x = 0.40, meaning that the samples are composed of an amorphous phase. The formation of amorphous phase might be related to the difference regions of sonochemical activity. It has been known that there are two regions of sonochemical activity, as postulated by Suslick and co-workers [26, 154]. One is the inside of the collapsing bubbles and the other is the interfacial region between the cavitation bubbles and the surrounding solution. The inside of the collapsing bubbles generate extremely high temperature (>5000 K), pressure (>20 MPa) and very high cooling rates (excess of 10^{10} $K.s^{-1}$), where the temperature in the interfacial region is much lower than the interior of the collapsing bubbles, it is still high enough to rupture chemical bonds and induce a variety of reactions [153]. If the reaction takes place inside the collapsing bubbles, the final product obtained is amorphous as a result of the extremely rapid cooling rate (>10^{10} $K.s^{-1}$) which occurs during the collapse. On the other hand, if the reaction occurs within the interfacial region, one would expect to get nanocrystalline products. In the present case, since amorphous powders were

obtained at low power of the ultrasound irradiation, we propose that the formation of $Ba(Zr_xTi_{1-x})O_3$ probably occurs inside the collapsing bubbles meanwhile the formation of $Ba(Zr_xTi_{1-x})O_3$ at high power of the ultrasound irradiation probably occurs at interfacial region of the collapsing bubbles.

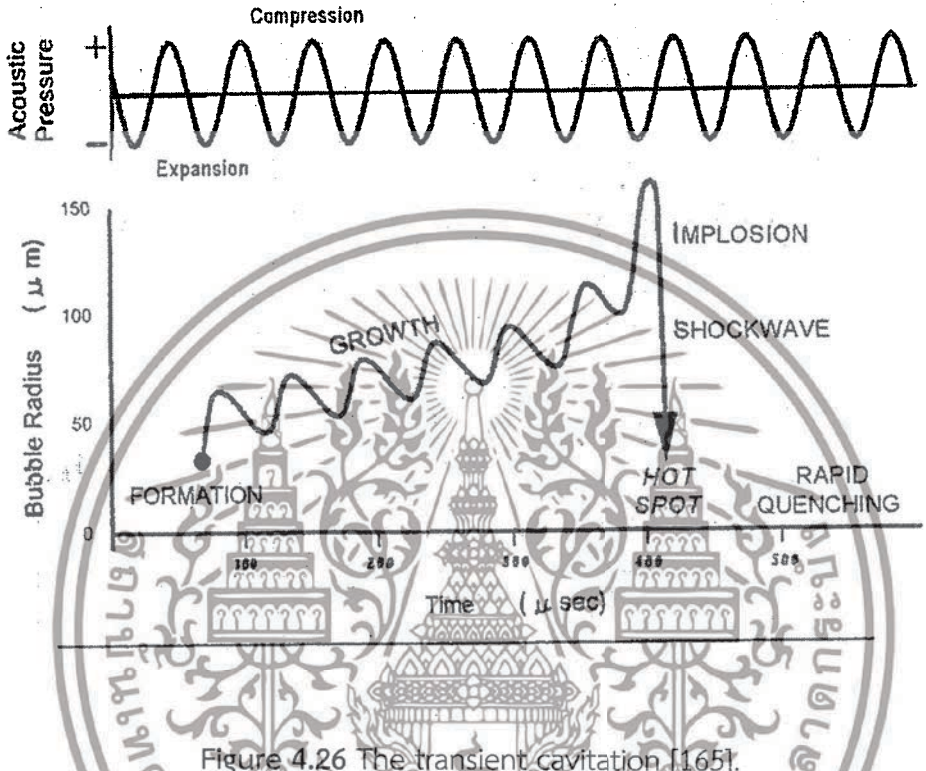

Figure 4.26 The transient cavitation [165].

This study exposed the power of ultrasound irradiation with a striking effects on the $Ba(Zr_xTi_{1-x})O_3$ (x = 0.0) phase formation. The sonochemical method uses an acoustic cavitation phenomenon from ultrasonic irradiation to generate or accelerate the chemical reaction. Acoustic cavitation is the formation, growth, and implosive collapse of bubbles in a liquid, which generates a localized hot spot, with a temperature of approximately 5,000 K, pressure of 20 MPa, and heating and cooling rates that exceed 10^{10} $K.s^{-1}$ [166]. These transient, localized hot spots can drive many chemical reactions, such as decomposition, dissolution, oxidation, reduction, and promotion of polymerization [166], as shown in Figure 4.26. Thus, the use high power of the ultrasound irradiation, spend less time at the lower power of the ultrasound irradiation.

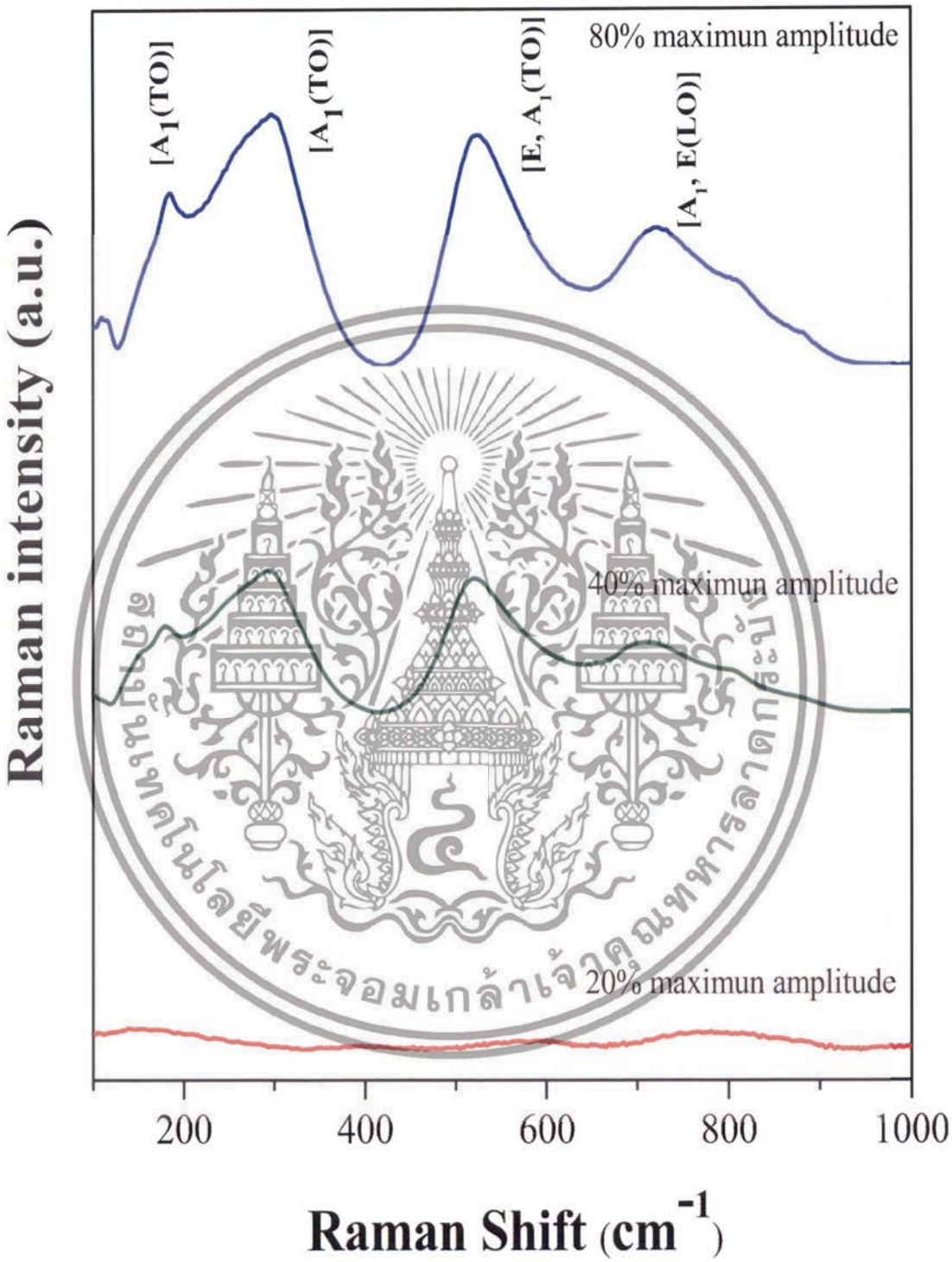

Figure 4.27 The Raman spectrum of $Ba(Zr_xTi_{1-x})O_3$, with x = 0.00, nanoparticles at different power of ultrasound irradiation.

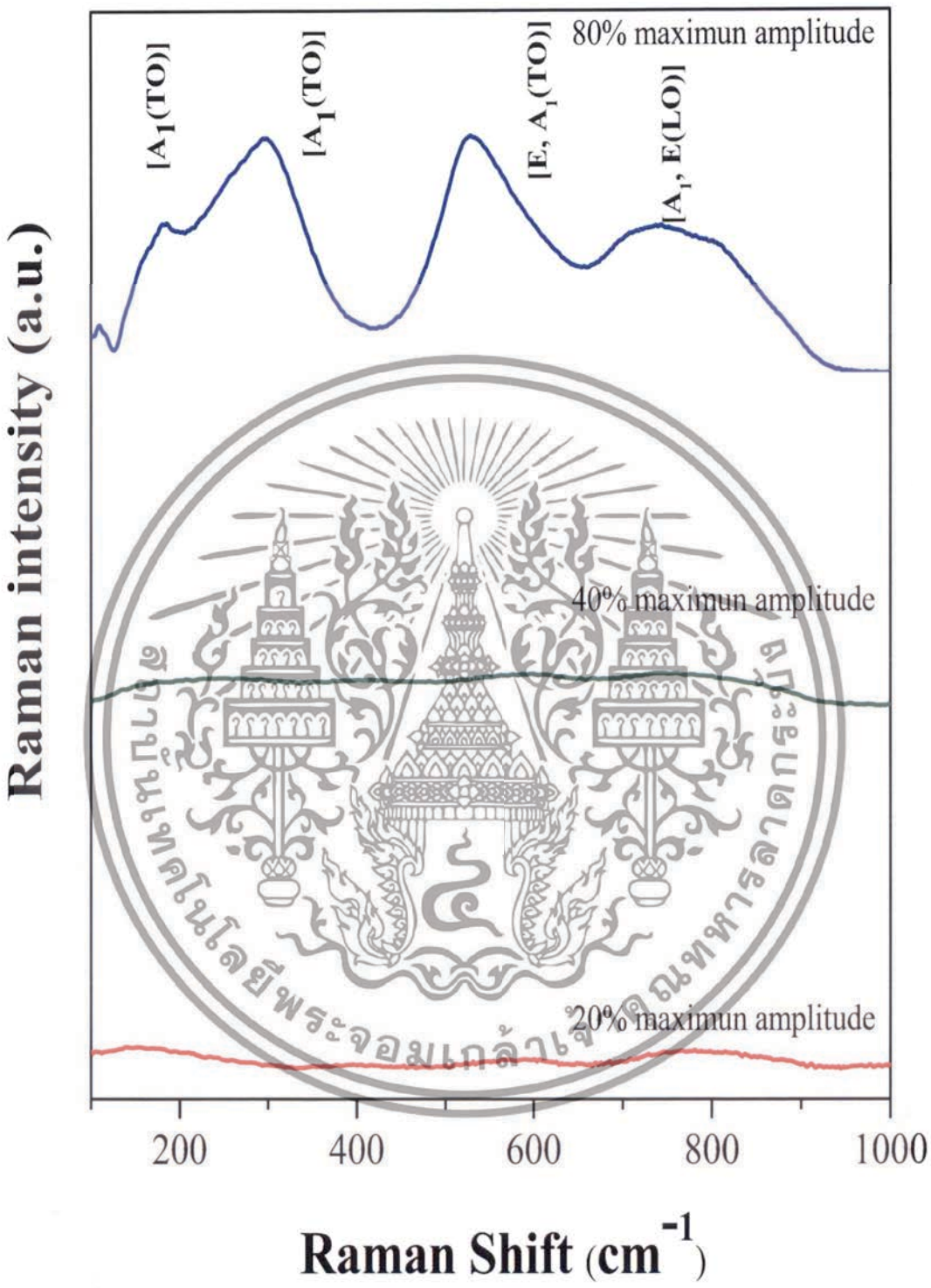

Figure 4.28 The Raman spectrum of $Ba(Zr_xTi_{1-x})O_3$, with x = 0.40, nanoparticles at different power of ultrasound irradiation.

The Raman spectra were clearly showed in Figure 4.27 and 4.28. All the Raman peaks of the composition x = 0.00, and 0.40, respectively were similarly observed. The 4 broadening peaks at around 186, 303, 522 and 715 cm^{-1} are assigned to the [A_1(TO) + E(LO)], [A_1(TO)], [E, A_1(TO)] and [A_1, E(LO)] Raman-active modes of tetragonal (*P4mm*) symmetry at 80% of the maximum ultrasound irradiation amplitude. From the XRD and Raman results indicated that increasing the Zr^{4+} substitution in $Ba(Zr_xTi_{1-x})O_3$ compound, the maximum amplitude of the ultrasound irradiation must be increased in order to obtain a pure perovskite phase.

4.7 Mechanism of crystal growth formation.

Based on the results achieved at different synthetic parameters, the perovskite phase formation of the $Ba(Zr_xTi_{1-x})O_3$ spheres involved the crystallization process and was similar to mechanical stirring [167]. A plausible mechanism to explain all of these data is shown in Figure 4.29.

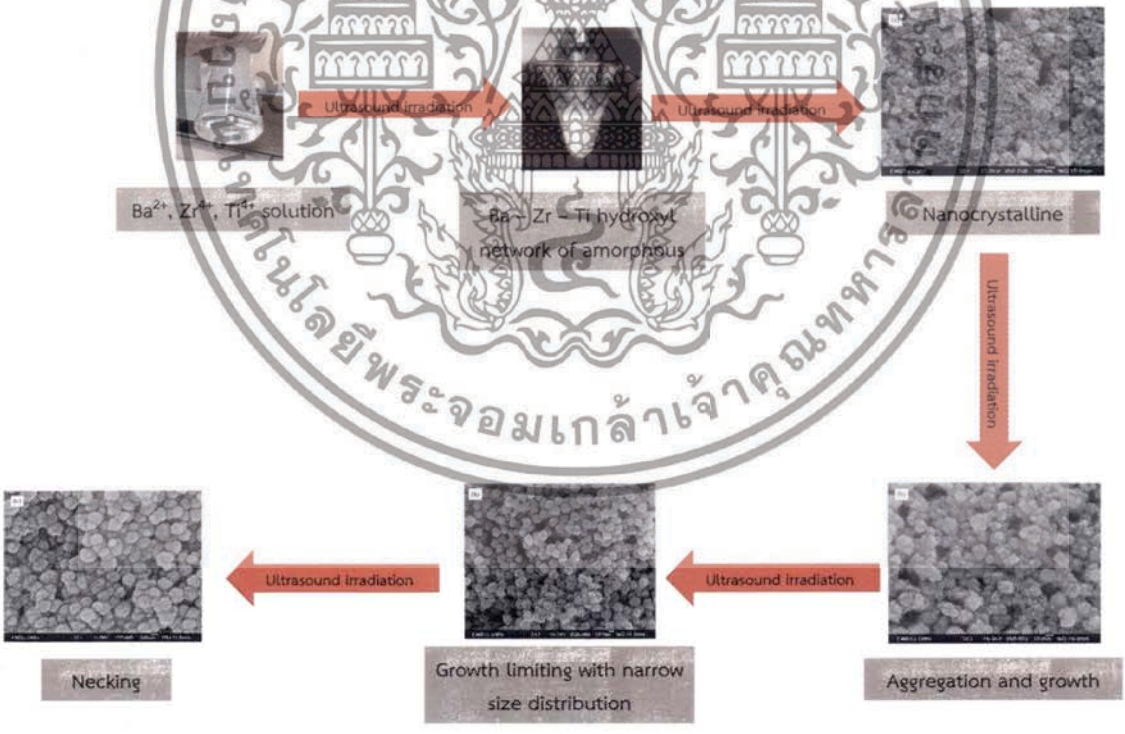

Figure 4.29 Schematic diagrams illustrating formation of the crystal growth mechanism.

The first stage of the synthesis is the formation of complex network of amorphous phase. The formation of complex network of amorphous phase was assumed to be as flows: barium cations formed $Ba(OH)^+$ species in the NaOH concentration. Furthermore, titanium and zirconium cations were readily hydrolyzed in NaOH solutions to form soluble $Ti(OH)_6^{2-}$ and $Zr(OH)_5^-$ anions. The formation of hexahydraxy titanate(IV) and pentahydraxy zirconate (IV) $[Zr(OH)_5]^-$ in the presence of strong alkaline condition were described also by N.C Pramanik *et al* [135] and Boshini *et al* [168] respectively. The reaction between $Ba(OH)^+$ $Zr(OH)_5^-$ and $Ti(OH)_6^{2-}$ initiated the formation of gels composed of entangled complex network of polymeric chains of trimetallic Ba-Ti-Zr hydroxides. The skeleton of the polymer corresponds to Ba, Ti and Zr atom linked by bridging O atoms.

The second stage of synthesis is the accelerated the formation of tiny primary particulates (crystallization) of BZT by ultrasonic irradiation. The results presented in the previous section indicate strongly that formation of BZT is dominated by a nucleation and growth mechanism. When the complex network of amorphous phase was irradiated by ultrasonic, the formation, growth, and implosive collapse of bubbles (microjet effect) in liquid medium generate extreme synthesis condition (localized hot spot with high temperature of ca. 5000 K, pressure of ca. 20 MPa, and a very high cooling rate of ca. 10^{10} $K.S^{-1}$). Also, due to vaporization of the solvent into bubbles, solubility of the reactants was enhanced, thus elevating supersaturation of the reactant solutions. In the conventional crystallization process from a solution, two steps are involved; nucleation and crystal growth, of which both have supersaturation as a common driving force. Crystals in the supersaturated solution can neither form nor grow. The nucleation rate in the crystallization process is small and only few nuclei can be generated at the initial time of growth. Then, nuclei grow in spatial orientations fixed by solute crystallized structures. However, nucleation in the sonocrystallization process was accelerated by the implosive collapse of bubbles, while the crystal growth process was inhibited or delayed by shock waves and turbulent flow created by ultrasonic radiation [26, 39]. This effect promoted nucleation over grain growth to form tiny primary particulates (crystalline), which tended to aggregate into large particles due to tremendous surface energy; and stability of the particles can be expressedas [169, 170]:

$$S = (R_a + R_b) \int_{R_a - R_b}^{\infty} \exp\left[\frac{V(C)}{k_B T}\right] \frac{dC}{C^2} \quad (4.4)$$

where S is the stability factor of the particles, R_a and R_b are the radius of the two particles, respectively, $V(C)$ is the function of potential energy interaction, C is the distance between the two particles, k_B is Boltzmann's constant (1.3806×10^{-23} $J.K^{-1}$)and T is the temperature (K). When the distance between particles is decreased to a certain extent, short-range reactions (van der Waal's forces and existence of an electrostatic barrier) lead to strong attraction between particles [169, 170].

The third stage of synthesis is forming spherical particles with a narrow size distribution. The turbulent flow and mechanical effects, such as microjet impact and shock waves that generate from the implosive collapse of bubbles under ultrasonication [32, 154], can create a relatively uniform reaction in fluid medium [32, 154], which improves the spherical shape of monodispersed BZT particles. Microjets with a high velocity of over 400 km/hcrush the aggregated cluster in all directions [128, 136], and nanocrystalline particles are driven together at extremely high speeds, thus inducing effective melting at the point of impact [26, 153]. These phenomena generate relatively monodispersed particles with a narrow size distribution. Furthermore, when increasing the sonication time further, neck formation was observed between the particles, caused by high velocity of the interparticle collision generated by ultrasonic irradiation [153]. Suslick *et.al.* [153, 154] proposed that the effects of cavitation in the phenomenon of interparticle collisions comes from the shock waves released into liquid and not from the temperature of the localized hot-spot formed within the collapsing bubble. It is interesting to note thatvolume shrinkage and densification did not originate, due to the sonochemical method that generated local thermal energy, which differed from thermal energy of the sintering process.

CHAPTER 5

CONCLUSIONS AND SUGGESTION

5.1 Conclusions

The complex perovskite structure $Ba(Zr_xTi_{1-x})O_3$ nanopowders were synthesized directly under ultrasonic irradiation in the sonochemical synthesis method without any calcination step. The concentration of NaOH, concentration of precursor, synthesized atmosphere and ultrasonic irradiation time played a key role in the formation of perovskite structure. The strong NaOH concentration and high precursor concentration not only initiated nucleation but also eliminated the formation of $BaCO_3$. The nanocrystalline was formed in a short period of time and then aggregated to form large particles. Narrow size distribution was acquired for the aggregated particles under ultrasonic irradiation. However, the synthesized powder has some OH group trapped into the crystal lattice coursed by strong OH concentration during the synthesis method. The plausible crystal growth mechanism was proposed in this work.

5.2 Suggestion and guidelines for further study

5.2.1 Should study the influence of the solvent on the morphology size distribution of the $Ba(Zr_xTi_{1-x})O_3$ nanopowders.

5.2.2 Study the preparation the high density of $Ba(Zr_xTi_{1-x})O_3$ ceramics from the $Ba(Zr_xTi_{1-x})O_3$ nanopowders.

5.2.3 Should study the electrical properties of $Ba(Zr_xTi_{1-x})O_3$ nanopowders; such as properties of the dielectric, piezoelectric and ferroelectric.

REFERENCES

[1] Y. I. Li, K. Moon, C. P. Wong, "Electronics without lead", science 308 (2005) 1419-1420.

[2] W. W. Wolny, "European approach to development of new mentally sustainable electroceramics", Ceram. Int. 30 (2004) 1079-1083.

[3] J. Rodel, W. Jo, K. T. P. Seifert, E. M. Anton, T. Granzow, D. Damjanovic, "Perspective on the development of lead-free piezoceramics", J. Am. Ceram. Soc. 92 (2009) 1153-1177.

[4] D. Maurya, M. Murayama, A. Pramanick, W. T. Reynolds, K. Song, M. H. Kim, W. J. Kim, "Origin of high piezoelectric response in A-site disordered morphotropic phase boundary composition of lead-free piezoelectric $0.93(Na_{0.5}Bi_{0.5})TiO_3$–$0.07BaTiO_3$", Apppl. Phys. 113 (2013) 114101.

[5] V. V. Shvartsman, D. C. Lupascu, "Lead-free relaxor ferroelectrics", J. Am. Ceram. Soc. 95 (2012) 1-26.

[6] MLB. Bernadi, E. Antoneli, AB. Lourenco, CAC. Feitosa, LJQ. Maia, AC. Hernades J Therm Anal Calorim 87 (2007) 725

[7] Landolt-Bornstein (1981) Landolt-Bornstein numerical data and functional relationship in science and technology. Springer-Verlag, Berlin, vol III/28a, p 268; vol III/16a, p 422.

[8] D. Hennings, A. Schnell, G. Simon, "Diffuse ferroelectrics phase transition in $Ba(Ti_{1-y}Zr_y)O_3$ ceramics", J. Am. Ceram. Soc. 65 (1982) 539-544.

[9] SM. Neirman, J Mater Sci, 23 (1988) 3973. doi: 10.1007/BF01106823.

[10] D McCauley, RE Newnham, CA Randall, J Am Ceram Soc, 81 (1998) 979.

[11] V. Vinothini, B. Vaidhyanathan, J Binner, "Microwave assisted synthsis of barium titanate nanopowders", J Mater sci. 46 (2011) 2155-2161.

[12] A. S. Bhalla, R. Guo and R. Roy, Mat. Res. Innovat., 4 (2000) 3.

[13] G. H. Haertling, Journal of the American Ceramic Society, 82 (1999) 797-818.

[14] J. Bera and S. K. Rout, "On the formation mechanism of $BaTiO_3$–$BaZrO_3$ solid solution through solid-oxide reaction". Materials Letters. 59(1) (2005) 135-138.

[15] A. J. Moulson and J. M. Herbert, Electroceramics: Materials, Properties, Applications, Wiley, 2003.

[16] M. Sopicka-Lizer, High-Energy Ball Milling: Mechanochemical Processing of Nanopowders, Elsevier Science, 2010.

[17] X. Hou and J. Yu, Journal of the American Ceramic Society, 96 (2013) 2218-2224.

[18] J. S. Reed, Principles of Ceramics Processing, Wiley, 1995.

[19] M. Veith, S. Mathur, N. Lecerf, V. Huch, T. Decker, "Sol-gel synthesis of nano-scaled $BaTiO_3$, $BaZrO_3$ and $BaTi_{0.5}Zr_{0.5}O_3$ oxides via single-source alkoxide precursors and semi-alkoxide routes", J. Sol-Gel. Sci. Techn. 17 (2000) 145.

[20] X. G. Tang, K. H. Chew, H. L. W. Chan, "Diffuse phase transition and dielectric tenability of $Ba(Zr_yTi_{1-y})O_3$ relaxor ferroelectric ceramics", Acta. Mater. 52 (2004) 5177.

[21] S. B. Reddy, K. P. Rao, M. S. R. Rao, "Nanocrystalline barium zirconate titanate synthesized at low temperature by an aqueous co-precipitation technique", J. Scripta. Mat. 57 (2007) 591.

[22] X. B. W. Lee, S. B. Cho, "Preparation of $BaZr_xTi_{1-x}O_3$ by the hydrothermal process from peroxide precursors", J. Eur. Ceram. Soc. 25 (2005) 2009.

[23] A. Outzourhit, M. A. E. I. Raghni, M. L. Hafid, "Characterization of hydrothermally prepared $BaTi_{1-x}Zr_xO_3$", J. Alloys Compd. 340 (2002) 214.

[24] P. Julphunthong, and T. Bongkarn, "Phase formation, microstructure and dielectric properties of $Ba(Zr_{0.1}Ti_{0.9})O_3$ ceramics prepared via the combustion technique". Current Applied Physics, 11(3, Supplement) (2011) S60-S65.

[25] X. Wang, J. Song, J. Liu and L. W. Zhong, "Direct-current nanogenerator driven by ultrasonic waves", Science, 316 (2007) 102-105.

[26] J. H. Bang and K. S. Suslick, "Applications of ultrasound to the synthesis of nanostructured materials". Advanced Materials, 2010, 22, 1039-1059.

[27] J. Janbua, J. Mayamae, S. Wirunchit, R. Baitahe and N. Vittayakorn, "Directed synthesis, growth process and optical properties of monodispersed $CaWO_4$ microspheres via a sonochemical route" RSC Advances, 5 (2015) 19893-19899.

[28] J. Guo, Z. Chen, Y. Li, Z. Yu, Q. Li, J. Li, C. Feng, D. Zhang, "Sonochemical synthesis of TiO_2 nanoparticles on graphene for use as photocatalyst", Ultrason. Sonochem. 18 (2011) 1082–1090.

[29] S. Anandan, G. J. Lee, J. J. Wu, "Sonochemical synthesis of CuO nanostructures with different morphology", Ultrason. Sonochem. 19 (2012) 682–686.

[30] I. A. Siddiquey, T. Furusawa, M. Sato, N. M. Bahadur, M. Alam, N. Suzuki, "Sonochemical synthesis, photocatalytic activity and optical properties of silica coated ZnO nanoparticles", Ultrason. Sonochem.19 (2012) 750–755.

[31] S. M. Meybodi, S. A. Hosseini, M. Rezaee, S. K. Sadmezhaad, D. Mahommadyani, "Synthesis of wide band gap nanocrystalline NiO powder via a sonochemical method", Ultrason. Sonochem. 19 (2012) 841–845.

[32] K. S. Suslick, "Sonochemistry", Science, 247 (1990) 1439-1445.

[33] J. H. Bang, and K. S. Suslick, "Applications of ultrasound to the synthesis of nanostructured materials". Advanced Materials, 22(10) (2010) 1039-1059.

[34] A. Gedanken, "Using sonochemistry for the fabrication of nanomaterials", J. Ult. Sonch. 11 (2004) 47.

[35] H. Xu, B.W. Zeiger, and K.S. Suslick, "Sonochemical synthesis of nanomaterials". Chemical Society Reviews, 42(7) (2013) 2555-2567.

[36] P. Charoonsuk, W. Vittayakorn, N. Atiwongsangthong, P. Seeharaj, N. Vittayakorn, "Synthesis of monodispersed perovskite barium zirconate ($BaZrO_3$) by the sonochemical method", Ferroelectrics 453 (2013) 54-61.

[37] S. Singh, et al., "Magnetodielectric effect in $BaTiO_3/ZnFe_2O_4$ core/shell nanoparticles". Journal of Alloys and Compounds, 587 (2014) 437-441.

[38] Y. Han, D. Radziuk, D. Shchukin and H. Moehwald, "Stability and size dependence of protein microspheres prepared by ultrasonication". Journal of Materials Chemistry, 18(42) (2008) 5162-5166.

[39] B. Zhou, et al., "Ultrasonic-assisted size-controllable synthesis of Bi_2Te_3 nanoflakes with electrogenerated chemiluminescence". Ultrasonics Sonochemistry, 14(2) (2007) 229-234.

[40] I. Haas, S. Shanmugam, and A. Gedanken, "Pulsed Sonoelectrochemical Synthesis of Size-Controlled Copper Nanoparticles Stabilized by Poly(N-

vinylpyrrolidone)". The Journal of Physical Chemistry B, 110(34) (2006) 16947-16952.

[41] T. Hyeon, M. Fang, and K.S. Suslick, "Nanostructured Molybdenum Carbide: Sonochemical Synthesis and Catalytic Properties". Journal of the American Chemical Society, 118(23) (1996) 5492-5493.

[42] J. Geng, L. Jiang, and J. Zhu, "Crystal formation and growth mechanism of inorganic nanomaterials in sonochemical syntheses". Science China Chemistry, 55(11) (2012) 2292-2310.

[43] C. Wu, B.P. Mosher, and T. Zeng, "Rapid Synthesis of Gold and Platinum Nanoparticles Using Metal Displacement Reduction with Sonomechanical Assistance. Chemistry of Materials", 18(13) (2006) 2925-2928.

[44] L. P. Jiang, et al., "Ultrasonic-Assisted Synthesis of Monodisperse Single-Crystalline Silver Nanoplates and Gold Nanorings". Inorganic Chemistry, 43(19) (2004) 5877-5883.

[45] J. N. Tiwari, R. N. Tiwari, K. S. Kim, "zero-dimensional, one-dimensional, two-dimensional and three-dimensional nanostructured materials for advanced electrochemical energy devices". Process in Materials Science, 57 (2012) 724-803.

[46] YT Kim, JH Han, BH Hong, YU Kwon. Adv Mater, 22 (2010) 515.

[47] G Zhang, D Wang. J Am Chem Soc, 130 (2008) 5616.

[48] Wang J, Lin M, Yan Y, Wang Z, Ho PC, Loh KP. J Am Chem Soc, 131 (2009) 11300.

[49] Gautam UK, Vivekchand SRC, Govindaraj A, Kulkarni GU, Selvi NR, Rao CNR. J Am Chem Soc, 127 (2005) 3658.

[50] Lee JY, Hong BH, Kim WY, Min SK, Kim Y, Jouravlev MV, et al. Nature, 460 (2009) 498.

[51] Mokerov VG, Fedorov YV, Velikovski LE, Scherbakova MY. Nanotechnology, 12 (2001) 552.

[52] Ustinov VM et al. Nanotechnology, 11 (2000) 397.

[53] W Lee, SH Kang, JY Kim, GB Kolekar, YE Sung, SH Han. Nanotechnology, 20 (2009) 335706.

[54] JW Stouwdam, RAJ Janssen. J Mater Chem, 18 (2008) 1889.

[55] Iijima S. Nature, 354 (1991) 56.

[56] Kuchibhatla SVNT, Karakoti AS, Bera D, Seal S. Prog Mater Sci, 52 (2007) 699.

[57] Huang L, Wang H, Wang Z, Mitra A, Zhao D, Yan Y. Chem Mater, 14 (2002) 876.

[58] Okada T, Kawashima K, Nakata Y, Ning X. Jpn J Appl Phys, 44 (2005) 688.

[59] Xia H, Feng J, Wang H, Lai MO, Lu L. J Power Sources, 195 (2010) 4410.

[60] Li GR, Feng ZP, Zhong JH, Wang ZL, Tong YX. Macromolecules, 43 (2010) 2178.

[61] Park JM, Nalwa KS, Leung W, Constant K, Chaudhary S, Ho KM. Nanotechnology, 21 (2010) 215301.

[62] Cao LM, Tian H, Zhang Z, Zhang XY, Gao CX, Wang WK. Nanotechnology, 15 (2004) 139.

[63] Yoon SM, Hwang IC, Kim KS, Choi HC. Angew Chem Int Ed, 48 (2009) 2506.

[64] Wang Y, Lee JY, Kim JS, Kim GH, Kim KS. Chem Mater, 19 (2007) 3912.

[65] Wang YW, Hong BH, Lee JY, Kim JS, Kim GH, Kim KS. J Phys Chem B, 108 (2004) 16723.

[66] Hong BH, Bae SC, Lee CW, Jeong S, Kim KS. Science, 294 (2001) 348.

[67] Hong BH, Lee JY, Lee CW, Kim JC, Bae SC, Kim KS. J Am Chem Soc, 123 (2001) 10748.

[68] Hong BH et al. Proc Nat Acad Sci USA, 102 (2005) 14155.

[69] Hong BH, Lee JY, Beetz T, Zhu Y, Kim P, Kim KS. J Am Chem Soc, 127 (2005) 15336.

[70] Hwang IC et al. J Phys Chem B, 114 (2010) 7216.

[71] Kim KS et al. J Am Chem Soc, 124 (2002) 14268.

[72] Kim WY, Choi YC, Kim KS. J Mater Chem, 18 (2008) 4510.

[73] Jun JW, Seo JW, Oh SJ, Cheon J. Coord Chem Rev, 249 (2005) 1766.

[74] Kim KS et al. Nature, 457 (2009) 706.

[75] Bae S et al. Nature Nanotechnol, 5 (2010) 574.

[76] Pradhan D, Leung KT. J Phys Chem C, 112 (2008) 1357.

[77] Tiwari JN, Pan FM, Tiwari RN, Nandi SK. Chem Commun, (2008) 6516.

[78] Nayak BB, Behera D, Mishra BK. J Am Ceram Soc, 93 (2010) 3080.

[79] Dong X, Ji X, Jing J, Li M, Li J, Yang W. J Phys Chem C, 114 (2010) 2070.

[80] Mann AKP, Skrabalak SE. Chem Mater, 23 (2011) 1017.

[81] Siril PF, Ramos L, Beaunier P, Archirel P, Etcheberry A, Remita H. Chem Mater, 21 (2009) 5170.

[82] Vizireanu S, Stoica SD, Luculescu C, Nistor LC, Mitu B, Dinescu G. Plasma Sources Sci Technol, 19 (2010) 034016.

[83] Jung SH, Oh E, Lee KH, Yang Y, Park CG, Park W, et al. Cryst Growth Des, 8 (2008) 265.

[84] Ren X, Zelenay P, Thomas S, Davey J, Gottesfeld S. J Power Sources, 86 (2000) 111.

[85] de Oliveira EC, Pires CTGVMT, Pastore HO. J Braz Chem Soc, 17 (2006) 16.

[86] Hu LB, Choi JW, Yang Y, Jeong S, La Mantia F, Cui LF, et al. Proc Natl Acad Sci USA, 106 (2009) 21490.

[87] Kamarudin SK, Achmad F, Daud WRW. Int J Hydrogen Energy, 34 (2009) 6902.

[88] Chen H, Cong TN, Yang W, Tan C, Li Y, Ding Y. Prog Nat Sci, 19 (2009) 291.

[89] Arico AS, Bruce P, Scrosati B, Tarascon JM, Van Schalkwijk W. Nature Mater, 4 (2005) 366.

[90] Ferreira-Aparicio P, Folgado MA, Daza L. J Power Sources, 192 (2009) 57.

[91] Li HQ, Wang YG, Wang CX, Xia YY. J Power Sources, 185 (2008) 1557.

[92] Jin YH, Lee SH, Shim HW, Ko KH, Kim WD. Electrochim Acta, 55 (2010) 7315.

[93] Dong Z, Kennedy SJ, Wu Y. J Power Sources, 196 (2011) 4886.

[94] Mastragostino M, Soavi F. J Power Sources, 174 (2007) 89.

[95] Winter M, Brodd R J. Chem Rev, 104 (2004) 4245.

[96] Armand M, Tarascon JM. Nature, 451 (2008) 652.

[97] Simon P, Gogotsi Y. Nature Mater, 7 (2008) 845.

[98] Hu CC, Chang KH, Lin MC, Wu YT. Nano Lett, 6 (2006) 2690.

[99] Shen Q, Jiang L, Zhang H, Min Q, Hou W, Zhu JJ. J Phys Chem C, 112 (2008) 16385.

[100] Teng XW, Liang XY, Maksimuk S, Yang H. Small, 2 (2006) 249.

[101] Lee H, Habas SE, Kweskin S, Butcher D, Somorjai GA, Yang PD. Angew Chem Int Ed, 45 (2006) 7824.

[102] Wang L, Yamauchi Y. Chem Mater, 21 (2009) 3562.

[103] Wang JN, Su LF, Wu ZP. Cryst Growth Des, 8 (2008) 1741.

[104] Liu J, Essner J, Li J. Chem Mater, 22 (2010) 5022.

[105] Lei W, Liu D, Zhang J, Zhu P, Cui Q, Zou G. Cryst Growth Des, 9 (2009) 1489.

[106] Hwang IC et al. Nanotechnology, 20 (2009) 245605.

[107] H. Kniekamp and W. Heywang, Phys., 6 [9] (1954) 385.

[108] G. H. Jonker and W. Noorlander, "Science of Ceramics", Academic Press, New York, 1 (1962) 255.

[109] N. C. Sharma and JE. R. McCartney, J. Austr. Ceram. Soc., 10 (1974) 16.

[110] R. J. Brandmayr, A. E. Brown, A. M. Dunlap, U. S. Technical Report No. E10M-2614, (1962) May.

[111] G. Arlt and P. Sasko, J. Appl. Phys., 51 (1980) 4956.

[112] G. Arlt, D. Hennings and G. de With, J. Appl. Phys., 58 [4] (1985) 1619.

[113] G. Arlt, Ferroelectrics 104 (1990) 217.

[114] G. Arlt and N. A. Pertsev, J. Appl. Phys., 70 [4] (1991) 2283.

[115] W. Heywang, Ferroelectrics, 49 (1983) 3.

[116] K. Kinoshita and A. Yamaji, J. Appl. Phys., 47 [1] (1976) 371.

[117] W. R. Buessem, L. E. Cross and A. K. Goswami, J. Am. Ceram. Soc., 49 (1966) 33.

[118] A. J. Bel, A. J. Moulson and L. E. Cross, Ferroelectrics, 54 (1984) 147.

[119] N. Kim, "Grain size effect on the dielectric and piezoelectric properties in compositions which are near the morphotropic phase boundary of lead zirconate titanate based ceramics". The Pennsylvania State University, U.S.A., 1994.

[120] D. Segal, .Chemical Synthesis of Advanced Ceramic Materials", Cambridge University Press, 1991.

[121] R. C. Kell, N. J. Hellicar, Structural transitions in barium titanate-zirconate transducer materials, Acustica. 6 (1956) 235-238.

[122] O. P. Thakur, C. Prakash, A. R. James, Enhanced dielectric properties of ceramics through improved processing, J. Alloys Compd. 470 (2009) 548-551.

[123] X. S. Wang, H. Yamada, C. N. Xu, Large electrostriction near the solubility limit in $BaTiO_3$–$CaTiO_3$ ceramics, Applied physics Letters. 85 (2005) 022905.

[124] S. Halder, P. Gerber, T. Schneller, R. Waser, Electromechanical properties of $Ba(Ti_{1-x}Zr_x)O_3$ thin films, Applied Physics. A. 81 (2005) 11-13.

[125] Z. L. Wang and J. Song, *Science*, 312 (2006) 242-246.

[126] J. Q. Qi, Y. Wang, W. P. Chen, L. T. Li and H. L. W. Chan, "Perovskite barium zirconate titanate nanoparticles directly synthesized from solutions". Journal of Nanoparticle Research, 8 (2006) 959-963.

[127] P. K. Dutta, R. Asiaie, S. A. Akbar and W. Zhu, "Hydrothermal Synthesis and Dielectric Properties of Tetragonal $BaTiO_3$" Chemistry of Materials, 6 (1994) 1542-1548.

[128] K. J. Leonard, S. Sathyamurthy and M. P. Paranthaman, "Characterization of BaZrO3 Nanoparticles Prepared by Reverse Micelle Synthesis". Chemistry of Materials, 17(15) (2005) 4010-4017.

[129] U.A. Peuker, U. Hoffmann, U. Wietelmann, S. Bandelin and R. Jung, "Sonochemistry ullmann's encyclopedia of industrial chemistry", Wiley-VCH, Weinheim, 2006.

[130] L.H. Thompson and L.K. Doraiswamy, "Sonochemistry: science and engineering", Ind. Eng. Chem. Res., 38 (1999) 1215.

[131] J T. Akita, T. Hiroki, S. Tanaka, T. Kojima, M. Kohyama, A. Iwase and F. Hori, "Analytical TEM observation of Au-Pd nanoparticles prepared by sonochemical method" Catalysis Today, 131 (2008) 90-97.

[132] P. Park, J.Y. Park, C.H. Hwang, M.-H. Choi, J.E. Kim, K.M. Ok and I.-W. Shim, "Synthesis of $LiCoO_2$ nanoparticles by a sonochemical method under the multibubble sonoluminescence conditions", Bull. Korean Chem. Soc., 2 (2010) 31.

[133] F. Dang, K. Kato, H. Imai, S. Wada, H. Haneda and M. Kuwabara, "A new effect of ultrasonication on the formation of $BaTiO_3$ nanoparticles", Ultrasonics Sonochemistry, 17, 310-314 (2010).

[134] Y. Waseda, E. Matsubara and K. Shinoda, X-Ray Diffraction Crystallography: Introduction, Examples and Solved Problems, Springer, 2011.

[135] N. C. Pramanik, S. I. Seok and B. Y. Ahn, "Wet-chemical synthesis of crystalline $BaTiO_3$ from stable chelated titanium complex: Formation mechanism and dispersibility in organic solvents", Journal of Colloid and Interface Science, 300(2) (2006) 569-576.

[136] M. M. Lencka and R. E. Riman, "Hydrothermal synthesis of perovskite materials: Thermodynamic modeling and experimental verification", Ferroelectrics, 151(1) (1994) 159-164.

[137] S. L. Swartz and T. R. Shrout, "Fabrication of perovskite lead mahnesium niobate", Mater. Res. Bull., 17 (10) (1982) 1245–1250.

[138] S. Wada, T. Tsurumi, H. Chikamori, T. Noma and T. Suzuki, "Preparation of nm-sized $BaTiO_3$ crystallites by a LTDS method using a highly concentrated aqueous solution". Journal of Crystal Growth. 229 (2001) 433-439.

[139] P. Pasierb, S. Komornicki, M. Rokita, M. Rkas, "Structural proper- ties of Li_2CO_3–$BaCO_3$ system derived from IR and Raman spectroscopy, Journal of Molecular Structure 596(1–3) (2001) 151–156.

[140] H. P. Kumar, C. Vijayakumar, C. N. George, *et al.*, "Characterization and sintering of $BaZrO_3$ nanoparticles synthesized through a sing-step combustion process". J Alloy Compd. 458 (2008) 528–531.

[141] N. Chakrabarti, H.S. Maiti, "Chemical synthesis of barium zirconate titanate powder by an autocombustion technique", Journal of Materials Chemistry 6 (7) (1996) 1169–1173.

[142] Y. Zhang, L. Wang, and D. Xue, "Molten salt route of well dispersive barium titanate nanoparticles". Powder Technol. 217 (2012) 629–633.

[143] E. B. Slamovich and I. A. Aksay, "Structure evolution in hydrothermally processed (<100 °C) $BaTiO_3$ films". 79 (1996). 239–247.

[144] Y. Shiratori, C. Pithan, J. Dornseiffer, and R.Waser, "Raman scattering studies on nanocrystalline $BaTiO_3$ Part I – isolated particles and aggregates". J. Raman. Spectrosc. 38 (2007) 1288–1299.

[145] S. Vuttivong, S. Niemcharoen, P. Seeharaj, W. C. Vittayakorn and N. Vittayakorn, "Sonochemical Synthesis of Spherical $BaTiO_3$ Nanoparticles". Ferroelectrics, 457 (2013) 44-52.

[146] P. S. Dobal, A. Dixit, R. S. Katiyar, Z. Yu, R. Guo, A. S. Bhalla, Phase transition behavior of $BaZr_xTi_{1-x}O_3$ ceramics", Journal of Raman Spectroscopy 32 (1) (2001) 69–71.

[147] N. G. Nelson, J. G. Skinner, "Raman spectrum of strontium titanate", J. Chem. Phys. 48 (1968) 2240.

[148] X. Wei, G. Xu, Z. Ren, Y. Wang, G. Shen and G. Han, "Size-controlled synthesis of $BaTiO_3$ nanocrystals via a hydrothermal route", Materials Letters, 62 (2008) 3666-3669.

[149] W. Wang, L. Cao, W. Liu, G. Su and W. Zhang, "Low-temperature synthesis of $BaTiO_3$ powders by the sol-gel-hydrothermal method", Ceramics International (Accepted 17 Feb 2013)

[150] M. B. Smith, K. Page, T. Siegrist, P. L. Redmond, E. C.Walter, R. Seshadri, L. E. Brus, andM. L. "Steigerwald, Crystal structure and the paraelectric-to-ferroelectric phase transition of nanoscale $BaTiO_3$". J. Am. Chem. Soc. 130 (2008) 6955–6963.

[151] Z. Deng, Y. Dai, W. Chen, X. Pei, and J. Liao, "Synthesis and characterization of bowl-like single-crystalline $BaTiO_3$ nanoparticles". Nanoscale Res. Lett. 5 (2010) 1217–1221.

[152] Pankaj, in Theoretical and Experimental Sonochemistry Involving Inorganic Systems, ed. M. Ashokkumar, Springer Netherlands, 2011, pp. 213-271.

[153] T. Prozorov, R. Prozorov and K. S. Suslick, Journal of the American Chemical Society, 126 (2004) 13890-13891.

[154] W. B. McNamara, Y. T. Didenko and K. S. Suslick, "Sonoluminescence temperatures during multi-bubble cavitation". Nature, 401(6755) (1999) 772.

[155] H. Wang, Y.-N. Lu, J.-J. Zhu and H.-Y. Chen, Inorganic Chemistry, 42 (2003) 6404-6411.

[156] H. Chen, C. Yang, C. Fu, J. Shi, J. Zhang, W. Leng, "Microstructure and dielectric properties of $Ba(Zr_xTi_{1-x})O_3$ ceramics", J. Mater. Sci. 19 (2008) 379-382.

[157] R. D. Shannon, "Revised effective ionic radii and systematic studies of interatomic distances in halides and chalcogenides", Acta Crystallogr., Sect. A: Cryst. Phys., Diffr., Theor. Gen. Crystallogr. A32 (1976) 751.

[158] H-H. Huang, H-H. Chiu, N-C. Wu, M-C. Wang, "Tetragonality and properties of $Ba(Zr_xTi_{1-x})O_3$ ceramics determined using the rietveld method", Metallurgical and materials transactions. 38A (2008) 3276-3282.

[159] B. H. Toby, "R factors in Rietveld analysis: How good is good enough?", Powder Diffraction. 21 (1) (2006) 67-70.

[160] T. Noma, S. Wada, M. Yano and T. Suzuki, "Analysis of lattice vibration in fine particles of barium titanate single crystal including the lattice hydroxyl group" Journal of Applied Physics, 80 (1996) 5223-5233.

[161] F. Baeten, B. Derks, W. Coppens and E. van Kleef, "Barium titanate characterization by differential scanning calorimetry.", Journal of the European Ceramic Society, 26 (2006) 589-592.

[162] M. H. Frey and D. A. Payne, Physical Review B - Condensed Matter and Materials Physics, 54 (1996) 3158-3168.

[163] R. Kota and B. Lee, J Mater Sci: Mater Electron, 18 (2007) 1221-1227.

[164] U. Weber, G. Greuel, U. Boettger, S. Weber, D. Hennings, R. Waser, "Dielectric properties of $Ba(Zr,Ti)O_3$-based ferroelectrics for capacitor applications", J. Am. Ceram. Soc. 84 (2001) 759-766.

[165] K. S. Suslick, "Applications of Ultrasound to Materials Chemistry", MRS BULLETIN/APRIL, (1995) 29-34.

[166] S. Wirunchit, T. Charoonsuk, N. Vittayakorn, "Facile sonochemical synthesis of nearly spherical barium zirconatetitanate ($BaZr_{1-y}Ti_yO_3$; BZT); perovskite stability and formation mechanism" RSC Advances., 5 (2015) 38061.

[167] A. Testino, M. T. Buscaglia, V. Buscaglia, M. Viviani, C. Bottino and P. Nanni, "Kinetics and Mechanism of Aqueous Chemical Synthesis of $BaTiO_3$ Particles". Chemistry of Materials, 16 (2004) 1536-1543.

[168] F. Boschini, A. Rulmont, R. Cloots and B. Vertruyen, Journal of the European Ceramic Society, 29 (2009) 1457-1462.

[169] K. S. Birdi, Handbook of Surface and Colloid Chemistry, Third Edition, CRC Press, 2008.

[170] W. B. Russel, D. A. Saville and W. R. Schowalter, Colloidal Dispersions, Cambridge University Press, 1992.

APPENDIXS

Miss Supamas Wirunchit
Electroceramics Research Labolatory, College of Nanotechnology
College of Nanotechnology, King Mongkut's Institute of Technology
Ladkrabang, THAILAND

Biography

Name	Supamas Wirunchit (นางสาวศุภมาส วิรุญจิตร)
Date of birth	21st September 1984 (๒๑ กันยายน ๒๕๒๗)
Place	Chantaburi Province (จังหวัดจันทบุรี)
Name of Father	Wanchai Wirunchit (นายวันชัย วิรุญจิตร)
Name of mother	Jumnien Wirunchit (นางจำเนียร วิรุญจิตร)
Address	69/86 Moo 4, MooBaan Wattana, Soi. 11, Ruampattana Road, Lumtoiting, Nongjog, Bangkok,Thailand, 10530

Education

2006	B.S. (Chemistry) King Mongkut's Institute of Technology Ladkrabang, Bangkok, Thailand
2007-2009	M.S. (Chemistry) King Mongkut's Institute of Technology Ladkrabang, Bangkok, Thailand
2010-2015	Ph.D. (Nanoscience and Nanotechnology) King Mongkut's Institute of Technology Ladkrabang, Bangkok, Thailand

Publications in International Journals

1. **S. Wirunchit**, R. Muanghlua, N. Atiwongsangthong, W. Vittayakorn, and N. Vittayakorn "Nanocrystalline barium zirconium titanate synthesized by the sonochemical process" *Advance Material Research*; Vols. 802 (2013) pp. 119-123.
2. P. Seeharaj, **S. Wirunchit**, P. Charoonsuk, P. Kim-Lohsoontorn and N. Vittayakorn "Spherical Nanocrystalline Barium Zirconate Titanate Prepared by Co-Precipitation in Highly Basic Aqueous Solution" *Ferroelectrics*,, Vol. 455, 2013 , pp.83-89. Impact factor 0.427
3. **S. Wirunchit**, T. Charoonsuk, N. Vittayakorn, "Facile sonochemical synthesis of nearly spherical barium zirconatetitanate ($BaZr_{1-y}Ti_yO_3$; BZT); perovskite stability and formation mechanism" *RSC Advances*., 5 (2015) 38061. Impact factor 3.84.
4. J. Janbua, J. Mayamae, **S. Wirunchit**, R. Baitahe and N. Vittayakorn, "Directed synthesis, growth process and optical properties of monodispersed

$CaWO_4$ microspheres via a sonochemical route" *RSC Advances*, 5 (2015) 19893-19899. Impact factor 3.84.

5. **S. Wirunchit**, R. Baitahe, W. Vittayakorn N. Vittayakorn and S. Maensiri "The effect of zirconium on the perovskite phase formation of barium zirconium titanate nanoparticles by the sonochemical method" *Ferroelectrics*, *In Press*. Impact factor 0.427

Presentations in International Conferences

Oral Presentations

1. Supamas Wirunchit, Rangson Muanghlua, Narin Atiwongsangthong, Wanwilai Vittayakorn, and Naratip Vittayakorn "Nanocrystalline barium zirconium titanate synthesized by the sonochemical process" The International Conference on Engineering, Applied Sciences, and Technology (ICEAST 2013), The Sukosol Hotel, Banhkok, Thailand, August 21-24, 2013.
2. Supamas Wirunchit, Rattanai Baitahe, Wanwilai Vittayakorn Naratip Vittayakorn and Santi Maensiri "The effect of zirconium on the perovskite phase formation of barium zirconium titanate nanoparticles by the sonochemical method" The 9th Asian Meeting on Ferroelectrics (AMF-AMEC 2014), Shanghai International Convention Center, Shanghai, China, October 26-30, 2014.

Advanced Materials Research Vol. 802 (2013) pp 119-123
© (2013) Trans Tech Publications, Switzerland
doi:10.4028/www.scientific.net/AMR.802.119

Nanocrystalline barium zirconium titanate synthesized by the sonochemical process

Supamas Wirunchit[1,a], Rangson Muanghlua[2,b], Narin Atiwongsangthong[2,c], Wanwilai Vittayakorn[1,d] and Naratip Vittayakorn[1,3,4,e]

[1]Electroceramics Research Laboratory, College of Nanotechnology, King Mongkut's Institute of Technology Ladkrabang, Bangkok 10520, Thailand

[2]Department of Chemistry, Faculty of Science, King Mongkut's Institute of Technology Ladkrabang, Bangkok 10520, Thailand

[3]Advanced Ceramic Research Unit, Faculty of Science, King Mongkut's Institute of Technology Ladkrabang, Bangkok 10520, Thailand

[4]Department of Electronics, Faculty of Engineering, King Mongkut's Institute of Technology Ladkrabang, Bangkok 10520, Thailand

[a]ester_cins@hotmail.com, [b]kmrangso@kmitl.ac.th, [c]kanarin@kmitl.ac.th [d]kvwanwil@kmitl.ac.th, [e]naratipcmu@yahoo.com

Keywords: Barium zirconium titanate, Sonochemical process, Nanocrystalline, BZT

Abstract. Nanocrystalline barium zirconium titanate, $BaZr_{0.4}Ti_{0.6}O_3$, was synthesized successfully via the sonochemical process. The effects of reaction time on the precipitation of $Ba(Zr,Ti)O_3$ particles were investigated briefly. The crystal structure as well as molecular vibrations and morphology were investigated. X-ray diffraction indicated that the powders exhibited a single phase perovskite structure, without the presence of pyrochlore or unwanted phases at the reaction time of 60 min. Nanocrystals were formed before being oriented and aggregated into large particles in aqueous solution under ultrasonic irradiation. A scanning electron microscopy (SEM) photograph showed the BZT powder as spherical in shape with uniform nanosized features.

Introduction

Due to environmental concerns, lead free ceramics, for example, KNN, BNT and BT[1] have growing interest in applications such as capacitors, actuators and sensors, with barium zirconium titanate ($Ba(Zr_xTi_{1-x})O_3$; BZT) being the most attractive because it is based on the solid solution of barium titanate ($BaTiO_3$) and barium zirconate($BaZrO_3$). This ceramic has been studied widely owing to its very high and broad relative permittivity maximum at the Curie temperature point [2-4]. However. It is know that the ferroelectric-related properties of the $Ba(Zr_xTi_{1-x})O_3$ system were significantly dependent on the Zr contents [5]. When the Zr content in less than 10 mol %, The BZT ceramics show normal ferroelectric behavior and the dielectric anomalies corresponding to the cubic to tetragonal (T_c), tetragonal to orthorhombic (T_2), and orthorhombic to rhombohedral (T_3) phases have been clearly observed. At around 27 mol %, Zr-concentration BZT ceramics exhibit typical diffuse paraelectric to ferroelectric phase transiton behavior in which T_c shifts to higher temperature with increase in frequency [6], which is caused by the inhomogeneous distribution of Zr ions on Ti sites and mechanical stress in the grain [7]. When increase of Zr (>30 mol %) content the BZT materials exhibit like relaxor ferroelectric behavior. In this case of $Ba(Zr_{0.4}Ti_{0.6})O_3$ ceramic, it is of great interest due to its high dielectric constant, low dielectric loss broad dielectric curve and the relaxor ferroelectric phase can be stabilized below the freezing temperature [8].

Conventional preparation of this ceramic is based on solid state reaction employing respective oxides, and requires repeated cycles of mixing and heat treatment to achieve complete phase formation. In contrast, chemical processing methods provide atomic level mixing of individual components, and they reduce the diffusion path in the nanometer scale to form

nanocrystalline materials at a much lower temperature than that from solid state reaction. While chemical processing methods such as sol-gel [9-10], hydrothermal [11-12], combustion [13-14] and co-precipitation techniques [15] have attracted great attention, these methods often require expensive precursor materials, longer processing time, complex procedure and a relatively high heat treatment temperature of the prepared powders to obtain single phase material.

The sonochemical technique is an effective method for improving the properties of synthesized nanoparticles. The main event in sonochemistry is the creation, growth and collapse of a bubble that forms in liquid. The stage that leads to bubble growth occurs through diffusion of solute vapor into the volume of the bubble. The last stage is collapse of the bubble, which occurs when its size reaches maximum value. An extremely high temperature of about 5,000K, pressure of ~20 MPa and a very high cooling rate of ~ 10^{10} K/S occur in a very localized space, when the small bubble generated in aqueous solution collapses during ultrasonication. Then, unique properties of the sonochemically synthesized particles are expected [16].

In this study, nanocrystalline barium zirconium titanate ($Ba(Zr_{0.4}\ Ti_{0.6})O_3$) was synthesized under ultrasonic irradiation. The effect of reaction time on the formation of $Ba(Zr_{0.4}\ Ti_{0.6})O_3$ particles was identified.

Experimental Procedure

Barium zirconium titanate nanoparticles, with a composition of $Ba(Zr_{0.4}\ Ti_{0.6})O_3$, were synthesized by a sonochemical process in a strong alkaline solution. Chemical routes had the advantage of mixing constituents on an atomic scale, with good control of stoichiometry therefore being possible. Appropriate proportions of high purity $BaCl_2.2H_2O$ (99%, Merck), $ZrOCl_2.8H_2O$ (99.5%, Advance Matherial) and $TiCl_4$ (99.5%, Wako) were weighed and used as raw materials for preparing precursor solution. Firstly, one concentration of molar precursor solution comprising titanium tetrachloride (1 M $TiCl_4$) was prepared by slowly adding concentrated $TiCl_4$ to near freezing distilled water (~ 278K), while stirring constantly. Secondly, both $ZrOCl_2.8H_2O$ and $BaCl_2.2H_2O$ were dissolved in distilled water to one concentration of molar precursor solution comprising zirconium (IV) oxychloride (1M $ZrOCl_2$), and one concentration of molar precursor consisting of barium chloride (1M $BaCl_2$). Then, 1M $TiCl_4$ and 1M $ZrOCl_2$ were mixed thoroughly before 1M $BaCl_2$ was added to this mixture. The precursor solutions were mixed continuously for 15 min. Twenty molar concentrations of sodium hydroxide (20M NaOH) were used for precipitation. After that, Ar gas bubbled the 20M NaOH for 30 min, and the precursor solution mixture was added to 20M NaOH. During the addition, Ti-based sol suspension began to form immediately. The suspension was irradiated with an ultrasonic horn for 15, 30 and 60 min, consecutively. After the synthesis, the precipitate was separated centrifugally and washed in deionized water, before drying at 80°C for 24 hr.

Characterization of the $Ba(Zr_{0.4}\ Ti_{0.6})O_3$ particles was conducted by X-ray diffraction (XRD), fourier transform infrared spectroscopy(FT-IR) and scanning electron microscope (SEM).

Result and discussion

The XRD patterns of $Ba(Zr_{0.4}\ Ti_{0.6})O_3$ particles, synthesized under irradiation of ultrasonic sound, with various reaction times (15, 30 and 60 min), are presented in Figure 1(A), in which low crystallinity and a small amount of amorphous material also are observed. This indicates (a) that the crystallization process remains incomplete for up to 15 min, after which the cubic $Ba(Zr_{0.4}\ Ti_{0.6})O_3$ phase can be identified clearly by the $Ba(Zr_{0.4}\ Ti_{0.6})O_3$ cubic structure from the JCPDS file No. 36-0019. However, in (b) the crystallization process renders the existence of intense diffraction in the $Ba(Zr_{0.4}\ Ti_{0.6})O_3$ phase for 30 min during the sonochemical process together with a few impure peaks corresponding to $BaCO_3$ from the JDPDS file No. 45-1471. At 60 min of the sonochemical process, (c) displays a complete crystallite of perovskite structure that is formed without the presence of an impure or unwanted phase. By increasing the reaction time from 15 to 60 min, the

yield of perovskite phase is significant until it reaches 60 min. This study also reflects the growth of powder crystallinity with increasing reaction time. The crystallite size can be estimated from the XRD result using Scherrer's equation : $L = \frac{K\lambda}{\beta cos\theta}$ Where L is the crystallite size, λ is the wavelength of X-ray radiation (0.15418 nm for Cu K_α), K is taken usually as 0.89, β is the line width at half-maximum of the 011 plane in the XRD pattern, and θ is the diffraction angle. With properly indexed peaks, a lattice parameter was determined using the UnitCell, which is a linear least squares refinement program. The calculated lattice parameter and crystallite size of $Ba(Zr_{0.4}Ti_{0.6})O_3$ particles are presented in Table 1.

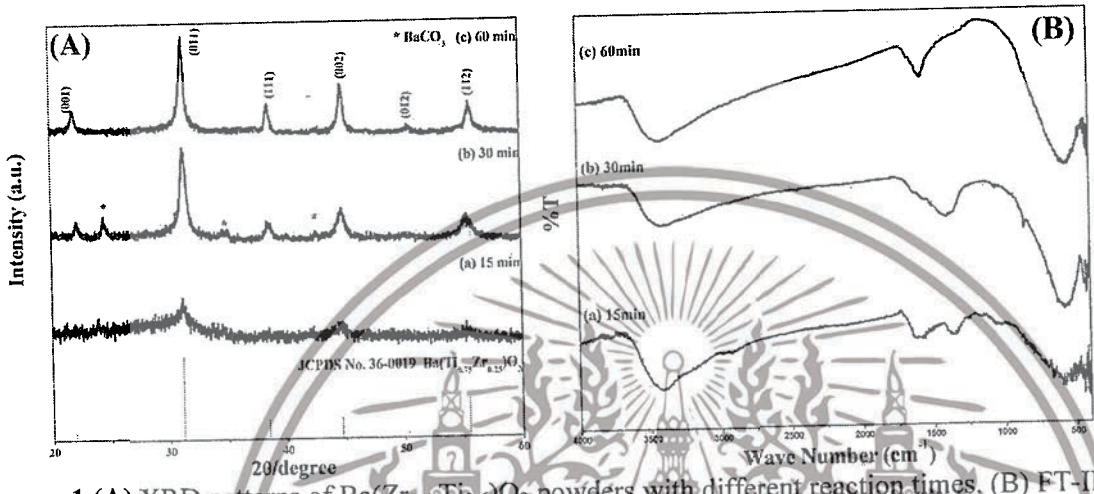

Figure. 1 (A) XRD patterns of $Ba(Zr_{0.4}Ti_{0.6})O_3$ powders with different reaction times. (B) FT-IR spectrums of $Ba(Zr_{0.4}Ti_{0.6})O_3$ powders with different reaction times.

The result of FT-IR spectroscopy supports the XRD patterns (Figure 1(A)) in that the perovskite phase is formed without the presence of a $BaCO_3$ phase at 60 min of the sonochemical process. The FT-IR spectrum of $Ba(Zr_{0.4}Ti_{0.6})O_3$ powders, with different reaction times, are shown in Figure 1(B). All of the FT-IR spectrums show metal-oxygen absorption of the perovskite phase in the region of 450-640 cm^{-1} [17] and hydrogen-oxygen vibration at 3,450 and 1,650 cm^{-1} [13]. Furthermore, the vibration band at 1,450 and 850 cm^{-1} of the $BaCO_3$ phase [18] was observed in the reaction time of 15 and 30 min in the XRD result.

Formation of $Ba(Zr_{0.4}Ti_{0.6})O_3$ aggregated particles in the sonochemical synthesis process was investigated. As shown in SEM photographs (Figure 2), $Ba(Zr_{0.4}Ti_{0.6})O_3$ nanoparticles formed under ultrasonic irradiation before the $Ba(Zr_{0.4}Ti_{0.6})O_3$ nanoparticles were aggregated by a short period under ultrasonic irradiation. Only sphere-like particles were obtained after 30 min, and the particle size increased after 60 min under ultrasonic irradiation. The size of $Ba(Zr_{0.4}Ti_{0.6})O_3$ particles is shown in Table 1.

Table 1 Preparatory condition and powder properties of the $Ba(Zr_{0.4}Ti_{0.6})O_3$ particles synthesized by the sonochemical process.

Reaction time (min)	Lattice constant (Å)	XRD Crystallite size (nm)	SEM Particle size (nm))
15	-	-	-
30	4.0617±0.0268	38.16	34.31±0.29
60	4.0867±0.0229	40.79	41.18±0.01

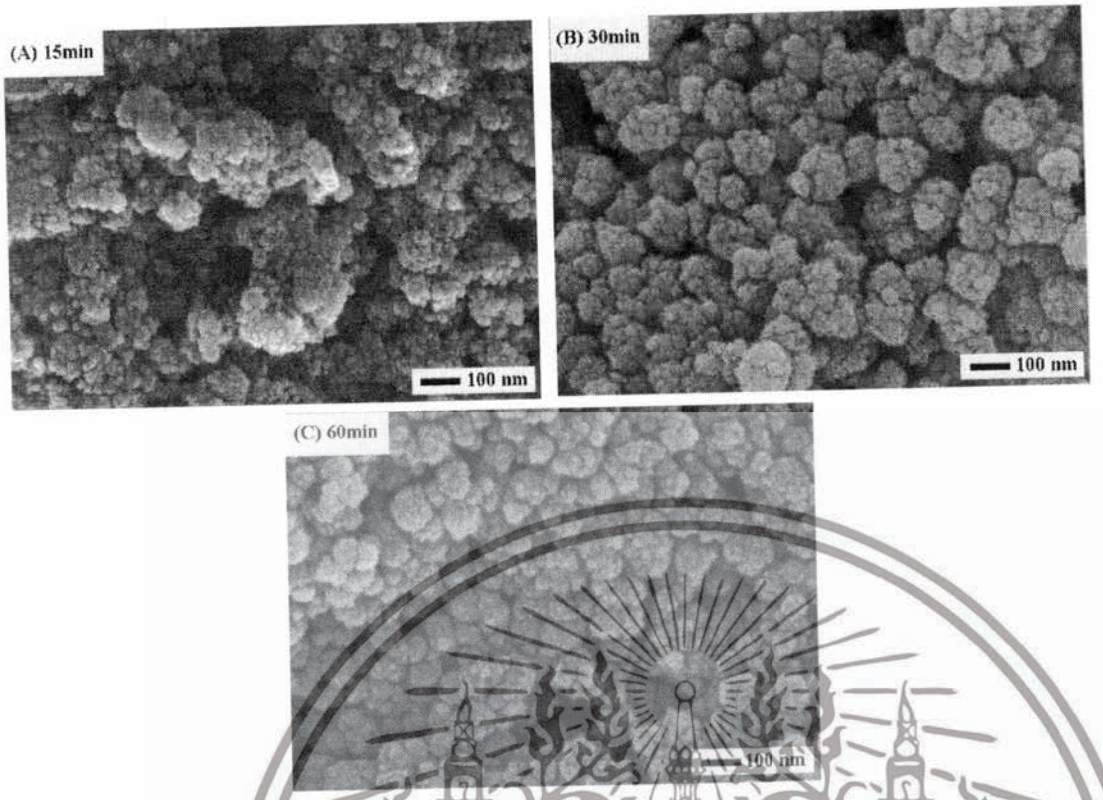

Figure. 2 SEM photographs of $Ba(Zr_{0.4}Ti_{0.6})O_3$ powders with different reaction times; (a) 15min, (b) 30 min and (c) 60 min.

Summary

At a reaction time of 60 min, the $Ba(Zr_{0.4}Ti_{0.6})O_3$ nanoparticles were completely crystallite with perovskite phase under ultrasonic irradiation in the sonochemical synthesis process. The shape of the nanoparticles was sphere-like and 34.31±0.29 and 41.18±0.01 nm at the reaction time 30 and 60 min, respectively.

Acknowledgments

This work has partially been supported by the KMITL Research Fund (KMITL Fund) and National Nanotechnology Center (NANOTEC), NSTDA, Ministry of Science and Technology, Thailand, through its "Center of Excellence Network" program, The Royal Golden Jubilee Ph.D. Program (RGJ) and Thailand Research Fund.

Reference

[1] R.T. Shrout, S.J. Zhang, Lead-free piezoelectric ceramics: Alternatives for PZT?, J. Electroceram. 19 (2007) 113.

[2] S.M. Neirmam, The Curie point temperature of $Ba(Ti_{1-x}Zr_x)O_3$ solid solutions, J. Mater. Sci. 23 (1988) 3973.

[3] D. Hennigs, A. Schnell, G. Simon, Diffuse ferroelectric phase transition in $Ba(Ti_{1-y}Zr_y)O_3$ ceramics, J. Am. Ceram. Soc. 65 (1982) 539.

[4] C.E. Ciomaaga, R. Calderone, M.T. Buscaglia, M. Viviani, V. Buscaglia, L. Mitoseriu, A. Stanca, P. Nanni, Relaxor properties of $Ba(Zr,Ti)O_3$ ceramics, J. Optoelectron. Adv. Mater. 8 (2006) 944.

[5] H. Chen, C. Yang, C. Fu, J. Shi, J. Zhang, W. Leng, Microstructure and dielectric properties of $Ba(Zr_xTi_{1-x})O_3$ ceramics, J. Mater. Sci. 19 (2008) 379-382.

[6] D. Hennings, A. Schnell, G. Simon, Diffuse Ferroelectric phase transition in $Ba(Ti_{1-y}Zr_y)O_3$ ceramics, J. Am. Ceram. Soc. 65 (1982) 539-544.

[7] U. Weber, G. Greuel, U. Boettger, S. Weber, D. Hennings, R. Waser, Dielectric properties of Ba(Zr, Ti)O_3-Based ferroelectrics for capacitor applications, J. Am. Ceram. Soc. 84 (2001) 759-766.

[8] A. Dixit, S. B. Majumder, R. S. Katiyar, A. S. Bhalla, Studies on the relaxor behavior of sol-gel derived $Ba(Zr_xTi_{1-x})O_3$ ($0.30 \leq x \leq 0.70$) thin films, J. Mater. Sci. 41 (2006) 87-96.

[9] M. Veith, S. Mathur, N. Lecerf, V. Huch, T. Decker, Sol-gel synthesis of nano-scaled $BaTiO_3$, $BaZrO_3$ and $BaTi_{0.5}Zr_{0.5}O_3$ oxides via single-source alkoxide precursors and semi-alkoxide routes, J. Sol-Gel. Sci. Techn. 17 (2000) 145.

[10] X.G. Tang, K.H. Chew, H.L.W. Chan, Diffuse phase transition and dielectric tenability of $Ba(Zr_yTi_{1-y})O_3$ relaxor ferroelectric ceramics, Acta. Mater. 52 (2004) 5177.

[11] X.B.W. Lee, S.B. Cho, Preparation of $BaZr_xTi_{1-x}O_3$ by the hydrothermal process from peroxo-precursors, J. Eur. Ceram. Soc. 25 (2005) 2009.

[12] A. Outzourhit, M.A.E.I. Raghni, M.L. Hafid, Characterization of hydrothermally prepared $BaTi_{1-x}Zr_xO_3$, J. Alloys Compd. 340 (2002) 214.

[13] C.N. Georde, J.K. Thomas, H.P. Kumar, M.K. Suresh, V.R. Kumar, P.R.S. Wariar, R. Jose, J. Koshy, Characterization, sintering and dielectric properties of nanocrystalline barium titanate synthesized through a modified combustion process, Mater. Charact. 60 (2009) 322.

[14] Q. Feng, X.H. Ma, Q.Z. Yan, C.C. Ge, Preparation of soft-agglomerated nano-sized ceramic powders by sol-gel combustion process, Mat. Sci. Eng. B-solid. 162 (2009) 53.

[15] S. B. Reddy, K.P. Rao, M.S.R. Rao, Nanocrystalline barium zirconate titanate synthesized at low temperature by an aqueous co-precipitation technique, J. Scripta Mat. 57 (2007) 591.

[16] A. Gedanken, Using sonochemistry for the fabrication of nanomaterials, J. Ult. Sonch. 11 (2004) 47.

[17] F.G. Garcia, C.R. Foschini, J.A. Varela, E. Longo, F. Moura, A.Z. Simoes, Structural and functional characterization of barium zirconium titanate/epoxy composites, Processing and Application Ceram. 54 (2011) 205.

[18] F. Boschini, A. Rulmont, R. Cloots, B. Vertruyen, Rapid synthesis of submicron crystalline barium zirconate $BaZrO_3$ by precipitation in aqueous basic solution below 100°C, J. Eur. Ceram. Soc. 29 (2009) 1457.

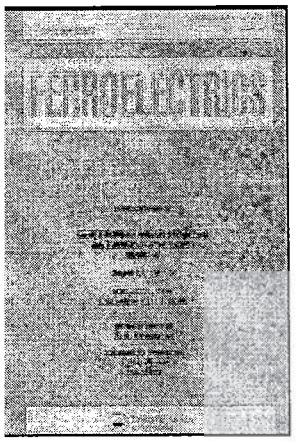

Ferroelectrics

Publication details, including instructions for authors and subscription information:
http://www.tandfonline.com/loi/gfer20

Spherical Nanocrystalline Barium Zirconate Titanate Prepared by Co-Precipitation in Highly Basic Aqueous Solution

Panpailin Seeharaj [a], Supamas Wirunchit [b], Piyanut Charoonsuk [b], Pattaraporn Kim-Lohsoontorn [c] & Naratip Vittayakorn [a b]

[a] Advanced Materials Research Unit, Department of Chemistry, King Mongkut's Institute of Technology Ladkrabang, Bangkok, 10520, Thailand

[b] Electroceramic Research Laboratory, College of Nanotechnology, King Mongkut's Institute of Technology Ladkrabang, Bangkok, 10520, Thailand

[c] Department of Chemical Engineering, Mahidol University, Nakorn Pathom, 73210, Thailand

Published online: 10 Dec 2013.

To cite this article: Panpailin Seeharaj, Supamas Wirunchit, Piyanut Charoonsuk, Pattaraporn Kim-Lohsoontorn & Naratip Vittayakorn (2013) Spherical Nanocrystalline Barium Zirconate Titanate Prepared by Co-Precipitation in Highly Basic Aqueous Solution, Ferroelectrics, 455:1, 83-89, DOI: 10.1080/00150193.2013.844054

To link to this article: http://dx.doi.org/10.1080/00150193.2013.844054

Ferroelectrics, 455:83–89, 2013

ISSN: 0015-0193 print / 1563-5112 online
DOI: 10.1080/00150193.2013.844054

Taylor & Francis
Taylor & Francis Group

Spherical Nanocrystalline Barium Zirconate Titanate Prepared by Co-Precipitation in Highly Basic Aqueous Solution

PANPAILIN SEEHARAJ,[1,*] SUPAMAS WIRUNCHIT,[2] PIYANUT CHAROONSUK,[2] PATTARAPORN KIM-LOHSOONTORN,[3] AND NARATIP VITTAYAKORN[1,2]

[1]Advanced Materials Research Unit, Department of Chemistry, King Mongkut's Institute of Technology Ladkrabang, Bangkok 10520, Thailand
[2]Electroceramic Research Laboratory, College of Nanotechnology, King Mongkut's Institute of Technology Ladkrabang, Bangkok 10520, Thailand
[3]Department of Chemical Engineering, Mahidol University, Nakorn Pathom 73210, Thailand

Spherical monosized barium zirconate titanate nanoparticles ($Ba(Zr_xTi_{1-x})O_3$ (BZT) when $x = 0.25$, 0.30 and 0.35) have been prepared by co-precipitation in a strongly alkaline solution (20 M NaOH) at 80°C. The phase formation of the as-precipitated powders was characterized by XRD, FT-IR and Raman spectroscopy as a single-phase BZT with cubic perovskite oxide structure. This indicates that crystalline BZT powders can be obtained from the co-precipitation in 20 M NaOH without the requirement of calcination process. SEM analysis showed that BZT had nanosized spherical morphology with uniform shape and size. The crystal sizes obtained by TEM analysis were 20-40 nm.

Keywords Co-precipitation; barium zirconate titanate; nanoparticles

Introduction

Barium zirconate titanate ceramics ($Ba(Zr_xTi_{1-x})O_3$ (BZT)) is one of the most promising microwave tuneable dielectric materials to be developed for tunable microwave devices such as tunable filters, phase shifters, antennas and actuators [1–3]. BZT with perovskite-type oxide structure (ABO_3) is formed by a solid solution of barium titanate ($BaTiO_3$) and barium zerconate ($BaZrO_3$). The substitution of isovalent cations, Zr^{4+}, for Ti^{4+} results in altering the crystal features together with broadening and shifting in the phase transition (Curie temperature, T_c) [3–5]. The dielectric properties and tunability of $Ba(Zr_xTi_{1-x})O_3$ ceramics can be optimized by manipulating the Zr:Ti concentration. BZT with x in the compositional range of $0.26 \leq \times \leq 0.42$ was reported to exhibit relaxor-like behavior (diffuse phase transition) with high thermal stability, high electric field tunability and low dielectric loss constant [4, 6].

Nanocrystalline BZT with homogeneous distribution of composition and uniform particle size and shape are required in order to improve the sinterability and dielectric properties

Received December 11, 2012; in final form March 13, 2013.
*Corresponding author's. E-mail: panpailin@hotmail.com

of electroceramics [4, 7]. To produce materials with the desired properties, many factors need to be taken into consideration *e.g.* nature of starting materials and processing routes. Various wet chemical methods including co-precipitation [7], sol-gel [8], hydrothermal [9] and sonochemical techniques [10] have been reported for preparing BZT powders. Comparing to the others, a co-precipitation is seemed to be a simplest and effective method to produce BZT nanoparticles. As a strong alkaline environment is favored for the chemical equilibrium of reaction of the BZT formation, BZT can simply be precipitated in a solution containing highly hydroxide ion (OH^-) concentration [7]. In addition, this method does not require expensive reagents, complex procedures, sophisticate instruments and high temperature calcination treatment steps. Reddy *et al.* has reported that nanocrystalline BZT ($Ba(Zr_xTi_{1-x})O_3$ for $x = 0.10$, 0.20 and 0.30) with mixture of shapes including spherical, elliptical, acicular and cube with truncated edged shapes can be obtained by co-precipitation in 15 M NaOH [7]. As increasing of hydroxide concentration was suggested to increase the purity [11] and decreasing the particle sizes of BZT [10]. This study focused on the investigation of the phase formation and microstructure BZT ($Ba(Zr_xTi_{1-x})O_3$ when $x = 0.25$, 0.30 0.35) prepared by co-precipitation in highly aqueous basic solution (20 M NaOH).

Experimental Procedure

BZT nanoparticles ($Ba(Zr_xTi_{1-x})O_3$ for $x = 0.25$, 0.30 and 0.35) were prepared by co-precipitation in 20 M NaOH at low temperature (80°C). The stoichiometric amounts of barium chloride dihydrate ($BaCl_2.2H_2O$, Fluka, 99% purity), zirconium oxychloride octahydrate ($ZrOCl_2.8H_2O$, Sigma-Aldrich, 99.5% purity) and titanium chloride ($TiCl_4$, Waka, 99% purity) were dissolved in de-ionized water. The mixed solution was slowly dropped into a 20 M (mol/l) sodium hydroxide solution (NaOH, Carla Erba, 97% purity) at a constant rate of 10 ml/min. The reaction was carried out at 80°C under flowing of argon gas and a pH of the synthesis solution was maintained at pH≈14. After the adding process was completed, the solution was continuously stirred at constant rate for 15 min. The precipitates were separated by centrifuge at 4000 rpm and washed with de-ionized water until the washed solution was neutralized (pH~7) followed by washing with formic acid (HCOOH, Carla Erba, 98% purity) to remove any possible carbonate contamination [12]. The as-precipitates were then dried in oven at 100°C for 24 hours. Phase formation and crystal structure of the synthesis powders was studied using X-ray diffraction (XRD, Bruker D8 Advance, CuKα, $2\theta = 20$–80°, the measurements were made relative to an external silicon standard and the phases were identified using the JCPDS (ICDD) index, the crystal sizes was calculated based on the Debye-Scherrer equation ($D = K\lambda/(\beta\cos\theta)$, where D is a crystal size, K is a constant taken as 0.9, λ is the wavelength of the X-ray radiation (CuKα radiation 1.5418 Å), β is a full width at half maximum of intensity of the diffraction peak and θ is the Bragg's angle) [3], Fourier-transform infrared spectroscopy (FT-TR, Perkin-Elmer GX 8500, KBr mixing, measuring in the range of 400–4000 cm^{-1}) and Raman spectroscopy (Thermo scientific DXR, measuring in the range of 100–1000 cm^{-1}). The microstructure was studied using scanning electron microscopy (SEM, Hitachi 54700) and transmission electron microscopy (TEM, Phillips TECNAI 20).

Results and Discussion

XRD studies of the as-prepared powders with different zirconium concentrations ($Ba(Zr_xTi_{1-x})O_3$ when $x = 0.25$, 0.3 and 0.35) obtained by co-precipitation in 20 M NaOH

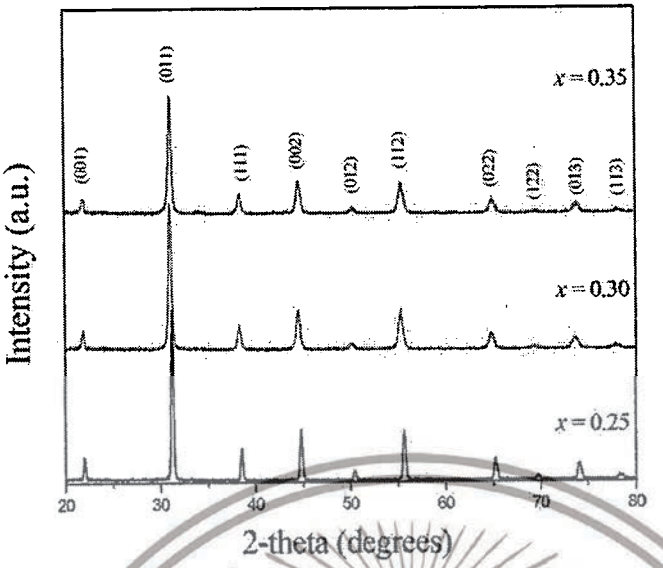

Figure 1. XRD patterns of as-precipitated $Ba(Zr_xTi_{1-x})O_3$ for x = 0.25, 0.3 and 0.35 obtained from co-precipitation in 20 M NaOH aqueous solution. (Color figure available online.)

solution are shown in Figure 1. The XRD patterns of all samples showed well-defined diffraction peaks with the phases identified to be cubic perovskite BZT phase (JCPDS no. 36-0019). No other diffraction peaks were observed in all samples. This indicates that single phase crystalline BZT can be obtained by precipitation in 20 M NaOH solution. By increasing of zirconium concentration, the XRD peaks are appeared to shift to slightly lower angles. This shift in angle is consistent with the increasing of zirconium concentration indicating the replacement of smaller titanium cations by larger zirconium cations (ionic radii (8-fold coordination) of Ti^{4+} = 0.745 Å and Zr^{4+} = 0.860 Å) [3]. The calculated crystallite sizes using Debye-Scherrer equation were 36.8 ± 0.02 nm, 28.3 ± 0.02 nm and 18.9 ± 0.02 nm for $Ba(Zr_{0.25}Ti_{0.75})O_3$, $Ba(Zr_{0.30}Ti_{0.70})O_3$ and $Ba(Zr_{0.35}Ti_{0.65})O_3$ powders, respectively.

The phase formation of the as-precipitated BZT ($Ba(Zr_xTi_{1-x})O_3$ for x = 0.25, 0.3 and 0.35 was further studied by FT-IR and Raman spectroscopy. IR spectra of BZT powders (Figure 2) showed the characteristic absorption bands of the perovskite phase (vibration of BO_6 octrahedra, when B = Ti or Zr) at 540 cm^{-1} [13]. It should be noted that absorption bands observed at 3400 cm^{-1} and 1600 cm^{-1} can be attributed to the asymmetric vibration of O—H stretching and O—H bending of physically absorbed moisture containing in the samples or in KBr during sample preparation.

Figure 3 shows room temperature Raman spectra of BZT powders prepared by a co-precipitation in 20 M NaOH aqueous solution. The Raman spectra of all samples are comparable with those have been reported in literatures [4, 5]. The characteristic Raman modes of BZT associating with the asymmetry within the BO_6 octrahedra were observed at 185, 220, 300 and 512 cm^{-1} (A_1(TO) modes) along with the modes corresponded to zirconium substitution (locally distorted ZrO_6 octrahedra) and a signature of the ferroelectric relaxor phase at region 600–800 cm^{-1}. The weak bands assigned to $BaCO_3$ were observed at 135, 155 and 694 cm^{-1} [14, 15], this carbonate contamination was probably formed during storing the samples. The results from XRD, FT-IR and Raman spectroscopy

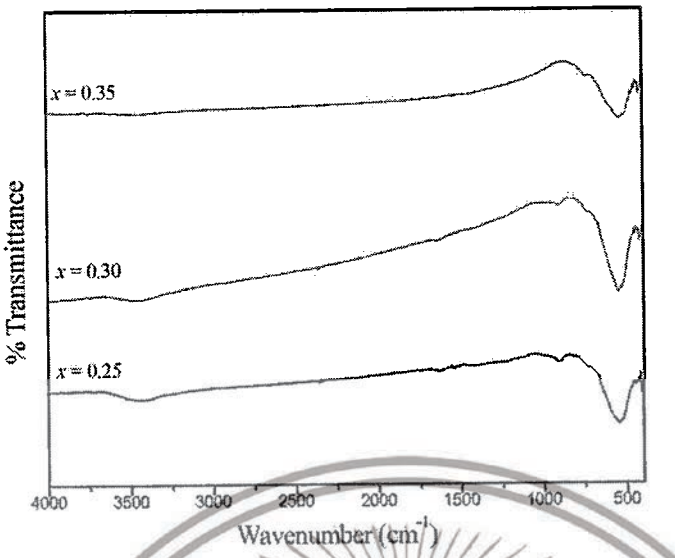

Figure 2. IR spectra of $Ba(Zr_xTi_{1-x})O_3$ for x = 0.25, 0.3 and 0.35. (Color figure available online.)

confirmed that high purity crystalline BZT powders can be prepared by co-precipitation in 20 M NaOH solution without a requirement of further calcination process.

The microstructure of the $Ba(Zr_{0.3}Ti_{0.7})O_3$ powders examined by SEM is presented in Figure 4. The BZT powders showed spherical morphology with high degree of uniformity with respect to shape and size. TEM micrographs of BZT ($Ba(Zr_xTi_{1-x})O_3$ for x = 0.25, 0.3 and 0.35) with particle size distributions are shown in Figure 5. As can be seen, TEM study supported the SEM analysis by showing spherical morphology with narrow size

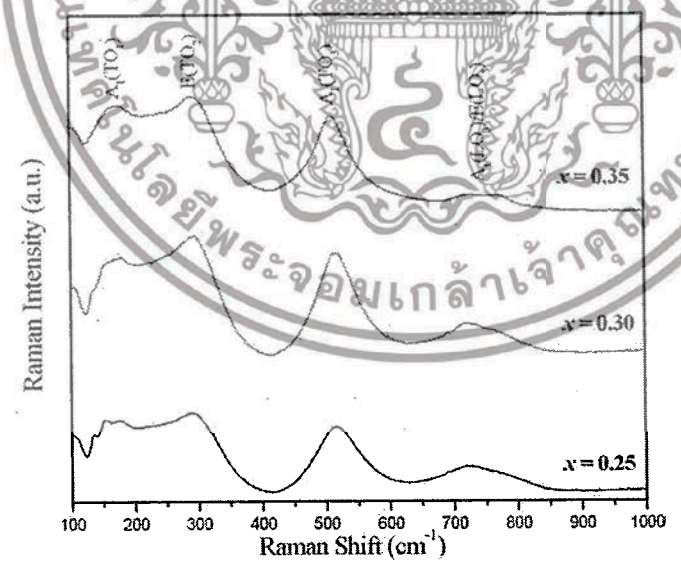

Figure 3. Room temperature Raman spectra of $Ba(Zr_xTi_{1-x})O_3$ for x = 0.25, 0.3 and 0.35. (Color figure available online.)

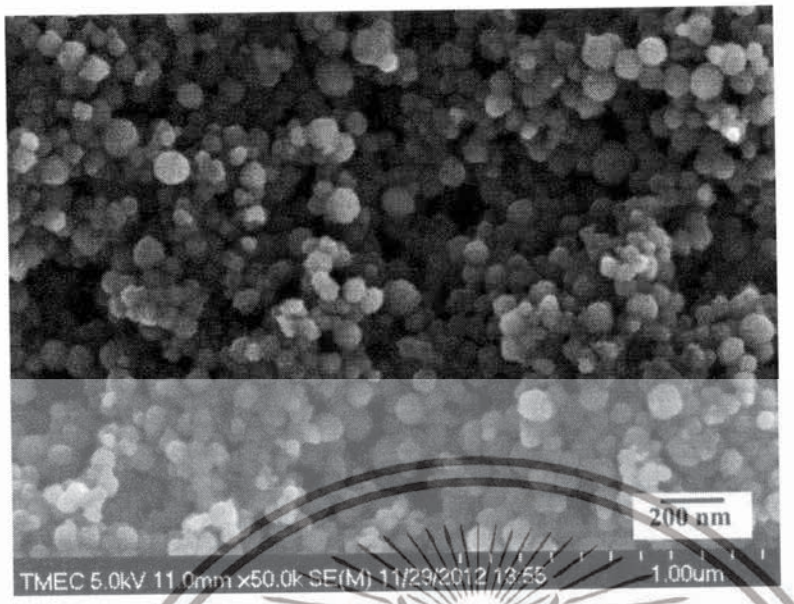

Figure 4. SEM image of $Ba(Zr_{0.3}Ti_{0.7})O_3$ powders obtained from precipitation in 20 M NaOH.

Figure 5. TEM images and size distributions of $Ba(Zr_xTi_{1-x})O_3$ for x = 0.25, 0.3 and 0.35. (Color figure available online.)

distribution. The BZT with spherical shape obtained from this study is different from that has been reported by Reddy *et al.* [7]. As the dispersive force and electrostatic interactions of ions are important factors to control the crystal formation, increasing hydroxide ion (OH^-) concentration of medium solution (20 M NaOH) could lead to the isoelectric condition which is favored for the spherical shape formation [16]. The average crystal sizes observed by TEM (26 ± 5 nm, 36 ± 8 nm and 31 ± 6 nm, for $Ba(Zr_{0.25}Ti_{0.72})O_3$, $Ba(Zr_{0.30}Ti_{0.70})O_3$, $Ba(Zr_{0.35}Ti_{0.75})O_3$ respectively) were in that same ranges with those calculated by XRD.

Summary

This study investigated the preparation of spherical monosized barium zirconate titanate nanoparticles ($Ba(Zr_xTi_{1-x})O_3$ for $x = 0.25$, 0.30 and 0.35) by co-precipitation in a highly basic solution (20 M NaOH) at 80°C using $BaCl_2.2H_2O$, $ZrOCl_2.8H_2O$ and $TiCl_4$ as the precursors. The phase formation of the as-precipitated powders characterized by XRD, FT-IR and Raman spectroscopy exhibited single-phase cubic perovskite BZT. These results indicate that high purity nanocrystalline BZT can be prepared directly by co-precipitation in 20 M NaOH without the need of any further calcination treatment. The microstructure examined by SEM and TEM showed that BZT powders had spherical morphology with uniform size and shape. The crystal sizes of BZT obtained by TEM analysis were 20–40 nm. This study exhibits that spherical nanocrystalline BZT with uniform size and shape can simply be prepared via co-precipitation in 20 M NaOH solution. This simple, effective and low cost procedure could probably be applied for producing some other perovskite oxide materials.

Acknowledgments

This work was supported by Thailand research fund (TRG5680019), KMITL research fund (KREF015420) and faculty of science KMITL.

References

1. T. Maiti, R. Guo, and A. S. Bhalla, Enhanced electric field tunable dielectric properties of $BaZr_xTi_{1-x}O_3$ relaxor ferroelectrics. *Appl. Phys. Lett.* **90**, 182901-3 (2007).
2. A. Dixit, *et al.*, Dielectric and Tunable Properties of $BaZr_xTi_{1-x}O_3$ Thin Films. *Ferroelectrics Letters*. **32**, 131–137 (2005).
3. J. Xu, *et al.*, Ferroelectric relaxor behavior and microwave dielectric properties of $Ba(Zr_{0.3}Ti_{0.7})O_3$ thin films grown by radio frequency magnetron sputtering. *Journal of applied Physics*. **106**(7), 074107 (2009).
4. P. S. Dobal, *et al.*, Micro-Raman scattering and dielectric investigations of phase transition behavior in the $BaTiO_3$–$BaZrO_3$ system. *J. Appl. Phys.*, 89(2001), 8085 (2001).
5. P. S. Dobal, *et al.*, Phase transition behavior of $BaZr_xTi_{1-x}O_3$ ceramics. *Journal of Raman Spectroscopy.*, **32**(1), 69–71 (2001).
6. A. Dixit, *et al.*, Phase transition studies of sol-gel deposited barium zirconate titanate thin films. *Thin Solid Films.*, **447-448**, 284–288 (2004).
7. S. B. Reddy, K. P. Rao, and M. S. R. Rao, Nanocrystalline barium zirconate titanate synthesized at low temperature by an aqueous co-precipitation technique. *Scripta Materialia.*, **57**(7), 591–594 (2007).
8. N. Binhayeeniyi, *et al.*, Physical and electromechanical properties of barium zirconium titanate synthesized at low-sintering temperature. *Materials Letters.*, **64**(3), 305–308 (2010).
9. B. W. Lee, and S.-B. Cho, Preparation of $BaZr_xTi_{1-x}O_3$ by the hydrothermal process from peroxo-precursors. *Journal of the European Ceramic Society.*, **25**(12), 2009–2012 (2005).

10. P. Seeharaj, *et al.*, Barium zirconate titanate nanoparticles synthesized by the sonochemical method. *Ceramics International,* 2012(In press Corrected proof).
11. F. Boschini, *et al.*, Rapid synthesis of submicron crystalline barium zirconate $BaZrO_3$ by precipitation in aqueous basic solution below 100°C. *Journal of the European Ceramic Society.*, **29**(8), 1457–1462 (2009).
12. K.-Y. Chen, and Y.-W. Chen, Preparation of barium titanate ultrafine particles from rutile titania by a hydrothermal conversion. *Powder Technology.*, **141**(1-2), 69–74 (2004).
13. N. Chakrabarti, and H. S. Maiti, Chemical synthesis of barium zirconate titanate powder by an autocombustion technique. *Journal of Materials Chemistry.*, **6**(7), 1169–1173 (1996).
14. P. Pasierb, *et al.*, Structural properties of Li_2CO_3-$BaCO_3$ system derived from IR and Raman spectroscopy. *Journal of Molecular Structure.* , **596**(1-3), 151–156 (2001).
15. F. Maxim, *et al.*, Kinetic Study of the Static Hydrothermal synthesis of $BaTiO_3$ using Titanate nanotubes precursors. Crystal Growth & Design., **11**(8), 3358–3365 (2011).
16. J. Subrt, *et al.*, Synthesis of spherical metal oxide particles using homogeneous precipitation of aqueous solutions of metal sulfates with urea. *Powder Technology.*, **169**(1), 33–40 (2006).

C Advances

APER

CrossMark

is: RSC Adv., 2015, 5, 38061

Facile sonochemical synthesis of near spherical barium zirconate titanate ($BaZr_{1-y}Ti_yO_3$; BZT); perovskite stability and formation mechanism

Supamas Wirunchit,[ac] Thitirat Charoonsuk[ac] and Naratip Vittayakorn*[abc]

The multicationic oxides of perovskite $Ba(Zr,Ti)O_3$ were synthesized successfully by the sonochemical method without a calcination step. Detailed exploration considering the role of sodium hydroxide (NaOH) concentration, synthesis atmosphere, ultrasonic reaction time and precursor concentration on the perovskite phase formation and particle size was presented. It was found that nanocrystals were formed directly before being oriented and aggregated into large particles in aqueous solution under ultrasonic irradiation. The nucleation in the sonocrystallization process was accelerated by the implosive collapse of bubbles, while the crystal growth process was inhibited or delayed by shock waves and turbulent flow created by ultrasonic radiation. A pure complex perovskite phase of spherical shape was formed completely in a short irradiation time without the calcination process. Sonochemical irradiation could accelerate spherical shape formation of the particles significantly. These results provide new insights into the development and design of better nanomaterial synthesis methods.

ved 10th March 2015
ɔted 21st April 2015

10.1039/c5ra04267d

rsc.org/advances

Introduction

ım zirconate titanate ($BaZr_yTi_{1-y}O_3$) and/or $BaZr_yTi_{1-y}O_3$-d ceramics have become among the most researched lead piezoelectric materials, due to their excellent piezoelectric erties.[1–4] The conventional solid state method is a tradi-al way of preparing $BaZr_yTi_{1-y}O_3$ ceramics. However, this ication method has several drawbacks such as a long pro-ing time,[5,6] multiple calcinations,[7,8] low purity,[9,10] sub-ometer size crystals[5,6,11] and a frequent need for grinding s,[10] and this technique is not suitable for obtaining narrow icle size distribution.[5,7,11] J. Bera *et al.*[5] investigated the ıation of $BaZr_yTi_{1-y}O_3$ solid solution by using solid state tion between $BaCO_3$, ZrO_2 and TiO_2. They reported that at a ɔerature of lower than 1300 °C, raw materials did not form $_yTi_{1-y}O_3$ solid solutin directly because it had a higher ıation of energy (133 kcal mol^{-1}) than $BaTiO_3$ (34.3 kcal $^{-1}$) and $BaZrO_3$ (48.4 kcal mol^{-1}). The formation mecha-ı can be explained by multistep reactions as follows: at the al stage, $BaTiO_3$ and $BaZrO_3$ are formed separately at a ɔerature ranging from 700 to 800 °C. Subsequently, the iO_3 diffuses into the $BaZrO_3$ to form a single perovskite phase of $BaZr_yTi_{1-y}O_3$ at a temperature as high as 1600 °C. In order to obtain perovskite $BaZr_yTi_{1-y}O_3$ nanoparticles with high quality, many new wet-chemical synthesizing methods have been developed to replace conventional solid state reaction, including the combustion method,[12] sol–gel method,[13,14] direct synthesis from solution (DSS),[15] and aqueous co-precipitation method.[16] Nanosized $BaZr_yTi_{1-y}O_3$ particles are synthesized by wet-chemical methods, which make the $BaZr_yTi_{1-y}O_3$ system very attractive for developing new electronic nanodevices.[17,18] P. Julphunthong *et al.*[12] synthesized barium zirconate titanate (BZT) powder *via* the combustion technique by using urea $(NH_2)_2CO$ as a fuel to reduce the reaction temperature. Unfortunately, the powder needed to be calcined at 1000 °C for 5 h after the combustion process in order to obtain a pure perovskite structure. Generally, submicron sizes with irregular morphology of the powder are observed always after the calcination process.[11,19] It is very difficult to obtain nanoparticles of uniform size under the calcination process,[11,19] which would therefore be an undesirable step during the fabrication process of nanopowder. M. Veith *et al.*[14] reported the synthesis of homogeneous $BaZr_{0.5}Ti_{0.5}O_3$ nanopowders that derived from a alkoxide sol–gel route. The hetero-trimetallic Ba–Ti–Zr framework was synthesized from $[TiZr(OPr^i)_8 \cdot Pr^iOH]_2$ and $[Ba(OPr^i_2)]$ and used as a precursor. The processing was performed under CO_2–free argon (Ar) or nitrogen atmosphere. The most advantageous characteristics of this method are the high purity and outstanding control of the composition of resulting powders. Nevertheless, the hydrolyzed dried gel needs to be calcined at temperatures above 400 °C in order to crystallize $BaZr_yTi_{1-y}O_3$. J. Q. Qi *et al.*[15] developed a new method called direct synthesis

*roceramics Research Laboratory, College of Nanotechnology, King Mongkut's ute of Technology Ladkrabang, Bangkok 10520, Thailand. E-mail: ipcmu@yahoo.com

rtment of Chemistry, Faculty of Science, King Mongkut's Institute of Technology abang, Bangkok 10520, Thailand

nced Materials Research Unit, Faculty of Science, King Mongkut's Institute of ology Ladkrabang, Bangkok 10520, Thailand

solution (DSS) to prepare $BaZr_yTi_{1-y}O_3$ nanoscaled ers near room temperature under ambient pressure. By lving barium hydroxide into warm water as a base solu- nanocrystalline $BaZr_yTi_{1-y}O_3$ powders can be obtained by ıg isopropanal solution of zirconium isopropoxide–iso- ınol and tetrabutyl titanate with hot base solution. When ; this, the particle size of the nanoparticles fell within the : of 25 to 120 nm. Recently, single phase nanocrystalline er of $BaZr_yTi_{1-y}O_3$ was obtained successfully by the ɔus co-precipitation method at a temperature <100 °C.[16] ɔrocess was as follows: a mixed chloride solution of Ba, Ti Zr ions was dripped slowly into a heated strong base ion (pH > 12.0). The nanocrystalline $BaZr_yTi_{1-y}O_3$ favored ing a strongly based concentration at a temperature of t 80 °C. The as-prepared powders showed an average :le size of 30 nm. The precipitant concentration and ıesis temperature play an important role as a parameter for asing product purity.[16] However, the particles have various es such as spherical, acicular, elliptical, and cubic with :ated edges.[16] The particle size and shape are not controlled ıis method. The different morphologic shape and wide : of particle size distribution have been the key problem to e the abnormal grain growth in the sintering process.[11] order to eliminate abnormal grain growth during the ring process, $BaZr_yTi_{1-y}O_3$ nanoparticles are expected to spherical morphology with a narrow particle size distri- n.[11] Among the wet-chemical methods developed so -16,20,21 sonochemical synthesis at ambient temperature s to be a new technique that fulfills the requirements for ıesizing extremely fine particles with spherical morphology a narrow size distribution.[22,23] The sonochemical method an acoustic cavitation phenomenon from ultrasonic irra- ɔn to generate or accelerate the chemical reaction. Acoustic ıtion is the formation, growth, and implosive collapse of les in a liquid, which generates a localized hot spot, with a erature of approximately 5000 K, pressure of 20 MPa, and ng and cooling rates that exceed 10^{10} K s^{-1}.[22,24] These ient, localized hot spots can drive many chemical reac- , such as decomposition, dissolution, oxidation, reduction, ɔromotion of polymerization.[22,24] By using these transient me conditions, various kinds of organic, inorganic and l materials, with unusual properties such as metals,[25,26] ous metals,[27,28] simple metal oxides,[29–35] nitrides,[29] des,[36] sulfides[29,37] and core/shell nanocomposites[37,38] were ıesized successfully. Up until now, few studies on the chemical synthesis of multicationic oxides based on a ɔlex perovskite structure $[A(B'B'')O_3]$ have been reported, ɔ the best of the authors' knowledge, there is no previous t on the direct sonochemical synthesis of $(BaZr_yTi_{1-y}O_3)$; y ı–0.6 powders.

ıis study used high-intensity ultrasound irradiation to ıesize nanosized complex ternary metal oxide ($BaZr_yTi_{1-y}$- y = 0.0–0.6. Various key synthesis parameters such as ıesis atmosphere, concentration of precipitating agent, entration of the starting solution, sonication time and Zr/Ti r ratio were investigated carefully in order to understand effect on the perovskite phase formation and morphology of the powders. The procedure of the sonochemical formation of nanosized BZT powders also was examined.

2. Experimental procedure

2.1 Solution preparation

In this study, all the reagents used in experiments were of analytical purity and used without further purification. The barium chloride dihydrate ($BaCl_2 \cdot 2H_2O$, 99.8% Merck), zirconium oxychloride octahydrate ($ZrOCl_2 \cdot 8H_2O$, 99.5% Advance material) and titanium tetrachloride ($TiCl_4$, 99.9% Wako) were used as the starting materials. Sodium hydroxide (Fisher Scientific 97.7%) was used as the precipitating agent. In order to obtain the stock of Ti-solution, $TiCl_4$ was dripped very slowly into deionized water at a temperature lower than 5 °C and stirred vigorously until the solution was clear. Then, the separate stoichiometric amounts of $BaCl_2 \cdot 2H_2O$ and $ZrOCl_2 \cdot 8H_2O$ were dissolved typically in de-ionized water in order to obtain the barium (Ba^{2+}) and zirconium (Zr^{4+}) solution, respectively. These stocks of starting solution were prepared freshly for each set of experiments.

2.2 Synthesis of $Ba(Zr_yTi_{1-y})O_3$ powders

The barium zirconate titanate ($Ba(Zr_yTi_{1-y})O_3$; BZT) powder products, with the composition (y) = 0.00, 0.05, 0.20, 0.04 and 0.60, were synthesized by the sonochemical method without the calcination process, which was in accordance with the reaction (1):

$$BaCl_2 \cdot 2H_2O_{(aq)} + (1-y)TiCl_{4(aq)} + yZrOCl_2 \cdot 8H_2O_{(aq)} + (6-2y)NaOH_{(aq)} \rightarrow Ba(Zr_yTi_{1-y})O_{3(s)} + (6-2y)NaCl_{(aq)} + (13-y)H_2O_{(aq)} \quad (1)$$

Firstly, the appropriate proportions of titanium and zirconium (withdrawn from the stock solution using a pipette) were mixed together to form a solution to which the barium solution was then added, with continuous stirring in order to obtain a homogeneous mixed solution. The concentrations of barium and titanium solution were varied from 0.01 mol L^{-1} to 1.5 mol L^{-1} in order to study the effect of Ba and Ti ion concentration on the perovskite phase formation. The Ba and Ti ion ratio in the mixed solution was targeted constantly at 1 : 1. After that, sonication equipment was set up for the sonochemical process. Regarding the synthesis system, the effect of synthesis atmosphere on the phase formation was studied. The powder synthesized in open air was compared with that in a closed system with Ar gas. After setting up the equipment, the sodium hydroxide (NaOH) solution was loaded into a sonication vessel for use as the precipitating agent. The concentration of NaOH solution was varied from 5 to 20 mol L^{-1} in order to study its effect. Then, the mixed starting solution was added into the sonication vessel, which contained the NaOH solution, drop by drop at a rate of about 25 ml min^{-1}. Therefore, a high pH value reached 14 during the process. In order to obtain nanoparticles of better quality, pulse ultrasonication (Sonics VCX-750, 20 kHz, 750 W) was conducted in the 2 s mode; and a pause in 1 s mode was performed in the experiments that followed. It has been

ted that synthesized powder in pulse ultrasonic mode a narrower particle size distribution than that in contin- ultrasonic mode.[39] This may be related to the uneven bution of ultrasonic energy in the ultrasonic vessel.[39] ıg the process of adding mixed solution, white precipita- vas formed instantaneously. After the irradiation time was the sonication vessel that contained the precipitate was d to room temperature by immersing in tap water. Then, ecovered precipitate was filtered out by centrifugal filtra- and washed with de-ionized water until the pH value ed to 7. The supernatant was checked with 0.1 mol L^{-1} of $)_3$ solution until no white sediment remained, which rmed that the chloride ion was not retained. Finally, the ed precipitates were dried at 80 °C in an oven overnight in to obtain the powder products.

Characterization

ierovskite phase formation, structure and crystallite size of roducts were carried out by X-ray powder diffraction using ray diffractometer (Philips PW3040, The Netherlands) with x radiation ($\lambda = 0.15406$ nm). The acceleration voltage was / with a 150 mA current flux. X-ray diffraction (XRD) was of the powders attached to a glass slide, and data were cted in the 2θ range from 20° to 60°, with a scanning rate of r min and sample interval of 0.02°. Crystallite size and)strain were calculated by the X-ray line broadening od using Scherrer[40] and Hall–Williamson methods.[41] The rrer equation relies on utilizing the following equation:

$$D = K\lambda/\beta \cos\theta, \quad (2)$$

e λ is the CuK_α radiation of wavelength (1.5406 Å), β is the vidth at haft-maximum (FWHM) in radian and θ is the ering angle. Also, K is the shape factor (a constant equal to and D is the crystallite size normalized to the reflecting s. The Hall–Williamson method provides a technique for ıg an average size of coherently diffracting domains and)strain. Strain-induced peak broadening arises due to rfect crystal and distortion, which is calculated by using)llowing formula:

$$\varepsilon = \frac{\beta_{hkl}}{4\tan\theta} \quad (3)$$

estimate microstrain from the XRD pattern, Hall and amson proposed a formula as follows:

$$\beta_{hkl}\cos\theta = \frac{\kappa\lambda}{D} + 4\varepsilon\sin\theta \quad (4)$$

e ε is the elastic strain. When $\beta_{hkl}\cos\theta$ is plotted *versus* ent diffraction planes, a linear fit is expected. Lattice ıs were obtained from the slope of this line. Raman ra were recorded in the 100–1000 cm^{-1} wave number s in order to support the crystal structure identification of esized powders with a Thermo Scientific DXR Raman)scope (532 nm excitation of the laser). The vibration of the bond in molecules was obtained from Fourier transform infrared (FT-IR spectrum Gx, Perkin Elmer, America) spectra. The morphology and particle size of the resulting as-prepared products were characterized initially by using a scanning electron microscope (SEM, Hitachi 54 700), equipped with energy-dispersive X-ray spectroscopy (EDX) capabilities. These samples were then coated conductively with gold by sputtering for 15 s in order to minimize charging effects under SEM imaging conditions. Regarding the study of phase transition, a differential scanning calorimeter (DSC 2920, TA Instrument) was used, and DSC curves were recorded in a temperature range from 30 °C to 200 °C with a scanning rate of 10°C min^{-1}.

3. Results and discussion

3.1 The effect of NaOH concentration on the perovskite phase formation

Changing the synthetic parameters greatly affected the perovskite phase formation. This study exposed the concentration of NaOH that had a notable effect on the perovskite phase formation. Fig. 1 shows the XRD patterns of $BaZr_yTi_{1-y}O_3$; $y = 0.0$ powders that evolved after sonication for 60 min in different NaOH concentrations in the open air system. As shown in Fig. 1, only X-ray peaks of whiterite-$BaCO_3$ and $Ba(OH)_2(H_2O)_3$ are present in powder synthesized with 5 mol L^{-1} NaOH. These kinds of unwanted phase correspond well with the literature.[21]

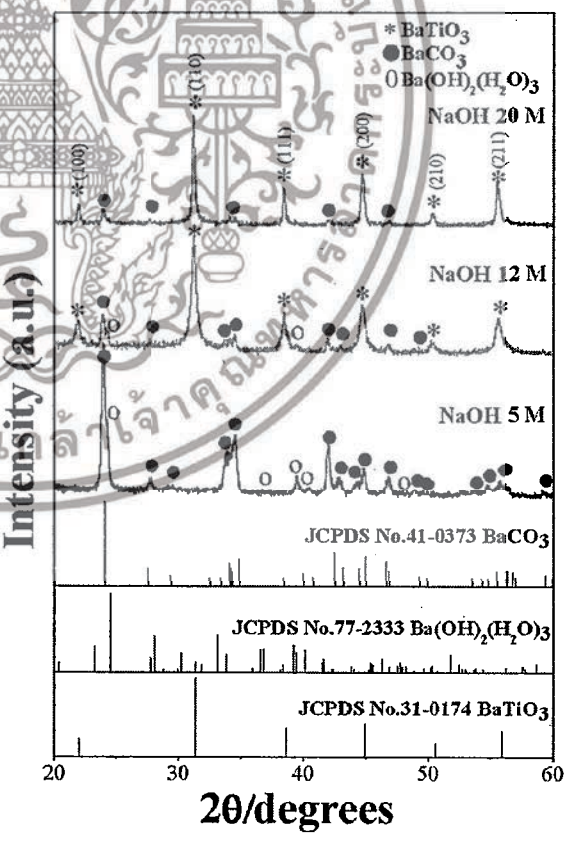

Fig. 1 XRD patterns of $BaZr_yTi_{1-y}O_3$; $y = 0.0$ powders evolved for 60 min at various NaOH concentrations in the open air system.

erovskite structure was characteristic of diffraction peaks, indicating no reaction had yet been triggered for synthesis 5 mol L^{-1} of NaOH concentration. Interestingly, the XRD rn presented no evidence of a Ti-precursor phase, indig that an amorphous phase might be formed.[42] When the vskite phase started to form with increasing NaOH entration, the $BaCO_3$ and $Ba(OH)_2(H_2O)_3$ phase decreased iatically. Diffraction peaks of the perovskite phase are ked with the $BaTiO_3$ cubic structure in the *Pm3m* space p from JCPDS card no. 31-0174. Intensity of the perovskite rn increased significantly with increasing NaOH concenon. The increase in perovskite phase at high hydroxide entration might be due to increasing formation of the plex polymeric chain network of bimetallic Ba–Ti hydrox-[43] Nevertheless, in the open air system, a peak of $BaCO_3$ low intensity was still present in products synthesized in 20 L^{-1} of NaOH concentration. The problem of forming $BaCO_3$ igh NaOH concentration should be attributed to use of the air synthesis system, in which the Ba-hydroxide in the ion can react easily with CO_2 in air or carbonate species in olution.

Effect of synthesis atmosphere on the perovskite phase ation

der to study the influence of synthesis atmosphere on the vskite phase formation, the powder was synthesized in n-air and Ar atmosphere. Fig. 2 shows XRD patterns of $_yTi_{1-y}O_3$; $y = 0.0$ powders that evolved after sonication for 5 0 min in 20 mol L^{-1} of NaOH concentrations in the (a) open ystem and (b) closed system with Ar gas. The XRD pattern in pen-air system showed a mixed phase of perovskite, $BaCO_3$ and $Ba(OH)_2(H_2O)_3$ phases. The $BaCO_3$ and $Ba(OH)_2(H_2O)_3$ phase remained in the pattern with increasing sonication time, indicating that the formation of $BaCO_3$ and $Ba(OH)_2(H_2O)_3$ phase are not related directly with the sonication irradiation time. Regarding powder synthesized in Ar atmosphere, the $BaCO_3$ phase disappeared after only five minutes sonication time. The relatively small XRD pattern agreed well with the perovskite structure. However, intensity of the perovskite phase was quite low, indicating that the product has low crystallinity. The crystallinity of the product was improved significantly by increasing the sonication period, and a sharp XRD pattern was observed clearly at 60 min sonication time. The observations clearly show that the $BaZr_yTi_{1-y}O_3$; $y = 0.0$ phase formation was completed during the sonochemical process itself, without the need of further calcination or a heating process. The XRD pattern indicated that the synthesized powder agreed well with the cubic $BaTiO_3$ structure in the *Pm3m* space group (JCPDS data no. 31-0174). Based on XRD results, Rietveld refinement analysis gave lattice parameters of $a = 4.0415 \pm 0.0004$ Å, which were slightly larger than those reported to value $a = 4.031$ Å (JCPDS data no. 31-0174). This slight expansion of lattice parameters (*a*) might be due to the presence of a trace amount of the OH group trapped in the crystal lattice, which can be confirmed by solvothermal treatment with dimethylformamide (DMF). The intensities and positions of the peaks match very well with those data reported in the literature.[15,16] No peaks in any other phase were detected, thus indicating high purity of the product. These results indicate that impurity of the $BaCO_3$ phase can be reduced or eliminated when the product is synthesized with a high concentration of precipitating agent (NaOH) and in the closed system with Ar atmosphere.

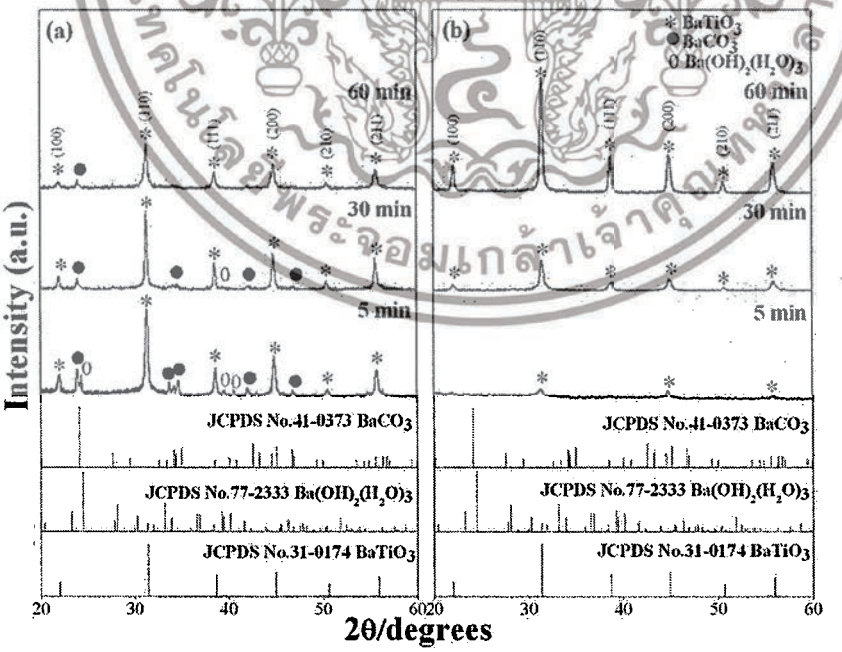

: XRD patterns of $BaZr_yTi_{1-y}O_3$; $y = 0.0$ powders obtained after sonication for 5 to 60 min in 20 mol L^{-1} of NaOH concentrations in the (a) air system and (b) closed system with Ar gas.

Effect of precursor concentration on the perovskite phase formation

Effect of Ba and Ti ion concentration in the starting solution on the perovskite phase formation was observed. The Ba to Ti ion ratio in the solution was kept constant at 1 : 1. The precursor concentration varied from 0.01 to 1.5 mol L^{-1}. Fig. 3(a) illustrates the XRD pattern of $BaZr_yTi_{1-y}O_3$; $y = 0.0$ powders at different precursor concentrations synthesized for 60 min with 20 mol L^{-1} of NaOH in Ar atmosphere. The XRD pattern displayed the $BaCO_3$ and $Ba(OH)_2(H_2O)_3$ phase at a low precursor concentration ($\leq$0.1 mol L^{-1}), the perovskite phase was not observed. The perovskite phase started to form at 0.5 mol L^{-1}. When the concentration increased to 0.5 mol L^{-1}, $BaCO_3$ peak disappeared, and the pure perovskite phase was obtained. Fig. 3(b)–(d) display the morphology of the product synthesized with different precursor concentrations. Two types of morphological particles were observed clearly at a low precursor concentration (0.01 mol L^{-1}); *i.e.* a large particle with irregular morphology and small one with agglomerated cluster. The energy dispersive X-ray (EDX) analysis [Fig. 3(b)] indicated that the large particle was the $BaCO_3$ phase, while the agglomerated cluster was the Ti-amorphous phase. The results corresponded well with the XRD pattern. The morphology of the particle changed significantly with increased precursor concentration to a more spherical shape, and a narrow size distribution was observed clearly. The histogram of particle size distribution in Fig. 3(d) illustrates nanoparticles with a narrow size distribution that ranges within the average particle dispersity (D_{SEM99}/D_{SEM50}) of 1.54. The average particle size decreased significantly with increasing precursor concentration, and when measured by SEM was found to be 123.2 $\pm$ 42.8 nm and 49.6 $\pm$ 11.2 nm for powder synthesized in 0.5 mol L^{-1} and 1.5 mol L^{-1} of precursor concentration, respectively. The intensity of the XRD pattern decreased when the precursor concentration increased to 1.5 mol L^{-1}, while the FWHM value was increased, thus indicating that nanocrystals tend to become smaller. The Hall–Williamson plot of $\beta_{hkl}\cos(\theta)/\lambda$ *versus* 4 sin θ gives the value of strain from the slop of the fit, as shown in Fig. 4(a)–(f). The crystalline size calculated from the Scherrer and Hall–Williamson methods is summarized in Table 1, where this assumption has been confirmed. The crystallite size of powder was found to be 36.61 $\pm$ 13.96 nm and 16.40 $\pm$ 01.46 nm when synthesized in 0.5 mol L^{-1} and 1.5 mol L^{-1} of precursor concentration, respectively. It is interesting to note that the particle size becomes close to the crystallite size with increasing precursor concentration, which indicates that particles synthesized at a high precursor concentration are composed of fewer crystallites. Generally, particle sizes that precipitate from solution are influenced by the relative rates of nuclei formation and crystallite growth, and a high nucleation

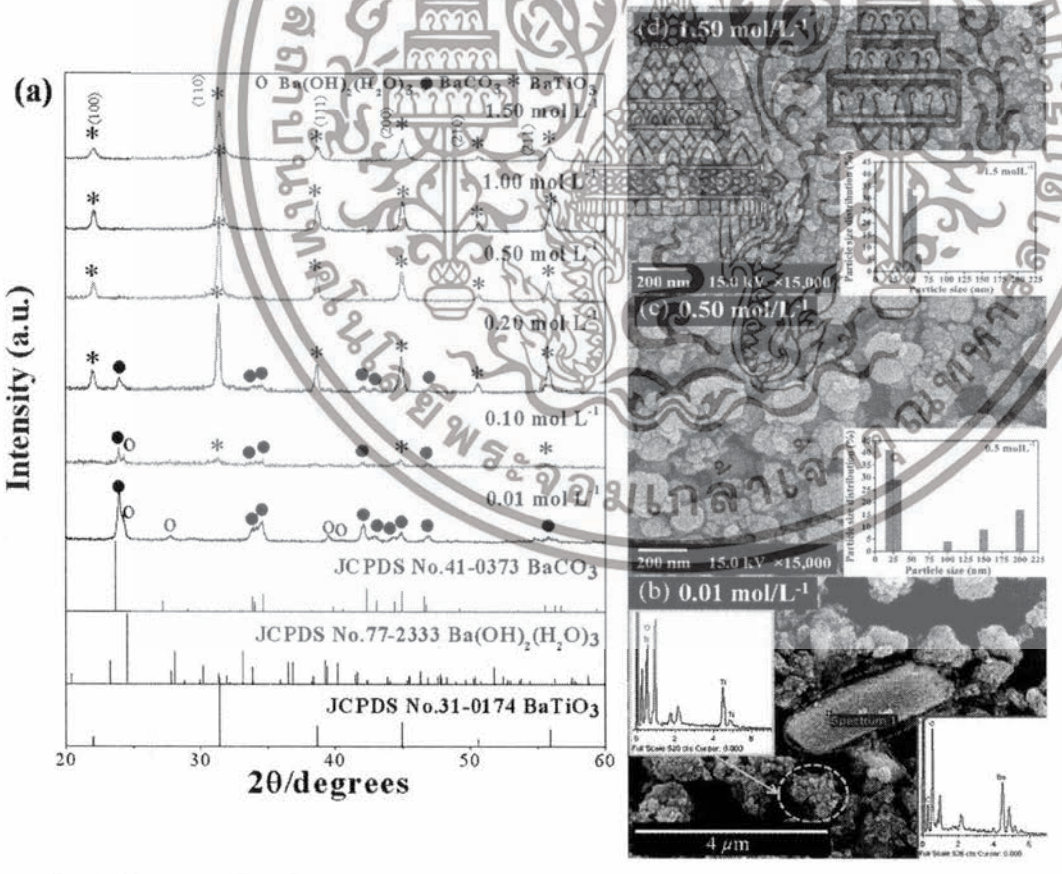

XRD pattern (a) and SEM images (b) to (d) of $BaZr_yTi_{1-y}O_3$; $y = 0.0$ powders synthesized for 60 min at various precursor concentrations in mol L^{-1} of NaOH in Ar atmosphere.

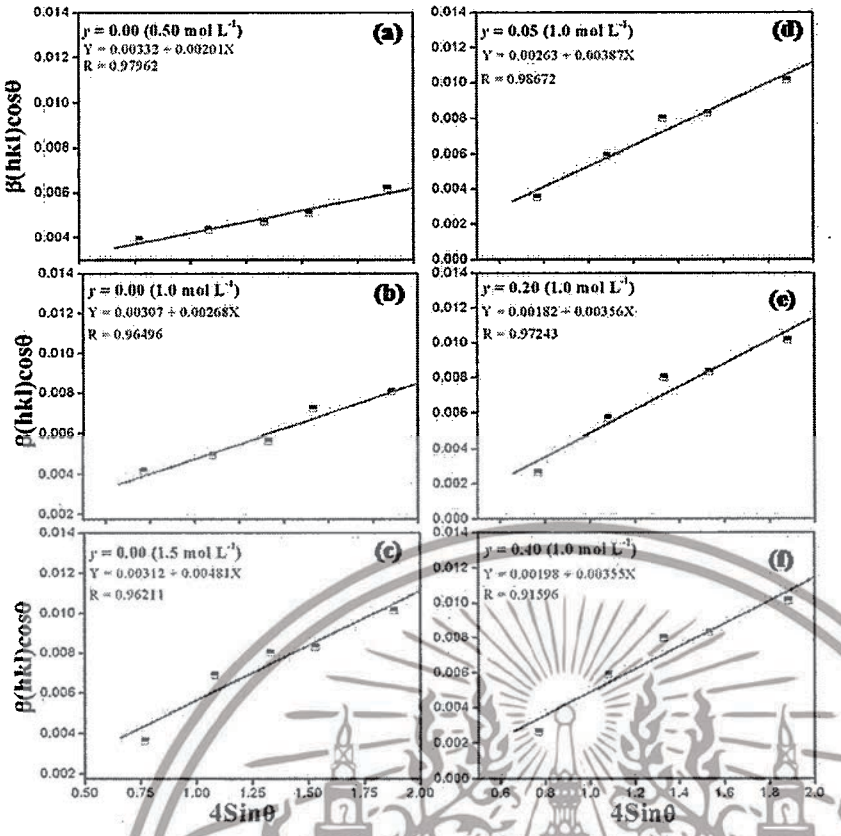

Hall–Williamson plot (a) $y = 0.0$ at 0.5 mol L^{-1} of precursor concentration, (b) $y = 0.0$ at 1 mol L^{-1} of precursor concentration, (c) $y = 0.0$ at ol L^{-1} of precursor concentration, (d) $y = 0.05$, (e) $y = 0.2$ and (f) $y = 0.4$.

1 Crystalline size (D) and lattice strain calculations of the $BaZr_yTi_{1-y}O_3$; $y = 0.0$, 0.05, 0.2 and 0.4 powders as determined by X-ray ction

le	Scherrer method	Hall–Williamson method		SEM
Conc. (mol L^{-1})	Crystalline size (nm)	Crystalline size (nm)	ε ($\times 10^{-3}$)	Particle size (nm)
0.50	36.6 ± 13.9	28.5	2.01 ± 0.002	123.2 ± 42.8
1.00	28.8 ± 09.4	26.4	2.68 ± 0.001	93.0 ± 28.2
1.50	16.4 ± 01.4	15.0	1.53 ± 0.003	49.6 ± 11.2
1.00	29.8 ± 07.4	18.6	3.87 ± 0.002	96.3 ± 14.0
1.00	33.2 ± 12.7	19.1	3.56 ± 0.003	108.1 ± 19.3
1.00	33.5 ± 12.3	19.4	3.55 ± 0.002	115.5 ± 11.0

can produce a large number of small crystallites.[19,44] A r number of cations at higher values of precursor entration diffuse in solution, thus leading to a higher e of supersaturation and higher nucleation rate.[11,29] As a t, the size of the final particles decreased with increasing ırsor concentration, while a large number of small crys- es were formed. The structural and morphological char- izations converged when demonstrating that the chemical synthesis process leads to forming the cubic O_3 phase, with 100 nm grade nanopowders and a narrow listribution.

3.4 Effect of sonication time on the morphology and particle size distribution

To investigate the details of sonochemical conversion from precursor to the final perovskite phase, a series of experiments employed different sonication times, without changing the conditions of other preparations. Fig. 5(a) shows the XRD pattern of as-prepared $BaZr_yTi_{1-y}O_3$; $y = 0.0$ powders synthesized by 1 mol L^{-1} of precursor concentration with 20 mol L^{-1} of NaOH in Ar atmosphere at different sonication times. The pure perovskite structure was observed clearly at 5 min sonication time by using a strong base solution (20 mol L^{-1} NaOH) and

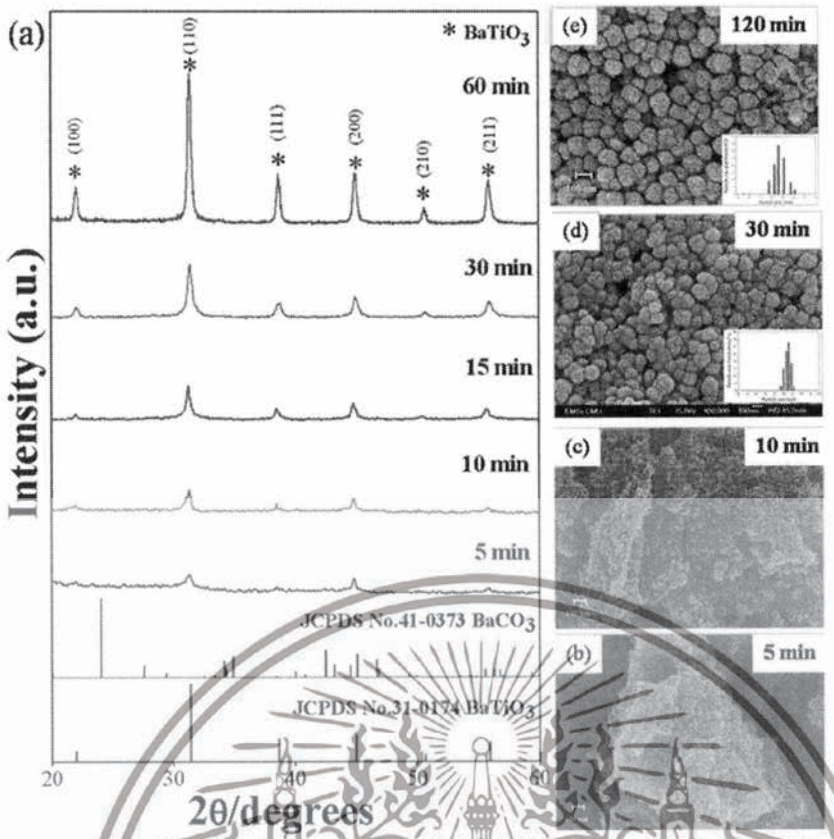

XRD pattern (a) and SEM images (b) to (e) of $BaZr_yTi_{1-y}O_3$; $y = 0.0$ powders synthesized at various reaction durations in 20 mol L^{-1} of l in Ar atmosphere.

precursor concentration (≥0.5 mol L^{-1}), with the powder ıesized in a closed system with Ar gas. No $BaCO_3$ phase or ınted phase was found, but intensity of the perovskite e was quite low. This indicated that the product had low allinity, which improved significantly with increasing sonic irradiation time. A sharp XRD pattern was observed ly at 60 min sonication time. Fig. 5(b)–(d) illustrate the ıdary electron images of $BaZr_yTi_{1-y}O_3$; $y = 0.0$ synthesized fferent sonication times. Fig. 5(b) and (c) show that nano- als of $BaZr_yTi_{1-y}O_3$; $y = 0.0$ were formed firstly under sonic irradiation, and then readily agglomerated into gated particles in a short period of time, in order to mize high surface energy. The particle size and shape of luster are difficult to identify. However, the spherical shape uniformity of the particle were observed clearly with ased sonication time [Fig. 5(d)–(f)]. Sphere-like particles achieved, evidently after 20 min sonication time, and the cle size increased slightly after 2 h under ultrasonic irra- ɔn. The particles showed a monosized spherical shape that different from that in other wet chemical synthesizing ıods.[12,14–16] The products had a slightly spherical ɔhology, and the particle size distribution was rather ɔw. Furthermore, by increasing the sonication time further, formation of neck between the particles was observed, h is caused by high velocity interparticle collision gener- by ultrasonic irradiation [Fig. 5(d)]. The high velocity of interparticle collision can make surface diffusion, as the melting point starts from the surface area of nanoparticles.[24] Surface diffusion is transportation of a typical mass in the sintering mechanism that produces surface smoothing,[29] particle joining,[23,45] grain boundary formation[24,45] and neck growth.[45] Nevertheless, densification and volume shrinkage did not originate, as the sonochemical method generated local thermal energy that differed from thermal energy of the sintering process.[24]

3.5 Effect of the Zr/Ti molar ratio on the perovskite phase formation

The evolution of XRD patterns of $BaZr_yTi_{1-y}O_3$; $y = 0.0$, 0.2, 0.4 and 0.6 powders synthesized in different sonication times is shown in Fig. 6(a)–(d). Strong influence of the Zr/Ti ratio was observed clearly on perovskite phase formation, which started for the composition, $y = 0.0$, at 5 minutes sonication time [Fig. 6(a)]. Otherwise, formation of the perovskite phase started to form at 10 and 15 minutes sonication time for the composition, $y = 0.2$ and 0.4, respectively [Fig. 6(b) and (c)]. However, as shown in Fig. 6(d), no strong crystal phases can be found from the XRD pattern for the composition, $y = 0.6$, meaning that the samples were composed of an amorphous phase, of which its formation might be related to different regions of sonochemical activity. Two regions of sonochemical activity are known to exist, as postulated by Suslick and co-workers.[22,46] One

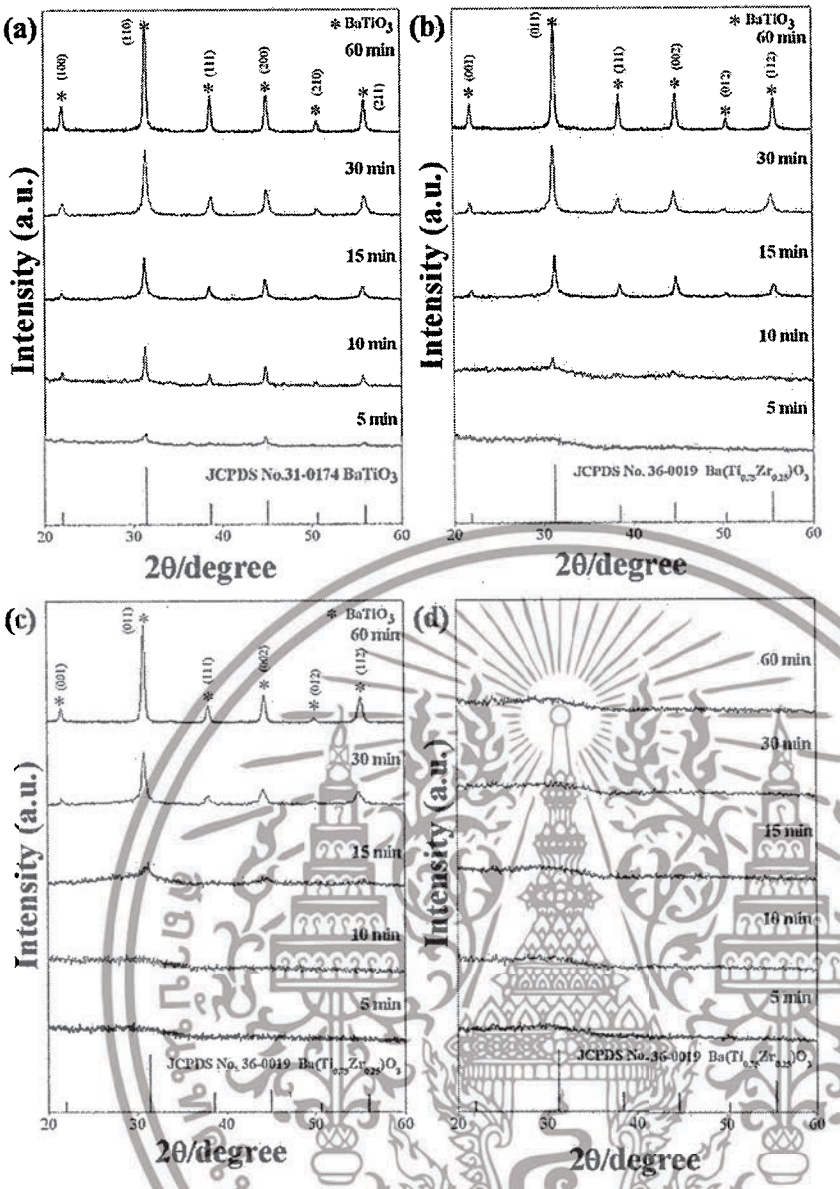

XRD patterns of $BaZr_yTi_{1-y}O_3$; $y = 0.0$, 0.2, 0.4 and 0.6 powders synthesized at various sonication times in 20 mol L^{-1} of NaOH solutions = 0.0, (b) $y = 0.2$, (c) $y = 0.4$ and (d) $y = 0.6$.

e inside of collapsing bubbles and the other the interfacial ɔn between the cavitation bubbles and surrounding solu- . The inside of collapsing bubbles generates extremely high ɔerature (>5000 K), pressure (>20 MPa) and very high cool- ɾates (excess of 10^{10} K s^{-1}), whereas the interfacial region ɾates a much lower temperature, which is still high enough ıpture chemical bonds and induce a variety of reactions.[45] ɴ a reaction takes place inside collapsing bubbles, the final luct is amorphous, as a result of the extremely rapid cooling (>10^{10} K s^{-1}) that occurs during the collapse. Conversely, if ıction occurs within the interfacial region, nanocrystalline lucts are expected to materialize. Since amorphous powders ɜ obtained in this study at a high Zr/Ti ratio, the authors ulate that the formation of $Ba(Zr/Ti)O_3$ at a high and low i ratio probably occurs inside and at the interfacial region of collapsing bubbles, respectively. Similar behavior was observed in stibnite (Sb_2S_3) nanorod that was synthesized by the sonochemical method.[47] Besides, another factor might relate to the difference in formation constant of the complex metallic hydroxide network. At a high Zr concentration, heterotrimetallic Ba–Ti–Zr-hydroxide may have difficulty in forming a network.[44] All compositions of powders synthesized at 60 min sonication time were selected in order to investigated the solid solution and identify the crystal structure. The XRD pattern of $BaZr_yTi_{1-y}O_3$; $y = 0.0$, 0.2, and 0.4 nanoparticles, synthesized for 60 min sonication time are presented in Fig. 7(a). All powders exhibit a pure perovskite structure without a trace of impurity, indicating that Zr^{4+} has diffused into the host lattice to form a solid solution. One symmetric peak observed at 2θ ~44° to 46° in all of the samples confirmed that all

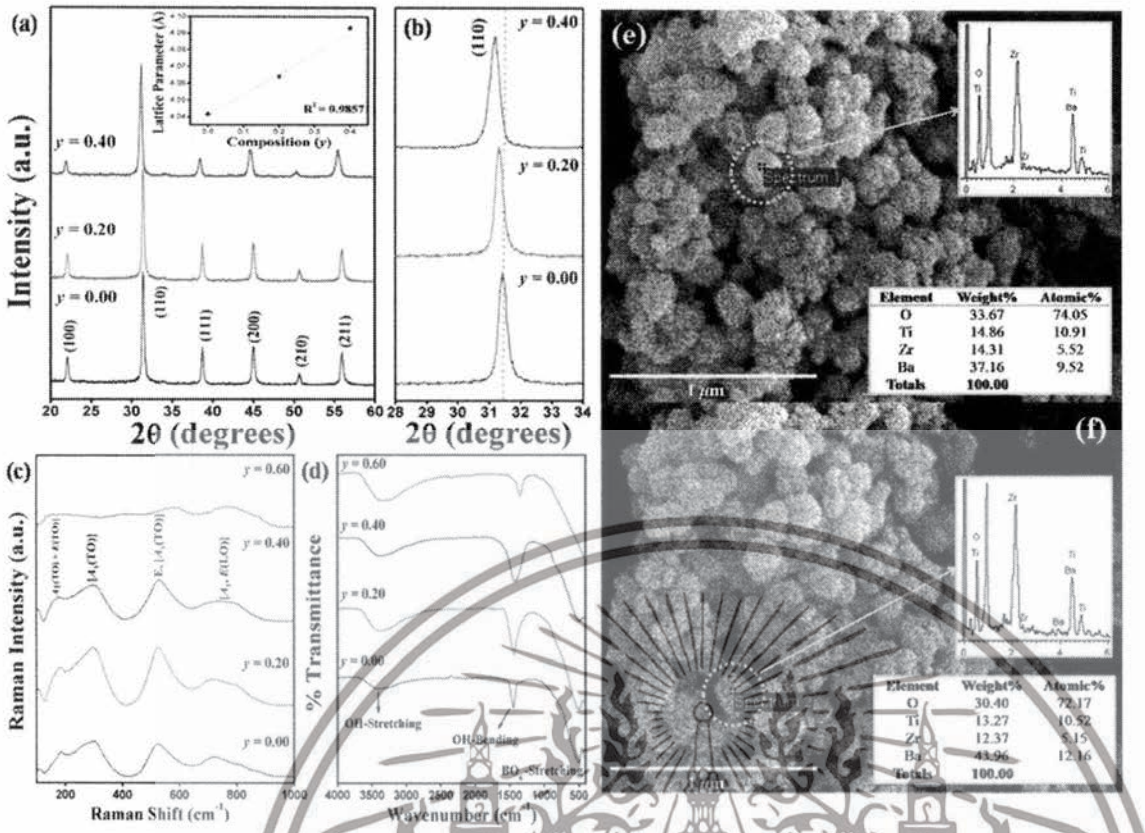

XRD patterns of $BaZr_yTi_{1-y}O_3$; $y = 0.0$, 0.2 and 0.4 powders synthesized at 60 min sonication time (a) enlarged ranges of 28–34°, (b) n spectrum (c) and FT-IR spectrum (d) SEM/EDX results of the composition $y = 0.4$ powders (e and f).

2 Lattice parameter (*a*), and unit cell volume (*v*) of the $BaZr_yTi_{1-y}O_3$; $y = 0.0$, 0.2 and 0.4 powders as determined by X-ray ction

le		
Conc. (mol L^{-1})	Lattice parameters (*a*)/(Å)	Unit cell volume (*v*)/(Å)^3
1.00	4.0415 ± 0.0004	65.42
1.00	4.0641 ± 0.0004	67.12
1.00	4.0931 ± 0.0011	68.57

positions had a cubic symmetry. This agreed well with ous reports that used the co-precipitation method.[16] tionally, the XRD pattern demonstrated a progressive peak toward the lower diffraction angle with increased Zr^{4+} 7(b)]. This phenomenon can be explained qualitatively respect to the unit cell volume caused by the substitution $^{4+}$ at the Ti-site. According to Shannon's effective ionic , with a coordination number of 6, the ionic radius of B-site (Zr^{4+}) is 0.86 Å, which is close to the radius of Ti^{4+} 5 Å).[48] The calculated lattice parameters (*a*) and unit cell me (*v*) of $BaZr_yTi_{1-y}O_3$; $y = 0.0$, 0.2, and 0.4 powders are rted in Table 2. These values increase with increased Zr ent by replacing Ti^{4+}-site (0.745 Å) with large Zr^{4+} (0.86 Å) . The Raman spectra are shown clearly in Fig. 7(c). All an peaks of the composition $y = 0.00$, 0.20 and 0.40 were observed similarly. The 4 broadening peaks at around 186, 303, 522 and 715 cm^{-1} are assigned to the $[A_1(TO) + B(LO)]$, $[A_1(TO)]$, $[E, A_1(TO)]$ and $[A_1, E(LO)]$ Raman-active modes of tetragonal (*P4mm*) symmetry.[49] It is noteworthy that despite the XRD data [Fig. 7(a)] showing the cubic (*Pm3m*) symmetry, the Raman spectra show the tetragonal (*P4mm*) crystal structure. This is because of the hydroxyl defect from a high basic environment. The $-OH$ groups can substitute the sub-lattice to form a metastable cubic phase. However, the hydroxyl defect existed as interstitial defects in many unit cells, but not all. Therefore, some unit cells can stabilize in a tetragonal structure. Nevertheless, characterization by XRD gives results in a static and average symmetry, while the result in a dynamic and local symmetry could be characterized by Raman spectroscopy.[49] Therefore, the results from Raman did not correlate with those from XRD data in this situation. In fact, the crystal structure of powder products may exhibit a mixture between the tetragonal and cubic crystal structure. However, the hydroxyl defects could be removed by chemical treatment with DMF, which is discussed later. Furthermore, Fig. 7(c) also reveals that all of the Raman peaks disappeared when the composition (*y*) of the Zr/Ti ratio was increased to 0.60. The presence of a very broad hump demonstrated a predominantly amorphous phase characteristic. This result confirms that the condition of powder products was stabilized in the amorphous phase. Furthermore, the FT-IR spectrum of powder products at various Zr/Ti ratios was studied

:eported in Fig. 7(d). The band appearing for all compo-ıs at around 3600 and 1600 cm^{-1} is attributed to O–H :hing and O–H bending vibration, respectively. In corre-ding with previous results, it could be said that the OH tion bands in the 0.00–0.40 compositions of the Zr/Ti ; come from the OH-defects, that existed on the surface :les and in the sub-lattice. On the other hand, the O–H tion band in the 0.60 composition of the Zr/Ti ratio may : from the mixture between OH^- species defects and –OH ɔs from the amorphous phase. In addition, the absorption at around 520 cm^{-1} was used to indicate the difference of :tallic Ba–Ti–Zr hydroxides amorphous and crystalline BZT es. This peak is assigned mainly to the characteristic peak e perovskite structure, while associating with the absorp-vibration of Ti–O and Zr–O asymmetric stretching in BO_6 ıedra.[14,50] The 0.00–0.40 compositions showed the strong ymmetric stretching in BO_6 octahedra, thus confirming the powder products in these conditions were formed as solid solution without the impurity or the other phases. estingly, the BO_6 vibration band disappeared at the 0.60 ɔosition of the Zr/Ti ratio, while the OH absorption band ɔited large intensity, thus suggesting that the BZT solid-ion phase was not found at this condition. Therefore, it ɔe confirmed that the product powder may stabilize in the of trimetallic Ba–Ti–Zr hydroxides in the amorphous e. The SEM/EDX analysis at different points on the surface dividual particles was performed in order to confirm the ogeneity of the powder products. Fig. 5(e) and (f) display :DX spectra at different points on the surface of individual cles. It can be seen from these figures that the concentra-: of various elements (Ba, Ti, Zr and O) involved in the ɾidual particle are very close to each other indicating to the ogeneity of the powder products. The result from SEM/EDX tra showed good correspondence with the result from XRD 7(a)]. This observation clearly demonstrates that the ıicationic perovskite $BaZr_yTi_{1-y}O_3$; $y = 0.0$–0.4 solid solu-was formed completely during the sonochemical process ;, without the need for further calcination or a heating ess.

Effect of chemical treatment on the crystal structure by g dimethyl formamide (DMF)

narily, hydroxyl (–OH) groups play an important role in the ıesis of perovskite nanopowders *via* wet-chemical esses, especially in a very high OH concentration (pH > [0,49–53] The powder products can contain much chemical ling with the two types of OH species. Weakly bonded OH^- ies are adsorbed on particle surfaces, while strongly led OH^- species are entrapped in the crystal lattice, to form :e OH^- defects.[20] These defects can affect the stability of :e vibration and decrease tetragonality to form a metastable c phase, which leads to the absence of phase transition.[20] n the literature, the OH^- species on particle surfaces could liminated by thermal heat treatment above 300 °C, and 'e 1100 °C for eliminating the lattice OH^- species.[20,52,53] This : investigated sonochemical $Ba(Zr_yTi_{1-y})O_3$ powder products and found hydroxyl defects similar to those in the $BaTiO_3$ reported in the literature.[20,53] Nevertheless, in this work, lattice hydroxyl defects could be removed completely by solvothermal treatment with DMF solution at only 170 °C. In studying the effect of DMF on the crystal structure, a selected region of XRD patterns in $2\theta = 42°$ to 48° of $Ba(Zr_yTi_{1-y})O_3$ ($y = 0.00$) powder products was compared between before and after treatment, as shown in Fig. 8(a). The results clearly show the difference of tetragonal *versus* cubic crystal structure. Before treatment, the powder products showed a single peak of (200) reflection, which agreed well with the characteristic of a cubic crystal structure. When the powder products were treated with DMF solution at 170 °C for 24 h, splitting of (200) reflected at a higher region, with a (002) shoulder at the lower region, and this corresponded to the characteristics of a tetragonal crystal structure. In accordance with a large amount of lattice OH^-, a high amount of protons (H^+) can link and exist in an oxygen sub-lattice. Therefore, the unit cell volume was enlarged with close correlation, and distortion of the tetragonal crystal structure was observed. Consequently, a cubic crystal structure was presented;[20] then, when the lattice OH^- was removed, the tetragonal structure returned to stabilize it. FT-IR spectroscopy was used to investigate the functional group of $Ba(Zr_yTi_{1-y})O_3$ ($y = 0.00$) powders. The spectrum is shown in Fig. 8(b). O–H stretching vibration of the hydroxyl group and Ti–O_6 stretching vibration of in BO_6 octahedra of $BaTiO_3$ were detected on $Ba(Zr_yTi_{1-y})O_3$ ($y = 0.00$) powders before treatment. Then, the band of O–H stretching disappeared, while TiO_6-stretching was still present after the treatment process. It could be seen that the hydroxyl species were desorbed more effectively after the treatment process. However, it is difficult to distinguish between the surfaced-adsorbed and lattice hydroxyl groups because the peak position of two OH^- species is very similar.[52,53] Furthermore, Raman scattering spectroscopy also was studied for further investigation. The Raman spectra of $Ba(Zr_yTi_{1-y})O_3$ ($y = 0.00$) compared before and after chemical treatment are shown in Fig. 8(c). All Raman-active modes in the powder products after chemical treatment clearly correspond to those in the $4E(TO + LO) + 3A_1(TO + LO) + B_1(TO + LO)$ of a tetragonal (*P4mm*) crystal structure.[19] However, there are 3 broadening peaks at around 303, 522 and 715 cm^{-1} in powder products before treatment, which are assigned to the Raman-active modes of tetragonal (*P4mm*) symmetry, indicating that the crystal structure of powder products before treatment may exhibit a mixture between tetragonal and cubic crystal structure. However, when the chemical treatment was preceded by DMF, the cubic crystal structure changed completely to be tetragonal. In addition, it is well known that the existence of OH^- defects leads to loss of phase transition in ferroelectric materials.[49,50] Therefore, DSC measurement was used for further investigation of $Ba(Zr_yTi_{1-y})O_3$ ($y = 0.00$) phase transition. The DSC data are shown in Fig. 8(d). The powder products before treatment show only the baseline, without the change of enthalpy (ΔH), while those after treatment clearly show the exothermic transition on cooling at temperatures of about 127.1 °C, which correlates to the phase transition temperature of tetragonal to cubic crystal structure. The relating change in

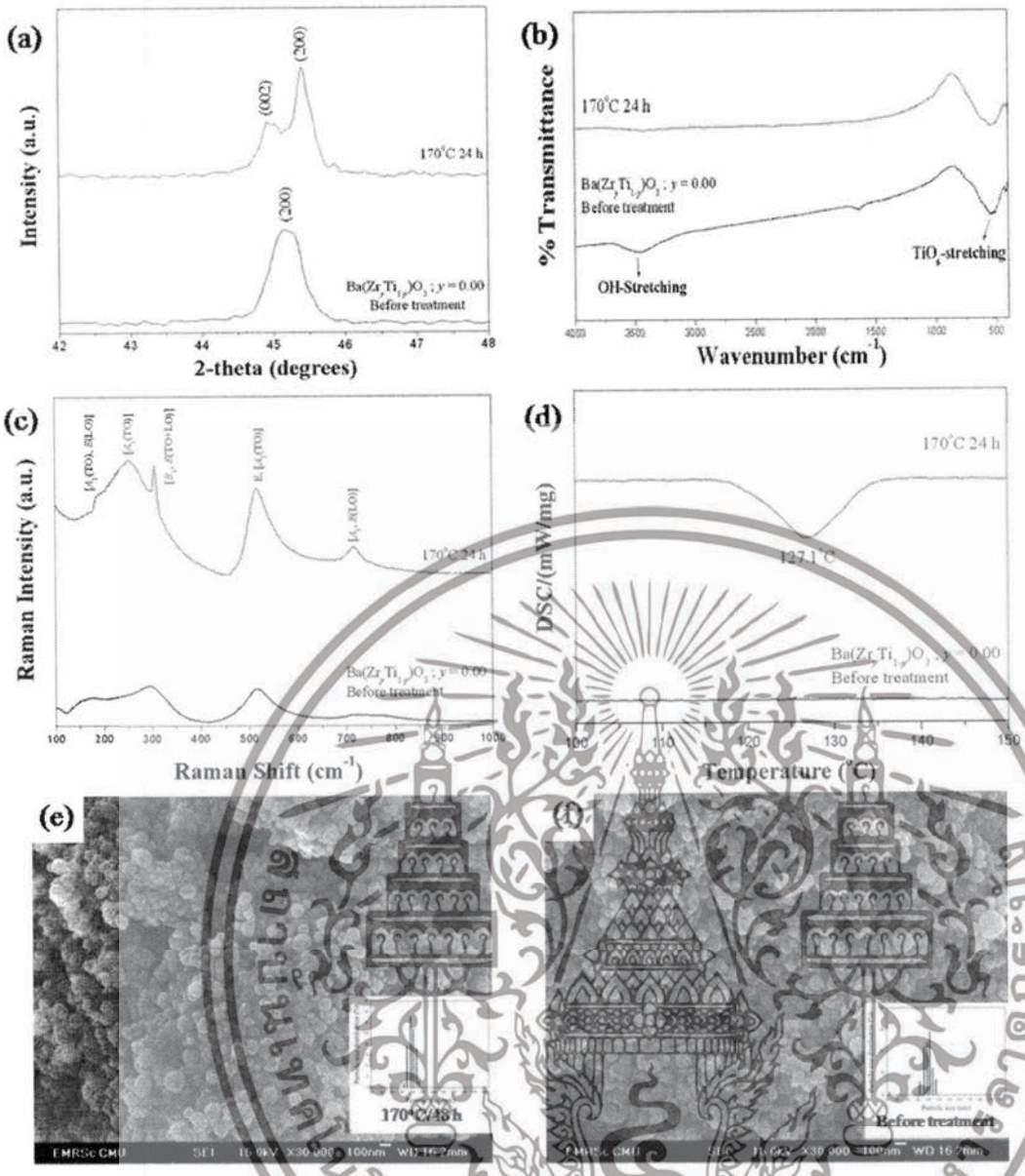

3 XRD pattern (a), FT-IR (b), Raman (c), DSC (d) and SEM image of $BaZr_yTi_{1-y}O_3$; $y = 0.0$ untreated powders (e) and chemically treated ders with DMF (f).

nalpy (ΔH) value of this transformation is 593 mJ g^{-1}, which esponds to 650 mJ g^{-1} of the commercial $BaTiO_3$ tetragonal cture. On the other hand, the Curie temperature observed n DSC data can be used to confirm the 1 : 1 stoichiometry Ti ratio in $Ba(Zr_yTi_{1-y})O_3$ ($y = 0.00$) powder products, which imilar to reports from F. Baeten.[51] Finally, all the results n this part of this study indicate that the use of chemical tment with DMF solution possibly eliminates OH^- defects n the oxygen sub-lattice. The tetragonal crystal structure was roved, and the phase transition observed at 127 °C. In lition, the chemical treatment with DMF had no significant ct on the particle shape, size or size distribution. The ticle size changed slightly from 97.4 ± 19.2 nm to 103.5 ± 3 nm with a narrow size distribution. The SEM micrographs of powder products before and after chemical treatment are shown in Fig. 8(e) and (f), respectively.

3.7 Mechanism of crystal growth formation

Based on the results achieved with different synthetic parameters, perovskite phase formation of the $BaZrTiO_3$ spheres involved the crystallization process and was similar to mechanical stirring.[54] A plausible mechanism that explains all these data is shown in Fig. 9. The first stage of the synthesis is forming a complex network of the amorphous phase, which is assumed to be flows: *i.e.* barium cations that form $Ba(OH)^+$ species in the NaOH concentration. Furthermore, titanium and zirconium cations were hydrolyzed readily in NaOH solutions to form soluble $[Ti(OH)_6]^{2-}$ and $[Zr(OH)_5]^-$ anions. The formation

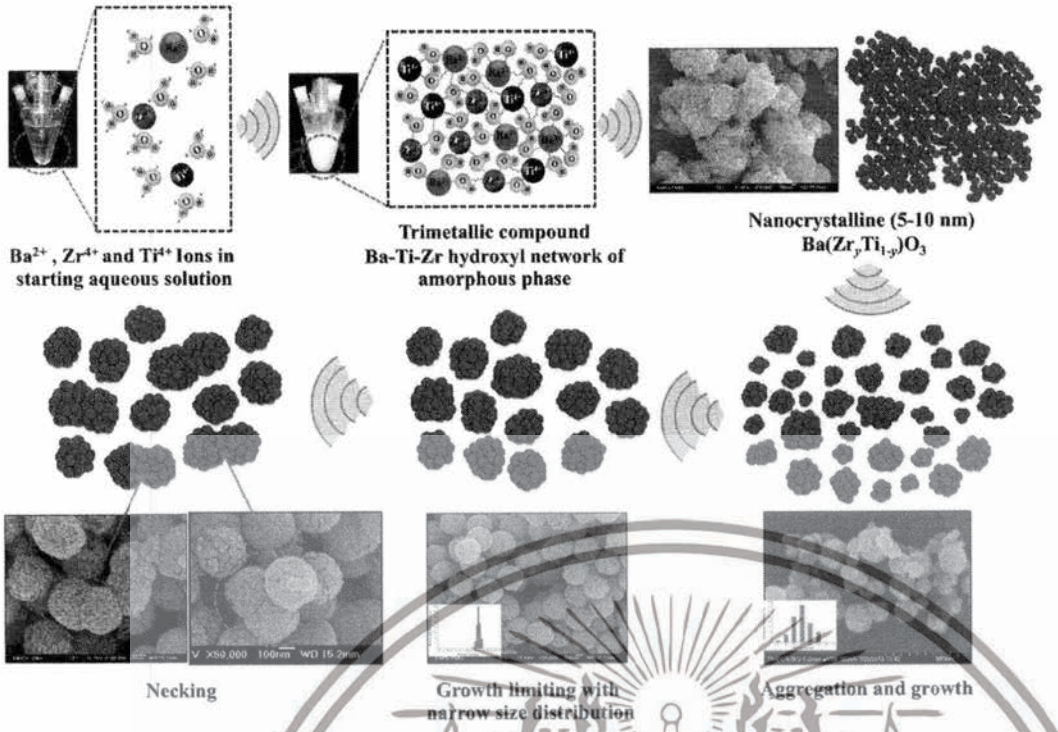

Schematic diagrams illustrating formation of the crystal growth mechanism.

exahydroxy titanate(IV) and pentahydroxy zirconate(IV) $)H)_5]^-$ in the presence of strong alkaline condition were ribed also by N. C Pramanik *et al.*[42] and Boschini *et al.*[55] ectively. The reaction between $Ba(OH)^+$, $[Ti(OH)_6]^{2-}$ and $)H)_5]^-$ initiated the formation of gels comprising an ngled complex network of polymeric chains of trimetallic i–Zr hydroxides. The skeleton of the polymer corresponds ıe Ba, Ti and Zr atom linked by bridging O atoms. The nd stage of the synthesis is accelerating the formation of primary BZT particulates (crystallization) by ultrasonic iation. The results presented in a previous section of this y strongly indicate that formation of BZT is dominated by a eation and growth mechanism. When the complex network norphous phases was irradiated ultrasonically, the forma- growth, and implosive collapse of bubbles (microjet effect) quid medium generated extreme synthesis conditions lized hot spot with high temperature of *ca.* 5000 K, pressure . 20 MPa, and a very high cooling rate of *ca.* 10^{10} K S^{-1}). due to vaporization of the solvent into bubbles, solubility ıe reactants was enhanced, thus elevating supersaturation ıe reactant solutions. In the conventional crystallization ess from a solution, two steps are involved; nucleation and al growth, of which both have supersaturation as a mon driving force. Crystals in the supersaturated solution neither form nor grow. The nucleation rate in the crystal- ion process is small and only few nuclei can be generated at nitial time of growth. Then, nuclei grow in spatial orien- ns fixed by solute crystallized structures. However, nucle- ı in the sonocrystallization process was accelerated by the osive collapse of bubbles, while the crystal growth process was inhibited or delayed by shock waves and turbulent flow created by ultrasonic radiation.[22,29] This effect promoted nucleation over grain growth to form tiny primary particulates (crystalline), which tended to aggregate into large particles due to tremendous surface energy, and stability of the particles can be expressed as:[36,57]

$$S = (R_a + R_b)\int_{R_a+R_b}^{\infty} \exp\left[\frac{V(C)}{k_B T}\right] \frac{dC}{C^2} \quad (5)$$

where S is the stability factor of the particles, R_a and R_b are the radius of the two particles, respectively, $V(C)$ is the function of potential energy interaction, C is the distance between the two particles, k_B is Boltzmann's constant (1.3806×10^{-23} J K^{-1}) and T is the temperature (K). When the distance between particles is decreased to a certain extent, short-range reactions (van der Waal's forces and existence of an electrostatic barrier) lead to strong attraction between particles.[36,57] The third stage of synthesis is forming spherical particles with a narrow size distribution. The turbulent flow and mechanical effects, such as microjet impact and shock waves that generate from the implosive collapse of bubbles under ultrasonication,[24,46] can create a relatively uniform reaction in fluid medium,[24,46] which improves the spherical shape of monodispersed BZT particles. Microjets with a high velocity of over 400 km h^{-1} crush the aggregated cluster in all directions,[21,43] and nanocrystalline particles are driven together at extremely high speeds, thus inducing effective melting at the point of impact.[22,45] These phenomena generate relatively monodispersed particles with a narrow size distribution. Furthermore, when increasing the sonication time further, neck formation was observed between

articles, caused by high velocity of the interparticle collisi- generated by ultrasonic irradiation.[45] Suslick *et.al.*[45,46] ›sed that the effects of cavitation in the phenomenon of ›article collisions come from the shock waves released into l and not from the temperature of the localized hot-spot ›d within the collapsing bubble. It is interesting to note ›olume shrinkage and densification did not originate, due .e sonochemical method that generated local thermal y, which differed from thermal energy of the sintering ›ss.

Conclusion

icationic oxides based on the complex perovskite structure $(Zr_yTi_{1-y})O_3$; $y = 0.0$–0.4 nanoparticles were synthesized tly under ultrasonic irradiation in the sonochemical ıesis process, without a calcination step. The concentration ıOH, the precursor and synthesized atmosphere play a key in forming the perovskite structure. Strong and high ›ntration of NaOH and the precursor, respectively, not only ıte nucleation, but also eliminate the formation of $BaCO_3$. ›crystalline was formed in a short period of time and then ›gated to form large particles. Narrow size distribution was ired for the aggregated particles under ultrasonic irradia- However, the synthesized powder had some of the OH p trapped in the crystal lattice, which was caused by strong ›concentration during the synthesis process. A plausible al growth mechanism was proposed by this study.

‹nowledgements

work was supported by the Thailand Research Fund (TRF) ›r grant no. BRG5680006 and S. Wirunchit would like to k The Royal Golden Jubilee (RGJ-Ph.D program) Scholar- program for financial support.

ferences

. G. Tang, K. H. Chew and H. L. W. Chan, *Acta Mater.*, 2004, **2**, 5177–5183.

7. Liu and X. Ren, *Phys. Rev. Lett.*, 2009, **103**, 257602.

. Zhang, M. Zhang, L. Wang, C. Zhou, Z. Zhang, Y. Yao, . Zhang, D. Xue, X. Lou and X. Ren, *Appl. Phys. Lett.*, 2014, **05**, 162908.

. Guo, B. K. Voas, S. Zhang, C. Zhou, X. Ren, S. P. Beckman nd X. Tan, *Phys. Rev. B: Condens. Matter Mater. Phys.*, 2014, **)**, 014103.

Bera and S. K. Rout, *Mater. Lett.*, 2005, **59**, 135–138.

. J. Moulson and J. M. Herbert, *Electroceramics: Materials, roperties, Applications*, Wiley, 2003.

I. Sopicka-Lizer, *High-Energy Ball Milling: Mechanochemical rocessing of Nanopowders*, Elsevier Science, 2010.

. Hou and J. Yu, *J. Am. Céram. Soc.*, 2013, **96**, 2218–2224.

. S. Bhalla, R. Guo and R. Roy, *Mater. Res. Innovations*, 2000, , 3.

. H. Haertling, *J. Am. Ceram. Soc.*, 1999, **82**, 797–818.

S. Reed, *Principles of Ceramics Processing*, Wiley, 1995.

12 P. Julphunthong and T. Bongkarn, *Curr. Appl. Phys.*, 2011, **11**, S60–S65.

13 N. Binhayeeniyi, P. Sukvisut, C. Thanachayanont and S. Muensit, *Mater. Lett.*, 2010, **64**, 305–308.

14 M. Veith, S. Mathur, N. Lecerf, V. Huch, T. Decker, H. P. Beck, W. Eiser and R. Haberkorn, *J. Sol-Gel Sci. Technol.*, 2000, **17**, 145–158.

15 J. Q. Qi, Y. Wang, W. P. Chen, L. T. Li and H. L. W. Chan, *J. Nanopart. Res.*, 2006, **8**, 959–963.

16 S. B. Reddy, K. P. Rao and M. S. R. Rao, *Scr. Mater.*, 2007, **57**, 591–594.

17 Z. L. Wang and J. Song, *Science*, 2006, **312**, 242–246.

18 X. Wang, J. Song, J. Liu and L. W. Zhong, *Science*, 2007, **316**, 102–105.

19 D. Segal, *Chemical Synthesis of Advanced Ceramic Materials*, Cambridge University Press, 1991.

20 P. K. Dutta, R. Asiaie, S. A. Akbar and W. Zhu, *Chem. Mater.*, 1994, **6**, 1542–1548.

21 K. J. Leonard, S. Sathyamurthy and M. P. Paranthaman, *Chem. Mater.*, 2005, **17**, 4010–4017.

22 J. H. Bang and K. S. Suslick, *Adv. Mater.*, 2010, **22**, 1039–1059.

23 J. Janbua, J. Mayamae, S. Wirunchit, R. Baitahe and N. Vittayakorn, *RSC Adv.*, 2015, **5**, 19893–19899.

24 K. S. Suslick, *Science*, 1990, **247**, 1439–1445.

25 B. Zhou, B. Liu, L.-P. Jiang and J.-J. Zhu, *Ultrason. Sonochem.*, 2007, **14**, 229–234.

26 I. Haas, S. Shanmugam and A. Gedanken, *J. Phys. Chem. B*, 2006, **110**, 16947–16952.

27 C. Wu, B. P. Mosher and T. Zeng, *Chem. Mater.*, 2006, **18**, 2925–2928.

28 L.-P. Jiang, S. Xu, J.-M. Zhu, J.-R. Zhang, J.-J. Zhu and H.-Y. Chen, *Inorg. Chem.*, 2004, **43**, 5877–5883.

29 H. Xu, B. W. Zeiger and K. S. Suslick, *Chem. Soc. Rev.*, 2013, **42**, 2555–2567.

30 D. Ghanbari, M. Salavati-Niasari and M. Ghasemi-Kooch, *J. Ind. Eng. Chem.*, 2014, **20**, 3970–3974.

31 F. Dang, K. Kato, H. Imai, S. Wada, H. Haneda and M. Kuwabara, *Ultrason. Sonochem.*, 2010, **17**, 310–314.

32 S. Vuttivong, S. Niemcharoen, P. Seeharaj, W. C. Vittayakorn and N. Vittayakorn, *Ferroelectrics*, 2013, **457**, 44–52.

33 M. Xu, Y. N. Lu, Y. F. Liu, S. Z. Shi, T. S. Qian and D. Y. Lu, *Powder Technol.*, 2006, **161**, 185–189.

34 K. Yasui, T. Tuziuti and K. Kato, *Ultrason. Sonochem.*, 2011, **18**, 1211–1217.

35 P. Charoonsuk, R. Baitahe, W. Vittayakorn, N. Atiwongsangthong, R. Muanghua, P. Seeharaj and N. Vittayakorn, *Ferroelectrics*, 2013, **453**, 54–61.

36 T. Hyeon, M. Fang and K. S. Suslick, *J. Am. Chem. Soc.*, 1996, **118**, 5492–5493.

37 J. Geng, L. Jiang and J. Zhu, *Sci. China: Chem.*, 2012, **55**, 2292–2310.

38 S. Singh, N. Kumar, R. Bhargava, M. Sahni, K. D. Sung and J. H. Jung, *J. Alloys Compd.*, 2014, **587**, 437–441.

39 Y. Han, D. Radziuk, D. Shchukin and H. Moehwald, *J. Mater. Chem.*, 2008, **18**, 5162–5166.

Waseda, E. Matsubara and K. Shinoda, *X-Ray Diffraction ystallography: Introduction, Examples and Solved Problems*, ringer, 2011.
Suryanarayana and G. Norton, *X-Ray Diffraction: A ictical Approach*, Springer, 1998.
C. Pramanik, S. I. Seok and B. Y. Ahn, *J. Colloid Interface .*, 2006, **300**, 569–576.
M. Lencka and R. E. Riman, *Ferroelectrics*, 1994, **151**, 159–4.
nkaj, in *Theoretical and Experimental Sonochemistry volving Inorganic Systems*, ed. M. Ashokkumar, Springer, therlands, 2011, pp. 213–271.
Prozorov, R. Prozorov and K. S. Suslick, *J. Am. Chem. Soc.*, 04, **126**, 13890–13891.
B. McNamara, Y. T. Didenko and K. S. Suslick, *Nature*, 99, **401**, 772–775.
Wang, Y.-N. Lu, J.-J. Zhu and H.-Y. Chen, *Inorg. Chem.*, 03, **42**, 6404–6411.
D. Shannon, *Acta Crystallogr., Sect. A: Cryst. Phys., Diffr., eor. Gen. Crystallogr.*, 1976, **32**, 751.
49 T. Noma, S. Wada, M. Yano and T. Suzuki, *J. Appl. Phys.*, 1996, **80**, 5223–5233.
50 S. Wada, T. Tsurumi, H. Chikamori, T. Noma and T. Suzuki, *J. Cryst. Growth*, 2001, **229**, 433–439.
51 F. Baeten, B. Derks, W. Coppens and E. Van Kleef, *J. Eur. Ceram. Soc.*, 2006, **26**, 589–592.
52 M. H. Frey and D. A. Payne, *Phys. Rev. B: Condens. Matter Mater. Phys.*, 1996, **54**, 3158–3168.
53 R. Kota and B. Lee, *J. Mater. Sci.: Mater. Electron.*, 2007, **18**, 1221–1227.
54 A. Testino, M. T. Buscaglia, V. Buscaglia, M. Viviani, C. Bottino and P. Nanni, *Chem. Mater.*, 2004, **16**, 1536–1543.
55 F. Boschini, A. Rulmont, R. Cloots and B. Vertruyen, *J. Eur. Ceram. Soc.*, 2009, **29**, 1457–1462.
56 K. S. Birdi, *Handbook of Surface and Colloid Chemistry*, CRC Press, 3rd edn, 2008.
57 W. B. Russel, D. A. Saville and W. R. Schowalter, *Colloidal Dispersions*, Cambridge University Press, 1992.

The effect of zirconium on the perovskite phase formation of barium zirconium titanate nanoparticles by the sonochemical method

Supamas Wirunchit,[1] Rattanai Baitahe[1], Wanwilai Vittayakorn,[1] Naratip Vittayakorn[1,2,3*] and Santi Maensiri[4]

[1]Electroceramics Research Laboratory, College of Nanotechnology, King Mongkut's Institute of Technology Ladkrabang, Bangkok 10520, Thailand

[2]Advanced Materials Research Unit, Faculty of Science, King Mongkut's Institute of Technology Ladkrabang, Bangkok 10520, Thailand

[3]Department of Chemistry, Faculty of Science, King Mongkut's Institute of Technology Ladkrabang, Bangkok 10520, Thailand

[4]School of Physics, Institute of Science, Suranaree University of Technology, Nakhon Ratchasima 30000, Thailand

Abstract

The sonochemical technique is a powerful synthetic method for the production of nanostructured inorganic powders. Monosized spherical barium zirconium titanate [$Ba(Zr_xTi_{1-x})O_3$; BZT], with x = 0.00, 0.05, 0.20 and 0.40 nanoparticles, were synthesized successfully through sonochemical reaction. The phase formation as well as crystal structure and morphology were investigated. The as-prepared powders were identified by X-ray diffraction (XRD). The cubic perovskite structure of BZT was formed completely in a short irradiation time without the calcination process. The lattice parameter (a) of the samples increased with increasing zirconium concentration. Furthermore, when the concentration of zirconium increased, the reaction time must be increased in order to obtain phase-pure perovskite. The BZT nanoparticles showed a monosized spherical shape that was different

from that in other preparation methods. The morphology of the products was very close to spherical, with the particle size distribution being rather narrow.

Keywords: Sonochemical method, ultrasonic irradiation, Barium zirconium titanate, Nanoparticle

* Corresponding author:

Asst. Prof. Naratip Vittayakorn, Department of Chemistry, Faculty of Science, King Mongkut's Institute of Technology Ladkrabang, Bangkok 10520, THAILAND

E-mail: naratipcmu@yahoo.com

1. Introduction

Many researchers have focused recently on lead-free ceramic materials and their applications in various electronic devices because of environmental and human health issues [1-4]. Barium titanate ($BaTiO_3$) was the first lead-free piezoelectric ceramic material to be studied widely since its discovery in the 1940s [5]. It is well known that doping is an effective way to improve the performance of material in electroceramics. In particular, substitution of Ti^{4+} with Zr^{4+} in $BaTiO_3$ has received much attention, due to the tunable structure and electrical properties of specific applications. Characteristics of the ferroelectric phase transition of $Ba(Zr_xTi_{1-x})O_3$ (BZT) ceramics depend strongly on Zr content from normal ferroelectric to relaxor ferroelectric behavior [6]. When the Zr content is less than 10 mol%, BZT ceramics show normal ferroelectric behavior, and dielectric anomalies that correspond to rhombohedral to orthorhombic (T_{R-O}), orthorhombic to tetragonal (T_{O-T}), and tetragonal to cubic (T_C) phases are observed clearly. The transition temperatures of BZT ceramics (T_{R-O}, T_{O-T} and T_C) became closer with increasing Zr content and merged near room temperature at 15 mol% Zr concentration. When Zr content increased further to around 27 mol%, the sample

showed typical diffuse paraelectric to ferroelectric phase transition behavior, in which T_C shifted to a higher temperature, with increased frequency caused by the inhomogeneous distribution of Zr ions on Ti sites, and mechanical stress in the grain [7-8]. When Zr content increased to more than 27 mol%, the BZT materials exhibited similar relaxor ferroelectric behavior. In a paraelectric state, which is just above T_C, BZT ceramics are attractive candidates for dynamic random access memories (DRAM) and tunable dielectric devices. The Zr^{4+} is an effective substituent in $BaTiO_3$, which decreases and shifts the Curie temperature to below room temperature [9]. Furthermore, the Zr^{4+} ion (0.86Å) is more stable chemically than Ti^{4+} (0.745Å) and has a larger ionic size that expands the lattice. Therefore, the conduction by electron hopping between Ti^{4+} and Ti^{3+} would be depressed by the substitution of Ti with Zr [10-12]. The production of high performance ceramic materials with functional devices requires the highest purities, homogeneity powders, well controlled particle morphology and narrow size distribution. Thus, many research groups have focused on the quality of processing for the synthesis of BZT high performance product powders. Conventional BZT powders are obtained by solid-state reaction between $BaCO_3$, ZrO_3 and TiO_2. However, the powders prepared by this method consist of rather coarse, poorly uniformed particles, with a broad particle size distribution and very high calcination temperature requiring more than 1,600°C for the synthesis of BZT powders [13]. In order to eliminate defects, a number of wet chemical synthesis methods are very popular such as sol-gel [14-15], hydrothermal [16-17], combustion [18-19] and co-precipitation techniques [20]. However, although these chemical methods are suitable for preparing high quality BZT nanopowders, the synthesis process is complicated and takes a very long time. In addition, the heat treatment step is still required to achieve complete phase formation. This research provides an interesting sonochemical method, which is one of the wet chemical processes. The sonochemical method can be employed to synthesize metallic and organic covers, and especially almost all inorganic

nanoparticles, in a short period of time [21-24]. It also can use the acoustic cavitation from an ultrasonic wave to generate or accelerate the chemical reaction. The main event in sonochemistry is the creation, growth and collapse of a bubble that forms in liquid. The stage that leads to bubble growth occurs through diffusion of solute vapor into the volume of the bubble. The last stage is collapse of the bubble, which occurs when its size reaches maximum value. An extremely high temperature of about 5,000 K, pressure of ~20 MPa and a very high cooling rate of $\sim 10^{10}$ K/S occur in a very localized space, when the small bubble generated in aqueous solution collapses during ultrasonication. Then, unique properties of the sonochemically synthesized particles are expected [25].

Previous work from the authors successfully synthesized $BaTiO_3$, $BaZrO_3$ and $Ba(Zr_{0.4}Ti_{0.6})O_3$ nanoparticles by the sonochemical method without a heat treatment process [26-28], which showed a monosized spherical shape at a short irradiation time and narrow size distribution. Therefore, the sonochemical method is a suitable way to synthesize high performance particle products. In this work, $Ba(Zr_xTi_{1-x})O_3$ powders, with x = 0.00, 0.05, 0.20 and 0.40, were synthesized successfully by the sonochemical method, without the calcination process. The effect of Zr^{4+} on the formation, structure and morphology, including the irradiation time, lattice constant, particle size and shape was discussed.

2. Experimental procedure

2.1 Powder synthesis

The $Ba(Zr_xTi_{1-x})O_3$ powders, with x = 0.00, 0.05, 0.20 and 0.40 nonoparticles, were synthesized by sonochemical synthesis in aqueous solution according to the overall reaction of

$$BaCl_2.2H_2O_{(aq)} + (1-x)TiCl_{4\,(aq)} + xZrOCl_2.8H_2O_{(aq)} + (6-2x)NaOH_{(aq)} \rightarrow Ba(Zr_xTi_{1-x})O_3 + (6-2x)NaCl_{(aq)} + (13-x)H_2O \quad (1)$$

where (aq) denotes a species in solution. This process is similar to the method described by Reddy et al. [20], except when applying powerful ultrasound irradiation. Appropriate proportions of high purity $BaCl_2.2H_2O$ (99%, Merck), $ZrOCl_2.8H_2O$ (99.5%, Advance Material) and $TiCl_4$ (99.5%, Wako) were weighed and used as raw materials. The deionized water used in this research had been boiled previously at 100 °C for 15 min in order to remove the CO_2 dissolved in it. Then, the dilution procedure involved adding 1 M of concentrated $TiCl_4$ slowly into deionized water at a temperature lower than 5 °C, while stirring until it turned into a homogeneous solution. Equal molar concentrated solutions of diluted $TiCl_4$ (1M solution) and $ZrOCl_2$ (1M solution) were mixed thoroughly at first, and 1 M $BaCl_2$ solution was added to this mixture. These solutions were mixed continuously for 10 minutes. NaOH with different molar concentrations was used for precipitation. NaOH solution was heated to 75 °C, with pH being maintained at ~14. The mixture of precursor solution was added to NaOH at the rate of 25 $ml.min^{-1}$, before being exposed to high-intensity ultrasound irradiation under ambient Ar gas for a given time. Ultrasound irradiation was accomplished with a high intensity ultrasonic probe (3 mm diameter; Ti-horn, 20 kHz) immersed directly in the reaction solution. Sonication was conducted without cooling in order that the temperature of the solution increased gradually from sonication to the end of the reaction. After the reaction had finished and cooled to room temperature, the precipitate was separated and washed with deionized water. The products were then dried in an oven at 80 °C for 24 hrs.

2.2 Powder characterization

The crystallographic information, including phase purity crystal structure and lattice constant of the powder products, was identify by the X-ray diffraction (XRD) technique using Ni-filtered Cu K_α radiation (λ = 0.1546 nm). The crystalline size (nm) was determined by

applying full-width half-maximum (FWHM) of the characteristic peak, according to Scherrer's equation: $d_{xrd} = k\lambda/\beta\cos\theta$, where λ is the X-ray wavelength (0.154 nm), k is the constant value (0.89), β represents the corrected peak width at half-maximum intensity, and θ is the diffraction angle. Furthermore, crystal structures also were identified by the Rietveld refinement method [28]. Then, Raman spectroscopy was the secondary technique used to investigate the crystal structure and ensure a single phase of powder products. Spectra of each sample were taken over a range from 100 to 1,000 cm^{-1}. Powder morphology and grain size were imaged directly using a field emission scanning electron microscope (SEM) and transmission electron microscope (TEM).

3. Results and Discussion

Figures 1(a) to (d) show the XRD results of BZT powders with various Zr^{4+} concentrations synthesized in 20M NaOH from 5 to 60 min sonication time. Figure 1(a) shows the XRD pattern of the perovskite phase as observed at 5 min sonication time. There was no detection of the $BaCO_3$ phase or unwanted phase, which indicated that powder synthesized in Ar-gas can eliminate formation of the $BaCO_3$ phase. However, intensity of the perovskite phase was quite low, which meant that the powder had low crystallinity. High crystallinity was achieved by increasing sonication time. Sharp peaks of perovskite phase were observed for powder synthesized at 60 min sonication time. A similar trend was observed for the composition, $x = 0.05$ [Figure1(b)]. By increasing the composition, $x = 0.2$ and 0.4, the XRD pattern of perovskite phase with low intensity started to form at 10 and 15 min sonication time, respectively [Figure 1(c) and (d)]. Intensity of the perovskite structure increased with increasing sonication time. XRD results indicated that when Zr concentration increases, the sonication time must be increased in order to obtain a pure perovskite phase. Sharp well-defined peaks were evident clearly in all products synthesized at 60 min

sonication time. When compared to traditional solid state synthesis, the result indicated that the BZT phase was formed completely during the sonochemical synthesis, without further heating or calcination. All compositions of powders synthesized at 60 min sonication time were selected in order to identify the crystal structure. Figure 2 displays the XRD pattern of $Ba(Zr_xTi_{1-x})O_3$, with x = 0.0, 0.05, 0.2 and 0.4 nanoparticles, synthesized for 60 min sonication time. Characteristics of the tetragonal perovskite structure such as splitting (002) and (200) in a range from 44° to 46° were not observed in all of the samples. One symmetric peak observed at $2\theta \sim 44°$ to 46° in all of the samples confirmed that all compositions had a cubic symmetry. This agreed well with previous reports that used a solid state and co precipitation method [6, 26-28]. Furthermore, the XRD pattern displayed a progressive peak shift toward the lower diffraction angle with increased Zr^{4+}. This phenomenon can be explained qualitatively with respect to the unit cell volume caused by the substitution of Zr^{4+} at the Ti-site. According to Shannon's effective ionic radii, with a coordination number of 6, the ionic radius of B-site ions (Zr^{4+}) has a radius of 0.86 Å, which is close to the radius of Ti^{4+} (0.745 Å) [28]. Therefore, Zr^{4+} can enter into the six fold coordinated B-site of the perovskite structure to substitute Ti^{4+}, due to radius matching. Rietveld refinement using data from 20° to 60° of the XRD results was conducted to achieve lattice parameters, as shown in Table 1. Lattice parameters increase in direct proportion to increasing Zr concentration. When compared with previous results of BZT powders prepared by a mixed oxide method, as reported by Chen et al. [6], the sonochemical BZT powder transition from tetragonal to cubic phase did not occur, whereas the solid state reaction power phase transition occurred at x = 0.20. The absence of phase transition in BZT powder synthesized by the sonochemical method might be related to some entrapped hydroxyl groups on the crystal surface or in the crystal lattice. It is well known that many wet chemical syntheses generate OH species in the solution during the process, and OH groups are incorporated

easily into the perovskite lattice, as defects are shown to be similar to a "loose packed" structure.

According to the literature [29, 31], the quality of data from structural refinement is checked generally by R-values (R_p, R_{exp}, R_{wp}), and the appropriate fit (G), which is defined by $G^2=X^2$. X^2 or "Chi squared", can be determined from the expected and weighted profile of R factors ($X^2 = (R_{wp}/R_{exp})^2$). Additionally, the difference between experimental profiles of XRD patterns and calculated data varies slightly in scale of intensity, as illustrated by the line, $Y_{observed}$-$Y_{calculated}$. Furthermore, the crystalline size of all compositions was calculated using the Scherer equation from the FWHM of the 110 planes in the XRD pattern, which is shown in Table 1. The crystalline size decreased with increasing the Zr^{4+} content. Since Raman spectroscopy or the Raman scattering technique is efficient for measuring the lattice vibration in discriminating the symmetry and asymmetry of a crystal structure, it can be used as a power tool that supports the identification of phase formation and structure of inorganic materials. Therefore, the Raman scattering technique was used together with the X-ray diffraction method to confirm the phase formation of BZT powder products [30]. Raman spectra of as-synthesized BZT powders, synthesized at different compositions of x, are presented in Figure 3. It is well known that $BaTiO_3$ has five atoms, and fifteen degrees of freedom divided into the optical representations, $3F_{1u} + F_{2u}$, while another F_{1u} symmetry mode corresponds to the acoustical branch. The $BaTiO_3$ spectra revealed the presence of a tetragonal structure, mainly characterized by the $A_1(TO_1)$, $A_1(TO_2)$, $E(TO_2)$, $A_1(TO_3)$ and $A_1(LO)/E(LO)$ Raman modes, while no Raman-active mode was predicted for the cubic phase ($Pm3m$) [30]. The Raman shift peak at the composition, $x = 0.00$ ($BaTiO_3$), is located at around 181, 295, 521 and 707 cm^{-1} and assigned to the transverse optical (TO) modes of A_1 symmetry. The peak at 181 cm^{-1} arises due to interference from harmonic coupling between the three $A_1(TO)$ phonons. The peak at 707 cm^{-1} is related to the highest frequency

of the longitudinal optical mode (LO) with A_1 symmetry [30]. Regarding the other compositions, the Raman spectra nearly corresponds to those of $BaTiO_3$ that present a cubic structure, which is in agreement with the XRD and Rietveld refinement result. The vibration of Ti atoms in octahedral oxygen created a peak at around 181 cm^{-1} ($A_1(TO_1)$ mode), which broadened and decreased in intensity with increasing Zr content.

The morphology and particle size were studied also by FE-SEM, and FE-SEM micrographs of all aggregated particle products, sonochemically synthesized for 60 minutes of ultrasonic irradiation, are demonstrated in Figures 4 (a) to (h), with the average particle size shown in Table 1. The difference between the XRD crystallite size and SEM particle size is thought to associate with the existence of a hierarchical structure [26]. The SEM particle size may stem from a secondary mesostructure consisting of a primary crystallite size. A large number of BZT nanocrystals were created initially from the Ti- and Zr- based precursor under ultrasound irradiation before aggregating BZT particles from large particles. The BZT particles showed a monosized spherical shape different from that in other preparation methods [6-8]. The products showed a spherical or almost spherical morphology, and the particle size distribution was rather narrow. Figure 5 shows TEM micrographs of the BZT nanoparticles. The large spherical BZT particles were characterized as aggregates of 5-10 nm of nanocrystals.

4. Conclusion

The $Ba(Zr_xTi_{1-x})O_3$, with x = 0.00, 0.05, 0.20 and 0.40 nanoparticles, was synthesized successfully by the sonochemical method without the calcination process. The as-prepared powders were identified by X-ray diffraction (XRD). The cubic perovskite structure of BZT was seen to form completely in a short irradiation time, and the lattice parameter (a) of the samples increases with increased zirconium concentration. Furthermore, when the concentration of zirconium increased, the reaction time must be increased in order

to obtain a phase-pure perovskite. The BZT nanoparticles showed a monosized spherical morphology and the particle size distribution was rather narrow. A TEM image indicated that the large spherical BZT particles were characterized as aggregates of 5-10 nm of nanocrystals.

Acknowledgements

This work was supported by the Thailand Research Fund (TRF) under the TRF Senior Research Scholar, Grant No. RTA5680008". S. Wirunchit would like to thank the Royal Golden Jubilee (RGJ) Ph.D. Program for its financial support.

References

[1] Y. I. Li, K. Moon, C. P. Wong, Electronics without lead, science 308 (2005) 1419-1420.

[2] W. W. Wolny, European approach to development of new mentally sustainable electroceramics, Ceram. Int. 30 (2004) 1079-1083.

[3] J. Rodel, W. Jo, K. T. P. Seifert, E. M. Anton, T. Granzow, D. Damjanovic, Perspective on the development of lead-free piezoceramics, J. Am. Ceram. Soc. 92 (2009) 1153-1177.

[4] D. Maurya, M. Murayama, A. Pramanick, W. T. Reynolds, K. Song, M. H. Kim, W. J. Kim, Origin of high piezoelectric response in A-site disordered morphotropic phase boundary composition of lead-free piezoelectric $0.93(Na_{0.5}Bi_{0.5})TiO_3$–$0.07BaTiO_3$, Apppl. Phys. 113 (2013) 114101.

[5] V. V. Shvartsman, D. C. Lupascu, Lead-free relaxor ferroelectrics, J. Am. Ceram. Soc. 95 (2012) 1-26.

[6] H. Chen, C. Yang, C. Fu, J. Shi, J. Zhang, W. Leng, Microstructure and dielectric properties of $Ba(Zr_xTi_{1-x})O_3$ ceramics, J. Mater. Sci. 19 (2008) 379-382.

[7] D. Hennings, A. Schnell, G. Simon, Diffuse ferroelectrics phase transition in $Ba(Ti_{1-y}Zr_y)O_3$ ceramics, J. Am. Ceram. Soc. 65 (1982) 539-544.

[8] U. Weber, G. Greuel, U. Boettger, S. Weber, D. Hennings, R. Waser, Dielectric properties of Ba(Zr,Ti)O_3-based ferroelectrics for capacitor applications, J. Am. Ceram. Soc. 84 (2001) 759-766.

[9] R. C. Kell, N. J. Hellicar, Structural transitions in barium titanate-zirconate transducer materials, Acustica. 6 (1956) 235-238.

[10] O. P. Thakur, C. Prakash, A. R. James, Enhanced dielectric properties of ceramics through improved processing, J. Alloys Compd. 470 (2009) 548-551.

[11] X. S. Wang, H. Yamada, C. N. Xu, Large electrostriction near the solubility limit in $BaTiO_3$–$CaTiO_3$ ceramics, Applied physics Letters. 85 (2005) 022905.

[12] S. Halder, P. Gerber, T. Schneller, R. Waser, Electromechanical properties of $Ba(Ti_{1-x}Zr_x)O_3$ thin films, Applied Physics. A. 81 (2005) 11-13.

[13] J. Bera, S. K. Rout, On the formation mechanism of $BaTiO_3$-$BaZrO_3$ solid solution through solid-oxide reaction, Materials Lett. 59 (2005) 135-138.

[14] M. Veith, S. Mathur, N. Lecerf, V. Huch, T. Decker, Sol-gel synthesis of nano-scaled $BaTiO_3$, $BaZrO_3$ and $BaTi_{0.5}Zr_{0.5}O_3$ oxides via single-source alkoxide precursors and semi-alkoxide routes,J.Sol-Gel.Sci.Techn.17 (2000) 145.

[15] X. G. Tang, K. H. Chew, H. L. W. Chan, Diffuse phase transition and dielectric tenability of $Ba(Zr_yTi_{1-y})O_3$ relaxor ferroelectric ceramics, Acta. Mater. 52 (2004) 5177.

[16] X. B. W. Lee, S. B. Cho, Preparation of $BaZr_xTi_{1-x}O_3$ by the hydrothermal process from peroxide precursors, J. Eur. Ceram. Soc. 25 (2005) 2009.

[17] A. Outzourhit, M. A. E. I. Raghni, M. L. Hafid, Characterization of hydrothermally prepared $BaTi_{1-x}Zr_xO_3$, J. Alloys Compd. 340 (2002) 214.

[18] C. N. Georde, J. K. Thomas, H. P. Kumar, M. K. Suresh, V. R. Kumar, P. R. S. Wariar, R. Jose, J. Koshy, Characterization sintering and dielectric properties of nanocrystalline

barium titanate synthesized through a modified combustion process, Mater. Charact. 60 (2009) 53.

[19] Q. Feng, X. H. Ma, Q. Z. Yan, C. C. Ge, Preparation of soft-agglomerated nano-sized ceramic powders by sol-gel combustion process, Mat. Sci. Eng. B-solid. 162 (2009) 53.

[20] S. B. Reddy, K. P. Rao, M. S. R. Rao, Nanocrystalline barium zirconate titanate synthesized at low temperature by an aqueous co-precipitation technique, J. Scripta. Mat. 57 (2007) 591.

[21] J. Guo, Z. Chen, Y. Li, Z. Yu, Q. Li, J. Li, C. Feng, D. Zhang, Sonochemical synthesis of TiO_2 nanoparticles on graphene for use as photocatalyst, Ultrason. Sonochem. 18 (2011) 1082–1090.

[22] S. Anandan, G. J. Lee, J. J. Wu, Sonochemical synthesis of CuO nanostructures with different morphology, Ultrason. Sonochem. 19 (2012) 682–686.

[23] I. A. Siddiquey, T. Furusawa, M. Sato, N. M. Bahadur, M. Alam, N. Suzuki, Sonochemical synthesis, photocatalytic activity and optical properties of silica coated ZnO nanoparticles, Ultrason. Sonochem.19 (2012) 750–755.

[24] S. M. Meybodi, S. A. Hosseini, M. Rezaee, S. K. Sadmezhaad, D. Mahommadyani, Synthesis of wide band gap nanocrystalline NiO powder via a sonochemical method, Ultrason. Sonochem. 19 (2012) 841–845.

[25] A. Gedanken, Using sonochemistry for the fabrication of nanomaterials, J. Ult. Sonch. 11 (2004) 47.

[26] S. Vuttivong, S. Niemcharoen, P. Seeharaj, W. C. Vittayakorn, N. Vittayakorn, Sonosynthesis of spherical $BaTiO_3$ nanoparticles, Ferroelectrics 453 (2013) 43-48.

[27] P. Charoonsuk, W. Vittayakorn, N. Atiwongsangthong, P. Seeharaj, N. Vittayakorn, Synthesis of monodispersed perovskite barium zirconate ($BaZrO_3$) by the sonochemical method, Ferroelectrics 453 (2013) 54-61.

[28] R. D. Shannon, Revised effective ionic radii and systematic studies of interatomic distances in halides and chalcogenides, Acta Crystallogr., Sect. A: Cryst. Phys., Diffr., Theor. Gen. Crystallogr. A32 (1976) 751.

[29] H-H. Huang, H-H. Chiu, N-C. Wu, M-C. Wang, Tetragonality and properties of $Ba(Zr_xTi_{1-x})O_3$ ceramics determined using the rietveld method, Metallurgical and materials transactions. 38A (2008) 3276-3282.

[30] N. G. Nelson, J. G. Skinner, Raman spectrum of strontium titanate, J. Chem. Phys. 48 (1968) 2240.

[31] B. H. Toby, R factors in Rietveld analysis: How good is good enough?, Powder Diffraction. 21 (1) (2006) 67-70.

Table Heading

Table 1 The lattice parameter, crystallite size and particles size of $Ba(Zr_xTi_{1-x})O_3$, with x = 0.0, 0.05, 0.2 and 0.4 nanoparticles

Figure Legends

Figure 1 The XRD pattern of $Ba(Zr_xTi_{1-x})O_3$, with x = 0.0, 0.05, 0.2 and 0.4 nanoparticles at different ultrasonic reaction times; (a) x = 0.0, (b) x = 0.05, (c) x = 0.2, and (d) x = 0.4.

Figure 2 Rietveld refinement that fits $Ba(Zr_xTi_{1-x})O_3$, with x = 0.0, 0.05, 0.2 and 0.4 nanoparticles synthesized at 60 minutes ultrasonic irradiation time.

Figure 3 Raman spectra of $Ba(Zr_xTi_{1-x})O_3$ nanoparticles synthesized at 60 minutes reaction time.

Figure 4 FE-SEM micrographs of $Ba(Zr_xTi_{1-x})O_3$ nanoparticles synthesized at 60 minutes reaction time; (a) $BaTiO_3$, (b) $BaZr_{0.05}Ti_{0.95}O_3$, (c) $BaZr_{0.20}Ti_{0.80}O_3$, and (d) $BaZr_{0.40}Ti_{0.60}O_3$, and particle size distribution; (e) $BaTiO_3$, (f) $BaZr_{0.05}Ti_{0.95}O_3$, (g) $BaZr_{0.20}Ti_{0.80}O_3$, and (h) $BaZr_{0.40}Ti_{0.60}O_3$).

Figure 5 TEM image of $BaZr_{0.05}Ti_{0.95}O_3$ nanoparticles synthesized at 60 minutes reaction time.

Table 1

Composition	Lattice parameter (a) (Å)	X^2	*Crystallite size (nm)*	*Perticle size (nm)*
$x = 0.00$	4.0295 ± 0.0004	1.1770	30.0	128.4 ± 18
$x = 0.05$	4.0432 ± 0.0003	1.0293	28.4	129.3 ± 17
$x = 0.20$	4.0589 ± 0.0004	1.2619	24.5	133.5 ± 22
$x = 0.40$	4.0931 ± 0.0011	1.3481	22.4	145.8 ± 46